ASSESSMENT OF MOLECULAR SIZE DISTRIBUTION EFFECTS ON THE NONSELECTIVE OXIDATION OF TRACE METAL HUMIC ACID BINARY SYSTEM

by

ESRA DEĞİRMENCİ İLHAN

B.S. in Environmental Engineering, Istanbul University, 2004

Submitted to the Institute of Environmental Sciences in partial fulfillment of
the requirements for the degree of
Master of Science
in
Environmental Technology

Bogazici University

2010

ASSESSMENT OF MOLECULAR SIZE DISTRIBUTION EFFECTS ON THE NONSELECTIVE OXIDATION OF TRACE METAL HUMIC ACID BINARY SYSTEM

APPROVED BY:

Prof. Dr. Miray Bekbölet . . . . . .
(Thesis Supervisor)

Prof. Dr. Ferhan Çeçen . . . . . .

Assist. Prof. Dr. Aslıhan Kerç . . . . . .

DATE OF APPROVAL . . . . . .

Dedicated to my family…

ACKNOWLEDGEMENTS

I owe my deepest gratitude to Prof. Dr. Miray BEKBÖLET for her invaluable, guidance, support, encouragement and help throughout this study. I am grateful for her extraordinary patience in all steps of the study and I feel so lucky to have a chance to work with her.

I would also like to express my appreciation to the members of my thesis jury; Prof. Dr. Ferhan ÇEÇEN and Assoc. Prof. Dr. Aslıhan KERÇ for their valuable time and comments.

I would express my special thanks to Dr. Ayşe Tomruk, Gülhan Özkösemen, Dr. Ceyda Uyguner Demirel, Sibel Şen Kavurmacı and Gül Geyik who helped me during this project.

I wish to thank my colleagues; Hülya Ünver, Hülya Aykaç, Müge Paçal and Sevinç İlgün for their support and friendship.

Finally, I would like to thank my family and my husband for their love, never-ending support, understanding and encouragement during my life.

ASSESSMENT OF MOLECULAR SIZE DISTRIBUTION EFFECTS ON THE NONSELECTIVE OXIDATION OF TRACE METAL HUMIC ACID BINARY SYSTEM

The objective of this research to investigate the effects of zinc ions on the nonselective photocatalytic degradation of humic acid in aqueous medium. The photocatalytic oxidation of humic was carried out using TiO_2 Degussa P-25 as the photocatalyst. The degradation kinetics was assessed based on pseudo first order. The adsorption experiments were also evaluated by using appropriate adsorption isotherms. The complex interactions between the surface properties of titanium dioxide and the molecular size dependent fractions of the humic acid were studied. The role of the metal ion complexation as expressed by the "binary system effect" on the photocatalytic degradation efficiency of humic acids with respect to molecular size fractions was deduced. The experiments were conducted with different molecular size fractions such as raw, 0.45 µm filtered fraction, 100 kDa fraction and 30 kDa fraction of Aldrich humic acid solution in the presence and the absence of zinc ion The molecular and structural characteristics of the humic acid molecule relative to changes during photocatalytic oxidation were evaluated on a comparative basis by UV-vis and fluorescence spectroscopy.

The declining trend of the specified UV-vis parameters, the related changes in the fluorescence spectra indicated the oxidative degradation of humic acid. As confirmed by the spectroscopic evaluation of the molecular size distribution, photocatalytic degradation of humic acid led to the formation of lower molecular size and higher UV-absorbing compounds. The complexity of the structure of humic acid molecule and the presence of zinc ions in the system can change the photocatalytic oxidation properties of humic acid through oxidation and adsorption processes. The reason of insignificant changes could be attributed to low concentrations of zinc with respect to humic acid concentration.

MOLEKÜLER BÜYÜKLÜK DAĞILIMININ HÜMİK ASİT- İZ METAL İKİLİ SİSTEMİNİN SELEKTİF OLMAYAN OKSİDASYONU ÜZERİNE ETKİLERİNİN DEĞERLENDİRİLMESİ

Bu araştırmanın amacı, sulu ortamdaki hümik asitlerin seçici olmayan fotokatalitik bozunma üzerinde çinko iyonlarının etkilerini araştırmaktır. Hümik asitlerin fotokatalitik oksidasyonu TiO_2 Degussa P-25 fotokatalizör kullanılarak yapılmıştır. Bozunma kinetiği birinci dereceden reaksiyon kinetik modelleri üzerinden değerlendirilmiştir. Adsorpsiyon deneyleri de uygun adsorpsiyon izotermleri kullanılarak değerlendirilmiştir. Titanyumdioksit yüzey özellikleri ve hümik asitin moleküler büyüklüğe bağımlı fraksiyonları arasındaki karmaşık etkileşimler araştırılmıştır. Hümik asidin fotokatalitik bozunma verimliliğinde moleküler büyüklüğe bağımlı fraksiyonlara bağlı olarak metal iyonu kompleksleşmesinin rolü "İkili sistem etkisi" ile ifade edilerek ortaya çıkarılmaktadır. Deneyler çinko varlığında ve yokluğunda Aldrich hümik asit solüsyonunun ham, 0.45 µm filtre edilmiş fraksiyonu, 100 kDa ve 30 kDa fraksiyonu gibi farklı moleküler boyut fraksiyonları ile yapılmıştır. Hümik asitlerin fotokatalitik oksidasyona bağımlı olarak değişen moleküler ve yapısal özellikleri UV-vis ve floresans spektroskopisi ile karşılaştırmalı olarak değerlendirilmektedir

Belirtilen UV-vis parametrelerinde düşüş eğilimi ve buna bağlı olarak floresans spektrumundaki değişiklikler hümik asitlerin oksidasyon parçalanmasını göstermektedir. Moleküler büyüklük dağılımı verilerinin spektroskopik olarak değerlendirilmesiyle onaylandığı gibi, hümik asitlerin fotokatalitik olarak parçalanması düşük moleküler ağırlıklı ve yüksek UV-absorbe eden bileşiklerin oluşumuna neden olmaktadır. Hümik asitlerin karmaşık molekül yapısı ve sistemde çinko iyonları varlığı oksidasyon ve adsorpsiyon proseslerinde hümik asitlerin fotokatalitik oksidasyon özelliklerini değiştirebilir. Önemsiz değişikliklerin nedeni çinkonun humik asit konsantrasyonuna göre düşük konsantrasyonlarda bulunması nedenine bağlanabilir.

TABLE OF CONTENTS

LIST OF FIGURES

LIST OF TABLES

LIST OF SYMBOLS/ABBREVIATIONS

	Explanation	Units Used
A	Related UV-vis parameter or	m^{-1}(UV-vis)
	TOC content of HA	mg L^{-1}(TOC)
AHA	Aldrich humic acid	
AOPs	Advanced oxidation processes	
BLF	Black Light Fluorescent Lamp	
C	Concentration	mg L^{-1}
C_e	Equilibrium concentration of adsorbate	mg L^{-1} (TOC)
		m^{-1} (UV-vis)
C_i	Initial concentration of adsorbate	mg L^{-1} (TOC)
		m^{-1} (UV-vis)
C_s	Amount of adsorbate adsorbed on adsorbent	mg L^{-1} (TOC)
		m^{-1} (UV-vis)
$Color_{436}$	Absorbance at 436 nm	cm^{-1} or m^{-1}
Da	Dalton	
DBPs	Disinfection byproducts	
DOC	Dissolved organic carbon	
DOM	Dissolved organic matter	
FI	Fluorescence intensity	
FI_{emiss}	Emission fluorescence intensity	
FI_{syn}	Synchronous fluorescence intensity	
FA	Fulvic acid	
GAC	Granular Activated Carbon	
HA	Humic acid	
HS	Humic substances	
ICP	Inductively Coupled Plasma Emission Spectroscopy	
K	Langmuir Adsorption Constant	mg L^{-1} (TOC)
		m^{-1} (UV-vis)

k	Pseudo first order reaction rate constant	min^{-1}
K_f	Freundlich Adsorption Capacity Constant	
K_{LH}	Adsorption coefficient	m
k_{LH}	Reaction rate constant	$m^{-1}min^{-1}$
L-H	Langmuir Hinshelwood	
NOM	Natural organic matter	
PAC	Powdered Activated Carbon	
q_A	Adsorbed amount per unit weight of adsorbent	$m^{-1}g^{-1}$
q_{max}	Maximum adsorption	$m^{-1}g^{-1}$
R	Pseudo first order rate	
R_{LH}	Rate of the reaction	$m^{-1}\ min^{-1}$
SCOA	Specific color absorbance	$m^{-1}\ mg^{-1}\ L$
$SCOA_{436}$	Specific color absorbance at 436 nm	$m^{-1}\ mg^{-1}\ L$
SUVA	Specific UV absorbance	$m^{-1}\ mg^{-1}\ L$
$SUVA_{254}$	Specific UV absorbance at 254 nm	$m^{-1}\ mg^{-1}\ L$
$SUVA_{280}$	Specific UV absorbance at 280 nm	$m^{-1}\ mg^{-1}\ L$
$SUVA_{365}$	Specific UV absorbance at 365 nm	$m^{-1}\ mg^{-1}\ L$
t	Irradiation time	min
$t_{1/2}$	Half life	min
THM	Trihalomethane	
TOC	Total Organic Carbon	$mg\ L^{-1}$
UF	Ultrafiltration	
UV-vis	Ultraviolet-Visible	
UV_{254}	Absorbance at 254 nm	cm^{-1} or m^{-1}
UV_{280}	Absorbance at 280 nm	cm^{-1} or m^{-1}
UV_{365}	Absorbance at 365 nm	cm^{-1} or m^{-1}
Zn	Zinc	
λ	Wavelength	nm
1/n	Freundlich adsorption intensity parameter	

1. INTRODUCTION

The decomposition of plant, animal and microbial material in soil and water produces a variety of complex organic molecules collectively defined as natural organic matter (NOM). NOM can be divided into two fractions; hydrophobic (humic substances), and hydrophilic (non-humic subtances). NOM is potentially important in binding and transport of inorganic and organic micropollutants; it may promote the formation of harmful byproducts during chlorination of drinking water. The functionality of NOM and its susceptibility to water treatment processes is governed by a number of factors such as polymeric molecular structure and molecular size fraction profiles. Chemical composition varies with molecular size and differences in the chemical composition between size fractions may have significant results on the environmental chemistry and geochemistry of humic substances. The differences in the structural characteristics, chemical environments and functional group contents of the humic acid fractions also affect the adsorption capability.

Humic acids are heterogeneous anionic macromolecules of low to moderate molecular weight containing both aromatic and aliphatic components with primarily carboxylic and phenolic functional groups. The high affinity of humic acids for complexation with various pollutants including heavy metals and pesticides causes contamination of ground and surface water. During chlorination step, humic acid can form very toxic disinfection (chlorinated organic compounds including trihalomethanes) by-products which exhibit mutagenic properties in drinking water treatment. Because of these reasons, several methods are used to remove the humic acids from water such as advanced oxidation processes (Benoit et al., 1993; Kainulaainen et al., 1994; Uyguner and Bekbolet, 2005b).

Molecular weight is one of the essential properties that need to be measured to understand the physical and chemical characteristics and chemical reactivity of humic acids. Lower molecular weight molecules have smaller radius, permitting nanopore adsorption, tend to be more hydrophilic resulting in greater bioavailability and increased mobility through porous media, and display rapid diffusion allowing for rapid adsorption

to mineral surfaces. On the other hand, higher molecular weight humic acid molecules tend to be more aromatic resulting in enhanced hydrophobic organic carbon partitioning, have higher electrostatic potential, greater metal binding capacity, and tend to increase the adsorption affinity resulting in decreased mobility.

Photocatalytic oxidation is used for breaking down organics into simpler components of water and CO_2, destroying organic pollutants, bacteria and viruses, detoxifying drinking water, purifying air streams and removing metals from waste streams. TiO_2 can be used in photocatalytic reactors for degrading contaminants in liquid and gas streams (Carp et al., 2004). Due to the surface oriented nature of photocatalysis, adsorption of humic acids onto TiO_2 should also be considered as an effective parameter for the efficiency of degradation. On the other hand, acid-base properties of TiO_2 also govern the adsorption process since the main functional groups residing on the humic molecule express pH dependent deprotonation capabilities.

The presence of dissolved metal ions is common in natural waters as well as in industrial wastes and they can affect the rate and efficiecny of photocatalytic reactions. Since humic substances display a key role in the cycling of many elements in the environment, the behavior of metal-humic acid complexes deserves to be investigated. The main objective of this research is to investigate the effects of zinc ions on the nonselective photocatalytic degradation of humic acid and its molecular fractions in aqueous medium. The spectroscopic properties of each size fraction were characterized and compared by UV-vis spectroscopy and fluorescence spectroscopy in emission and synchronous scan modes. The molecular and structural characteristics of the humic acid molecular size fractions relative to changes during both photocatalysis and adsorption experiments were monitored by UV-vis and fluorescence spectroscopy.

2. THEORETICAL BACKGROUND

2.1. Natural Organic Matter

Natural organic matter is the broken down organic matter that comes from plants and animals in the environment. Basic structure of NOM is comprised of cellulose, tannin, cutin, lignins, proteins, lipids, aminoacids and simple sugars. NOM displays wide range properties in terms of acidity, molecular weight and molecular structure (Goslan et al., 2002).

NOM is present throughout the ecosystem and provides nutrition to living plant and animal species in the environment. Because of its solubility, it has an important role in transporting the contaminants in the environment. It can pass through soil and mainstream water with waterflow. NOM in water is usually arised from living or decayed vegetation and microbial decomposition processes. One of the most important source of organic matter in fresh water supply is algal and cyanobacterial biomass, which is mostly aliphatic and devoid of lignins. The NOM in many water sources is comprised of hydrophobic (humic and fulvic acids), hydrophilic (non-humic substances), carboxylic acids, amino acids, carbohydrates and hydrocarbons.

NOM affects potable water quality in the areas of disinfection by-products (DBPs) formation, biological regrowth in the distribution system, affects organoleptic properties of water, such as; color, taste and odour (Siddiqui et al., 1997; Khan et al., 1998). For this reason, the treatment of water to remove natural organic matter has a significant importance. The characteristics (molecular weight, charge, hydrophobic and, aromatic nature etc.) of natural organic matter with its main constituent, humic substances, give the opportunity of several removal methods. Because of the large molecular size, filtration through nanofiltration membranes can be used when NOM concentration and color is high. Because of the charge and colloidal nature, NOM can be removed by coagulation and flocculation. The color of NOM may effectively be removed by ozonation (or another strong oxidative method.

The methods to remove natural organic matter in drinking water treatment include coagulation, ion exchange, chemical oxidation, membrane filtration and activated carbon adsorption (Letterman, 1999). Recently researches on advanced oxidation processes (AOPs) such as ozone (Siddiqui et al., 1997) and/or hydrogen peroxide (Toor and Mohseni, 2007), with or without being photoassisted with UV light are performed. The combination of these treatment processes has resulted in an improved removal efficiency of NOM compared to that of single process (Fearing et al., 2004). Oxidation processes have also been applied in the treatment of drinking water. The main purpose of these processes is to improve the biodegradability of NOM (Hoigné, 1998).

2.1.1. Humic Substances

Humic substances are the natural organic polyelectrolytes that form by the microbial degradation of plant and animal tissues and biomolecules (lipids, proteins, carbohydrates and lignin) dispersed in the environment after the death of living cells. Humic substance is a supramolecular structure of small bio-organic molecules (having molecular mass < 1000 Da) self-assembled mainly by weak dispersive forces such as van der Waals force, π-π, and CH-π bonds into only large molecular sizes (Piccolo, 2002). It is known that humic substances are the most stable fraction of organic matter is soils and can persist for thousands of years (Stevenson, 1994).

Humic substances are classified into three categories depending on the solubility in alkali or acid solutions: (i) fulvic acids (FA), which are soluble in water under all pH conditions. Fulvic acids remain in solution after removal of humic acid by acidification. Fulvic acids are light yellow to yellow-brown in color; (ii) humic acids (HA); which are not soluble in water under acidic conditions (pH < 2) but are soluble at higher pH values. They can be extracted from soil by reagents. They are dark brown to black in color. Humic acids are completely soluble only in strongly basic solution. Their solubility increase with increasing pH and decrease with increasing inert electrolyte concentration (Kipton et al., 1992); (iii) humin, which is not soluble in water at any pH value. Humins are black in color. There are not so much differences between humic acids, fulvic acids and humins. They are all part of a heterogeneous supramolecular system and the differences between the subdivisions are because of variations in chemical composition, acidity, size, molecular

weight, degree of hydrophobicity and self-associations of molecules. The chemical properties of humic substances are presented in Figure 2.1 (Stevenson, 1982).

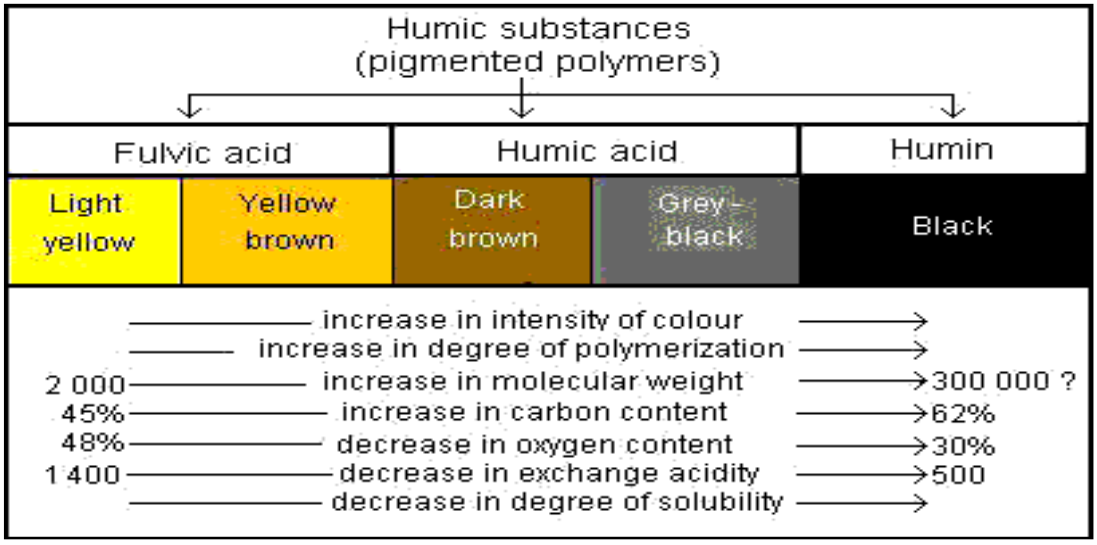

Figure 2.1. Chemical properties of humic substances (Stevenson, 1982).

Humic substances (HS) represent most of total organic carbon in global carbon cycle, forming the major organic fraction in soils (between 70% and 80%) and the largest fraction of natural organic matter in stream, river, wetland, lake, sea, and ground waters (Senesi and Loffredo, 1999). The removal of humic substances has become increasingly important in light of the potential to form carcinogenic disinfection by products (Hu et al., 2006).

2.1.1.1. Structure and Composition of Humic Substances. Humic substances vary in composition depending on their source, location and the method of extraction. The elemental composition ranges cover the three types of humic substances, the carbon content of a humic material could display a variation trend in the following series, FA < HA < Humin (van Loon and Duffy, 2000). Humic acids contain more hydrogen, carbon, nitrogen and sulfur than fulvic acids. The range of elemantal composition of humic substances is 40-60% carbon, 30-50% oxygen, 4-5% hydrogen, 1-4% nitrogen, 1-2% sulfur and 0- 0.3% phosphorus.

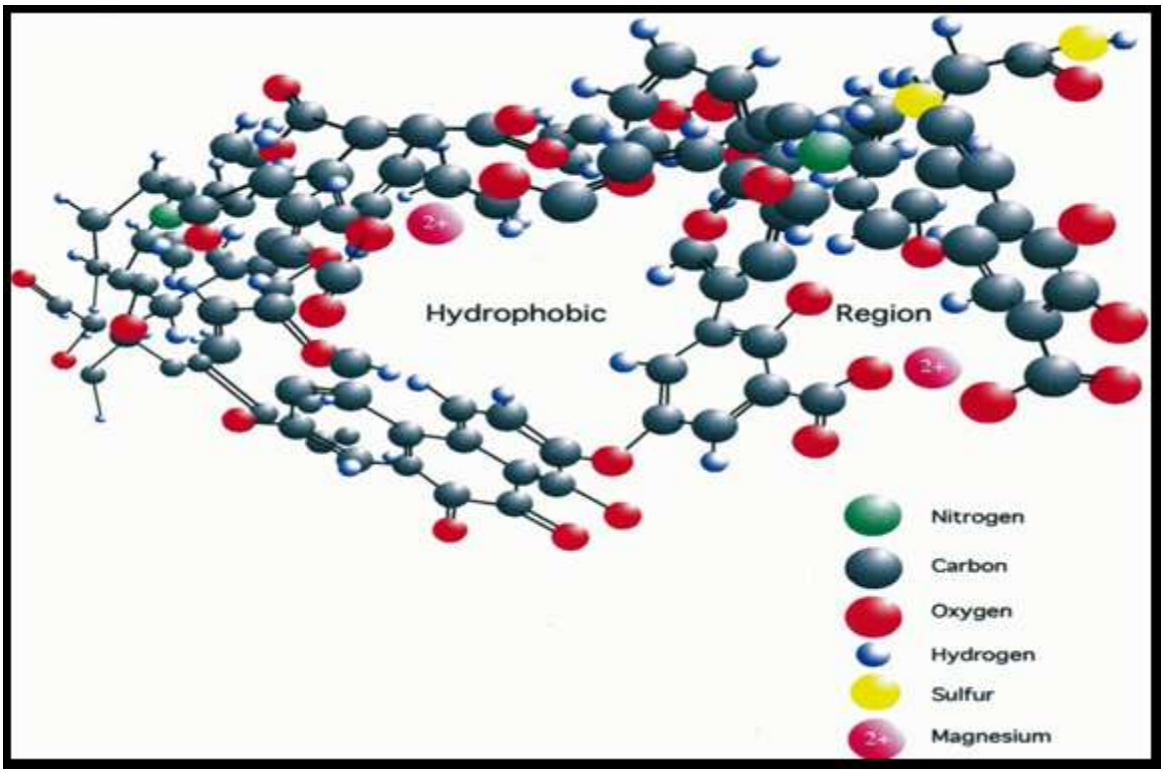

Figure 2.2. Portion of the structure of humic acid (Wandruszka, 2000).

Three general properties representing the major characteristics of humic substances could be explained by their polyfunctionality, macromolecular change and hydrophilicity. The structural diversity of humic acids could also be displayed by computer simulation studies (Figure 2.2).

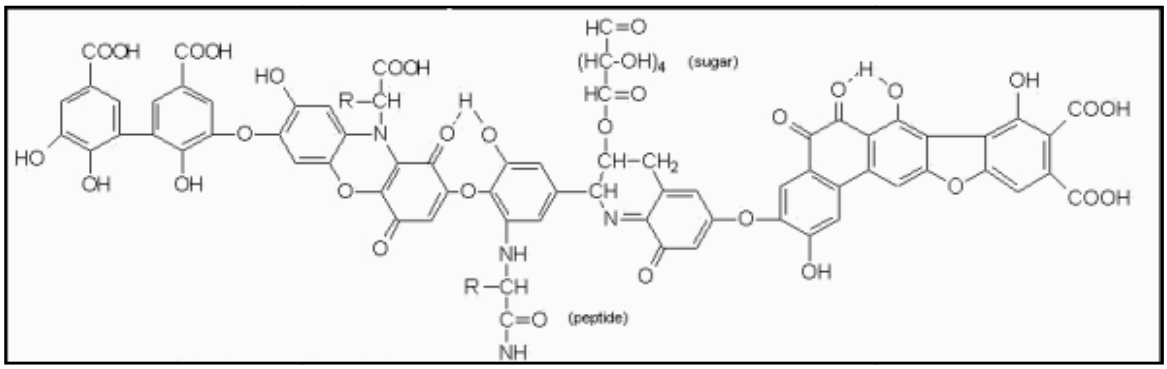

Figure 2.3. The model structure of humic acid (Stevenson, 1982).

Studies related to the structural analysis have shown that humic substances have both aromatic and aliphatic characteristics (Figure 2.3). The dominant functional groups which cause to surface charge and reactivity of humic substances are phenolic and carboxylic groups (Stevenson, 1994). Humic substances are complex aromatic macromolecules with aminoacids, aminosugars, peptides, aliphatic compounds includes linkages between the aromatic groups. The hypothetical structure for humic acid contains free and bound phenolic OH groups, quinone structures, nitrogen and oxygen as bridge units and COOH groups placed on aromatic rings. It contains carboxyl, amine, hydroxyl, and phenol groups (Brady, 1990).

2.1.1.2. Environmental Effects of Humic Substances. Humic substances have important physiological properties; many of these are connected to their sorptive properties. Chemical influences include physicochemical reactions of the compounds such as sorption, coagulation, acid-base interactions, complexation reactions and chemical changes such as oxidation, reduction, hydrolysis and photochemical reactions. Physical influences include processes that transport or disperse chemicals. Biological influences are uptake and depuration by organisms and food chain (Suffet and MacCarthy, 1989).

Humic substances in drinking water are removed because of many reasons. They give brown/yellow colour and undesirable taste to the water that is not aesthetically pleasing for domestic consumers. The colour is unsuitable for the paper, beverage and textile industries. It is also well known that humic substances upon chlorination form mutagenic halogenated compounds such as trihalomethanes (Aiken et al., 1985). The undesirable trihalomethanes formation may lead to the deterioration of human health (Rook, 1974; Singer, 1999). Humic acids are the most important sunlight absorbers in natural waters and they can photosynthesis the oxidation of certain aquatic pollutants and biologically important substances (Aiken et al., 1985).

2.1.1.3. Influences of Aquatic Humic Substances On Treatment Processes. Humic substances compete for adsorption sites with target compounds in coagulation treatments and activated carbon adsorption (Goel et al., 1995), cause plugging and fouling problems on membranes (Yoon et al., 1998; Kulovaara et al., 1999), form soluble complexes with many heavy metal ions and organo-pollutants (Suffet and MacCarthy, 1989), promote the

formation of bio-film in water distribution pipelines (Volk and LeChevallier, 2002), increase the bacteria regrowth potential in distribution system resulting in pipe corrosion (Camper, 2004) and most importantly they can also react with chlorine during water disinfection process to form disinfection byproducts such as trihalomethanes (THMs), haloacetic acids, and haloacetonitriles (Richardson, 1998).

Humic acids (HA) are among the most widely occurring natural products and are present in lakes and rivers as water-soluble compounds (Suffet and MacCarthy, 1989). Humic acids show colloidal behavior and interact with other chemical species in the natural environment. They can form complexes with metals and organic pollutants such as pesticides, insecticides and herbicides (Bennet and Drikas, 1993).

Many different treatment technologies such as enhanced coagulation, advanced oxidation methods (Kitis and Kaplan, 2007), adsorption (Peng et al., 2006; Uyguner et al., 2007), biofiltration (Melin and Odegaard, 1999; Sobecka et al., 2006), membrane processes (Petala and Zouboulis, 2006), and photocatalysis (Bekbolet et al., 1998; Selcuk et al., 2003; Murray and Parsons, 2004) were applied in order to remove humic acid from water. By using low-cost adsorbent for adsorption is one of the most efficient methods in humic acid removal. In the past years, different adsorbents have been used for humic acid adsorption including activated carbon, clays, zeolite and metal oxides. It is necessary to understand the behavior of HAs, in established and alternative processes, especially those inducing chemical changes in the humic structure.

Lots of different humic molecules in diverse physical associations are mixed together in natural environments. Hence, it is difficult to measure their exact concentrations and separate them to a certain class of bio-organic molecules. The concentrations of humic acid classes can be estimated out of concentrations of organic matter (typically from concentrations of total organic carbon (TOC) or dissolved organic carbon (DOC)). The presence of humic acid in water intended for potable or industrial use can have a significant effect on the treatability of that water and the success of chemical disinfection processes. The suitable methods of determining humic acid concentrations are essential in preserving water supplies, especially from upland peaty catchments in temperate climates.

Humic substances generally constitute 30–50% of the dissolved organic carbon (DOC) of natural DOM in surface waters (Thurman and Morgan, 1981). In surface waters, the humic content which is dissolved organic carbon (DOC) varies from 0.1 to 50 mg L^{-1} in dark-water swamps. In ocean waters, the DOC varies from 0.5 to 1.2 mg L^{-1} at the surface, and the DOC in samples from deep groundwaters is between 0.1 and 10 mg L^{-1}. About 10% of the DOC in surface waters is found in suspended matter, either as organic or organically coated inorganic particulates.

2.2. Trace Metals

Trace metals are the metals in small quantities, nearly at molecular level, that present in animal and plant cells and tissue. They may enter the water through corrosion products or simply by the dissolution of small amounts of metals with which the water comes in contact.

Trace metals may interact with other components which present in the natural system, such as dissolved low-molar-mass organic or inorganic ligands, high-molar-mass particulate organic or inorganic materials, and living organisms. Although they are a necessary part of nutrition; if they are taken high quantities, they can be toxic. Trace metals such as iron, copper, chromium, cadmium, lead, mercury, manganese and zinc are the major constituents of the aquatic systems. Atomic Absorption Spectrometer and Inductively Coupled Plasma Emission Spectroscopy (ICP) can be used to identify these metals. The natural concentration of metals in fresh water varies dependent on the metal concentration in the soil and the underlying geological structures, the acidity of the water, its humus content and particulate matter concentration. The toxicity of metals is dependent on their solubility, pH, different types of anions and cations.

Metal ions, especially form of metal salts, are dissolved in groundwater and surface water when the water contact with rock or soil that contains metals. Metals can also enter with discharges from sewage treatment plants, industrial plants, and other sources. The metals found in the highest concentrations in natural waters are calcium and magnesium. These are usually connected with the carbonate anion (CO_3^{2-}). Calcium and magnesium are non-toxic and absorbed by living organisms easier than the other metals. If the water is

hard, the toxicity of a toxic metal is reduced. On the other hand, in soft water, the same concentrations of metals may be more toxic (Kavcar et al., 2009). From the point of view of health; metals can be divided into two groups; metals with an undesired effect (Fe, Mn, Cu, Zn, Co, Ba, Ag) and metals giving a negative toxic effect (As, Cd, Cr, Hg, Ni, Pb, Sb, Se). Heavy metals have a tendency to accumulate in the body and the food chain, because of this reason they can give chronic damage in time (Apostoli et al., 2006).

2.2.1. Zinc

Zinc is an essential trace element in all biological systems studied and plays a fundamental role in the structure and function of numerous proteins, including metalloenzymes, transcription factors, and hormone receptors. After ingestion, zinc in humans is initially transported to the liver and distributed throughout the body, where it is found in all tissues, organs, and fluids. Zinc shortages can even cause birth defects. Zinc is naturally present in water. Zinc does not volatilize from water but is deposited primarily in sediments through adsorption and precipitation. It is found in the environment primarily in the +2 oxidation state. The primary anthropogenic sources of zinc in the environment (air, water, soil) are related to mining and metallurgic operations involving zinc and use of commercial products containing zinc. Waste streams from zinc and other metal manufacturing and zinc chemical industries, domestic waste water, and run-off from soil containing zinc can discharge zinc into waterways. Suspended (i.e. undissolved) zinc may be dissolved with changes in water conditions (e.g. pH, solution speciation) or may sorb on to suspended matter. It dissolves in acids to form hydrated Zn^{2+} cations and in strong bases to form zincate anions, which are hydroxo complexes, e.g. $[Zn(OH)_3]^-$ and $[Zn(OH)_4]^{2-}$ (Essington, 2004).

Environmental toxicity of zinc in water is dependent upon the concentration of other minerals and the pH of the solution, which affect the ligands that associate with zinc (Heijerick et al., 2002; Paquin et al., 2002; Santore et al., 2002). Zinc has a strong tendency to react with acidic, alkaline, and inorganic compounds. Zinc processing plants have attempted to limit releases to the environment by using techniques such as water reuse and control of particulate emissions. In addition, liquid effluents are limed and allowed to settle so that zinc can precipitate out as the hydroxide (Lloyd and Showak,

1984). Desorption of zinc from sediments occurs as salinity increases (Helz et al., 1975), apparently because of displacement of the adsorbed zinc ions by alkali and alkaline earth cations, which are abundant in brackish and saline waters.

Zinc in aerobic waters is partitioned into sediments through sorption onto hydrous iron and manganese oxides, clay minerals, and organic material. The efficiency of these materials in removing zinc from solution varies according to their concentrations, pH, redox potential, salinity, nature and concentrations of complexing ligands, cation exchange capacity, and the concentration of zinc. Precipitation of soluble zinc compounds appears to be significant only under reducing conditions in highly polluted water. Zinc can occur in both suspended and dissolved forms in surface water. Dissolved zinc may occur as the free (hydrated) zinc ion or as dissolved complexes and compounds with varying degrees of stability. The transport of zinc in the aquatic environment is controlled by anion species. In natural waters, complexing agents, such as humic acid, can bind zinc.

Zinc usually remains adsorbed to soil and does not volatilize from soil. Zinc accumulation in soil resulting from waste disposal occurred primarily as inorganic precipitates. The mobility of zinc in soil also depends on the solubility of the speciated forms of the element and on soil properties such as cation exchange capacity, pH, redox potential, and chemical species present in soil; under anaerobic conditions, zinc sulfide is the controlling species.

Zinc undergoes reactions in sediment and soil involving precipitation/dissolution, complexation/dissociation, and adsorption/desorption. In acidic sediments and soils, more zinc is available in ionic forms, and cation exchange processes influence its fate. Depending on the nature and concentrations of other mobile metals in sediments and soils, competition for the binding sites probably occurs. In the absence of suitable binding sites, zinc may be mobilized. In alkaline soils, the chemistry of zinc is dominated by interactions with organic ligands.

As an element, zinc does not degrade in the environment. Degradation of an element is a nuclear process by definition, and stable elements, such as zinc, typically undergo such processes only at insignificant rates in the environment. Zinc can change from one form to

another, sometimes reversibly, in numerous chemical reactions that can proceed under a wide range of common environmental conditions.

Elementary zinc does not react with water molecules. The stability of zinc complexes depends on the pH of the water and the nature of the complex. When the pH of the water decreases, the concentration of zinc ions in the water phase increases at the same rate as that of the release of zinc from the sediment. Solubility increases with increasing acidity. Above pH 11, solubility increases. At lower pH values, zinc remains as the free ion. The free ion (Zn^{2+}) tends to be adsorbed and transported by suspended solids in unpolluted waters. In polluted waters in which the concentration of zinc is high, removal of zinc by precipitation of the hydroxide is possible. Zinc can occur in both suspended and dissolved forms in surface water. Dissolved zinc may occur as the free (hydrated) zinc ion or as dissolved complexes and compounds with varying degrees of stability. In anaerobic environments and in the presence of sulfide ions, precipitation of zinc sulfide limits the mobility of zinc. The relative mobility of zinc in soil is determined by the same factors that affect its transport in aquatic systems (i.e. solubility of the compound, pH, and salinity) (Selim and Iskandar, 1999). Zinc dissolves in water as $ZnOH^{+}_{aq}$ or Zn^{2+}_{aq}. In the following reaction; the zinc ion form a protective, water insoluble zinc hydroxide ($Zn(OH)_2$) layer with dissolved hydroxide ions:

$$Zn^{2+} + 2OH^{-} \leftrightarrow Zn(OH)_2(s) \tag{2.1}$$

If zinc, Zn(s) reacts with H^{+} ions, hydrogen gas is released that could further react with oxygen;

$$Zn(s) + 2H^{+} \rightarrow Zn^{2+}(aq) + H_2(g) \tag{2.2}$$

The average zinc concentration in seawater is 0.6-5 µg L^{-1}. River waters contain 5-10 µg L^{-1} zinc. Algae contain 20-700 mg L^{-1}, sea fish and shells contain 3-25 mg L^{-1}, oysters contain 100-900 mg L^{-1} and lobsters contain 7-50 mg L^{-1}. The World Health Organization (WHO) stated a legal limit of 3 mg L^{-1} Zn^{2+} in drinking water. The limit set by EPA is 5 mg L^{-1} Zn^{2+}. When ISKI (İstanbul Su ve Kanalizasyon İdaresi) Water Quality Reports were checked, it was observed that the Zn concentration is less than 0.1 mg L^{-1} in finished

İstanbul drinking water. At concentrations of about 2 mg L^{-1} Zn^{2+}, zinc may give an unwanted flavour to water (İSKİ, 2010).

The binding of protons and metal ions by humic substances cause many environmental problems such as the transport and bioavailability of heavy metals, the impacts of acid rain on soils and the migration of radionuclides in groundwaters (Tipping, 1998). For these reasons, metal–HS complexation plays an important role in the environment, since heavy metals are continuously and increasingly released into the environment by numerous human activities (Baker, 2001; San Vicente de la Riva et al., 2002). The binding of metal ions by humic substances is one of the most important environmental qualities of humic substances. This binding can occur as chelation between a carboxyl group and a phenolic hydroxyl group, as chelation between two carboxyl groups, or as complexation with a carboxyl group (Figure 2.4).

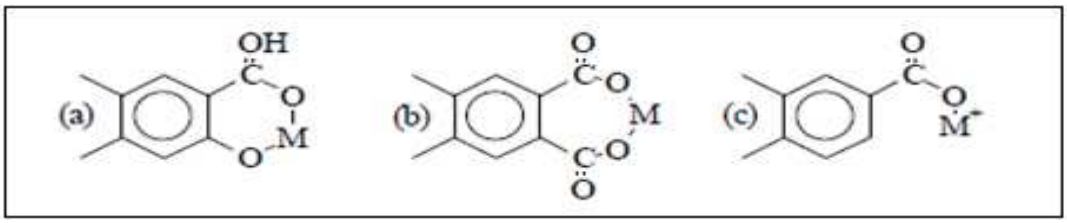

Figure 2.4. Binding of a metal ion, M^{2+}, by humic substances (a) by chelation between carboxyl and phenolic hydroxyl, (b) by chelation between two carboxyl groups, and (c) by complexation with a carboxyl group (Manahan, 2001).

Zinc-humic acid complexes may be 50% dissociated at pH 5.5 and the dissociation rate may be higher as the pH decreases (Guy and Chakrabarti, 1976). Therefore, as the pH of the water decreases, the concentration of zinc ions in the water phase increases at the same rate as that of the release of zinc from the sediment.

The presence of a strong metal-complexing ligand could further influence the effect of pH on the release of zinc. The zinc in the solution phase was determined by the interactions between concentration of the complexing ligand, the competing cation in the solution and the pH (Lombnæs et al, 2008).

2.3. Photocatalysis

Photocatalysis is a reaction which uses light to activate a substance which further modifies the rate of a chemical reaction without being involved itself. In chemistry, photocatalysis is the acceleration of a photoreaction in the presence of a catalyst. In catalysed photolysis, light is absorbed by an adsorbed substrate. In photogenerated catalysis the photocatalytic activity depends on the ability of the catalyst to create electron–hole pairs, which generate free radicals (hydroxyl ions; OH^-) able to undergo secondary reactions. Its comprehension has been made possible ever since the discovery of water electrolysis by means of the titanium dioxide (Figure 2.5).

The photocatalysis is based on the combined use of low energy UV-A light and semiconductor photocatalysts. The anatase form of TiO_2 is the preferred semiconductor photocatalysts, because it is inexpensive, non-photocorrosive, non-toxic, capable of photooxidative destruction of most organic pollutants, chemically and biologically inert and commercially available. Photoinduced reactivity of titanium dioxide has been extensively discussed by Carp and co-workers (Carp et al., 2004).

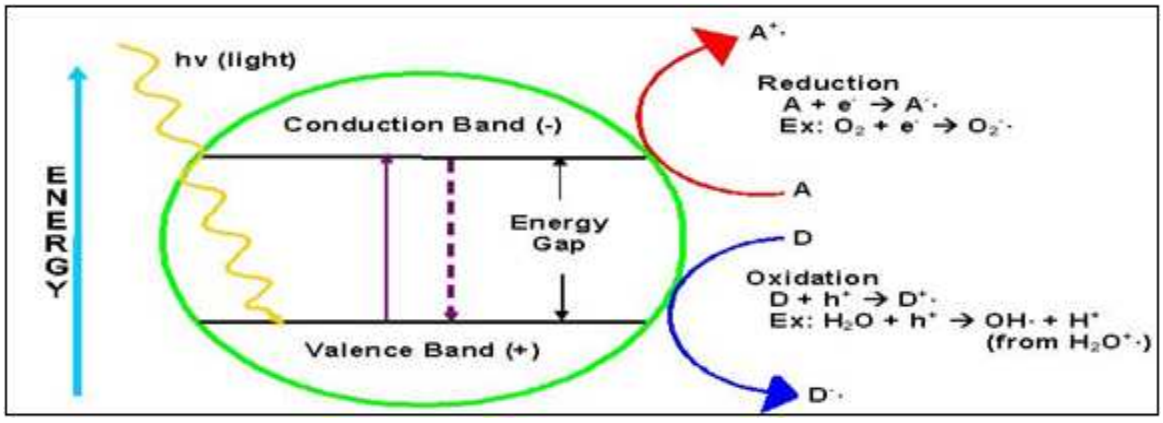

Figure 2.5. Simplified TiO_2 photocatalytic mechanism.

The most important feature of this process is the generation of the •OH radicals upon irradiation. The oxidation reactions of the adsorbed OH^- ions or H_2O molecules with the photogenerated holes yield HO• radicals which can degrade a great variety of organic compounds (Mills and Le Hunte, 1997; Pichat, 1997).

Photocatalysis over a semiconductor oxide such as TiO_2 is initiated by the absorption of a photon with energy equal to or greater than the band gap of the semiconductor (3.2 eV for TiO_2), producing electron-hole (e^-/h^+) pairs. Following irradiation, the TiO_2 particle can act as either an electron donor or acceptor for molecules in the surrounding media. However, the photoinduced charge separation in bare TiO_2 particles has a very short lifetime because of charge recombination. Therefore, it is important to prevent hole-electron recombination before a designated chemical reaction occurs on the TiO_2 surface. The formation of redox pair could be followed by respective reactions or a recombination reaction resulting in the dissipation of the reactive species (Equations 2.3-2.4).

(i) Formation of redox pair through light absorption ($E_{h\nu} \geq E_{bg}$):

$$TiO_2 + h\nu\ (UV) \rightarrow TiO_2\ (e^-_{CB} + h^+_{VB}) \quad (2.3)$$

(ii) Direct recombination reaction leading to the inactivation of the electron hole pair:

$$TiO_2\ (e^-_{CB} + h^+_{VB}) \rightarrow TiO_2 + \text{heat} \quad (2.4)$$

(iii) Photogenerated holes (h^+_{VB}) may directly oxidize the organic substrate, S anchored to the oxide surface. The principal hole traps are adsorbed H_2O molecules and OH^- forming $HO^\bullet$ radicals. The $HO^\bullet_{(s)}$ radicals adsorbed on the semiconductor surface are the prominent reactive species due to their high oxidant power (E= +2.80 V) and possible competing reaction leads to the formation of hydrogen peroxide.

$$h^+_{VB} + S \rightarrow S^{\bullet+} \quad (2.5)$$

$$h^+_{VB} + H_2O \rightarrow HO^\bullet + H^+ \quad (2.6)$$

$$h^+_{VB} + OH^- \rightarrow HO^\bullet \quad (2.7)$$

$$HO^\bullet + HO^\bullet \rightarrow H_2O_2 \quad (2.8)$$

(iv) On the other hand, in the presence of electron scavengers (i.e. O_2) reduction reactions may take place leading to the following sequence of the reactions:

$$e^-_{CB} + O_2 \rightarrow O_2^{\bullet -} \quad (2.9)$$

$$e^-_{CB} + H_2O_2 \rightarrow OH^- + HO^{\bullet} \quad (2.10)$$

$$O_2^{\bullet -} + H^+ \rightarrow HO_2^{\bullet} \quad (2.11)$$

$$O_2^{\bullet -} + HO_2^{\bullet} \rightarrow HO_2^- + O_2 \quad (2.12)$$

$$HO_2^{\bullet} + HO_2^{\bullet} \rightarrow O_2 + H_2O_2 \quad (2.13)$$

$$H_2O_2 \leftrightarrow HO_2^- + H^+ \qquad pK_a=11.6 \quad (2.14)$$

$$HO^{\bullet} + HO_2^{\bullet} \rightarrow H_2O + O_2 \quad (2.15)$$

Heterogeneous photocatalytic process takes place through a complex sequence of reactions. The relevant reactions at the TiO_2 surface causing the degradation of the organic compounds could be outlined by equations (2.3)-(2.15). Hydroxyl radicals are created from water when UV light is absorbed by the titanium dioxide layer. The energy causes electrons to move to the conduction band of the TiO_2. The positive holes remaining in the valance band can accept electrons from molecules. A •OOH radical is formed from the reduction of the dissolved oxygen in the aqueous solution combining with a hydroxyl radical.

Photocatalytic oxidation is used for breaking down organics into simpler components of water and CO_2, destroying organic pollutants, bacteria and viruses, detoxifying drinking water, purifying air streams and removing metals from waste streams. TiO_2 can be used in photocatalytic reactors for degrading contaminants in liquid and gas streams.

Adsorption plays a prominent role in catalytic photodegradation of organic molecules. Photodegradation of humic substance molecules occurs soon after adsorption of the molecules almost reaches equilibrium. Photocatalysis takes place at the surface; the concentration of substrate adsorbed to the surface directly influences the overall rate of adsorption.

The presence of dissolved metal ions can induce various effects on the rate and efficiency of photocatalytic reactions. The effect is strongly dependent on the type and concentration of the metal ion resulting in either an increase in the photocatalytic rate or in an inhibitory effect (Litter, 1999). Photocatalytic removal of humic acids is influenced by the presence of metal ions (Karabacakoğlu, 1998; Uyguner, 1999).

2.4. Adsorption

Adsorption is a process that occurs when a gas or liquid solute accumulates on the surface of a solid or a liquid (adsorbent), forming a molecular or atomic film (the adsorbate). Adsorption can be classified as physical adsorption, chemical adsorption, and exchange adsorption. In the physical adsorption, there are weak forces of attraction or Van der Waals' forces between molecules and it is reversible. In the chemical adsorption, adsorbed molecules form a layer on the surface. There are much stronger forces between the molecules, so it is rarely reversible. Exchange adsorption refers to electrical attraction between the molecules due to opposite charge on the surface. Adsorption is operative in most natural physical, biological, and chemical systems, and is used in industrial applications such as activated charcoal, synthetic resins and water purification. Decolorization can be efficient by adsorption and with negligible loss of other materials (Weber, 1972).

The most common industrial adsorbents are activated carbon, silica gel, and alumina, because they present large surface areas per unit weight. Adsorption is related with surface area of adsorbent, pore size distribution and the characteristics of the adsorbed molecules. There are other factors that affect the adsorption such as pH and temperature. Generally, adsorption increases at pH ranges where the species have not any charge. Many organics form negative ions at high pH, positive ions at low pH, and neutral species in intermediate pH ranges. Moreover, pH affects the charge on the surface, altering its ability to adsorb materials. Many organic pollutants in water are highly adsorbed by decreasing pH because of neutralization of negative charges at the carbon surface with increasing hydrogen concentration.

When temperature is increased the adsorption extent decreases because adsorption reactions are exothermic. The total amount of heat evolved in the adsorption of a definite quantity of solute on an adsorbent is termed the heat of adsorption, ΔH which is the change in the heat content of the system when adsorption occurs. Since temperature effects on adsorption are important, measurements are usually carried out at a constant temperature therefore graphs of the data are called isotherm.

2.4.1. Adsorption Isotherms

In the process of adsorption, adsorbate gets adsorbed on adsorbent.

$$\text{Adsorbate} + \text{Adsorbent} \rightleftarrows \text{Adsorption} \tag{2.16}$$

$$A + B \rightleftarrows AB \tag{2.17}$$

According to Le-Chatelier principle, the direction of equilibrium would shift in the direction where the stress can be relieved. In case of application of excess of pressure to the equilibrium system, the equilibrium will shift in the direction where the number of molecules decreases. Since number of molecules decreases in forward direction, with the increases in pressure, forward direction of equilibrium will be favored.

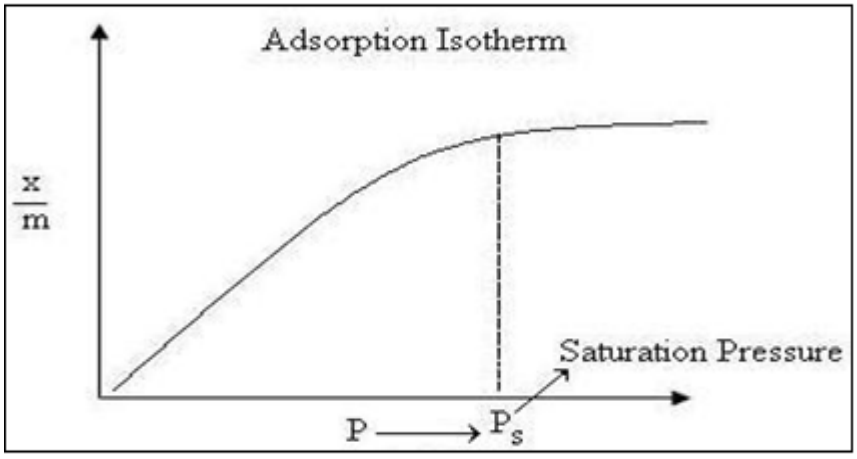

Figure 2.6. Basic adsorption isotherm.

Figure 2.6 is the graph between the amounts of adsorbate (x) adsorbed on the surface of adsorbent (m) and pressure at constant temperature. From the Figure 2.6, it can be seen that after saturation pressure P_s, adsorption does not occur anymore. It can be explained by the reason that there are limited numbers of vacancies on the surface of the adsorbent. At high pressure, when all the sites are occupied, a stage is reached and further increase in pressure does not cause any difference in adsorption process.

Adsorption isotherms for solutes in dilute solution can be classified to according to initial slope. Different solutes show different behavior on the adsorbent (Weber, 1972), so their adsorption isotherms can be termed according to their shapes resembling the letters, such as “S” type, “L” type, “H” type, “C” type (Giles et al., 1960). The four main classes are shown in Figure 2.7.

The S-curve isotherm is characterized by an initially small slope that increases with adsorptive concentration. This shows that at low concentration the affinity of the soil solid phases for the adsorbate is less than that of the soil solution for the adsorptive. When the metal concentration exceeds the complexing capacity of these ligands, adsorption on the solid soil particles increases and the isotherm takes on its characteristic S-shape. The S-curve isotherm occurs also as a result of interactions among adsorbed organic molecules that cause the adsorbate to become stabilized on the solid surface and cause to enhanced affinity of the surface for the adsorbate with increasing amounts adsorbed.

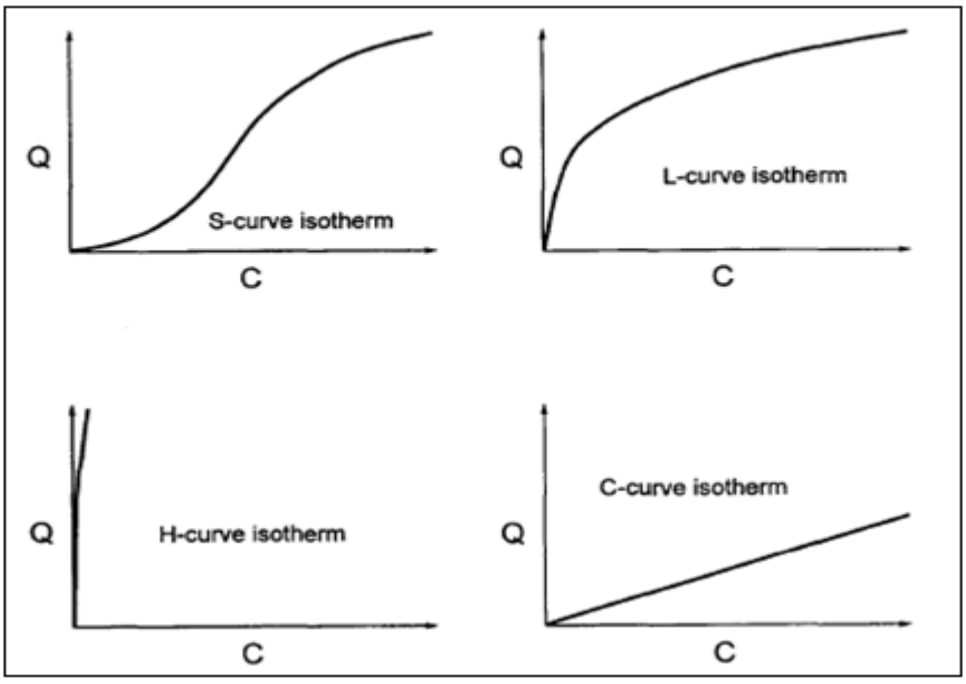

Figure 2.7. The four general categories of adsoption isotherm (Sposito, 1989).

The L-curve isotherm, which typically is concave to the concentration axis, shows an initial slope that does not increase with adsorptive concentration. This is the result of high

affinity of the soil solid phases for the adsorbate at low surface coverage combined with a decreasing amount of adsorbing surface with progressing adsorption. While the concentration of the adsorbate increases, the amount of the remaining adsorbing surface is decreased.

The H-curve isotherm, that large initial slope indicates very high affinity of the soil solid phases for the adsorbate, which is caused by specific interactions between the solid phases and the adsorbate or by significant van der Waals interactions in the adsorption process.

The C-curve isotherm shows an initial slope that remains independent of adsorptive concentration until the maximum possible adsorption. This type of isotherm is produced by a constant partitioning of a substance between the interfacial region and the soil solution or by an increase in the amount of adsorbing surface as the amount adsorbed increases.

2.4.1.1. Freundlich Isotherm. Freundlich isotherm is a non-linear adsorption equilibrium model that describes the adsorption occurrences on heterogenous surfaces composed of different adsorption sites. The corresponding formula is:

$$q_A = K_f C_e^{1/n} \qquad (2.18)$$

Where ;

q_A = Amount of solute adsorbed per unit weight of solid adsorbent, mg adsorbate/g adsorbent

C_e = Concentration of the solute remaining in the solution at equilibrium, mgL^{-1}

K_f = Constant which relates to adsorption capacity

1/n = Constant which relates to adsorption intensity.

The equation does not imply any particular mechanism of adsorption. It is purely empirical, and has been found to be most satisfactory in the low concentration range (vanLoon and Duffy, 2000) and it is very useful because it accurately describes much adsorption data.

2.4.1.2. Langmuir Isotherm. It is based on the assumptions that the sorption for each molecule is independent of surface coverage and same; in addition sorption occurs only on localised sites and involves no interactions between sorbed molecules. This model is predicated on the assumptions that the energy of sorption for each molecule is the same and independent of surface coverage and that sorption occurs only on localized sites and involves no interactions between sorbed molecules. Equilibrium is reached when the rate of adsorption of molecules onto the surface is the same as the rate of desorption of molecules from the surface. The corresponding formula is:

$$\frac{1}{q_A} = \frac{1}{q_{max}} + \frac{1}{K\ q_{max}\ C_e} \qquad (2.19)$$

q_A = Amount of solute adsorbed per unit weight of solid adsorbent, mg adsorbate/g adsorbent

C_e = Concentration of the solute remaining in the solution at equilibrium, mgL^{-1}

K = Binding constant

q_{max} = Maximum quantity adsorbable when all adsorption sites are occupied.

The Langmuir adsorption isotherm was for single layer adsorption and gives a curve that describes the fraction of the surface area of the adsorbent covered with solute, as a function of the concentration of the solute in the contacting liquid phase. The Langmuir isotherm is a curve, convex to the solute concentration axis, and flattens out when the total surface is covered with solute. The isotherm for double layer adsorption is similar to single layer adsorption but the initial convex part of the curve is sharper. The adsorption isotherm only tends to linearity at very low concentrations of solute (at very low surface coverage) and so symmetrical peaks will only be achieved with very small samples.

Although the Freundlich equation is basically empirical, it generally agrees quite well with the Langmuir equation at very high concentrations, since *n* must reach some limit when the surface is fully covered.

2.4.1.3. BET Isotherm. The BET (Brunauer, Emmet, Teller) model assumes that a number of layers of adsorbate molecules form at the surface. Further assumption of the BET model is that a given layer need not complete formation prior to initiation of subsequent layers.

2.5. Summary of the Previous Studies Performed for the Assessment of Photocatalytic Treatment and Adsorptive Interactions of Humic Acids

In recent years, many studies were focused on the destructive removal of humic acids in natural waters since these substances are known to be major precurcors of carcinogenic disinfection by-products that produced during chlorination. Bekbolet and co-workers have been studying about photocatalytic degradation and adsorption of humic substances since 1996.

2.5.1. Photocatalytic Treatment Studies

Bekbolet and co-workers (1996) studied the effect of TiO_2 photocatalyzed oxidation on the degradation and decolorization of humic acid. Adsorptive behavior of humic acid was studied followed by TiO_2 photocatalytic oxidation of humic acid. After the photocatalytic oxidation of humic acid, a decrease in organic compounds and decolorization and an increase in biodegradability were observed. A slight decrease of adsorptivity was also observed after irradiation.

Bekbolet and Balcıoglu (1996) investigated the influence of hydrogen peroxide and bicarbonate ion on the photocatalytic degradation of humic acid. Bekbolet and Balcıoglu reported that in the presence of $1x\ 10^{-2}$ M H_2O_2, which was the optimum amount, reaction rate for TOC and color removal of 50 mg L^{-1} humic acid were increased by 1.6-1.8 times.

Bekbolet and Ozkosemen (1996) reported the destructive removal of humic acid in aqueous medium by photocatalytic degradation process. The effects of the photocatalyst concentration, pH and humic acid concentration were investigated during photocatalytic degradation of humic acid. The optimum TiO_2 concentration was found as 1.0 mg mL^{-1}. It was also found that acidic medium was more favorable for experiments because of positively charged surface characteristic of TiO_2. It was concluded that photocatalytic

oxidation of humic acid by using TiO_2 could be effective pretreatment method to keep the trihalomethane levels below the limit of 100 μgL^{-1}.

Bekbolet and co-workers (2002) investigated the photocatalytic degradation efficiencies of the two commercial titania samples, Degussa P-25 and Hombikat UV-100, in aqueous solution by using humic acid. The photocatalytic degradation efficiencies and adsorption capacities for Degussa P-25 were found to be higher than for Hombikat UV-100. It was concluded that there was certain dependency between the adsorption characteristics and the photocatalytic decolorization rates but no dependency onto the surface area of TiO_2 powders.

Uyguner and Bekbolet (2005a) studied on the spectral changes of humic acids during oxidation processes and the effects of the molecular size distribution of photocatalytically treated humic acid samples. It was found that the degradation of the higher molecular size fractions of humic acid to lower molecular weight compounds leads to decreasing in the TOC value for raw humic acid comparing with the corresponding treated humic acid fractions. It is also observed that the fluorescence spectra of all the fractions of treated humic acid have lower wavelengths than raw humic acid fractions.

Uyguner and Bekbolet (2005b) studied the photocatalytic removal of model humic and fulvic acids of different origins by using TiO_2 Degussa P-25 as the photocatalyst. It was reported that there were substantial differences in photocatalytic removal efficiencies of humic and fulvic acids on the basis of their diverse chemical and physical properties such as molecular weight, molecular size, elemental composition and source of origin.

Uyguner and Bekbolet (2007) examined the impact of aqueous Cr (VI) and Mn (II) species on the photocatalytic oxidation of humic acids as a major component of natural organic matter in aquatic systems. The experiment results were evaluated in terms of Langmuir-Hinshelwood rate with respect to $Color_{436}$ because of the pseudo-first-order rate constant explains the overall removal tendency covering all competitive and consecutive reactions. The presence of these ions affected the adsorptive properties of the photocatalyst and the photocatalytic oxidation rate of humic acids. The impact of manganese ion on the photocatalytic oxidation could be better explained in terms of L-H kinetics where 15%

increase was observed with respect to $Color_{436}$ while 54% decrease observed in the presence of chromium.

Selcuk and Bekbolet (2008) studied the photocatalytic and photoelectrocatalytic treatment methods for removing humic acid under different experimental conditions. Photoelectrocatalytic system was performed for humic acid oxidation in the presence of chloride anion and humic acid to observe the selectivity of photoelectrocatalytic system. To investigate the inhibitory effect of carbonate species, the system was performed in the presence and absence of carbonate species. It was reported that the attraction of humic acid to the surface of TiO_2 was stronger than that of chloride ions and carbonate ions retarded HA degradation at basic condition.

Uyguner and Bekbolet (2010) investigated the removal efficiency of aqueous humic acid solutions by TiO_2 photocatalytic degradation in the presence of Cu (II) species. The photocatalytic oxidation studies of the molecular size fractions of humic acid were also performed. The photocatalytic removal of humic acid decreased when the system contained both humic acid and Cu (II) compared to humic acid alone. Both in the presence and absence of copper ions the removal rate constants of the size fractions displayed an increasing trend as Raw < 0.45µm filtered fraction, 100 kDa, 30 kDa. Batch equilibrium adsorption experiments were also evaluated for probable binary and ternary systems. Even though the presence of Cu (II) species significantly altered the isotherm shape irrespective of the spectral parameters, no significant difference was attained for TOC. K_f values displayed an inconsistent effect of Cu (II) species, while adsorption intensity factor 1/n, 1 denoted a prevailing favorable type of adsorption for UV_{254} and $Color_{436}$. TOC adsorption profile showed a rather linear-type adsorption as expressed by $1/n < 1$ both in the absence and presence of Cu (II) species.

2.5.2. Adsorption Studies

Uyguner and Bekbolet (2004) investigated the effect of the chromium ion concentration on the adsorption of humic acid onto TiO_2. The adsorption of chromium ions on TiO_2 in the absence of humic acid has also been studied and no direct relationship could be assessed between K_f values and increasing chromium ion concentration. $Color_{436}$ and

UV_{254} are used as parameters to evaluate the adsorption effects of humic acid and chromium ions on the oxide surface. It was found that the presence of chromium inhibit the adsorption capacity of humic acid onto TiO_2.

Uyguner and colleagues (2007) investigated the adsorption and coagulation characteristics of humic acid samples that following to ozonation, photocatalysis and sequential oxidation systems. The structural properties of humic acid significantly changed after the applied oxidation systems that supported by the low values of $Color_{436}$, UV_{254}, TOC and decrease of fluorescence intensities. Uyguner et al. (2007) used two types of activated carbons in adsorption experiments (PAC and GAC) and aluminum sulfate and ferric chloride in coagulation experiments. It was found that $Color_{436}$ removal efficiencies for untreated, photocatalytically oxidized, ozonated, and sequentially oxidized humic acids increased for PAC, respectively. $Color_{436}$ removal efficiencies for untreated, sequentially oxidized, photocatalytically oxidized, and ozonated humic acids increased for GAC, respectively. On the other hand, UV_{254} removal efficiencies for untreated, photocatalytically oxidized, ozonated, and sequentially oxidized humic acids decreased for PAC, respectively. UV_{254} removal efficiencies for untreated, ozonated, sequentially oxidized, and photocatalytically oxidized humic acids decreased for GAC, respectively. The adsorption capacities at $Color_{436}$ are higher than at UV centers after treatment. Amongst all treatment methods, ozonation shows the least removal efficiency for both coagulants. Between the two coagulants, alum coagulation was favored for each treatment step with removal efficiencies no less than 91%.

Ulker (2008) studied the effect of molecular size fractionation on the sorption properties of humic acid onto metal ion doped TiO_2 (Fe), and TiO_2 modified with an organic substance (ascorbic acid) samples in comparison to TiO_2 Degussa P-25. It was aimed to investigate the complex interactions between the surface properties of titanium dioxide and the molecular size dependent fractions of the humic acid in order to provide information in relation to the photocatalytic degradation of humic acids with surface modified TiO_2 powders. The adsorption profiles of the selected UV-vis parameters of humic acid and its molecular size fractions onto bare TiO_2 displayed various characteristics that were followed by fluorescence properties. The adsorption profiles of the $Color_{436}$ and UV_{254} of humic acid and its molecular size fractions and Fe doped TiO_2

exhibited distinct differences with respect to the conditions of the humic acid and bare TiO_2 system. The use of ascorbic acid modified TiO_2 expressed comparatively different adsorption patterns respect to bare TiO_2 as well as the Fe doped TiO_2. Molecular size fractions of humic acid displayed higher K_f values and lower 1/n values. The observed differences in adsorption behavior of raw humic acid as well as the molecular size fractions could be explained by the probable diversity of the attraction sites on both of the organic moieties.

3. MATERIALS AND METHODS

3.1. Materials

3.1.1. Humic Acid

Humic acid was supplied from Aldrich (Aldrich Co. Ltd., USA). Stock humic acid (1000 mg L^{-1}) solution was prepared by dissolving 1 g humic acid in 1000 mL distilled deionized water. In this step, the ultrasonic sonication bath is used to provide complete dissolution of humic acid. Stock humic solution was stored in a dark glass container and was protected from light to prevent light induced degradation. 20 mg L^{-1} solutions, which were used during experiments, were prepared from the stock solution by using distilled deionized water. Humic acid samples were filtered from 0.45 µm Millipore cellulose acetate membrane filters. After filtration with 0.45 µm filters, all humic acid samples were fractionated using ultrafiltration stirred cells into appropriate molecular fractions such as 100 kDa and 30 kDa.

3.1.2. Titanium Dioxide Powder

Semiconducter metal oxide, TiO_2 powders was provided from Degussa (P25 grade). TiO_2 P-25 had a BET surface area of 50 ± 15 m^2 g^{-1} and average particle size of 20-30 nm. TiO_2 P-25 powders were mainly anastase in crystal form (70% anatase and 30% rutile). Homogeneous slurry of TiO_2 was obtained by sonicating the solution for 3 minutes.

3.1.3. Zinc

Stock zinc solution (1000 mg L^{-1}) was prepared from Zinc (Fluka) Atomic Spectroscopy Standard Solution according to the Standard Methods using distilled deionized water (APHA, AWWA, WPCF, 1999). 0.1 mg L^{-1} concentrations of zinc solutions were prepared from 1000 mg L^{-1} stock zinc solution before experiments. The required concentrations of zinc ions were added from prepared stock solutions directly to the humic acid solutions

3.1.4. Laboratory Equipments

3.1.4.1. Specific Instruments. Molecular size fractionation of humic acid and specified measurements for humic acid samples such as UV-vis spectroscopic measurements, fluorescence spectroscopic measurements and TOC (Total Organic Carbon) measurements were done by using following instruments:

Perkin Elmer Lamda 35 UV-vis Double Beam Spectrophotometer was used to record the UV- visible absorption spectra employing Hellma quartz cuvettes of 1.0 cm optical path length. Perkin Elmer LS 55 Luminescence Spectrophotometer was used to measure the fluorescence spectra in emission and synchronous scan modes employing Perkin Elmer quartz cuvettes of 1.0 cm optical path length. Shimadzu TOC-V WP Total Organic Carbon Analyzer was used for analyzing TOC. Amicon Model 8050 Ultrafiltration Stirred Cell System was used for molecular size fractionation of humic solutions.

3.1.4.2. General Laboratory Instruments and Materials. The other general laboratory applications and measurements were done by using the following instruments:

Memmert Water Bath Shaker Model WB/OB 7-45, Hettich EBA 20 Centrifuge, Ultra Sonic Waterbath LC30, IKA-Labortechnik Magnetic Stirrer, Memmert Oven, Scaltec SBA 31 Balance, Sterile Millex-HA Millipore Filter and several types of glassware.

3.2. Methods

3.2.1. Photocatalytic Degradation

3.2.1.1. Experimental Set-Up. During experiments, the used light source was 125 W Black Light Fluorescent Lamp (BLF) which had an output spectrum ranging between 320-440 nm. The lamp exhibited a maximum emission at 365 nm and no emission below 300 nm and above 500 nm. The intensity of incident light, measured using ferrioxalate actinometery (Hatchard and Parker, 1956) was 2.854×10^{16} quanta s^{-1}. The lamp was built into a lamp housing which provides a location of 10 cm above the surface of the solution. The experimental set up was prepared as detailed in previous literature (Bekbolet et al.,

2002). A cylindrical pyrex reaction wessel with a diameter of 7.5 cm and a height of 3.5 cm was used as the photoreactor. The volume of reaction mixtures was 50 mL. During experiments, continuous stirring was provided by a magnetic stirrer. The photoreactor was enclosed by a mirror casing and the whole system was placed in a box. The inner walls of the box were covered with Al-foil.

3.2.1.2. Experimental Procedure. All experiments were conducted under neutral pH conditions (pH≈6.7). The photocatalytic degradation of humic acid solution was performed in the absence and presence of zinc ions. In order to assess the direct interaction of light with humic acid reactions were carried out in the absence of photocatalyst. Dark reactions were also carried out to evaluate the probable initial adsorption of humic acid onto TiO_2. Also, the preliminary reactions were performed in the absence of photocatalyst.

For each set of experiments, 20 mg L^{-1} humic acid solution was prepared by dilution from the Aldrich humic acid stock solution. (In some of these experiments, the required amounts of zinc were added to humic acid solutions). 50 mL of 20 mg L^{-1} humic acid was added directly to reaction vessel onto weighted 0.1 mg mL^{-1} TiO_2. First of all, the prepared slurry was sonicated for three minutes to provide a homogenous mixture. Than, it was placed on a magnetic stirrer to be irradiated for certain reaction periods. The distance between the BLF lamp and the solution surface was 10 cm. After these steps, the mixture was poured into 50 mL volumetric flask and filled with distilled deionized upto 50 mL limit to compensate the volume loss due to the evaporation of water observed especially at longer irradiation periods. Prior to analysis, TiO_2 was removed from the suspension by filtering through 0.45 µm filters. The clear humic acid samples were analysed by means of UV-vis spectra and fluorescence spectra as well as by the specified UV-vis and fluorescence parameters. All of the experiments were carried out both in the presence and absence of zinc.

3.2.2. Adsorption

3.2.2.1. Experimental Procedure. Adsorption experiments were conducted to determine the effects of molecular size dependent fractions of humic acid solution on TiO_2 surfaces. 100 mL Erlenmeyer flasks were used for experiments. Each flask was filled with 50 mL humic acid solution. Increased amounts of TiO_2 were added into each Erlenmeyer flask in the range of 0.1 mg mL^{-1} to 1.0 mg mL^{-1}. One extra flask was filled with only raw humic acid solution to compare with other sets. Each sample was sonicated for evenly distribution of TiO_2 in the slurry. The samples were immersed in the water-bath at room temperature which is equipped with shaking device. The flasks were kept shaking for 24 hours. After this time period, the samples were centrifuged for 10 minutes at 5000 cycles min^{-1}. The supernatant was filtered by the 0.45µm Millipore syringe filter.

The effect of metal ions (Zn) on the adsorption was studied in the presence of zinc ions at different molecular fractions such as 0.45 µm filtered fraction, 100 kDa fraction and 30 kDa fraction of humic acid. The clear humic acid samples were evaluated by specified UV-vis parameters, fluorescence parameters and DOC.

3.2.3. Molecular Size Fractionation with Ultrafiltration

Humic acid solutions were fractionated using a 50 mL Amicon Model 8050 ultrafiltration stirred cells into appropriate molecular sizes; 100 kDa and 30kDa. Following filtration through 0.45 µm filters, humic acid samples were fractionated into different molecular size fraction such as 100 kDa and 30 kDa by using ultrafiltarion stirred cell system and Millipore YM series cellulose membranes. The cell was run on a magnetic stirrer with 50 mL samples. A nitrogen gas tube equipped with a pressure control valve was attached to the stirrer reactor to provide the operating pressure inside the cell (Figures 3.1-3.2).

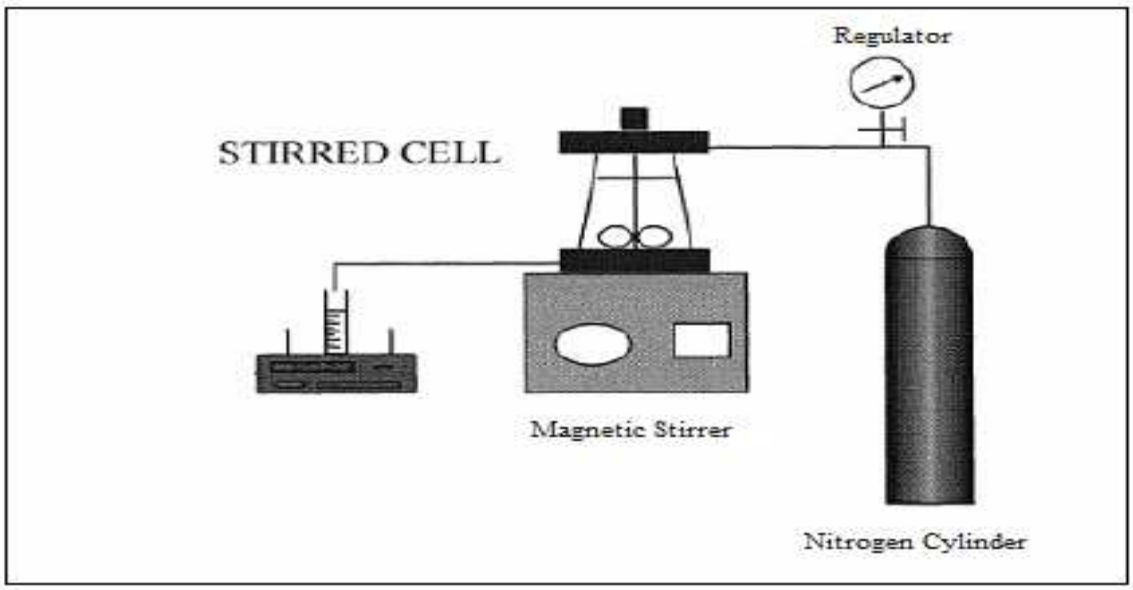

Figure 3.1. Schematic diagram of stirred cell system.

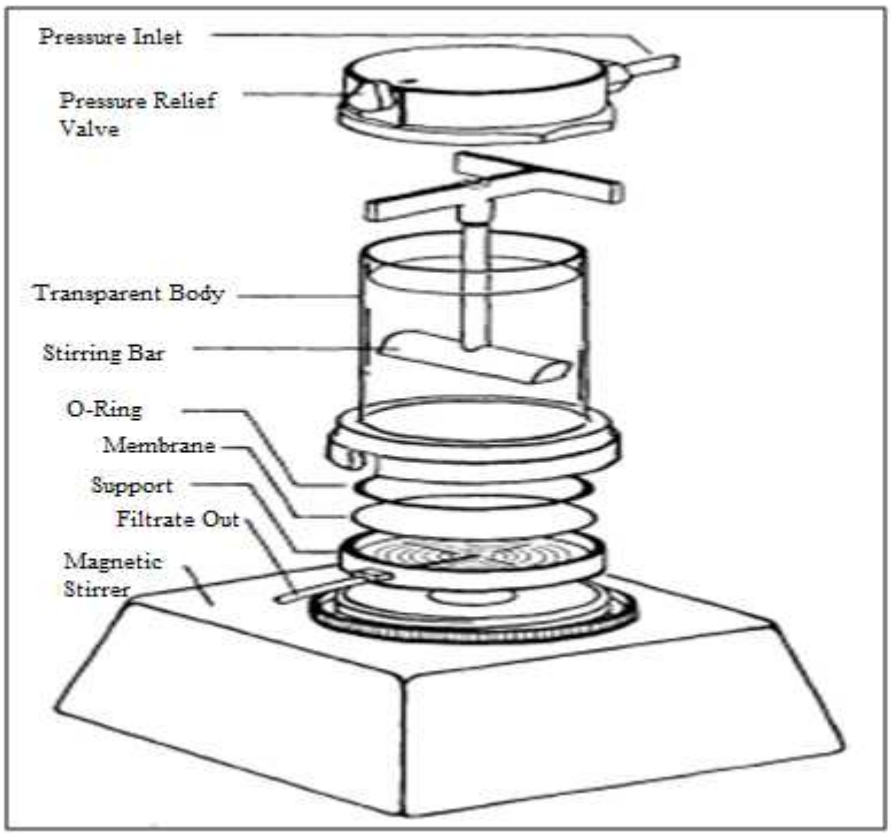

Figure 3.2. The parts of Amicon 8050 stirred ultrafiltration cells.

Millipore YM series cellulose membrane filters with 25 mm diameter and with nominal molecular weight cutoffs 100 kDa and 30 kDa were used within stirred cell. At the beginning of each run, the membranes were kept in distilled deionized water for 15 minutes and then the cell was operated on a magnetic stirrer and run with 50 mL distilled deionized water. After use prior to storage YM membranes were washed with 0.1 M NaOH solution and stored in 10% ethanol/water solution at refrigerator. Fractionated humic acid solutions were stored in dark glass bottles at cold rooms.

3.2.4. Analytical Methods

3.2.4.1. Total Organic Carbon (TOC) Analysis. Total organic carbon (TOC, mg L^{-1}) measurements of humic substances were performed on a Shimadzu TOC Vwp Total Organic Carbon Analyser. TOC is determined as total organic matter in water. Dissolved organic carbon (DOC) is the organic carbon remaining in a sample after filtering the sample typically using 0.45 µm filters.

3.2.4.2. UV-vis Spectroscopic Measurements. UV-vis absorption spectra were recorded on a Perkin Elmer Lamda 35 UV-vis double beam spectrophotometer employing Hellma quartz cuvettes of 1.0 cm optical path length. Humic acid samples were characterized by UV/vis spectra. The UV-vis absorbance values were recorded for specified UV-vis parameters such as $Color_{436}$, UV_{365}, UV_{280} and UV_{254}.The specified parameters are explained as follows;

$Color_{436}$: Color forming moieties, absorbance at 436 nm, m^{-1}
UV_{365} : Organic matter content, absorbance at 365 nm, m^{-1}
UV_{280} : Organic matter content, absorbance at 280 nm, m^{-1}
UV_{254} : Organic matter content, absorbance at 254 nm, m^{-1}.

3.2.4.3. Fluorescence Spectroscopic Measurements. Fluorescence spectra in the emission and synchronous scan modes were recorded on a Perkin Elmer LS 55 Luminescence Spectrometer equipped with a 150W Xenon arc lamp and a red sensitive photomultiplier tube. 1-cm path length quartz cells were used. The method of measuring fluorescence is that the cuvette holder excites the sample over the entire path length and reads the emitted

light at right angles. Both the excitation and the emission slits of the instrument were 10 nm. A scan speed of 400 nm min^{-1} was used with a slit width opening of 10 nm. Opening the slit wider allows more light energy from the xenon light source to excite the molecules in the sample. The emission spectra were scanned over the range of 380-550 nm at a constant excitation wavelength of 360 nm. Synchronous scan spectra were recorded in the excitation wavelength range of 200-600 nm excitation wavelength range using the bandwidth of $\Delta\lambda$ = 18 nm between the excitation and emission monochromators (Senesi, 1990).

4. RESULTS AND DISCUSSIONS

In this study, photocatalytic degradation and adsorption experiments were carried out to investigate the complex interactions between the surface properties of titanium dioxide and the molecular size dependent fractions of the humic acid. In order to assess the effects of zinc on these experiments, the reactions were also conducted in the presence of this ion. The role of the metal ion complexation as expressed by the "binary system effect" on the photocatalytic degradation efficiency of humic acids with respect to molecular size fractions will be deduced.

Photocatalytic degradation experiments were conducted with different molecular size fractions such as 0.45 µm filtered fraction, 100 kDa fraction and 30 kDa fraction of Aldrich humic acid solution. The humic acid fractions were photocatalytically degraded in the presence of 0.1 mg mL^{-1} TiO_2 Degussa P-25 for certain reaction periods up to 120 minutes. The experiments were carried out at neutral pH conditions. The preliminary experiments were also performed; i. in the presence of light and absence of TiO_2 and ii. under dark conditions in the presence of catalyst. In the absence of light, the catalyst doses were chosen as 0.25 mg mL^{-1} TiO_2 Degussa P-25 in the absence of zinc and 0.1 mg mL^{-1} TiO_2 Degussa P-25 in the presence of 2.5 mg L^{-1} zinc.

Complementary adsorption experiments were performed with raw humic acid and different molecular size fractions, such as 0.45 µm filtered fraction, 100 kDa fraction and 30 kDa fraction of humic acid solution. The TiO_2 loadings changed in the range of 0.1-1.0 mg $mL^{-1}$and zinc concentration was kept constant in all experiments as 0.1 mg L^{-1}.

4.1. Material Specification

Humic acid molecular size fractions were prepared according to the methods outlined in Materials and Methods section. Following filtration through 0.45 µm filters, humic acid samples were fractionated into different molecular size fraction such as 100 kDa and 30 kDa.

4.1.1. Spectroscopic Analysis of Humic Acid and Its Molecular Size Fractions

The characterization of the humic acid and its molecular size fractions i.e. 0.45 µm filtered fraction, 100 kDa fraction and 30 kDa fractions were assessed with respect to their UV-vis spectroscopic and fluorescence spectroscopic properties. Fluorescence spectra were recorded both in emission and synchronous scan modes. DOC contents were also determined.

4.1.1.1. UV-vis Spectroscopic Properties of Humic Acid and Its Molecular Size Fractions.

The UV-vis absorbance values were measured between 200-600 nm wavelength region. For the humic acid solutions, absorbance values of samples were recorded at 436 nm, 365 nm, 280 nm and 254 nm wavelengths for specified parameters of $Color_{436}$, UV_{365}, UV_{280} and UV_{254}. The absorbance values of humic acid were decreased with increasing wavelentgh.

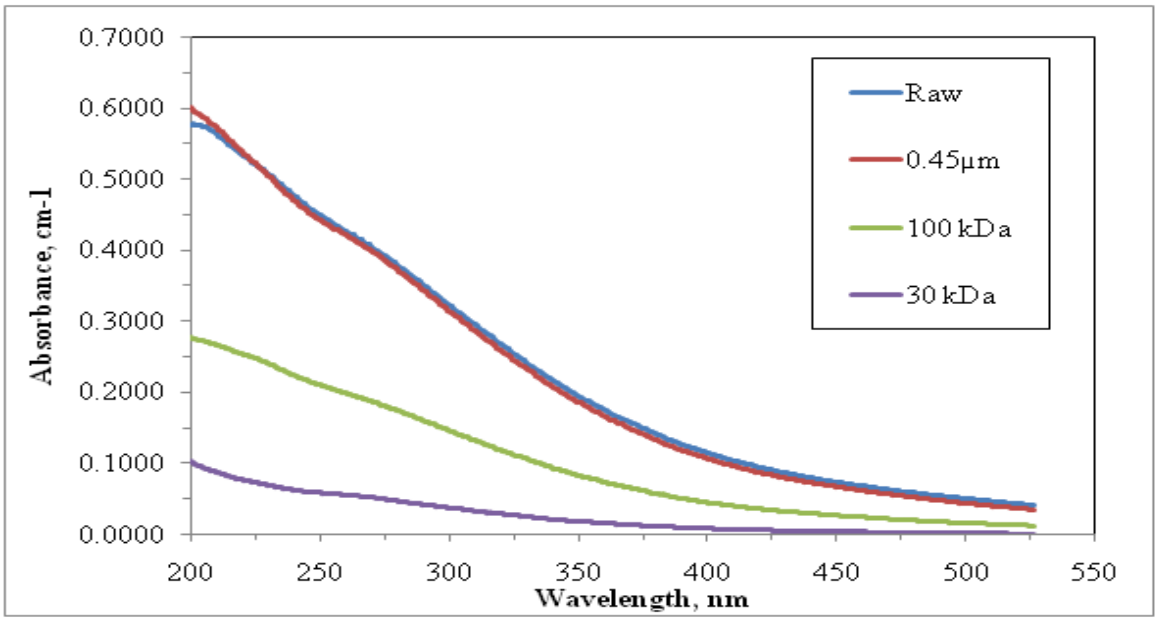

Figure 4.1. UV-vis spectra of raw, 0.45µm filtered fraction, 100 kDa fraction and 30 kDa fraction of humic acid.

In the Figure 4.1, it could be also easily observed that the absorbance values showed a gradually decreasing trend with decreasing molecular size fraction. As expected,

absorbance values of the raw and 0.45µm filtered fraction of humic acid were very close to each other. The absorbance values of 30 kDa fraction of humic acid recorded to be significantly lower than other molecular size fractions at all wavelengths as shown in Figure 4.1. 30 kDa fraction of humic acid exhibited very low absorbance values causing to difficulties while recording absorbance values. UV-vis absorbance values of different fractions of humic acids as represented by the indicated parameters followed an order as Raw > 0.45µm filtered fraction > 100 kDa > 30 kDa. As an indicator of organic carbon content, UV_{254} was found to be 0.440 cm^{-1} for raw humic acid, 0.4337 cm^{-1} for 0.45 µm filtered fraction, 0.2052 cm^{-1} for 100 kDa fraction and 0.0567 cm^{-1} for 30 kDa fraction.

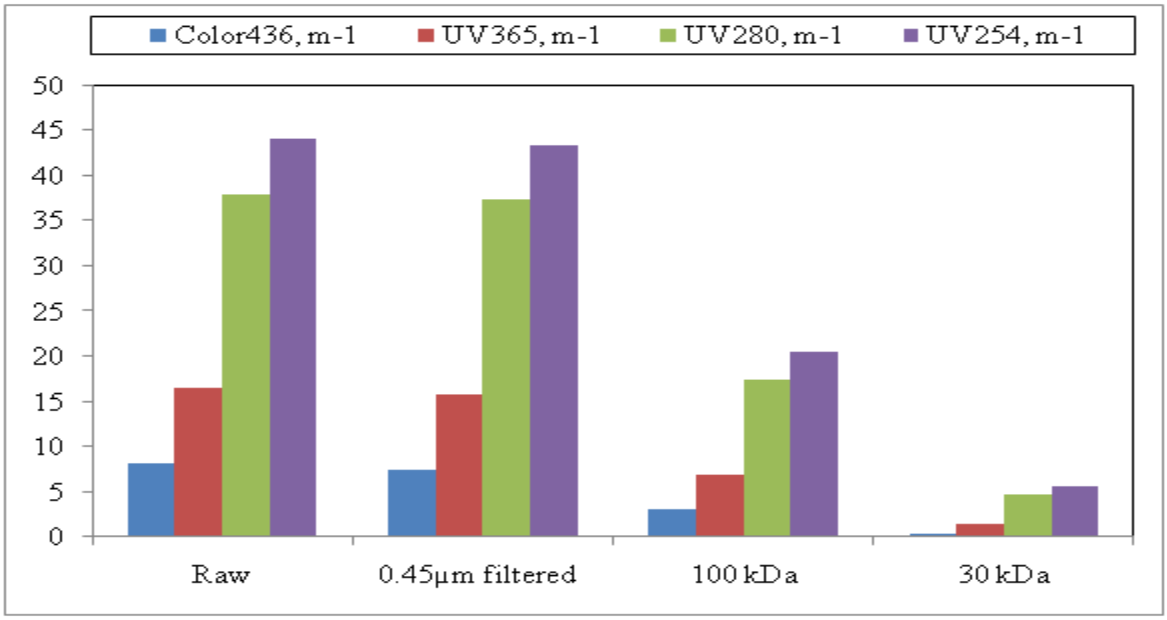

Figure 4.2. Comparative presentation of the specified UV-vis parameters of raw, 0.45µm filtered fraction, 100 kDa fraction and 30 kDa fraction of humic acid.

Since humic acid was supposed to pass through 0.45µm fitler, raw and 0.45µm filtered fraction of humic acid displayed nearly the same absorbance values as illustrated in Figure 4.2. On the other hand, the absorbance values of 100 kDa fraction of humic acid was less than the half of the raw humic acids' absorbance values for specified parameters of $Color_{436}$, UV_{365}, UV_{280} and UV_{254}. Moreover 30 kDa fraction of humic displayed significantly lower organic content as expressed by the specified UV-vis parameters.

It was reported that while UV-vis absorbance values displayed a decreasing order, the contents of carbon, hydrogen, nitrogen and sulfur should also decrease with decreasing molecular weight of the fraction. On the other hand, the oxygen contents should increase. Carboxylic and phenolic carbon contents of the humic acid molecular size fractions tended to increase with decreasing molecular weight (Christl and Kretzschmar, 2001).

4.1.1.2. Fluorescence Spectroscopic Properties of Humic Acid and Its Molecular Size Fractions. Emission scan fluorescence spectra of raw, 0.45µm filtered fraction, 100 kDa fraction and 30 kDa fraction of humic acid were displayed in Figure 4.3. The emission scan spectra were scanned in the range of 380-560 nm at a constant excitation wavelength of 360 nm.

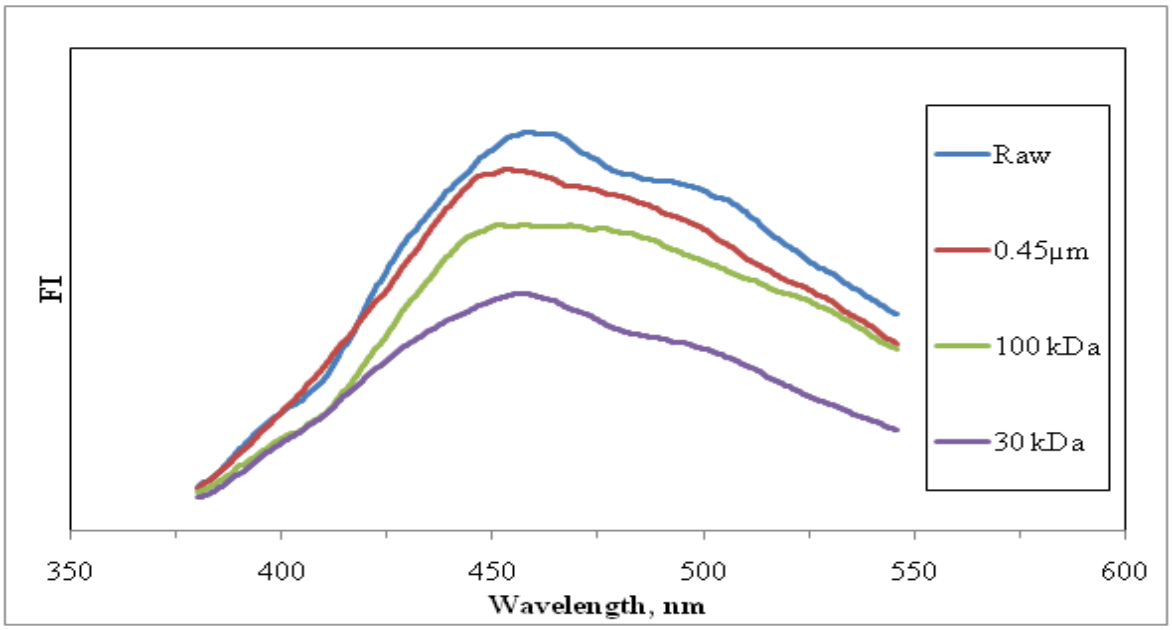

Figure 4.3. Emission scan fluorescence spectra of raw, 0.45µm filtered fraction, 100 kDa fraction and 30 kDa fraction of humic acid.

In Figure 4.3, the emission scan spectra gave decreasing emission fluorescence intensity with decreasing molecular size fractions. There was a characteristic peak at ~ 450 nm wavelength for raw, 0.45µm filtered fraction, 100 kDa fraction and 30 kDa fraction of humic acid. Upto about 425 nm wavelength, the trend of raw humic acid and 0.45 µm filtered fraction of humic acid were overlapping. After 425 nm wavelength, raw humic

acid gave higher fluorescence intensities than 0.45 µm filtered fraction of humic acid with little changes. On the other hand, trend of 100 kDa fraction and 30 kDa fraction of humic acid were crossed over in the region of 380-410 nm wavelength. After this wavelength region, 30 kDa fraction of humic acid gave the lowest fluorescence intensities in spectra.

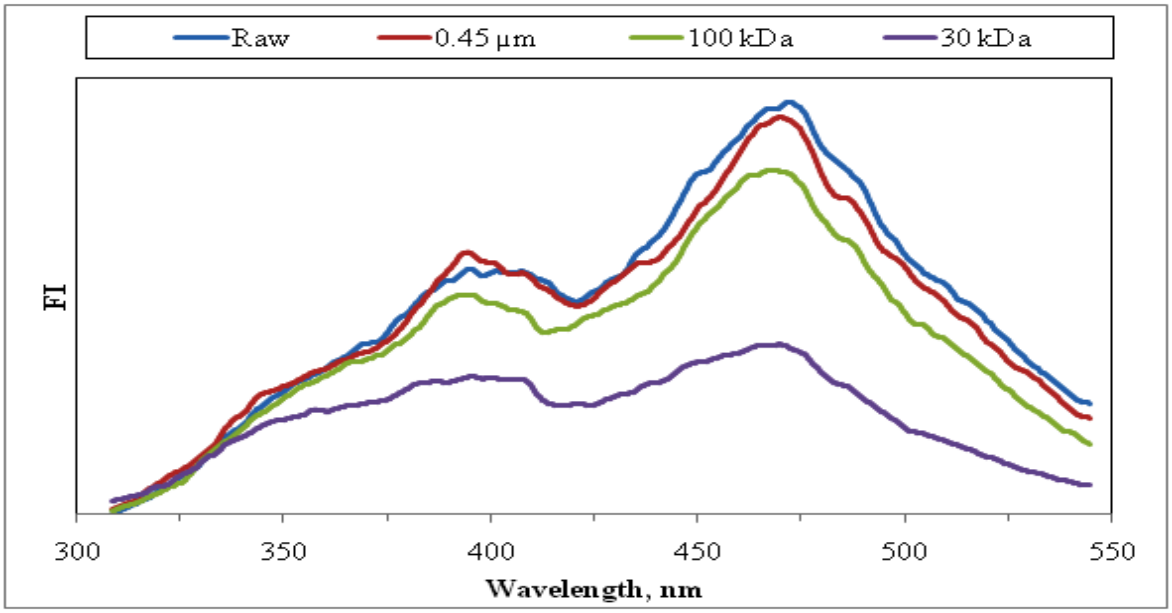

Figure 4.4. Synchronous scan fluorescence spectra of raw, 0.45µm filtered fraction, 100 kDa fraction and 30 kDa fraction of humic acid.

Synchronous spectra was recorded in the range of 200-600 nm excitation wavelength by using the bandwidth of $\Delta\lambda$ =18 nm between the excitation and emission monochromators. On the other hand, the synchronous spectra was presented in the range of 300-550 nm wavelength because of very low absorbance values at the region that was lower than 300 nm wavelength. In Figure 4.4, the synchronorous scan fluorescence spectra gave decreasing fluorescence intensities with respect to decreasing molecular size fraction. Two main peaks were observed at 400 and 470 nm wavelengths. While raw, 0.45 µm filtered fraction and 100 kDa fraction of humic acid had similar fluorescence intensities with small changes, 30 kDa fraction of humic acid had very low fluorescence intensities. Also, for 30 kDa fraction of humic acid, the peak at ~ 400 nm wavelength was found to be nearly indistinguishable.

4.1.1.3. Specific Parameters of Humic Acid. All of the specific parameters as UV-vis spectral parameters ($Color_{436}$, UV_{365}, UV_{280} and UV_{254}), fluorescence spectral parameters (FI_{emiss} and FI_{syn}), dissolved organic carbon (DOC) and derived parameters ($ScoA_{436}$, $SUVA_{365}$, $SUVA_{280}$, $SUVA_{254}$**,** SFIemiss and SFI_{syn}) for raw, 0.45 µm filtered fraction, 100 kDa fraction and 30 kDa fraction of humic acid were presented in Table 4.1.The highest fluorescence intensities were recorded at 460 nm and 470 nm wavelengths therefore the fluorescence spectral parameters (FI_{emiss} and FI_{syn}) recorded at these wavelengths were chosen for emission scan and synchronous scan fluorescence intensity indicators respectively.

Specific UV absorbance ($SUVA_{254}$, m^{-1} $mg^{-1}L$) was used to present DOC normalized aromatic moieties (UV_{254}) whereas specific color absorbance ($SCoA_{436}$, m^{-1} $mg^{-1}L$) was defined as $Color_{436}$/DOC to signify organic carbon normalized color forming moieties. $SUVA_{365}$ was also calculated in a similar fashion as the ratio of the UV_{365} absorbing species to DOC. SFI_{emiss} was calculated as the ratio of the FI_{emiss} values to DOC. SFI_{syn} could be explained as DOC normalized FI_{syn}.

The order of $Color_{436}$ was shown as; Raw > 0.45 µm filtered fraction > 100 kDa fraction > 30 kDa fraction as expected. The same order was also observed for other UV-vis spectral parameters, such as; UV_{365}, UV_{280} and UV_{254}. As seen in Table 4.1, the order for fluorescence intensities and the DOC values of humic acids could also be presented as; Raw > 0.45 µm filtered fraction > 100 kDa > 30 kDa

While the $SCoA_{436}$, $SUVA_{365}$, $SUVA_{280}$ and $SUVA_{254}$ values for raw, 0.45µm filtered fraction and 100 kDa humic acid were nearly equal each other with low changes, values for 30 kDa fraction of humic acid was observed to be ≤ 50% of other fractions of humic acid for $SCoA_{436}$, $SUVA_{365}$, $SUVA_{280}$ and $SUVA_{254}$. SUVA values greater than 4 reflect the presence of highly hydrophobic fractions. For SUVA ratios in the range of 2 – 4, humic acids were normally dominated with mixture hydrophobic and hydrophilic fractions. SUVA < 2 significantly represented hydrophilic properties (Edzwald et al., 1985). The calculated $SUVA_{365}$ and $SCoA_{436}$ parameters for both raw and treated humic acid samples showed a generally decreasing trend directly proportional to the size fractions (Uyguner and Bekbolet, 2005a).

Table 4.1. Specific parameters of raw, 0.45µm filtered fraction, 100 kDa fraction and 30 kDa fraction of humic acid.

Humic Acid	Raw	0.45µm	100kDa	30kDa
UV-vis spectral parameters				
$Color_{436}$, m^{-1}	8.19	7.51	3.01	0.41
UV_{365}, m^{-1}	16.56	15.77	6.92	1.40
UV_{280}, m^{-1}	37.85	37.25	17.40	4.66
UV_{254}, m^{-1}	44.00	43.37	20.52	5.67
Fluorescence spectral parameters				
FI_{emis}	115.7	104.9	88.7	68.9
FI_{syn}	32.8	31.3	27.5	13.5
Dissolved organic carbon				
DOC, mg L^{-1}	6.750	6.469	3.104	1.608
Derived parameters: $SCoA_{436}$, $SUVA_{365}$, $SUVA_{280}$, $SUVA_{254}$ (m^{-1} mg^{-1} L) SFI_{emiss}, SFI_{syn} (cm^{-1} mg^{-1} L)				
$SCoA_{436}$	1.213	1.161	0.970	0.255
$SUVA_{365}$	2.453	2.438	2.229	0.871
$SUVA_{280}$	5.607	5.758	5.606	2.898
$SUVA_{254}$	6.519	6.704	6.611	3.526
SFI_{emis}	17.14	16.22	28.58	42.85
SFI_{syn}	4.859	4.838	8.860	8.396

For SFI_{emis} parameters, the order was 30 kDa fraction > 100 kDa fraction> Raw > 0.45 µm filtered fraction. For SFI_{syn}, the order was changed as 100 kDa fraction> 30 kDa fraction > Raw ≥ 0.45 µm filtered fraction. The differences could be attributed to the possible conformational changes attained during ultrafiltration process leading to the formation and dissappearance of the fluorophoric groups (Kulovaara et al, 1999).

4.2. Photocatalytic Degradation of Humic Acid

Prior to the photocatalytic degradation experiments using raw, 0.45µm filtered fraction, 100 kDa fraction and 30 kDa fraction of humic acids in the presence and the absence of zinc, the preliminary experiments were carried out.

4.2.1. Preliminary Experiments

Preliminary experiments were carried out under dark conditions as well as in the absence of the photocatalyst. The preliminary studies were performed also in the presence of zinc ion to observe the effects of humic acid and zinc ions as a binary system.

4.2.1.1. Experiments Carried Out Under Dark Conditions. To observe the effect of light in photocatalytic degradation of humic acids and the plusable adsorptive interactions, the experiments were carried out under dark conditions. The dark experiments were performed in the presence of 0.25 mg mL^{-1} TiO_2 dose with raw humic acid.

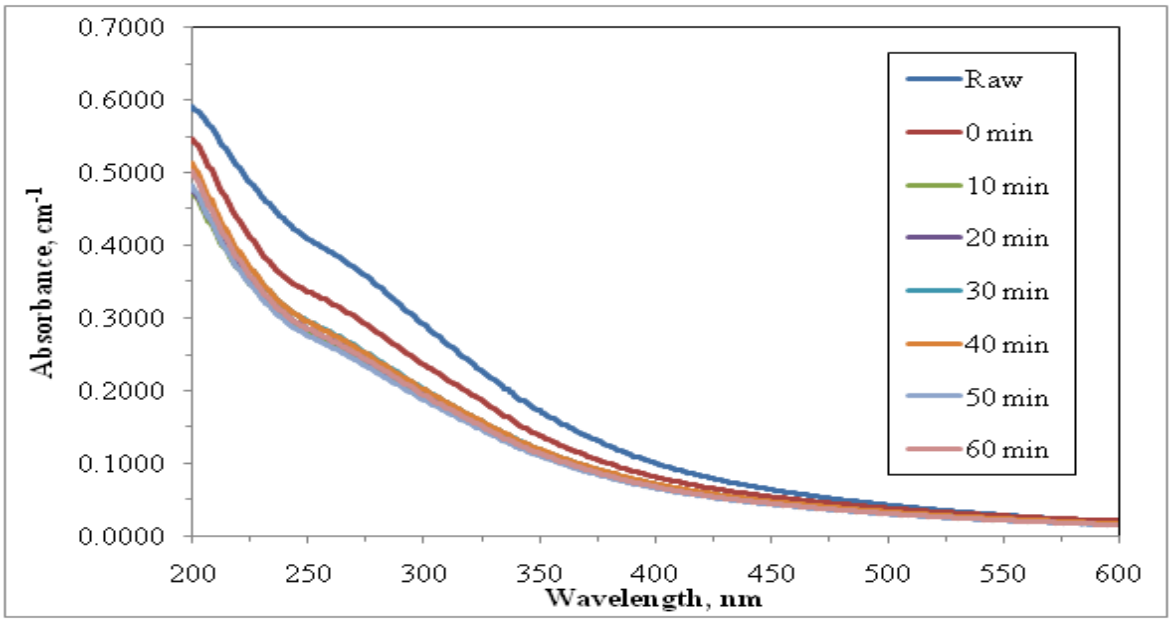

Figure 4.5. UV-vis spectra of raw humic acid during preliminary experiments conducted under dark conditions in the presence of 0.25 mg mL^{-1} TiO_2.

For UV-vis spectroscopic evaluation of raw humic acid during preliminary experiments in the absence of light, UV-vis absorbance values were recorded in the 200-600 nm wavelength region. As seen in Figure 4.5, the UV-vis spectra of humic acids monotonously decreased with increasing wavelength in a broad and featureless trend. As expected, no significant change was observed with increasing time. Dark experiments were also carried out in the presence of 0.1 mg mL^{-1} TiO_2 and 2.5 mg L^{-1} zinc. The UV-vis absorbance spectra were recorded in the region of 200-600 nm wavelength (Figure 4.6).

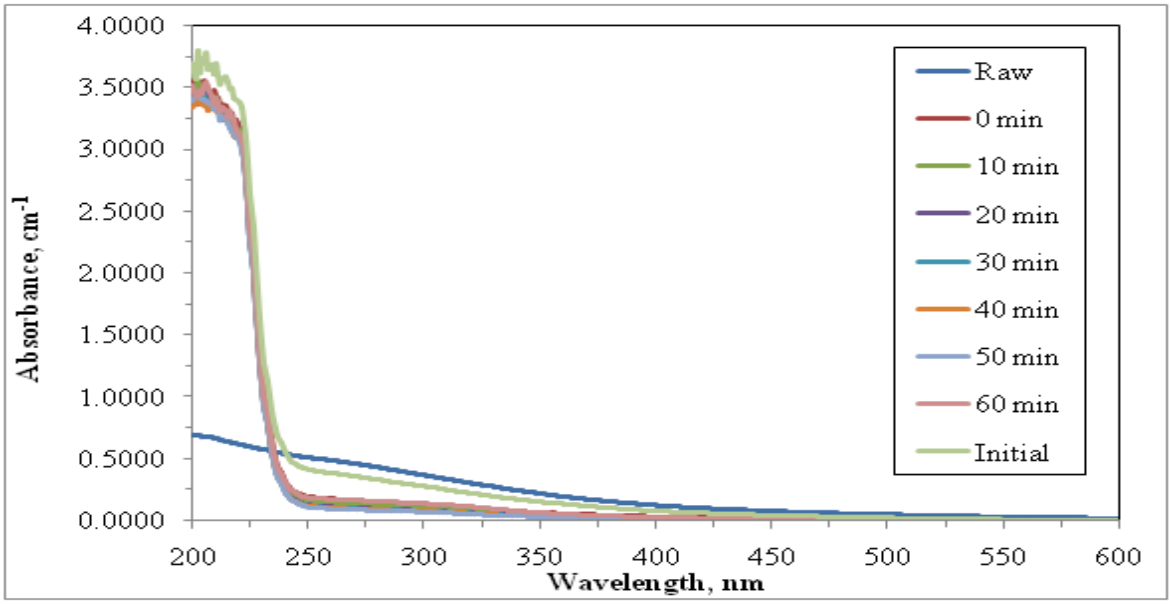

Figure 4.6. UV-vis spectra of raw humic acid during preliminary experiments conducted under dark conditions in the presence of 0.1 mg mL^{-1} TiO_2 and 2.5 mg L^{-1} Zn (Initial represents raw humic acid and zinc binary system).

As seen in Figure 4.6, significant increases in UV-vis absorbance values of the samples were observed in the spectral region of 200-235 nm. After ~240 nm wavelength, the UV-vis spectra of raw humic acid and zinc binary system followed the similar trend of raw humic acid with lower absorbance values. The data obtained from dark reactions of humic acid for $Color_{436}$ and UV_{254} were given in Figure 4.7. Raw humic acid and 0.25 mg mL^{-1} TiO_2 interaction resulted in an initial adsorptive removal of 53% and 48% for $Color_{436}$ and UV_{254}, respectively. The same trend was observed throughout the experimental periods.

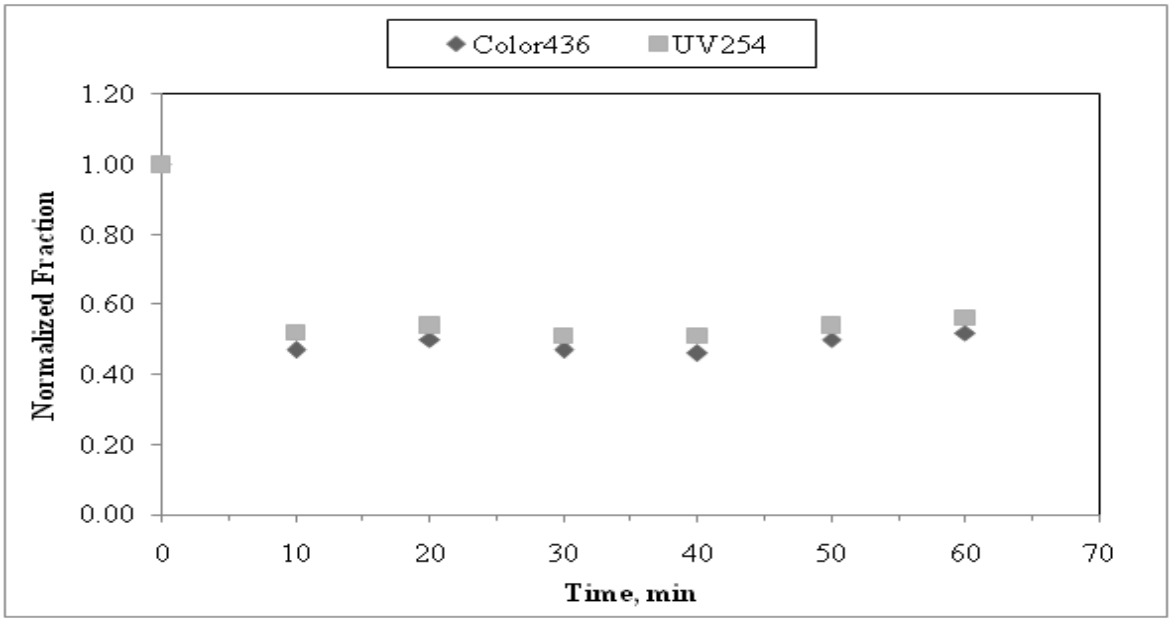

Figure 4.7. Normalized $Color_{436}$ and UV_{254} values of raw humic acid with respect to time in the presence of 0.25 mg mL^{-1} TiO_2.

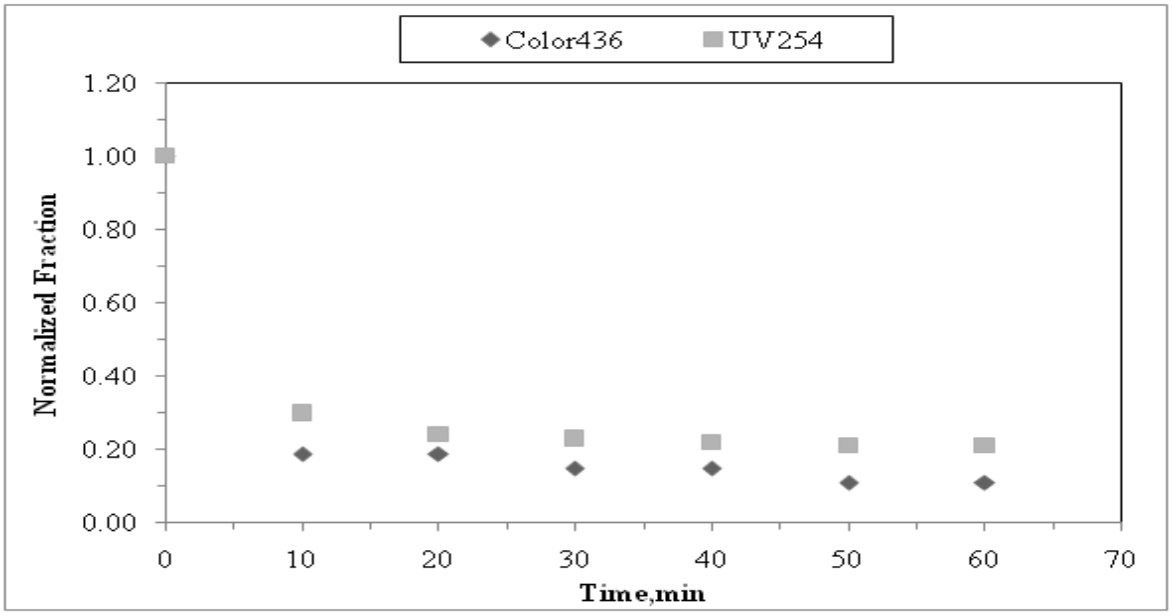

Figure 4.8. Normalized $Color_{436}$ and UV_{254} values of raw humic acid with respect to time in the presence of 0.1 mg mL^{-1} TiO_2 and 2.5 mg L^{-1} Zn.

The removal percentages for $Color_{436}$ and UV_{254} were obtained from dark reactions of humic acid in the presence of 0.1 mg mL^{-1} TiO_2 and 2.5 mg L^{-1} Zn were resulted with 81% and 70%, respectively (Figure 4.8). Although lower TiO_2 dose was utilized, significantly higher adsorptive removal was attained.

In the study of Uyguner and Bekbolet (2007), preliminary experiments of humic acid (10 mg L^{-1}) and 0.05 mg L^{-1} manganese ion without irradiation in the presence of catalyst (0.25 mg mL^{-1} TiO_2) revealed an initial adsorptive removal of approximately 35% with respect to UV_{254} removal of humic acid. This condition was explained by a surface complexation model. Moreover, in the study of Uyguner and Bekbolet, 2007, preliminary experiments were also conducted in the presence of chromium ion concentrations ranging from 0.05 mg L^{-1} to 0.20 mg L^{-1} and 0.25 mg mL^{-1} TiO_2 as catalyst. The presence of humic acid decreased the adsorption efficiency of chromium ions because of the competitive adsorption on the active sites of TiO_2 (Uyguner and Bekbolet, 2004). In adsorbed state, the coordination of metals by ligands such as carboxyl, phenolic or sulfhydryl groups is similar to the equivalent process taking place in solution (Uyguner and Bekbolet, 2007).

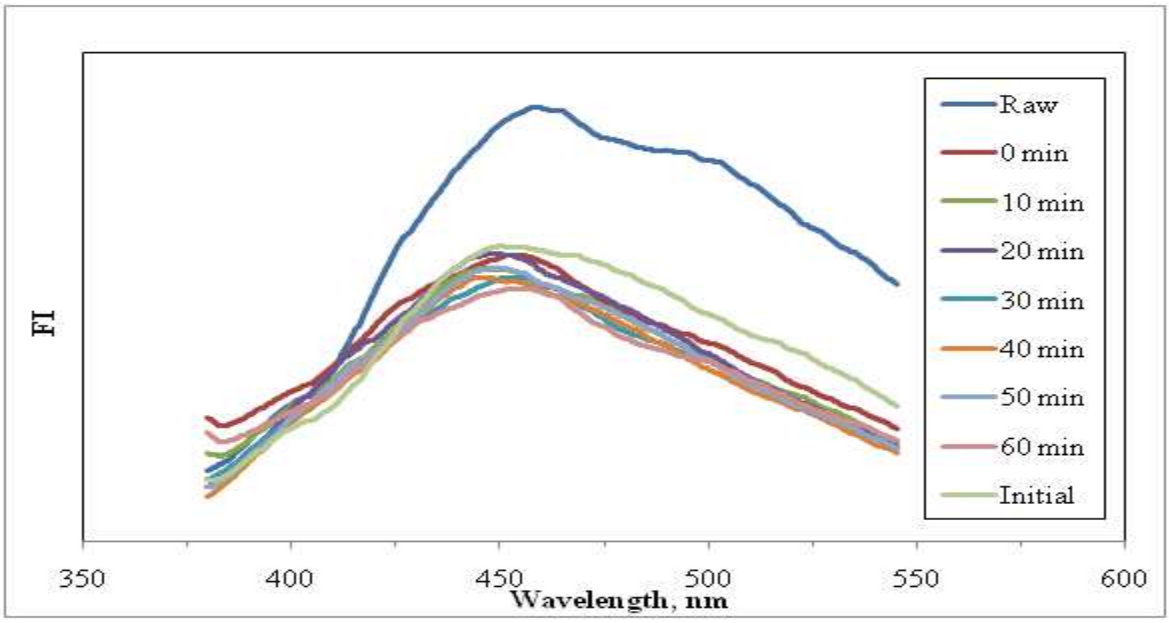

Figure 4.9. Emission scan fluorescence spectra of raw humic acid during preliminary experiments conducted under dark conditions in the presence of 0.1 mg mL^{-1} TiO_2 and 2.5 mg L^{-1} zinc (Initial represents raw humic acid and zinc binary system).

For fluorescence spectroscopic evaluation of raw humic acid during preliminary experiments in the absence of light, the emission scan spectra was scanned in the range of 380-560 nm at a constant excitation wavelength of 360 nm. The emission scan fluorescence spectra of raw humic acid gave a peak at about 450 nm wavelength. As expected, no significant difference was observed for FI trend during 60 minutes of time displaying nearly same fluorescence intensity values with overlapping trend under all conditions (Figure 4.9).

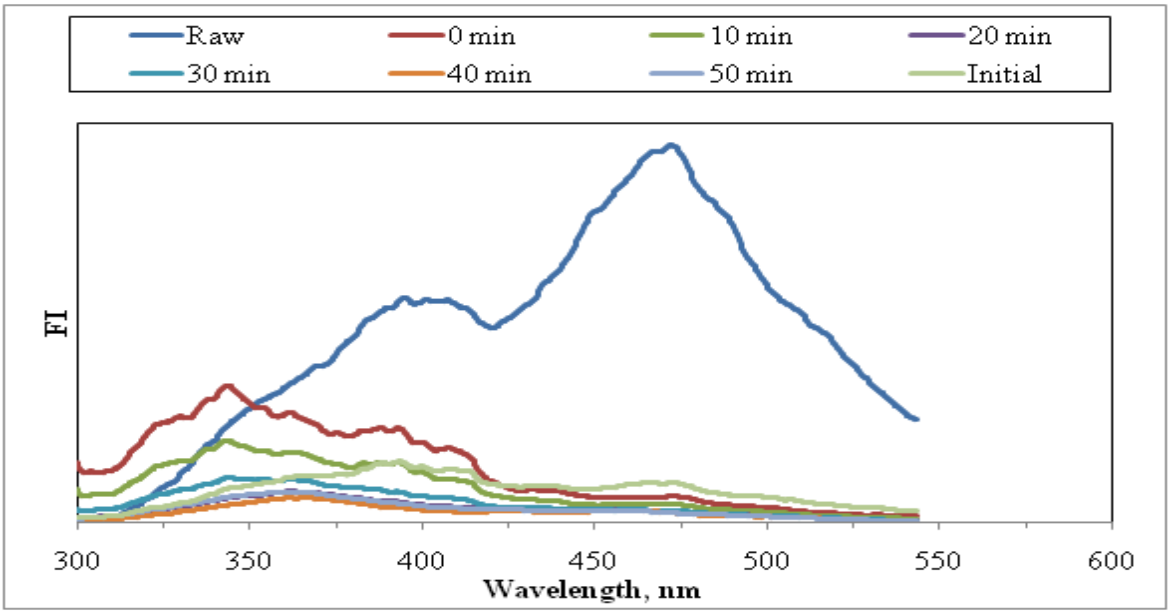

Figure 4.10. Synchronous scan fluorescence spectra of raw humic acid during preliminary experiments conducted under dark conditions in the presence of 0.1 mg mL^{-1} TiO_2 and 2.5 mgL^{-1} zinc (Initial represents raw humic acid and zinc binary system).

The synchronous scan fluorescence spectra recorded for the preliminary experiments of humic acid in the presence of zinc were shown in Figure 4.10. The synchronous scan fluorescence spectra for raw humic acid displayed a sharp peak around wavelength of 470 nm. There was also a moderate peak at 390 nm wavelength with a comparatively lower intensity. By the addition of TiO_2 and zinc to the system, minor decreases were observed for FI values up to 400 nm wavelength. After 450 nm wavelength, all samples were showed nearly same trend with low FI values.

4.2.1.2. Experiments Carried Out in the Absence of TiO_2. To observe the effect of light intensity in photocatalytic degradation of humic acids, the experiments were carried out in the absence of TiO_2. Similar experiments were also performed in the presence of 2.5 mg L^{-1} zinc. The UV-vis spectra were recorded between 200-600 nm wavelength region for UV-vis spectroscopic evaluation of raw humic acid during preliminary experiments in the absence of TiO_2.

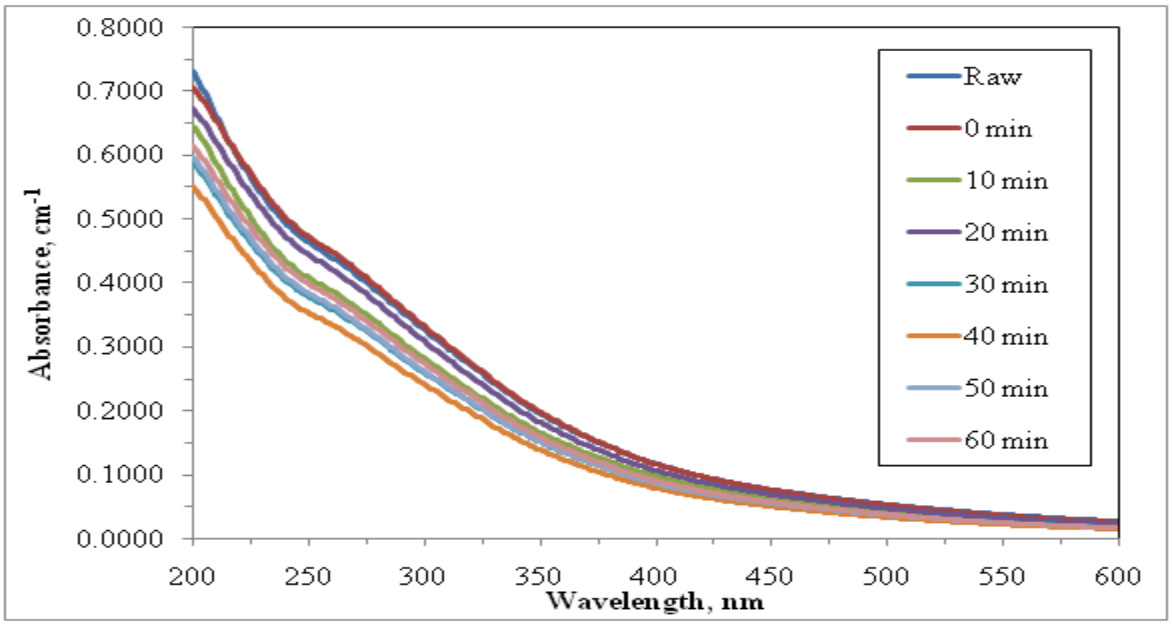

Figure 4.11. UV-vis spectra of raw humic acid during preliminary experiments conducted in the absence of TiO_2.

UV-vis spectra of of all of the humic acid samples displayed a broad, featureless and monotonously decreasing trend with increasing wavelength. Besides the expected trend, slightly significant changes in absorbances were observed by increasing time (Figure 4.11). Furthermore, as seen in Figure 4.12, a significant increase in UV-vis absorbance values was observed in the spectral region of 200-240 nm for humic acid and zinc binary system. After ~240 nm wavelength, the UV-vis spectra of raw humic acid and zinc binary system followed the similar trend of raw humic acid with lower absorbance changes. As expected, there was no significant absorbance change with increasing time and all trends were overlapping except raw humic acid.

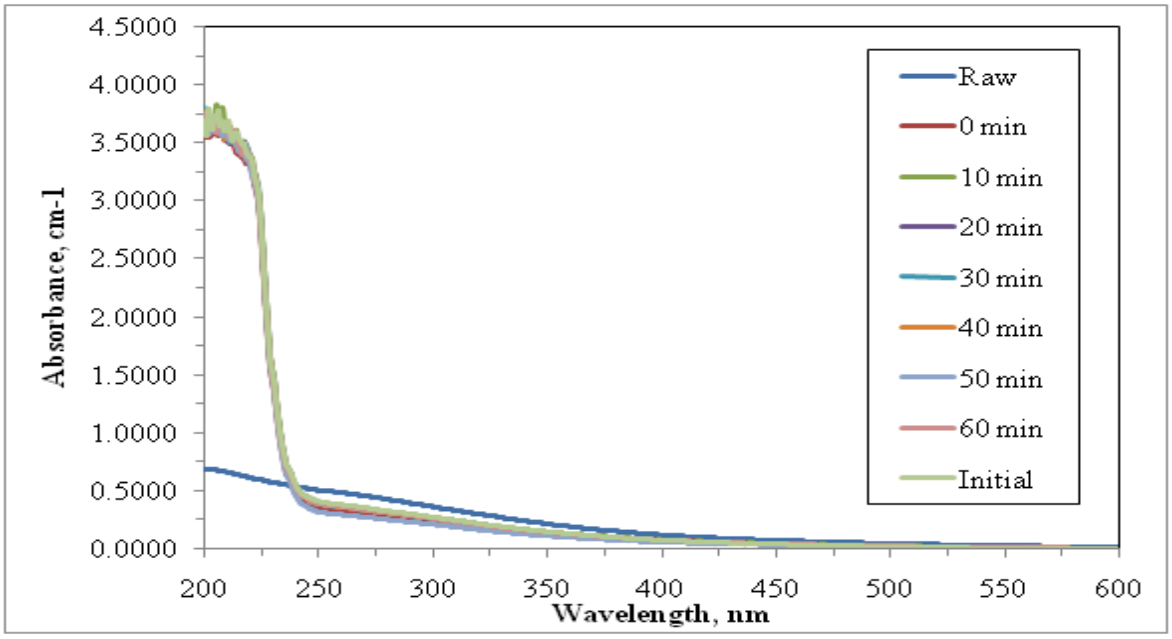

Figure 4.12. UV-vis spectra of raw humic acid and zinc binary system during preliminary experiments conducted in the absence of TiO_2 (Zn = 2.5 mg L^{-1}, initial represents raw humic acid and zinc binary system).

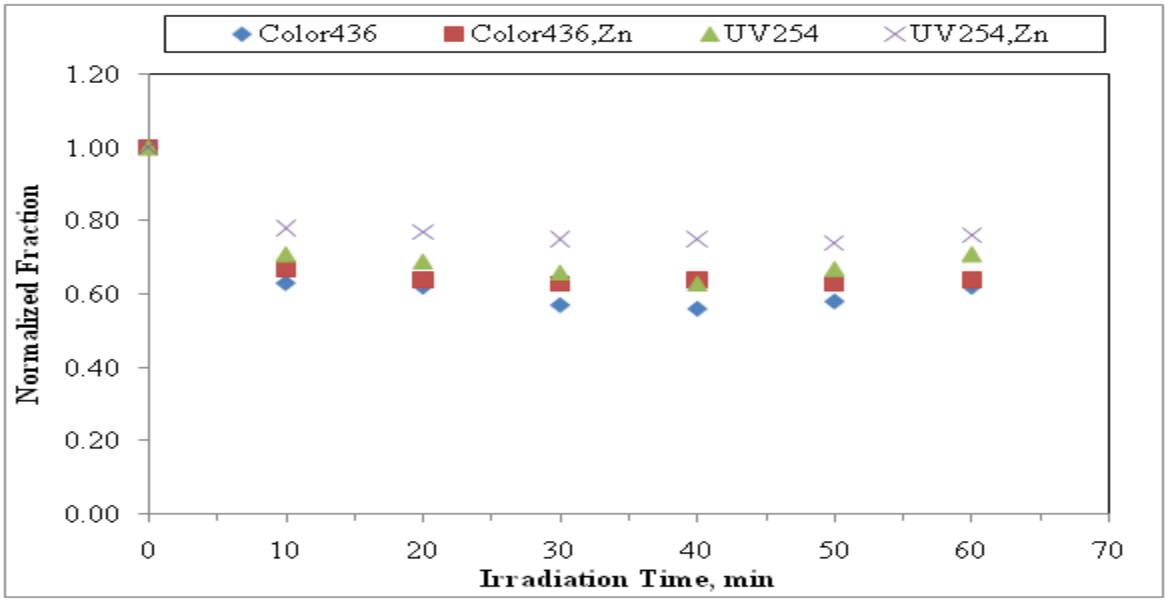

Figure 4.13. Normalized $Color_{436}$ and UV_{254} values of raw humic acid and zinc binary system with respect to irradiation time in the absence of TiO_2 (Zn = 2.5 mg L^{-1}).

As illustrated in Figure 4.13, in the absence of zinc, normalized fraction of $Color_{436}$ and UV_{254} were found to be nearly the same. Moreover, in the presence of zinc, $Color_{436}$ had similar normalized fraction. On the other hand, the removal efficiency was decreased in the presence of zinc for UV_{254} and showed the highest remaining ratio with 75% as shown in Figure 4.13. The retardation effect observed on the photocatalytic degradation of humic acid could be explained by the adsorption of zinc ions on humic acid or the surface of TiO_2 resulting in blockage of active sites of the photocatalyst.

The emission scan fluorescence spectra was scanned in the range of 380-560 nm at a constant excitation wavelength of 360 nm for fluorescence spectroscopic evaluation of raw humic acid in the presence 2.5 mg L^{-1} zinc (Figure 4.14).

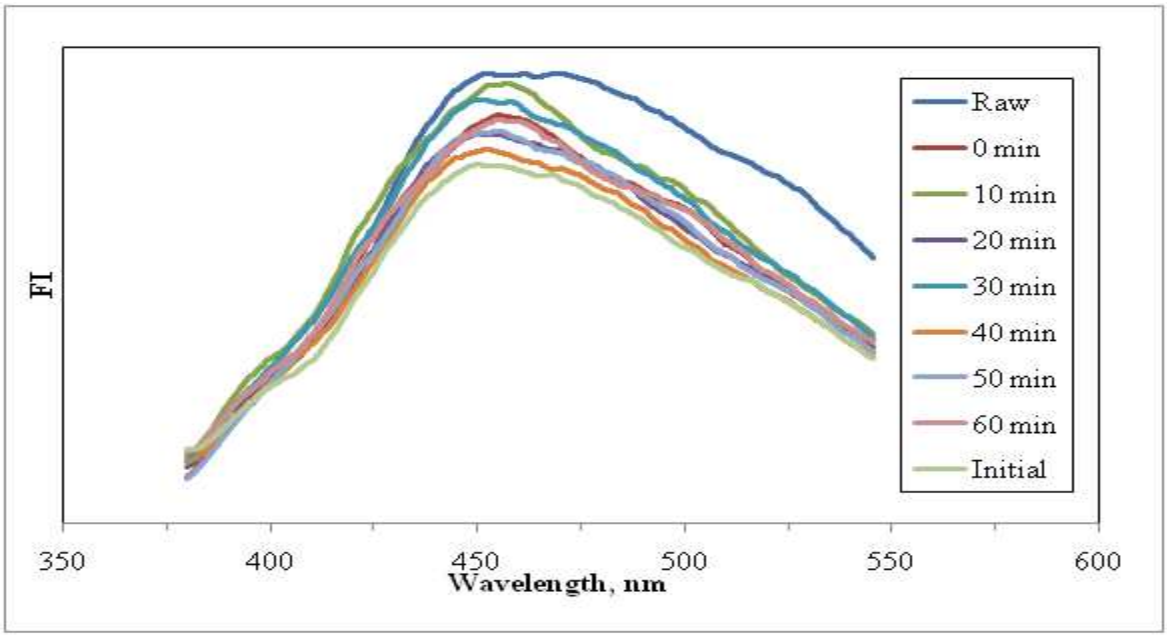

Figure 4.14. Emission scan fluorescence spectra of raw humic acid and zinc binary system during preliminary experiments conducted in the absence of TiO_2 (Initial represents raw humic acid and zinc binary system).

The emission scan fluorescence spectra of raw humic acid gave a peak at about 450 nm wavelength. As expected, no significant changes were observed for FI trend up to 60 minutes. Nearly the same fluorescence intensity values with overlapping trend were recorded for all time periods.

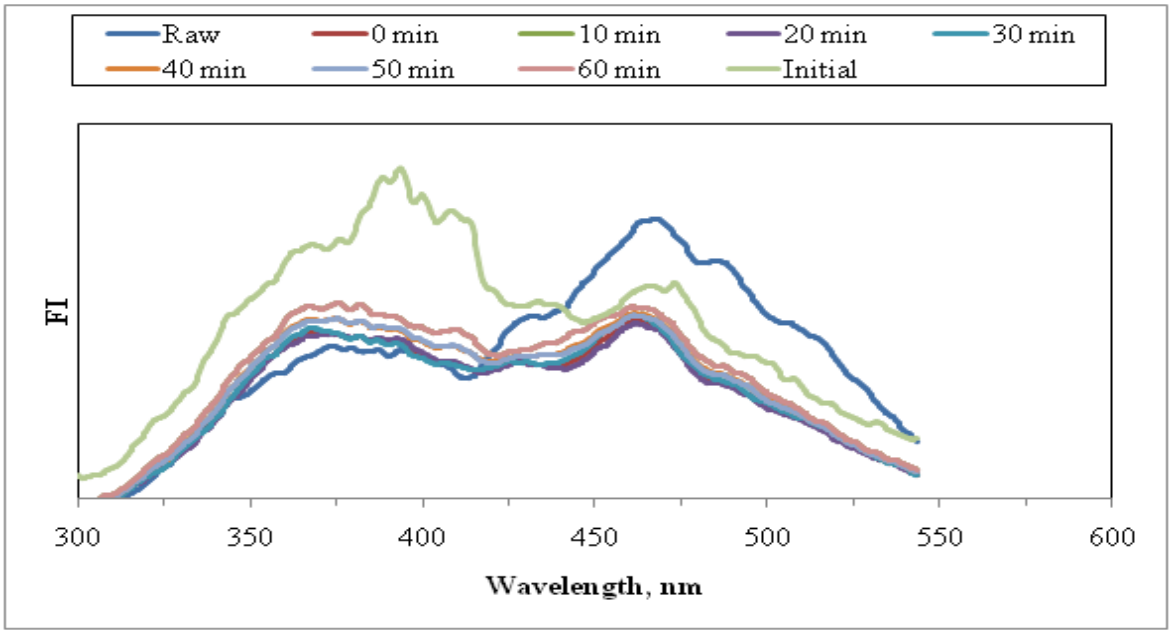

Figure 4.15. Synchronous scan fluorescence spectra of raw humic acid and zinc binary system during preliminary experiments conducted in the absence of TiO_2 (Initial represents raw humic acid and zinc binary system).

The synchronous scan fluorescence spectra for raw humic acid displayed a sharp peak around wavelength of 470 nm (Figure 4.15). There was also a moderate peak about 380 nm wavelength with a comparatively lower intensity. With the addition of zinc to humic acid, two new peaks were observed at 395 nm and 475 nm wavelengths. On the other hand, there was no significant change in the trend of synchronous fluorescence spectra of preliminary experiments conducted in the absence of TiO_2.

4.3. Photocatalytic Degradation of Humic Acid and Zinc Binary System

For the assessment of the photocatalytic degradation of humic acid (AHA), different molecular size fractions such as 0.45 µm filtered fraction, 100 kDa fraction and 30 kDa fraction were also used. Moreover, the experiments were also carried out in the absence and in the presence of zinc ion for comparison purposes. Photocatalyst, TiO_2 loadings were kept constant as 0.1 mg mL^{-1} and zinc concentration was also constant as 0.1 mg L^{-1} in all experiments.

The physical-chemistry of humic acid-cation interactions were less understood due to the complex structure and heterogeneity of humic acids expressing a wide distribution of types and number of metal binding sites (Kinniburgh et al., 1999). Trace metals did not necessarily compete for the same sites on the humic acid, since they had different affinities for different binding sites. Conformational changes that occured when trace metals bound to the different sites caused either a competing or enhanced effect (Cao et al., 1995). The overall effect of these interactions could be either enhancement or retardation of the photocatalytic degradation efficiency.

4.3.1. Photocatalytic Degradation of Raw Humic Acid

Humic acid solution was subjected to photocatalytic oxidation according to the method explained in the Materials and Methods section. The oxidized humic acid samples were evaluated by UV-vis spectra and fluorescence spectra as well as by the specified UV-vis and fluorescence parameters. The results were presented under appropriate subheading for the humic acid and molecular size fractions in the presence and absence of zinc.

4.3.1.1. UV-vis Spectroscopic Evaluation of Raw Humic Acid During Photocatalytic Degradation. The UV-vis spectrum of humic acid showed a gradually declining trend with the respect to increasing wavelength in the 200-600 nm region as seen in Figure 4.16. Uyguner and Bekbolet (2005a) also reported that the UV-vis spectra of humic acids broad, featureless and monotonously decrease with increasing wavelength during photocatalytic degradation. Irradiation time dependent changes were also followed by spectroscopic properties during humic acid photocatalytic degradation starting with t = 0 min which was the initial titanium dioxide introduction to humic acid solution prior to irradiation (Uyguner and Bekbolet, 2005a). Initial adsorptive removal of raw humic acid could also be visualized by examining the recorded UV-vis spectra of raw humic acid under dark conditions. Moreover, the UV-vis spectra of raw humic acid during photocatalytic degradation showed that t=0 min and t=10 min had similar trend. Also, for irradiation periods of t=20 min and t=30 min, the UV-vis spectra followed the same trend with lower absorbance values than t= 0 min. After irradiation time of 30 minutes, the degradation of humic acid displayed a significant decrease in the UV-vis absorbance retaining the similar trend.

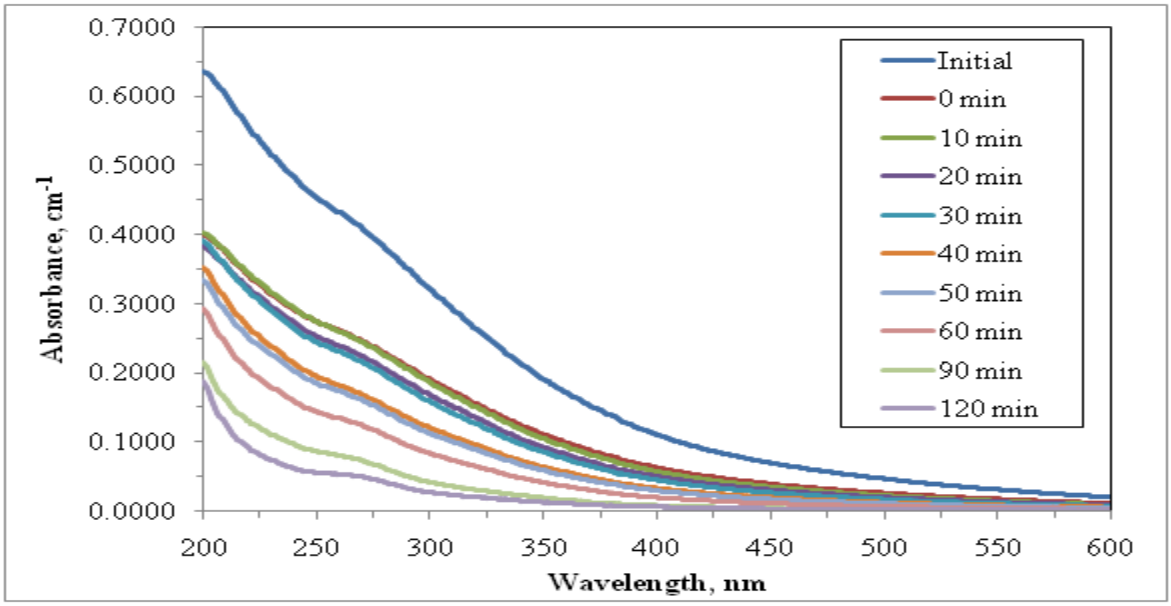

Figure 4.16. UV-vis spectra of raw humic acid during photocatalytic degradation (Initial represents raw humic acid).

The effect of prolonged irradiation time was shown by the spectra recorded for 90 and 120 minutes. It could be easily noticed that there were no significantly characteristic absorbance recordings ($\lambda \leq 300$ nm, UV_{300}=0.030 cm^{-1}) after long irradiation time periods such as 120 minutes.

Furthermore, the photocatalytic degradation of humic acid was evaluated in terms of UV-vis parameters as expressed by $Color_{436}$, UV_{365}, UV_{280} and UV_{254}. The remaining fractions of the specified parameters were displayed with respect to irradiation time for simplicity purposes (Figure 4.17). Initial adsorptive removal of humic acid could also be assessed by the specified UV-vis parameters. The removal efficiencies were 43%, 42%, 40% and 40% for $Color_{436}$, UV_{365}, UV_{280} and UV_{254}, respectively. While 49% of $Color_{436}$ was removed in 10 minutes of irradiation, following photocatalysis 83% removal was achieved after 60 minutes. In long irradiation time periods such as 120 minutes, $Color_{436}$ was detected as < 1% for humic acid that could be considered as an overall removal of the color forming moieties.

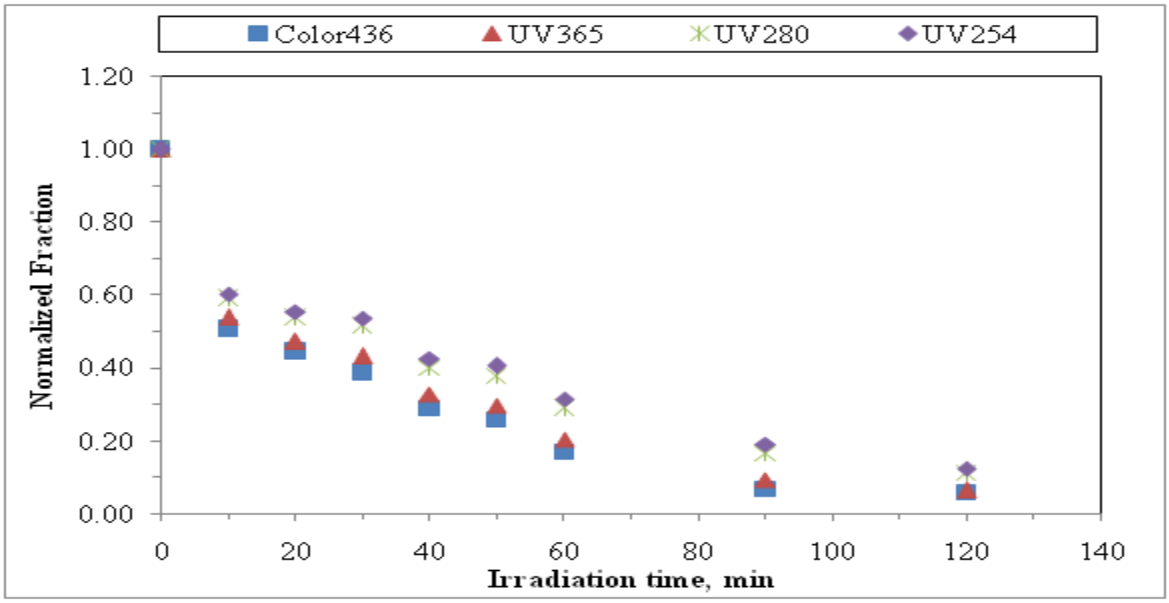

Figure 4.17. Normalized $Color_{436}$, UV_{365}, UV_{280}, and UV_{254} values of raw humic acid with respect to irradiation time.

For UV_{254}, 40% removal was observed in 10 minutes of irradiation time. Similar to $Color_{436}$, UV_{254} was removed from the suspension in significant amounts as 69% and 88% after 60 and 120 minutes irradiation times, respectively. Moreover, almost 80% and 71% degradation was achieved in 60 minutes for UV_{365} and UV_{280}, respectively. In longer time periods, the removal percentages reached to 94% and 89% for UV_{365} and UV_{280}, respectively. The removal efficiencies followed a basic trend of $Color_{436}$ > UV_{365}>UV_{280} >UV_{254} irrespective of the irradiation time.

4.3.1.2. Fluorescence Spectroscopic Evaluation of Raw Humic Acid During Photocatalytic Degradation. The fluorescence spectra of treated humic acid samples showed general decreasing intensity profiles with increasing photocatalytic irradiation time (Uyguner and Bekbolet, 2005a). The emission scan fluorescence spectra of humic acid samples were displayed in Figure 4.18. The fluorescence spectra of the samples were recorded by excitation at 360 nm causing a major peak at the wavelength of 450 nm. Although an irradiation time dependent general decreasing trend in fluorescence intensity could be visualized, the maximum fluorescence intensity was observed for 40 minutes of irradiation time with reference to the raw humic acid.

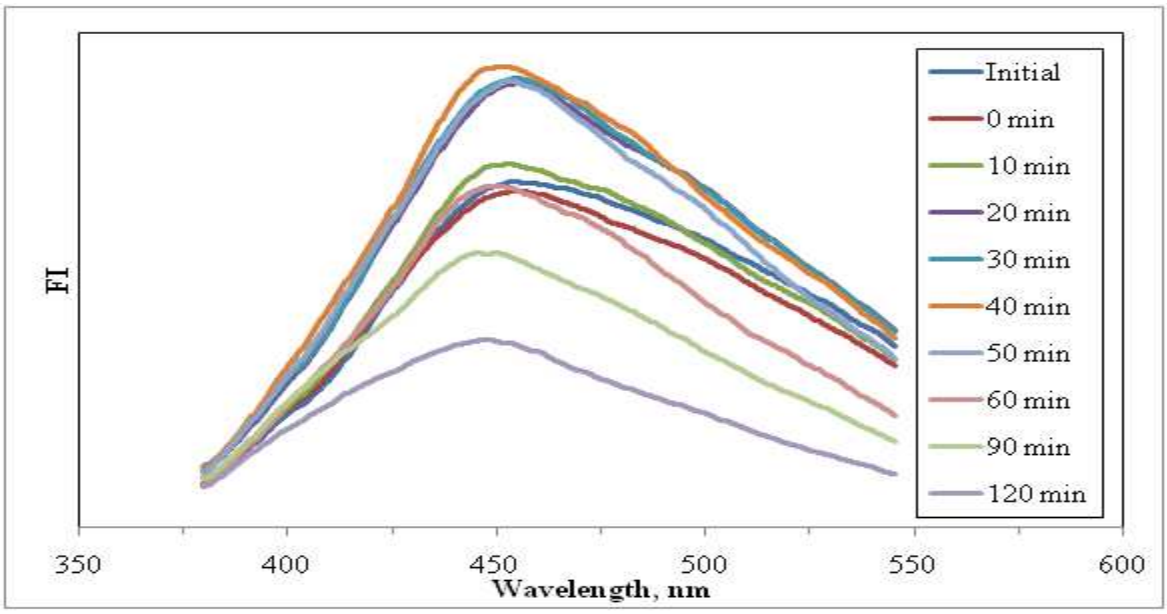

Figure 4.18. Emission scan fluorescence spectra of raw humic acid during photocatalytic degradation (Initial represents raw humic acid).

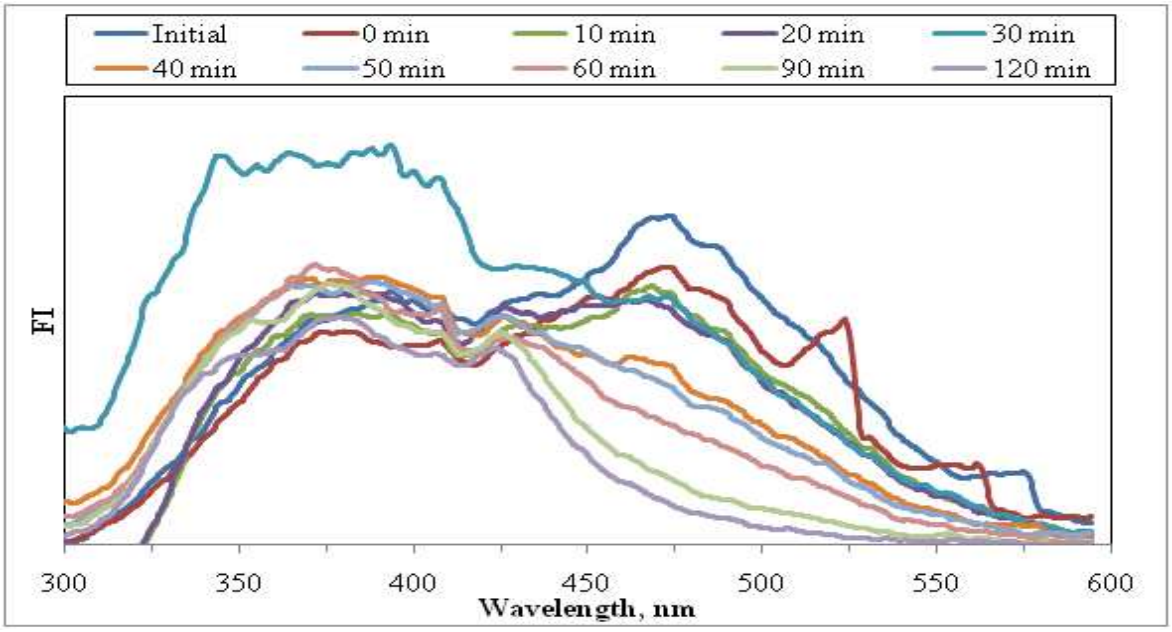

Figure 4.19. Synchronous scan fluorescence spectra of raw humic acid during photocatalytic degradation (Initial represents raw humic acid).

The synchronous scan fluorescence spectra recorded for the photocatalytically treated humic acid were shown in Figure 4.19. The synchronous scan fluorescence spectra for raw humic acid displayed a sharp peak around wavelength of 470 nm. There was also a moderate peak around 390 nm wavelength with a comparatively lower intensity. Uyguner and Bekbolet (2005a) reported that raw humic acid had a sharp peak around 473 nm and a moderate peak around 400 nm. Peuravuori and co-workers (2002), ascribed the peak around 460 nm wavelength to polycyclic aromatic consisting of seven fused benzene rings. The synchronous scan fluorescence spectra of humic acids photodegradation led to the gradual decrease of FI in the region of 470-600 nm wavelengths. It could be indicated the degradation of the high molecular weight components of humic acids and formation of lower molecular size fractions of humic acidswere expected during photocatalysis (Uyguner and Bekbolet, 2005a). After long irradiation time periods, the characteristic sharp peak of raw humic acid at 470 nm wavelength completely disappeared. On the other hand, emergence of new peaks at 375 and 425 nm wavelengths were also noticed. At these wavelengths, comparatively similar fluorescence intensities were recorded for extended irradiation time of 120 minutes.

4.3.2. Photocatalytic Degradation of 0.45µm Filtered Fraction of Humic Acid

Photocatalytic degradation of 0.45µm filtered fraction of humic acid samples were evaluated by both UV-vis spectra and fluorescence spectra recorded in emission scan and synchronous modes. The specified UV-vis and fluorescence parameters were also presented.

4.3.2.1. UV-vis Spectroscopic Evaluation of 0.45µm Filtered Fraction Humic Acid During Photocatalytic Degradation. As followed for raw humic acid, a similar declining decay trend in UV-vis absorbance spectra were also recorded for 0.45µm filtered fraction of humic acid (Figure 4.20). Comparison of UV-vis spectra of raw and 0.45µm filtered fraction of humic acid reveals the role of filtration through 0.45 µm fitler as observed by the elimination of overlapping chromophoric groups displaying “shoulder effect” (Figure 4.16).

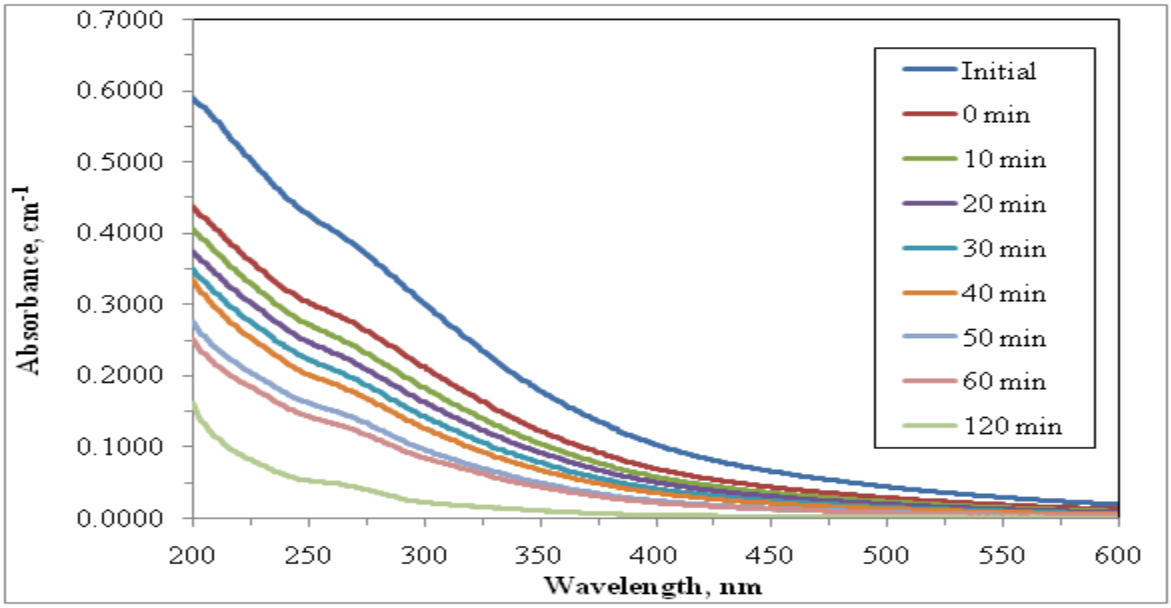

Figure 4.20. UV-vis spectra of 0.45µm filtered fraction of humic acid during photocatalytic degradation (Initial represents 0.45µm filtered fraction of humic acid).

Moreover, UV-vis spectra of the photocatalytically treated 0.45µm filtered fraction of humic acid could be distinctly differentiated with respect to the duration of the exposure to the light intensity (e.g. 60 mins). Following prolonged irradiation conditions (120 mins), significantly lower UV-vis absorbance recordings were attained as could be expressed by very low UV_{254} (0.050 cm^{-1}) and complete elimination of color forming moities (i.e. $Color_{436}$).

Photocatalytic degradation of 0.45µm filtered fraction of humic acid was also evaluated in terms of UV-vis parameters as expressed by $Color_{436}$, UV_{365}, UV_{280} and UV_{254} (Figure 4.21). Initial adsorptive removal efficiencies of 0.45µm filtered fraction of humic acid were 34%, 32%, 29% and 29% for $Color_{436}$, UV_{365}, UV_{280} and UV_{254}, respectively. The general descreasing trend detected for all of the UV-vis parameters displayed the same approach as was recoreded for raw humic acid. While 45% of $Color_{436}$ was removed in 10 minutes of irradiation, 81% removal was achieved after 60 minutes. In 120 minutes of irradiation time, the removal of $Color_{436}$ reached to 97%.

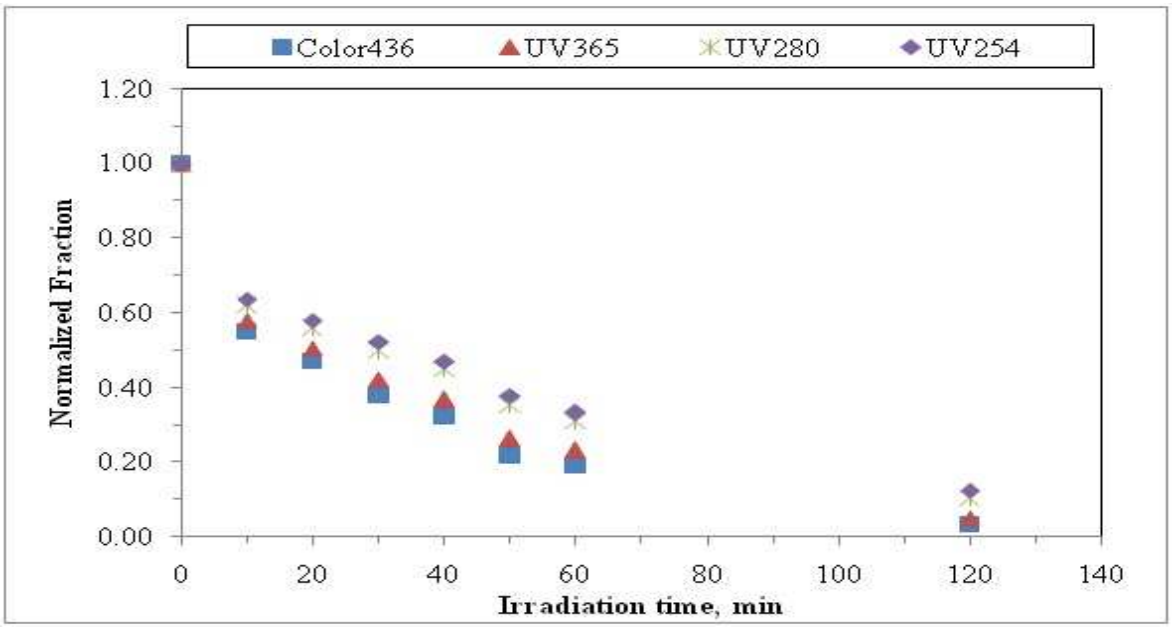

Figure 4.21. Normalized $Color_{436}$, UV_{365}, UV_{280} and UV_{254} values of 0.45 µm filtered fraction of humic acid with respect to irradiation time.

Significantly lower removal trend was observed for UV absorbing centers as UV_{254}. 36% removal was observed in 10 minutes irradiation time followed by a slightly slower rate reaching to removals to about 67% and 88% after 60 and 120 minutes irradiation times, respectively. However, 77% and 69% degradation was achieved in 60 minutes for UV_{365} and UV_{280}, only 0.05% of UV_{365} and 0.10% UV_{280} was remained in solution in 120 minutes of irradiation time. Almost complete elimination of the UV-vis parameters (≤ 10 %) explains the removal of humic acid moities by photocatalysis in 120 mins.

4.3.2.2. Fluorescence Spectroscopic Changes of 0.45µm Filtered Fraction of Humic Acid During Photocatalytic Degradation. The emission scan scan fluorescence spectra recorded under post-irradiation conditions for the photocatalytially oxidized samples 0.45µm filtered fraction of humic acid were shown in Figure 4.22. A general decreasing trend was attained for the emission fluorescence index recorded at maximum wavelength of 450 nm with resspect to irradiation period. The fluorescence intensity could still be detected for 120 min of irradiation time.

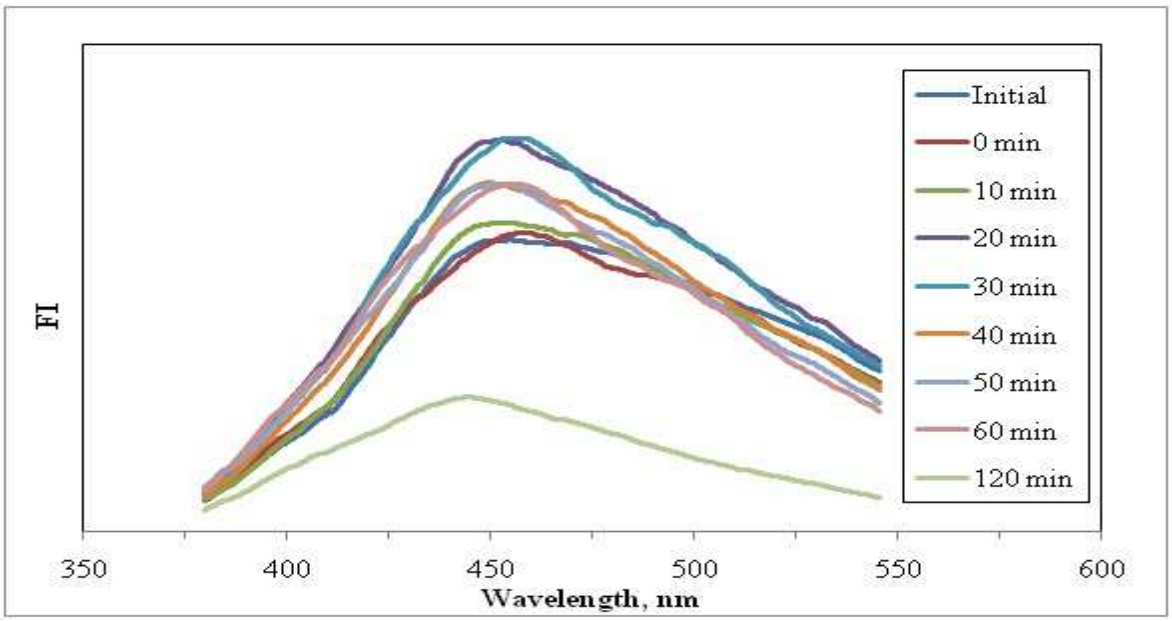

Figure 4.22. Emission scan fluorescence spectra of 0.45µm filtered fraction humic acid during photocatalytic degradation (Initial represents 0.45µm filtered fraction of humic acid).

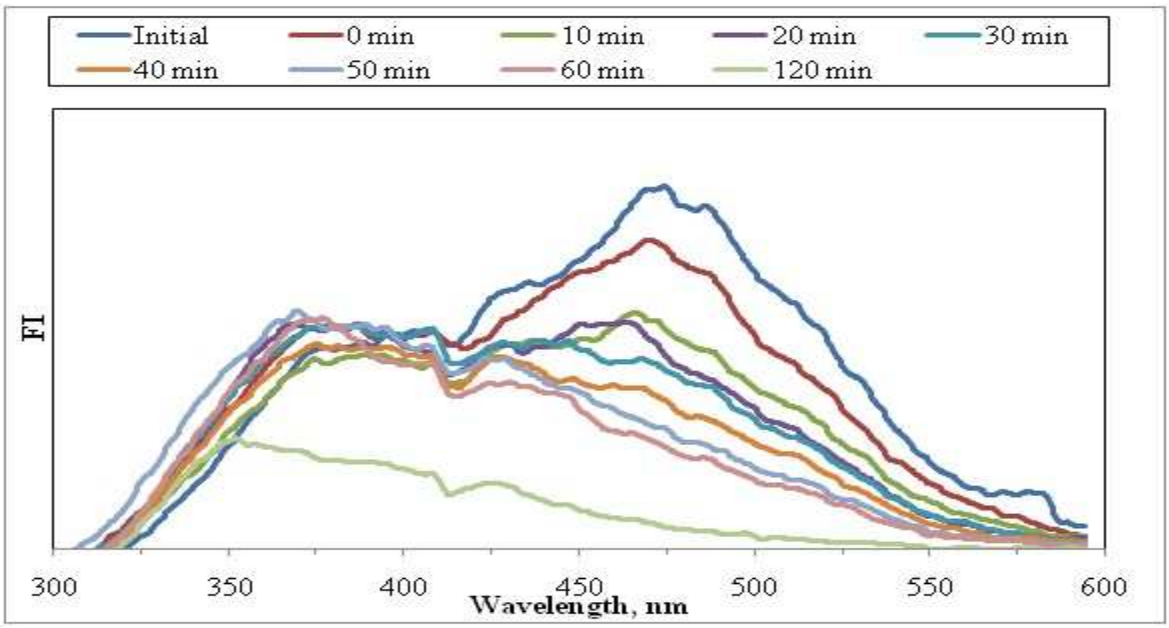

Figure 4.23. Synchronous scan fluorescence spectra of 0.45µm filtered fraction humic acid during photocatalytic degradation (Initial represents 0.45µm filtered fraction of humic acid).

No significant change was attained in the emission fluorescence intensity of 0.45µm filtered fraction of humic acid for the initial adsorptive removal of humic fractions. The photocatalytically treated humic fractions displayed a consistent formation tendency of fluorescent moieties during oxidative degradation. The decrease of the fluorescence maxima was indicative for the destruction of the high degree of conjugation and aromatic structures of humic acids (Uyguner, 2005). Approximately 50% FI removal at emission fluorescence maximum wavelength of 450 nm was attained for 120 minutes of irradiation time.

Synchronous scan fluorescence spectra of 0.45 µm filtered fraction of humic acid displayed a major peak around ~470 nm and a minor peak around ~370 nm with comparatively similar fluorescence intensities (Figure 4.23). Synchronous scan spectra of 0.45 µm filtered fraction of humic acid exhibited similar fluorescence properties in comparison to raw humic acid (Figure 4.19 and Figure 4.23). Parallel to the findings of Korshin et al., 1999, and Carvalho et al., 2004, a general decrease around 470-600 nm wavelengths was observed for all of the applied oxidation systems. It was reported that in large humic molecules, intrafluophore energy transfer shortened the apparent decay lifetimes of fluorophores whereas in smaller molecules, lifetimes of fluorophores increase because of weaking of excitation energy. While the applied oxidation methods decreased the size of humic acid molecule and destroyed some of the aromatic chromophores involved in the energy transfer, the decrease of FI in oxidized humic acid samples correlated with this hypothesis (Uyguner and Bekbolet, 2007).

The characteristic peak of humic acid was significantly quenched even with the sole action of TiO_2 prior to irradiation. These conditions showed the importance of initial adsorption of humic acid on to TiO_2. After 120 minutes of irradiation, the characteristic sharp peak of 0.45 µm filtered fraction of humic acid completely disappeared, the major peak around 370 nm decayed in intensity and another peak of low intensity around 350 nm wavelength emerged. The disappearance of the characteristic peak of humic acid after photocatalysis was observed and this could be attributed to the removal of carboxylic functional groups (Uyguner and Bekbolet, 2005a).

Considering the expected complete filtration of humic acid through 0.45 µm membrane filter, observed similarity for both of the humic acid samples could possibly be related to the structural properties. However, the recorded synchronous scan fluorescence spectra of both of the samples under post treatment conditions indicated the presence of structural changes leading to diverse reactivities during photocatalysis.

4.3.3. Photocatalytic Degradation of 100 kDa Fraction of Humic Acid

Photocatalytic degradation of 100 kDa fraction of humic acid samples were evaluated by UV-vis spectra and fluorescence spectra as well as by the specified UV-vis and fluorescence parameters.

4.3.3.1. UV-vis Spectroscopic Evaluation of 100kDa Fraction of Humic Acid During Photocatalytic Degradation. 100 kDa fraction of humic acid was subjected to photocatalysis and evaluated in the same manner as reported for raw humic acid and 0.45µm filtered fractions of humic acid. Following the general trend observed for humic acids, The UV-visible spectra displayed a descending trend with increasing irradiation time periods from time zero to 90 minutes (Uyguner and Bekbolet, 2005a).

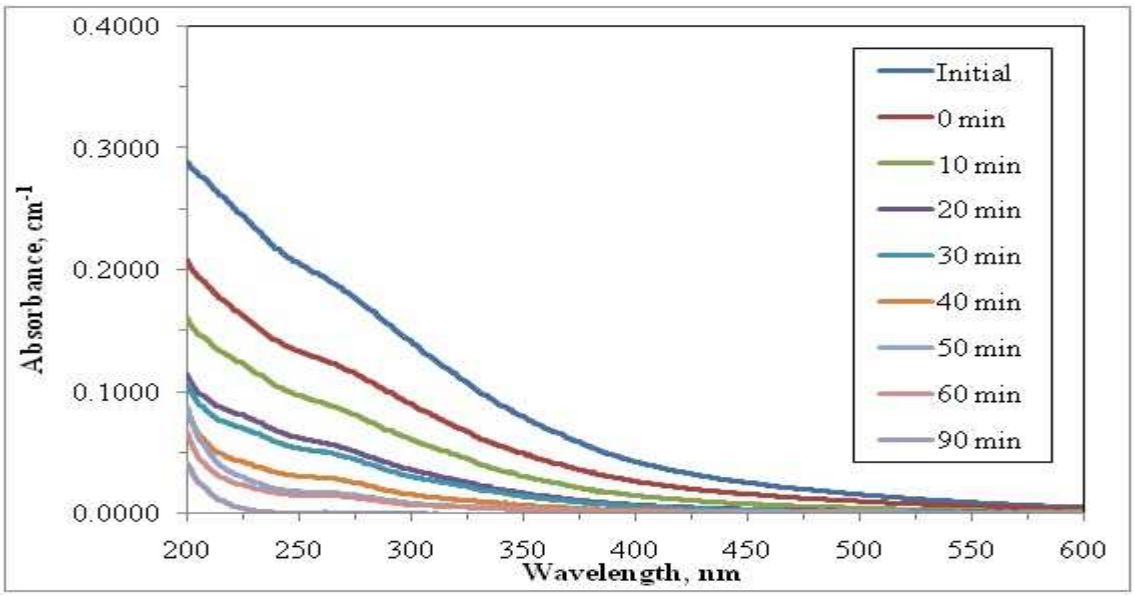

Figure 4.24. UV-vis spectra of 100 kDa fraction of humic acid during photocatalytic degradation (Initial represents 100 kDa fraction of humic acid).

Taking into account the initial UV-vis spectral features of the 100 kDa fraction of humic acid, the attained absorbance recordings were significantly lower than the considerably higher molecular weight fractions (Figure 4.24). The decrease of the UV absorbing properties of each humic acid fraction could be a consequence of the decomposition of the humic acid to smaller molecular size fractions (Uyguner and Bekbolet, 2005a). Consequently for longer irradiation time conditions, UV-vis absorption spectra approached to very low absorbance values. Considering the lower initial UV-vis absorbance of 100 kDa fraction with respect to humic acid and 0.45µm filtered fractions of humic acid, UV-vis spectra were recorded significantly up to irradiation period of 60 minutes. Especially after 30 minutes of irradiation period, $Color_{436}$ values became close to zero, while UV_{254} absorbance could be still detected ($UV_{254} \leq 0.050$ cm^{-1}). As presented absorbance values recorded for wavelength region of 200-375 nm could be considered as significant irrespective of the irradiation period (0- 60 mins).

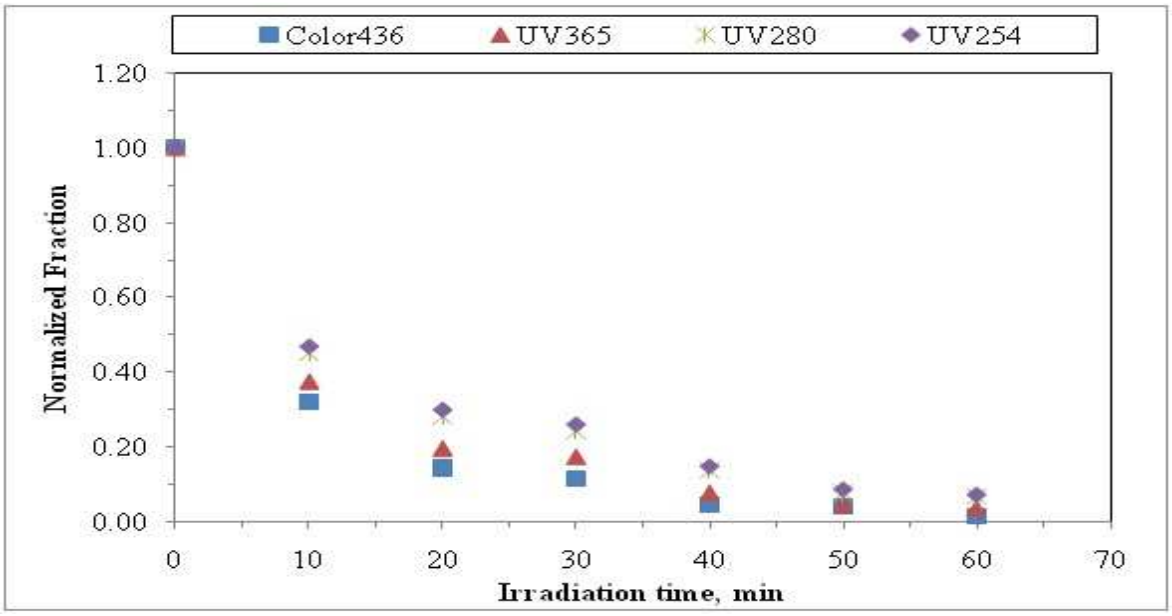

Figure 4.25. Normalized $Color_{436}$, UV_{365}, UV_{280} and UV_{254} values of 100 kDa fraction of humic acid with respect to irradiation time.

Photocatalytic degradation of 100 kDa fraction of humic acid was also evaluated in terms of UV-vis parameters as expressed by $Color_{436}$, UV_{365}, UV_{280} and UV_{254} (Figure 4.25). Initial adsorptive removal of 100 kDa fraction of humic acid could also be assessed by the specified UV-vis parameters. The removal efficiencies were 38%, 39%, 35% and

35% for $Color_{436}$, UV_{365}, UV_{280} and UV_{254}, respectively. Moreover, 68% removal of $Color_{436}$ and 53% removal of UV_{254} were recorded at the end of 10 minutes of photocatalytic treatment that could also be explained by the adsorptive and desorptive interactions taking place during the early stages of photocatalysis. On the other hand, in 40 minutes, the removal efficiecies of all of the UV-vis parameters were found to be ≥ 80 % followed by irradiation period of 60 minutes at which the removal efficiency reached up to 99%. At the end of 60 minutes of irradiation time, all of the UV-vis parameters i.e. $Color_{436}$, UV_{365}, UV_{280}, and UV_{254} expressed an almost complete degradation of 100 kDa fraction of humic acid (≤ 1%) (Figure 4.25).

4.3.3.2. Fluorescence Spectroscopic Evaluation of 100 kDa Fraction Humic Acid During Photocatalytic Degradation. Emission scan fluorescence spectra of photocatalytically treated 100kDa fraction humic acid samples were displayed in Figure 4.26. It could be noticed that excitation wavelength of 360 nm caused a major peak in the region of 450 nm as recorded for the raw humic acid and 0.45µm filtered fraction of humic acid.

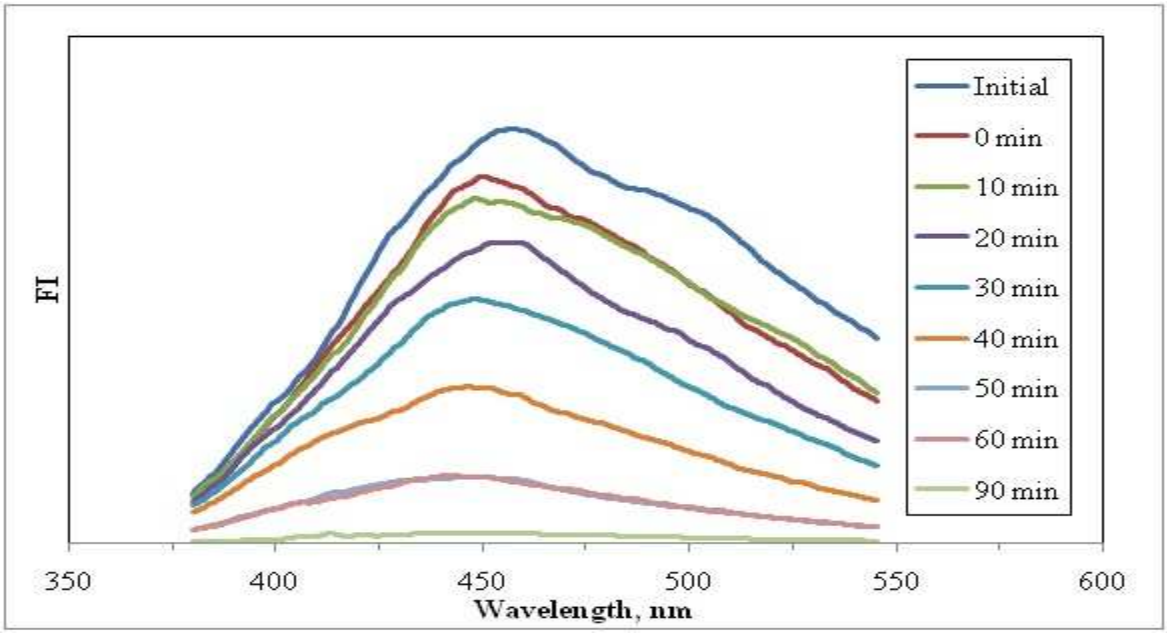

Figure 4.26. Emission scan fluorescence spectra of 100 kDa fraction of humic acid during photocatalytic degradation (Initial represents 100 kDa fraction of humic acid).

Although a slight shift to lower wavelengths (~ 5 nm) was recorded in the emission maxima of fluorescence emission scan spectra, comparisons were based on the λ_{max} at 450 nm. A significant decrease in FI was recorded for initial adsorption of 100 kDa fraction of humic acid. Starting from time zero to 90 minutes of experimental sequence emission fluorescence intensities slightly declined. Especially after 40 minutes of irradiation time, the major started to disappear. At 90 minutes of irradiation time, there was no detectable peak in the emission scan fluorescence spectra.

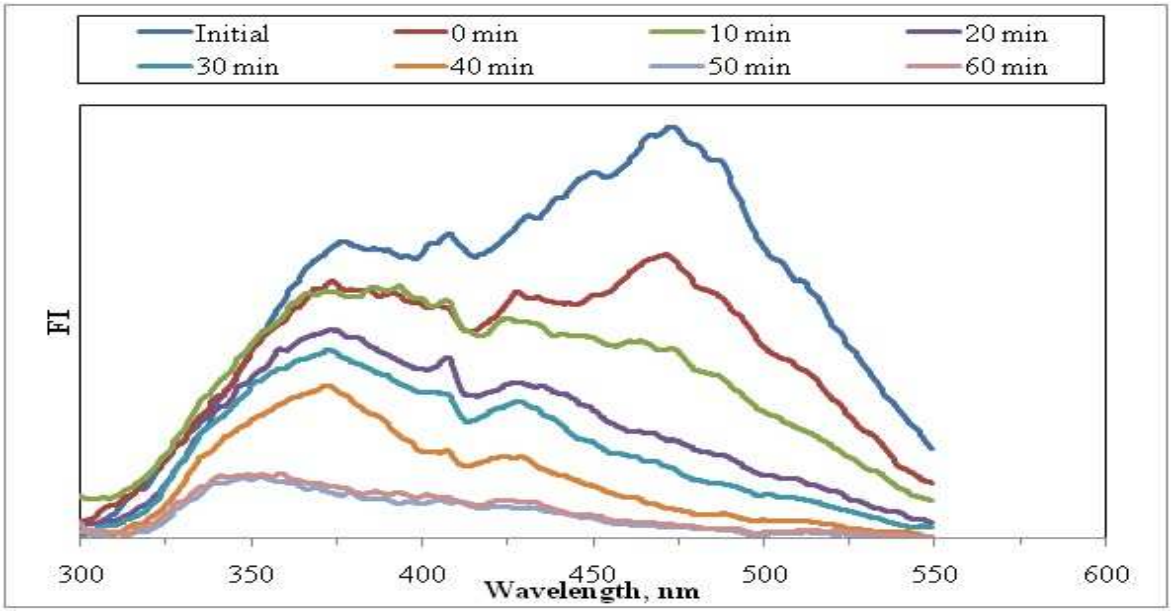

Figure 4.27. Synchronous scan fluorescence spectra of 100 kDa fraction of humic acid during photocatalytic degradation (Initial represents 100 kDa fraction of humic acid).

Synchronous scan spectra of 100 kDa fraction of humic acid as shown in Figure 4.27, displayed a major peak around ~470 nm and a minor peak around ~370 nm. Initial adsorptive removal of 100 kDa fraction of humic acid could also be visualized by the synchronous scan fluorescence spectra displaying a quite significant FI decrease at 470 nm wavelength. Following oxidative treatment both the fluorescence spectral features as well as the FI were changed. Even after 10 minutes of irradiation time, the peak at λ_{max} 470 nm started to disappear.

Upon irradiation during photocatalysis, the oxidatively treated 100 kDa fraction of humic moieties displayed synchronous scan fluorescence spectra exhibiting a shift to lower

wavelengths. For the irradiation period of 40 minutes, the minor peak detected at the wavelength of 370 nm could still reflect the presence of fluoresence emitting humic moities. For longer irradation periods of 50 minutes and 60 minutes, the synchronous scan fluorescence spectra demostrated a featureless regime.

4.3.4. Photocatalytic Degradation of 30 kDa Fraction of Humic Acid

Photocatalytic degradation of 30 kDa fraction of humic acid samples were evaluated by UV-vis spectra and fluorescence spectra as well as by the specified UV-vis and fluorescence parameters

4.3.4.1. UV-vis Spectroscopic Evaluation of 30kDa Fraction Humic Acid During Photocatalytic Degradation. 30 kDa fraction of humic acid was subjected to photocatalysis and evaluated in the same manner as reported for raw, 0.45µm filtered fraction and 100 kDa fraction of humic acid.

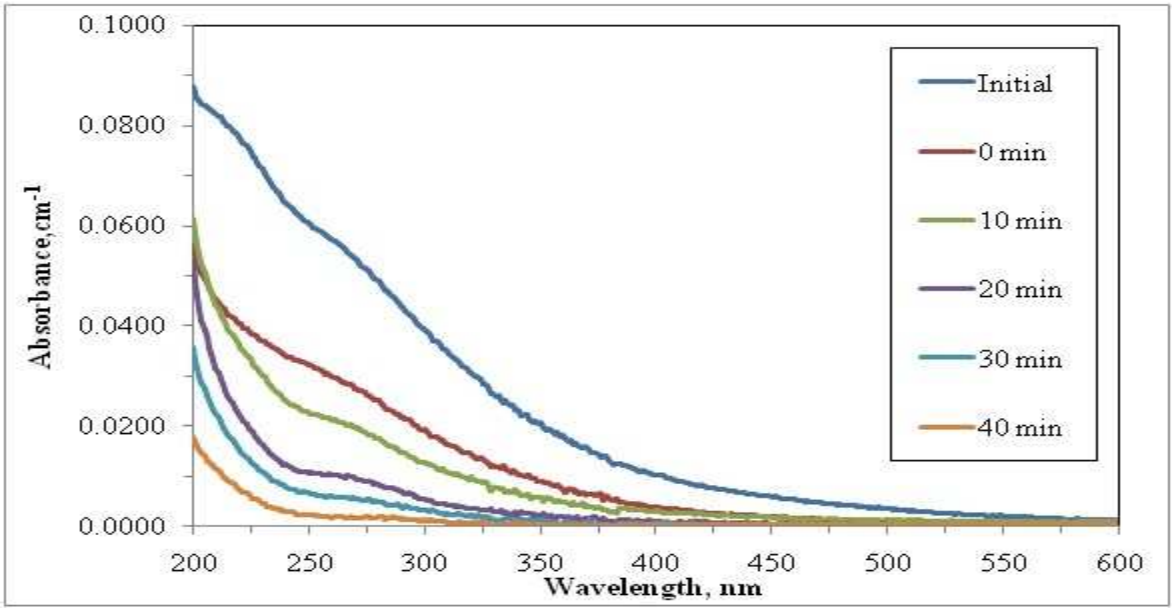

Figure 4.28. UV-vis spectra of 30 kDa fraction of humic acid during photocatalytic degradation (Initial represents 30 kDa fraction of humic acid).

UV-vis spectra of the 30 kDa fraction of humic acid displayed a decaying shape for all of the samples in the 200-600 nm wavelength region. The general decline in specific

absorbance values towards smaller size fractions was consistent with the findings of Alberts and co-workers (2002), who have studied the molecular size fractions of fresh water natural organic matter. Considering the initial UV-vis spectral features of the 30 kDa fraction of humic acid, the attained absorbance recordings were significantly lower than the considerably higher molecular weight fractions. Even for comparatively shorter irradiation time conditions (i.e. 20 minutes), UV-vis absorption spectra approached to very low absorbance values. Considering the lower initial UV-vis absorbance of 30 kDa fraction of humic acid with respect to raw, 0.45µm filtered fraction and 100 kDa fraction of humic acid, UV-vis spectra could only be recorded significantly up to irradiation period of 30 minutes.

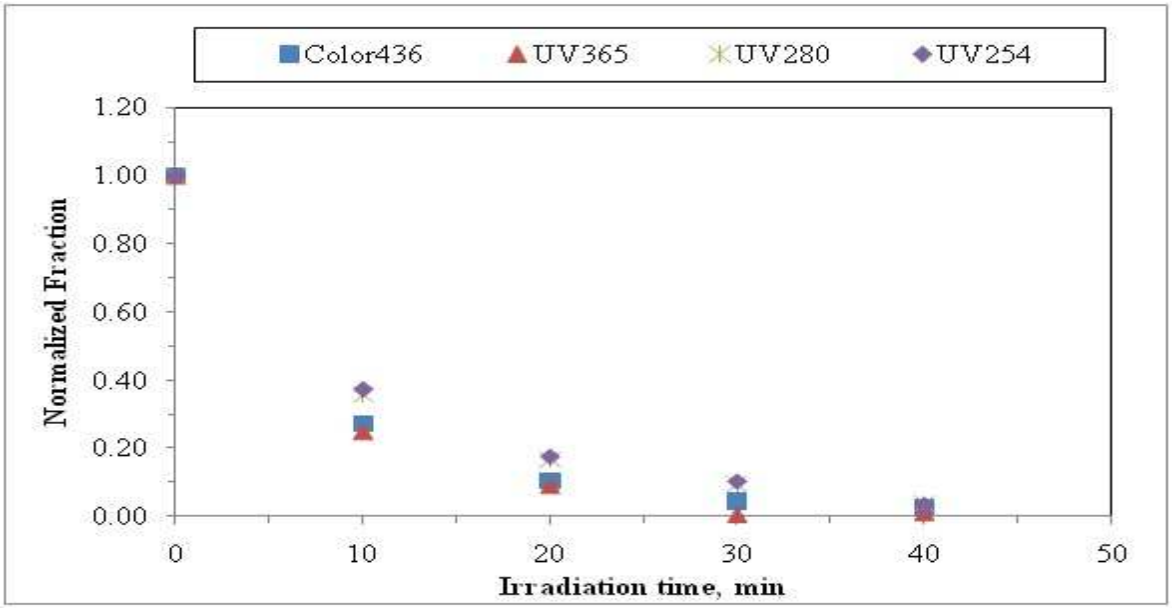

Figure 4.29. Normalized $Color_{436}$, UV_{365}, UV_{280} and UV_{254} values of 30 kDa fraction of humic acid with respect to irradiation time.

Photocatalytic degradation of 30 kDa fraction of humic acid was also evaluated in terms of UV-vis parameters as expressed by $Color_{436}$, UV_{365}, UV_{280} and UV_{254} (Figure 4.29). Initial adsorptive removal of humic acid could also be assessed by the specified UV-vis parameters. The removal efficiencies were 68%, 59%, 49% and 47% for $Color_{436}$, UV_{365}, UV_{280} and UV_{254}, respectively.

For the irradiation period of 10 minutes, the removal efficiency of 30 kDa fraction of humic acid was higher than all of the other higher molecular size fractions irrespective of the expressed UV-vis parameter. While 73% of $Color_{436}$ was removed in 10 minutes of irradiation, 97% removal was achieved after 40 minutes. For UV_{365}, the removal of 30 kDa fraction of humic acid was reached to 97% upon irradiation period of 40 minutes. UV_{254} was removed from the suspension about 63% and 97% after 10 and 40 minutes irradiation times, respectively.

4.3.4.2. Fluorescence Spectroscopic Evaluation of 30 kDa Fraction of Humic Acid During Photocatalytic Degradation. Emission scan fluorescence spectra of photocatalytically treated 30kDa fraction of humic acid samples were displayed in Figure 4.30. It could be noticed that excitation wavelength of 360 nm caused a major peak in the region of 450 nm as recorded for the raw humic acid, 0.45µm filtered fraction of humic acid and 100 kDa fraction of humic acid. Although a slight shift to lower wavelengths (~ 10 nm) was recorded in the emission maxima of fluorescence emission scan spectra, comparisons were based on the λ_{max} at 450 nm.

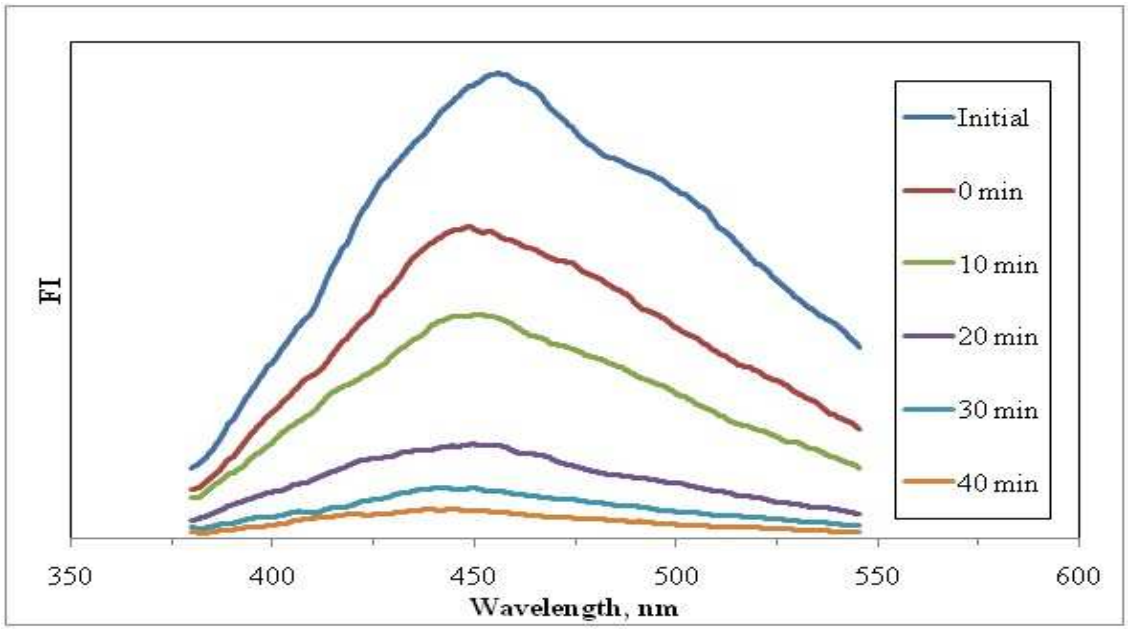

Figure 4.30. Emission scan fluorescence spectra of 30 kDa fraction of humic acid during photocatalytic degradation (Initial represents 30 kDa fraction of humic acid).

A significant decrease in FI was recorded for initial adsorption of 30 kDa fraction of humic acid. Starting from time zero to 20 minutes of experimental sequence, emission fluorescence intensities declined. Especially after 30 minutes of irradiation time, the major started to disappear and even at 40 minutes of irradiation time, there was no detectable peak in the emission scan fluorescence spectra.

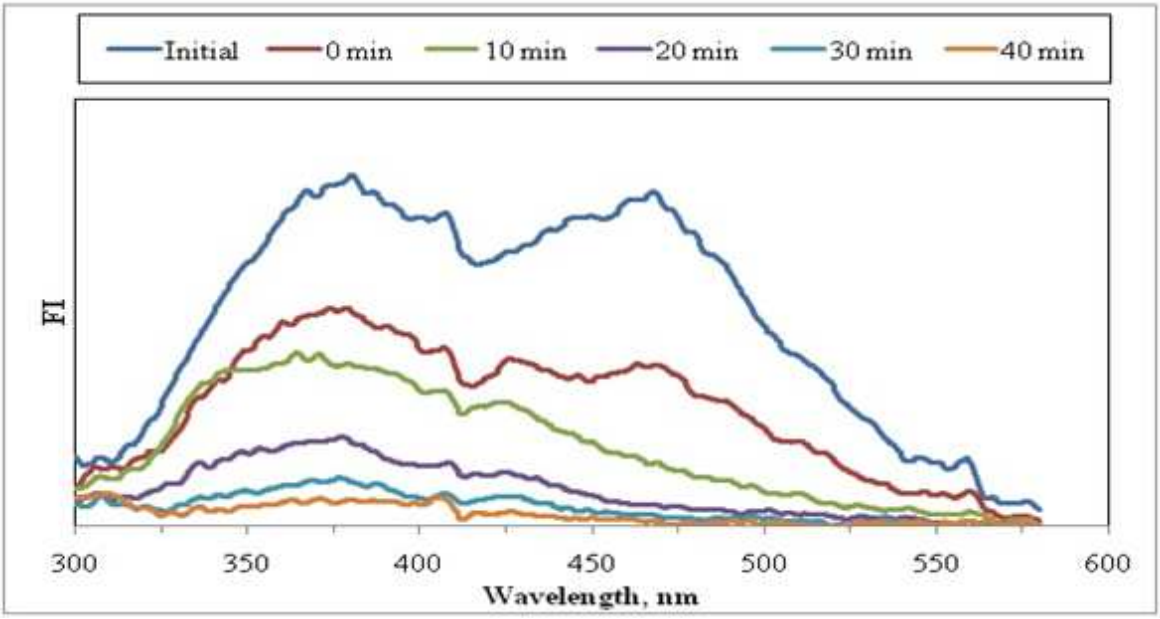

Figure 4.31. Synchronous scan fluorescence spectra of 30 kDa fraction of humic acid during photocatalytic degradation (Initial represents 30 kDa fraction of humic acid).

Synchronous fluorescence scan spectra of each molecular size fractions such as 100 kDa and 30 kDa fraction of humic acids exhibited a decreasing trend in terms of fluorescence intensity (Uyguner and Bekbolet, 2005a). Synchronous scan spectra of 30 kDa fraction of humic acid as shown in Figure 4.31, displayed two main peaks around wavelengths of 470 nm and 370 nm. Initial adsorptive removal (t=0) of 30 kDa fraction of humic acid could also be visualized by the synchronous scan fluorescence spectra displaying a quite significant FI decrease at both of the fluorescence maxima wavelengths.

Following oxidative treatment both the fluorescence spectral features as well as the FI were significantly changed that could also be visualized by the spectra recorded even after 10 minutes of irradiation time. Further irradiation conditions (20 min) resulted in

decreased fluorescence intensities and for the irradiation period of 30 minutes the absence of both of the peaks demonstrated the formation of different fluoresence emitting humic centers revealing a contnium of fluorescence intensities. Upon further irradiation period of 40 minutes, the synchronous scan fluorescence spectra demostrated a featureless regime.

4.3.5. Photocatalytic Degradation of Raw Humic Acid in the Presence of Zinc

For the assessment of the photocatalytic degradation of humic acid in the presence of 0.1 mg L^{-1} zinc, different molecular size fractions such as 0.45µm filtered fraction, 100 kDa fraction and 30 kDa fraction were also used in a comparative manner as presented previously for the humic acid fractions. The oxidized raw humic acid samples in the presence of zinc were evaluated by UV-vis spectra and fluorescence spectra as well as by the specified UV-vis and fluorescence parameters.

4.3.5.1. UV-vis Spectroscopic Evaluation of Raw Humic Acid During Photocatalytic Degradation in the Presence of Zn. UV-vis spectra of the raw humic acid in the presence of zinc showed a gradually declining trend with respect to increasing wavelength in the 200-600 nm region (Figure 4.32). Contrary to the UV-vis spectra of humic acid, a substantial increase in absorption was observed in the spectral region of 200-235 nm. The UV-vis spectra of “initial” followed the same trend of raw humic acid in the 235-600 nm wavelength region. In the study of Uyguner and Bekbolet, 2007, the similar conditions were observed in the UV-vis spectra of humic acid in the presence of manganese ions. Irradiation time dependent changes were also followed by spectroscopic properties during humic acid photocatalytic degradation starting with t = 0 min which was the initial titanium dioxide introduction to the humic acid solution prior to irradiation. Initial adsorptive removal of humic acids could also be visualized by examining the UV-vis spectra with respect to the UV-vis spectra recorded humic acids under dark conditions. Moreover, in the absence of zinc the UV-vis spectra of raw humic acid showed that the irradiation period of 10 min didnot significantly alter the removal profile as seen by the UV-vis spectra recorded for t=0 min and t=10 min had the similar trend (Figure 4.16). After irradiation time of 30 minutes, the degradation of humic acid displayed a significant decrease in the UV-vis absorbance retaining the similar trend.

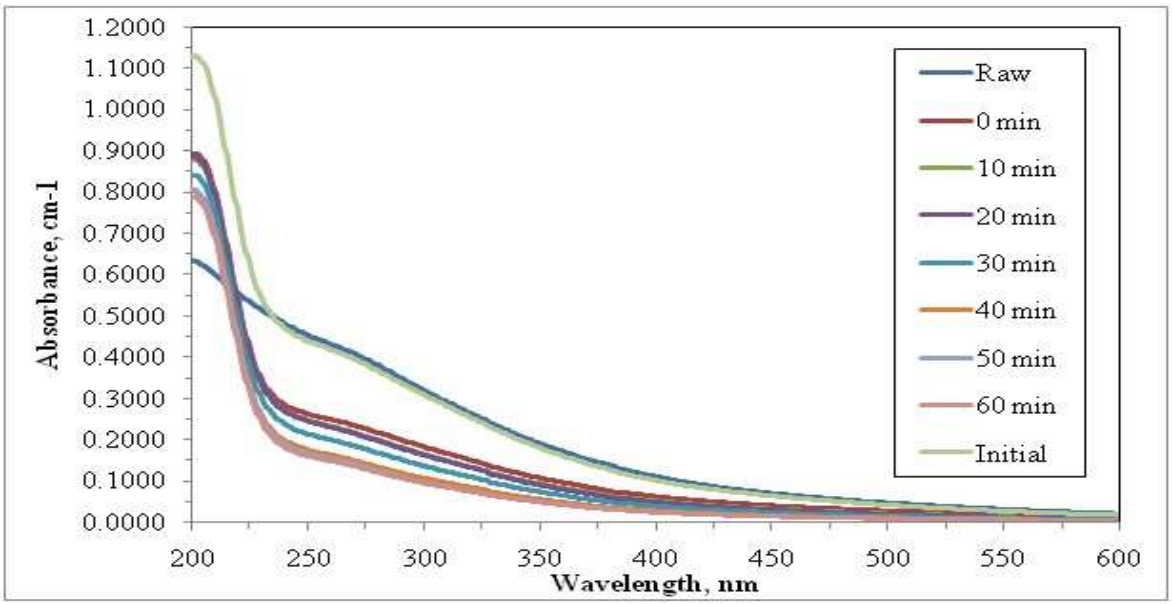

Figure 4.32. UV-vis spectra of raw humic acid during photocatalytic degradation in the presence of zinc (''Raw'' represents raw humic acid, ''Initial'' represents raw humic acid and zinc binary system).

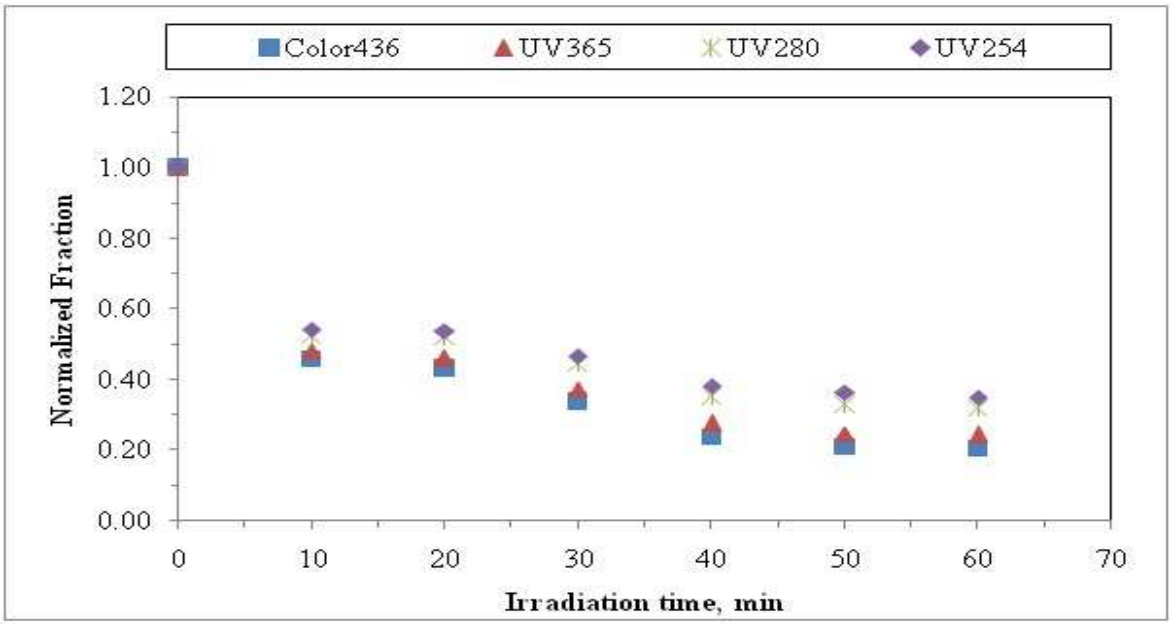

Figure 4.33. Normalized $Color_{436}$, UV_{365}, UV_{280}, and UV_{254} values of raw humic acid with respect to irradiation time in the presence of zinc.

Furthermore, the photocatalytic degradation of humic acid in the presence of zinc was evaluated in terms of UV-vis parameters as expressed by $Color_{436}$, UV_{365}, UV_{280} and UV_{254}. The remaining fractions of the specified parameters were displayed with respect to irradiation time for simplicity purposes (Figure 4.33). Initial adsorptive removals of humic acid were found to be 42%, 44%, 43% and 42% for $Color_{436}$, UV_{365}, UV_{280} and UV_{254}, respectively. The presence of zinc did not alter significantly ($\leq$ 5%) the initial adsorptive removal of humic acid onto TiO_2. In 30 minutes of irradiation time, all of the UV-vis parameters expressed more than 50 % removal efficiencies. While 54% of $Color_{436}$ was removed in 10 minutes of irradiation, following photocatalysis 79% removal was achieved after 60 minutes. 46% removal was observed in 10 minutes irradiation time for UV_{254}. Similar with $Color_{436}$, UV_{254} was removed from the suspension about 65% after 60 minutes irradiation times. Comparatively lower removal efficiencies were expected for UV_{254} with refence to $Color_{436}$ (Uyguner and Bekbolet, 2007; Uyguner and Bekbolet, 2010). In case of UV_{365} and UV_{280} parameters, 76% and 68% degradation efficiencies were achieved in 60 minutes, respectively.

With reference to the UV-vis spectral features as shown in Figure 4.32, to fulfill the purpose of the maintaining a reliable absorbance recordings in the visible region, no further irradiation period was applied.

4.3.5.2. Fluorescence Spectroscopic Evaluation of Raw Humic Acid During Photocatalytic Degradation in the Presence of Zn. Emission scan fluorescence spectra of humic acid in the presence of zinc were displayed in Figure 4.34. In accordance with the conditions set forward for raw humic acid, the fluorescence spectra of the samples were also recorded by excitation at 360 nm which resulted in a major peak at the wavelength of 450 nm. Although no general decreasing trend in emission fluorescence intensity could be visualized with respect to irradiation time, the maximum fluorescence intensity could still be detected significantly for 60 minutes of irradiation time with reference to the raw humic acid (Figure 4.18). In relation to the fluorescence emission scan spectra recorded for raw humic acid, no distinct comparative evaluation could be deduced for the assessment of the effect of the zinc ions in binary system. However, the role of initial adsorptive interaction could still be visualized by the fluorescence emission scan spectra recorded for t=0 condition.

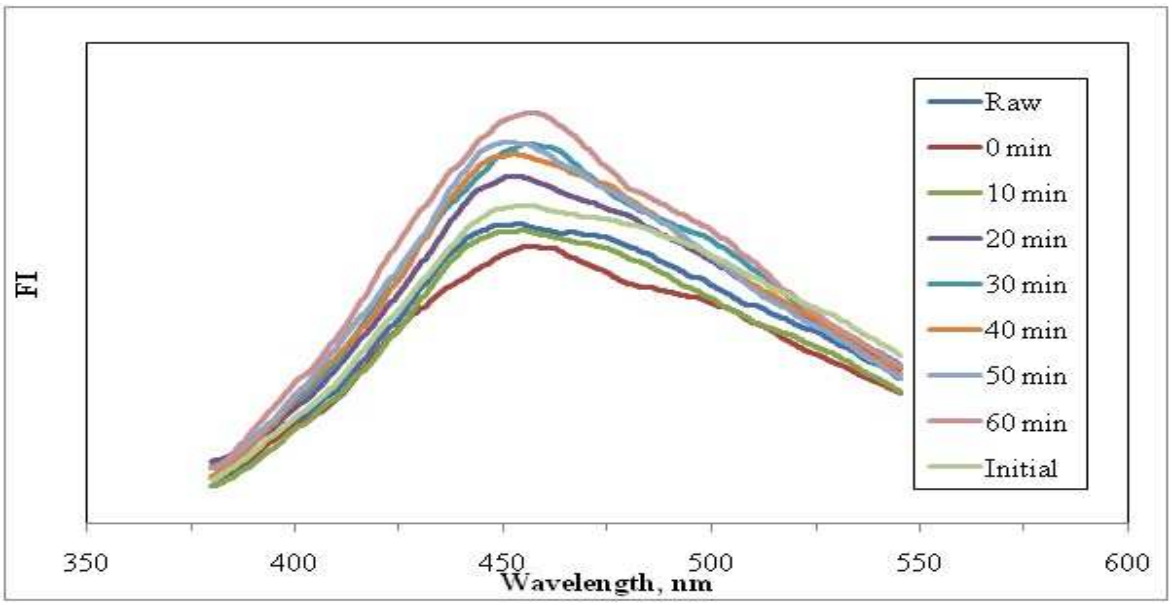

Figure 4.34. Emission scan fluorescence spectra of raw humic acid in the presence of zinc during photocatalytic degradation (‘’Raw’’ represents raw humic acid, ‘’Initial’’ represents raw humic acid and zinc binary system).

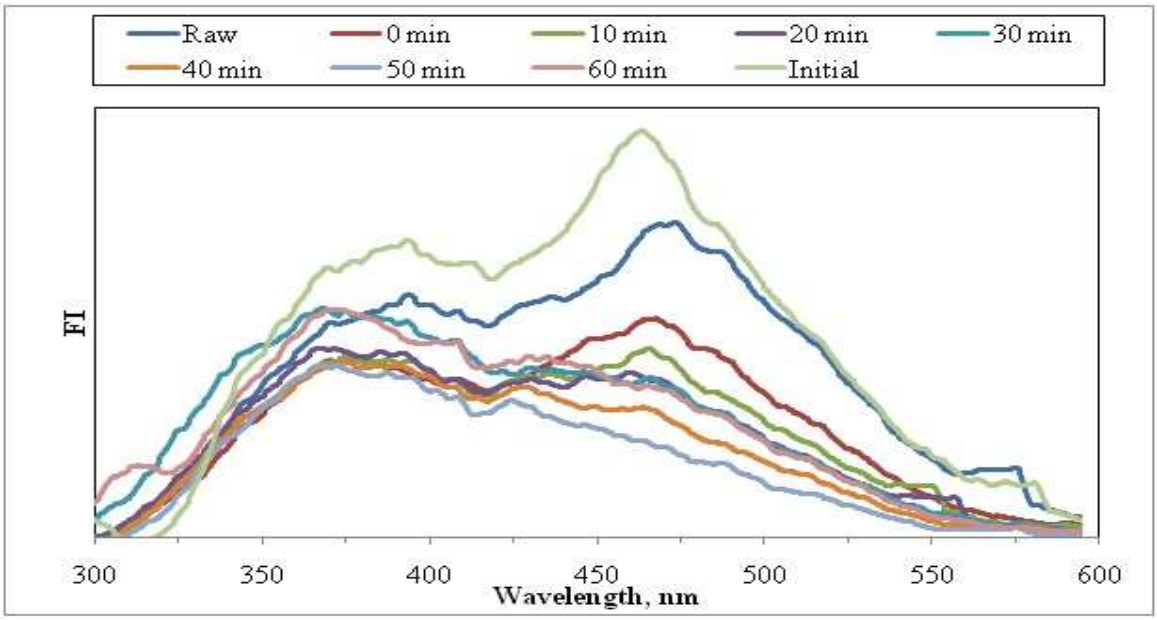

Figure 4.35. Synchronous scan fluorescence spectra of raw humic acid in the presence of zinc during photocatalytic degradation (‘’Raw’’ represents raw humic acid, ‘’Initial’’ represents raw humic acid and zinc binary system).

Synchronous scan fluorescence spectra recorded for the photocatalytically treated humic acid in the presence of zinc were shown in Figure 4.35. Synchronous scan fluorescence spectra for raw humic acid in the presence of zinc displayed a sharp peak around wavelength of 470 nm. There was also a moderate peak at 390 nm wavelength with a comparatively lower intensity. When the synchronous scan fluorescence spectra of photocatalytic degradation of humic acid in the absence of zinc was compared to the synchronous scan fluorescence spectra in the presence of zinc, it was observed that the high fluorescence trend of 30 min irradiation time was disappeared by the addition of zinc (Figure 4.19). Under prolonged irradiation conditions (60 mins), the fluorescence intensity maxima at 470 nm was completely removed and a new fluorescence intensity maxima at 375 nm was found to be significantly evident with a detectable intensity value. The shift of fluorescence maxima to lower wavelengths could be expalined by the formation of new fluorophores during photocatalysis (Uyguner and Bekbolet, 2005a). Moreover, the observed shift was also found to be present in the absence of zinc.

4.3.6. Photocatalytic Degradation of 0.45µm Filtered Fraction of Humic Acid in the Presence of Zinc

Photocatalytic degradation of 0.45µm filtered fraction of humic acid in the presence of zinc were evaluated by UV-vis spectra and fluorescence spectra as well as by the specified UV-vis and fluorescence parameters.

4.3.6.1. UV-vis Spectroscopic Evaluation of 0.45µm Filtered Fraction of Humic Acid During Photocatalytic Degradation in the Presence of Zn. UV-vis spectra displayed a logarithmic decaying shape for all of the samples obtained after photocatalytic treatment of 0.45µm filtered fraction of humic acids in the presence of zinc (Figure 4.36). The presence of zinc ions caused a dramatic effect on the UV-vis spectra of humic acid. A substantial increase in absorption was observed in the spectral region of 200-235 nm. The UV-vis spectra followed the same trend of raw humic acid in the 235-600 nm wavelength region. For longer irradiation time periods, the spectra showed very low absorbance values especially at ~ 250 nm wavelength.

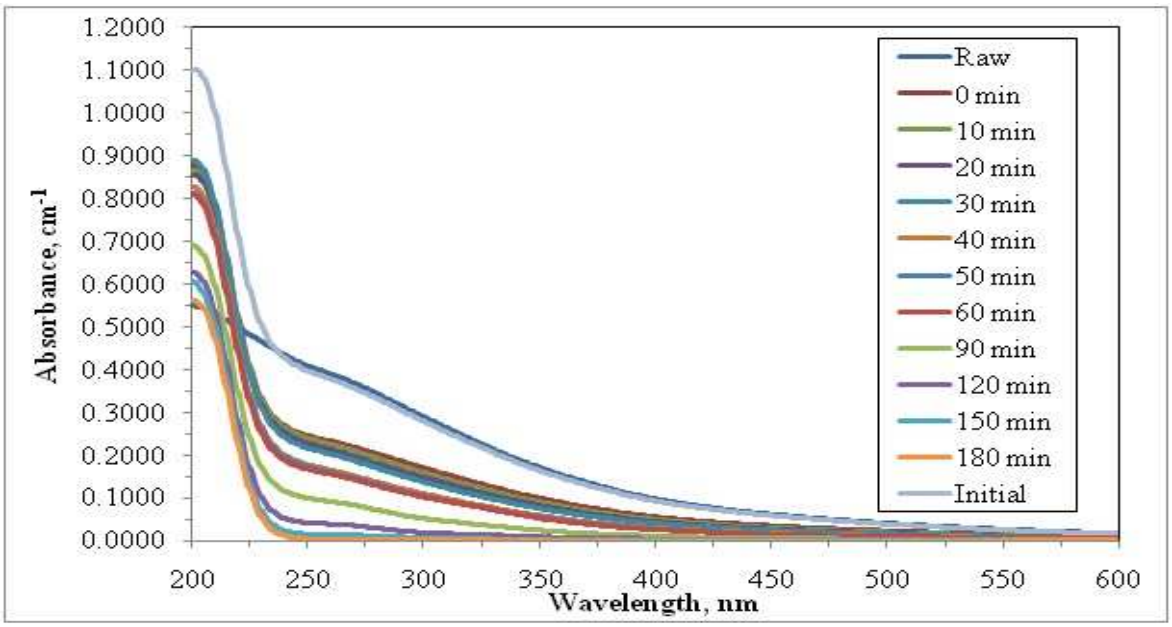

Figure 4.36. UV-vis spectra of 0.45µm filtered fraction of humic acid during photocatalytic degradation in the presence of zinc (‘’Raw’’ represents 0.45µm filtered fraction of humic acid, ‘’Initial’’ represents 0.45µm filtered fraction of HA and zinc binary system).

The photocatalytic degradation profile of humic acid in the presence of metal ions displayed the same basic, featureless pattern of monotonous decline as a function of wavelength and a decrease in the absorbance values was observed with the increasing irradiation time during photocatalytic oxidation (Uyguner and Bekbolet, 2007, Uyguner and Bekbolet, 2010). In general, chromophores that are responsible for the absorbances in the UV-vis spectral region consist of conjugated double bonds and lone pair of electrons like those associated with oxygen, sulphur, and halogen atoms. It was assumed that the interactions of natural organic matter with metals took place primarily at the sites that form the strongest bond i.e. coordinate bonding and chelating sites followed by the attraction with the weaker sites i.e. electrostatic bonding and water bridging sites (Stevenson, 1994). However, the effect of these interactions could not be verified clearly by the observed featureless UV-vis spectra that were recorded under all experimental conditions, therefore more specific spectroscopic tools should be employed for the elucidation of the structural and conformational changes (Uyguner, 2005).

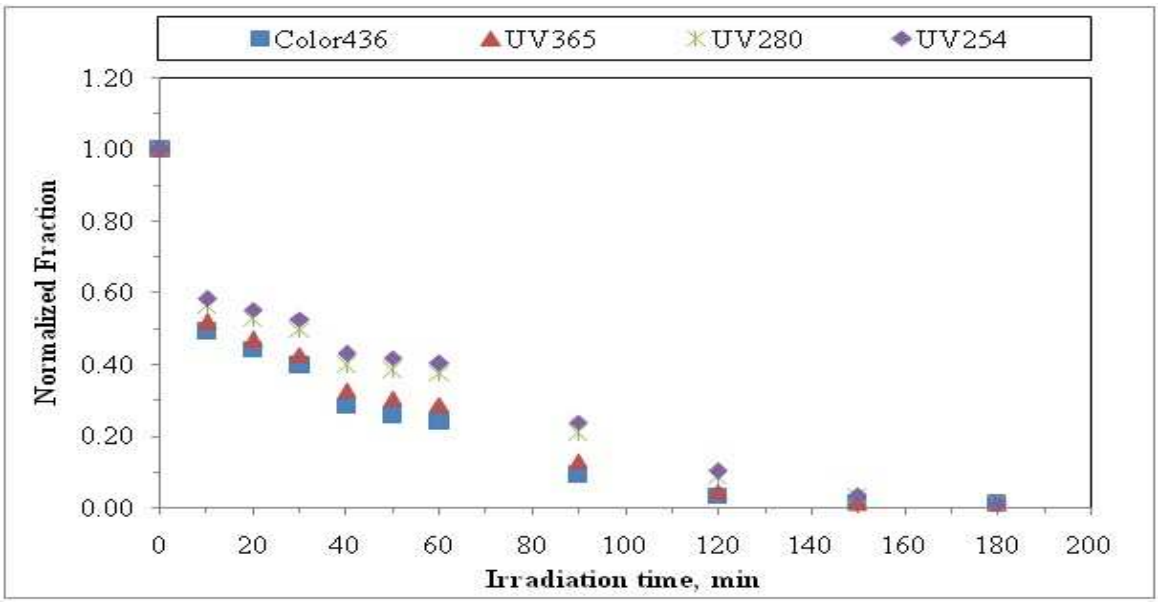

Figure 4.37. Normalized $Color_{436}$, UV_{365}, UV_{280} and UV_{254} values of 0.45µm filtered fraction of humic acid with respect to irradiation time in the presence of zinc.

Photocatalytic degradation of 0.45µm filtered fraction of humic acids in the presence of zinc was also evaluated in terms of UV-vis parameters as expressed by $Color_{436}$, UV_{365}, UV_{280} and UV_{254} (Figure 4.37). Initial adsorptive removal efficiencies of 0.45µm filtered fraction of humic acid in the presence of zinc were found to be 43%, 42%, 41% and 40% for $Color_{436}$, UV_{365}, UV_{280} and UV_{254}, respectively. The presence of zinc ions altered initial adsorptive removal of 0.45µm filtered fraction of humic acid by approximately 20%. The removal percentage for photocatalytic degradation of 0.45µm filtered fraction humic acid in the presence of zinc is higher than in the absence of zinc in short time periods, such as 10 minutes. 48% removal of UV_{365} and 44% removal of UV_{280} were also recorded at the end of 10 minutes.While 51% of $Color_{436}$ was removed in 10 minutes of irradiation period, 76% removal was achieved after 60 minutes.UV_{254} was removed from the suspension about 42% and 60% after 10 and 60 minutes irradiation times respectively. Furthermore at the end of 120 minutes of irradiation time, $\leq$ 10% of humic acid was found to be present as expressed by all of the specified UV-vis parameters. After 180 minutes of irradiation time period, no detectable UV-vis parameter could be attained for the photocatalytic degradation of 0.45µm filtered fraction of humic acid in the presence of zinc.

4.3.6.2. Fluorescence Spectroscopic Evaluation of 0.45µm Filtered Fraction of Humic Acid During Photocatalytic Degradation in the Presence of Zn. Emission scan fluorescence spectra of photocatalytically treated 0.45µm filtered fraction of humic acid in the presence of zinc samples were displayed in Figure 4.38.

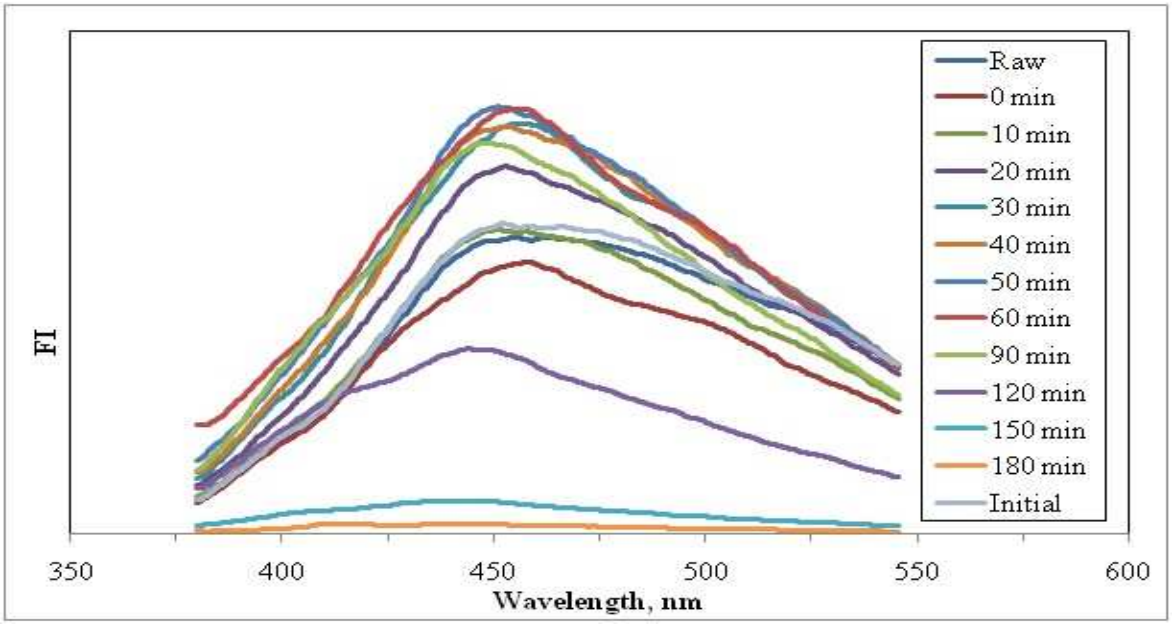

Figure 4.38. Emission scan fluorescence spectra of 0.45µm filtered fraction of humic acid during photocatalytic degradation in the presence of zinc (''Raw'' represents 0.45µm filtered fraction of humic acid, ''Initial'' represents 0.45µm filtered fraction of HA and zinc binary system).

It could be stated that through the excitation of humic moities at wavelength of 360 nm caused a major peak in the region of 450 nm as was also recorded for the raw 0.45µm filtered fraction of humic acid in the absence of zinc. The fluorescence intensities displayed an increasing trend with respect to increasing irradiation period from time 0 to 60 minutes. While the trend observed for the emission scan fluorescence spectra of the 0.45µm filtered fraction of humic acid and zinc binary system at t=0 min condition displayed the lowest fluorescence intensity profile, the spectrum of 50 minutes of reaction period crossed over with the recorded emission scan spectrum for the photocatalytically treated sample for 60 minutes. The highest fluorescence intensities were obtained at 60 minutes of reaction time expressing the formation of new highly fluorescent centers. After

prolonged irradiation time periods, the emission scan fluorescence peak at 450 nm disappeared and the trend became close to a linear form.

Synchronous scan spectra of 0.45 µm filtered fraction of humic acid in the presence of zinc displayed a continuum of fluorescence intensities with respect to wavelength except for certain irradiation time periods (Figure 4.39).

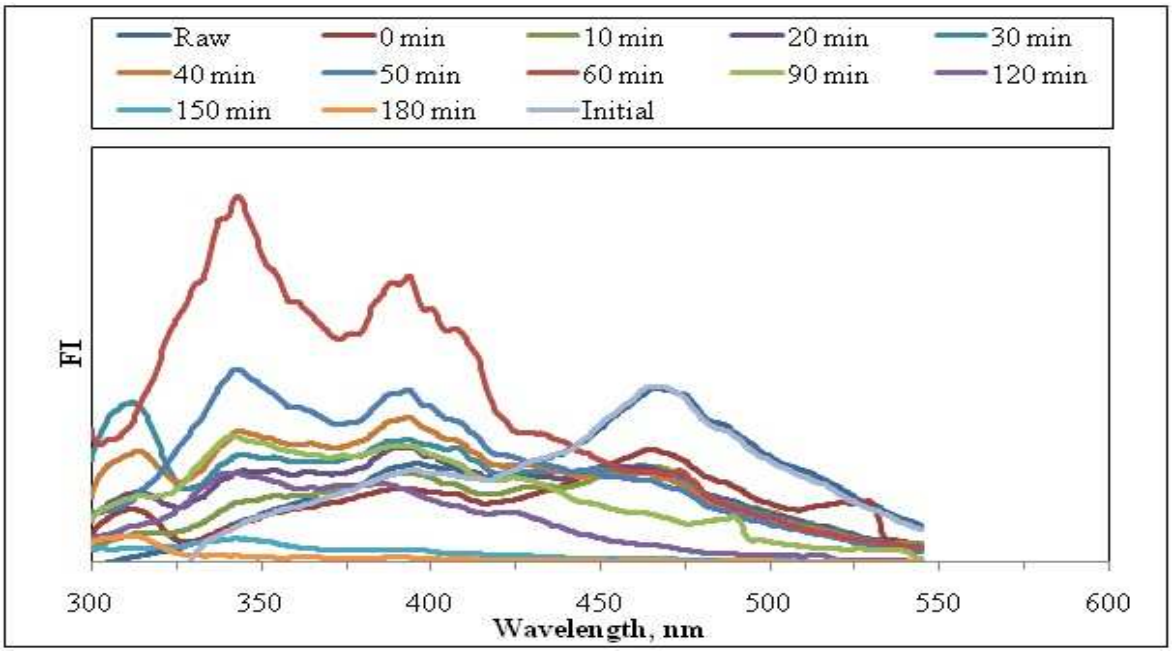

Figure 4.39. Synchronous scan fluorescence spectra of 0.45µm filtered fraction of humic acid during photocatalytic degradation in the presence of zinc (‘’Raw’’ represents 0.45µm filtered fraction of humic acid, ‘’Initial’’ represents 0.45µm filtered fraction of HA and zinc binary system).

Synchronous scan fluorescence spectra of 0.45 µm filtered fraction of humic acid did not exhibit similar fluorescence properties in comparison to raw humic acid. After increased irradiation time periods, while the major peak at 450 nm was disappeared, the new peaks were occurred at 345 and 395 nm. The presence of different peaks at different wavelengths could be attributed to the presence of zinc. For “initial” representing 0.45µm filtered fraction of HA and zinc binary system and raw humic acids, the UV-vis spectra followed the same trend.

The recorded synchronous scan fluorescence spectra of the photocatalytically treated 0.45 µm filtered fraction of humic acid in the presence of zinc samples under posttreatment conditions indicated the presence of structural changes leading to the formation and removal of fluorescent centers during photocatalysis. The increase in the FI for 60 minutes irradiation time had been associated with the increasing content of C=O, aromatic C and COOH groups (Senesi, 1990).

4.3.7. Photocatalytic Degradation of 100 kDa Fraction of Humic Acid in the Presence of Zinc

Photocatalytic degradation of 100 kDa fraction of humic acid in the presence of zinc were evaluated by UV-vis spectra and fluorescence spectra as well as by the specified UV-vis and fluorescence parameters.

4.3.7.1. UV-vis Spectroscopic Evaluation of 100 kDa Fraction of Humic Acid during Photocatalytic Degradation in the Presence of Zn. 100 kDa fraction of humic acid in the presence of zinc was subjected to photocatalysis and evaluated in the same manner as reported for 100 kDa humic acid in the absence of zinc (Figure 4.24). In general, the UV-vis spectra of 100 kDa fraction of humic acid in the presence of zinc showed a gradually decreasing trend with the respect to wavelength in the 200-600 nm region. The presence of zinc ions caused a dramatic effect on the UV-vis spectra of humic acid (Figure 4.40). A substantial increase in absorption was observed in the spectral region of 200-235 nm. Under all irradiation conditions, the UV-vis spectra followed the same trend of 100 kDa fraction of humic acid in the 235-600 nm wavelength region. Moreover, the UV-vis spectra displayed a $\Delta Abs \leq 0.003$ in the wavelength region of 230-350 nm followed by a complete overlapping trend in the wavelength region of 350-600 nm indicationg the role of overlapping chromophores rather than the elimination of the UV-vis absorbing centers. It should also be considered that the recorded absorptivities were quite low to be considered as significantly discriminative. Moreover, the UV-vis spectra displayed the importance of the UV-absorbing centers (UV_{365}, UV_{280} and UV_{254}) with respect to the color forming moities ($Color_{436}$) for the assessment of an indicative parameter that could be used the photocatalytic degradation of humic acid.

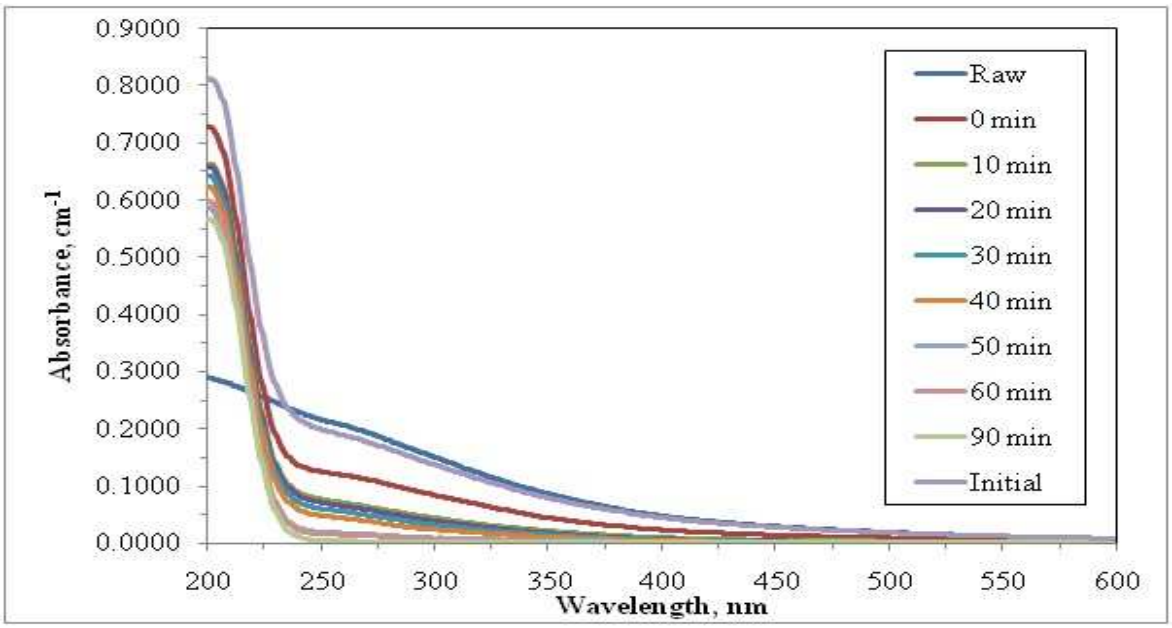

Figure 4.40. UV-vis spectra of 100 kDa fraction of humic acid during photocatalytic degradation in the presence of zinc (''Raw'' represents 100 kDa fraction of humic acid, ''Initial'' represents 100 kDa fraction of HA and zinc binary system).

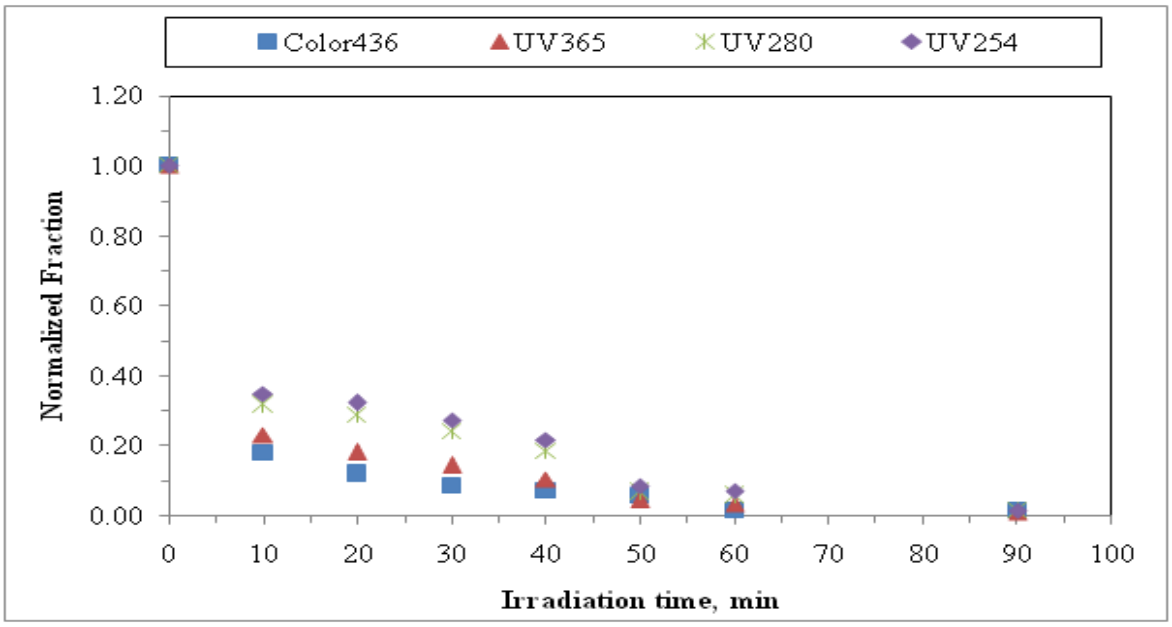

Figure 4.41. Normalized $Color_{436}$, UV_{365}, UV_{280} and UV_{254} values of 100 kDa fraction of humic acid with respect to irradiation time in the presence of zinc.

The effect of prolonged irradiation time was also shown by the UV-vis spectra recorded for 60 and 90 minutes. It was observed that there were no characteristic absorbance recordings after long irradiation time periods. For example, in 90 minutes the absorbance values nearly reached to zero at 350 nm wavelength. These conditions were provided for 0.45 µm filtered fraction of humic acid at 180 minutes irradiation time.

Photocatalytic degradation of 100 kDa fraction of humic acid in the presence of zinc was also evaluated in terms of UV-vis parameters as expressed by $Color_{436}$, UV_{365}, UV_{280} and UV_{254} (Figure 4.41). The detected initial adsorptive removal efficiency of 100 kDa fraction of humic acid were 53%, 50%, 43% and 42% for $Color_{436}$, UV_{365}, UV_{280} and UV_{254}, respectively. The effect of zinc ions on the initial adsorption of 100 kDa fraction of humic acid could be regarded as significantly greater than the effect observed for 100 kDa fraction of humic acid in the absence of zinc. While 45% of $Color_{436}$ was removed in 10 minutes of irradiation period, 81% removal was achieved after 60 minutes. In 120 minutes of irradiation time, the removal of $Color_{436}$ reached to 97%. For UV_{254}, 36% removal was observed in 10 minutes irradiation time. UV_{254} was removed from the suspension about 67% and 88% after 60 and 120 minutes irradiation times, respectively. In early stages of irradiation; such as 10 minutes, removal efficiency of 100 kDa fraction of humic acid in the presence of zinc is more than the removal efficiency attained for 100 kDa fraction of humic acid in the absence of zinc. While 82% of $Color_{436}$ removed in 10 minutes of irradiation, 65% removal achieved for UV_{254}. The removal of UV_{365} and UV_{280} are about 14% more than the photocatalytic degradation of 100 kDa fraction of humic acid in the absence of zinc. At the end of 60 minutes of irradiation time, 98%, 97%, 94% and 93% of removal was achieved for 100 kDa fraction of humic acid in the presence of zinc, for $Color_{436}$, UV_{365}, UV_{280}, UV_{254}, respectively.

4.3.7.2. Fluorescence Spectroscopic Evaluation of 100 kDa Fraction of Humic Acid During Photocatalytic Degradation in the Presence of Zn. Noticeable changes in the shape of the emission scan fluorescence spectra of 100 kDa fraction of humic acid were seen in Figure 4.42. The maximum fluorescence intensity peak was also recorded at 450 nm wavelength in accordance with the previously investigated humic acid and humic acid zinc binary systems.

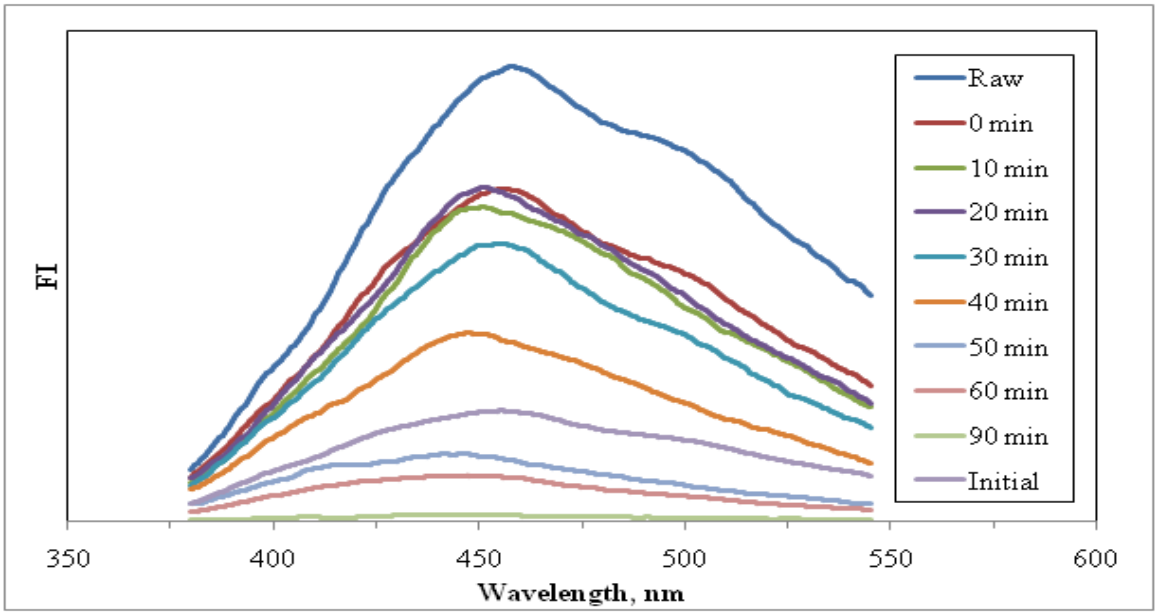

Figure 4.42. Emission scan fluorescence spectra of 100 kDa fraction of humic acid during photocatalytic degradation in the presence of zinc (‘’Raw’’ represents 100kDa fraction of humic acid, ‘’Initial’’ represents 100 kDa fraction of HA and zinc binary system).

In general it was observed that from time zero to 90 minutes of experimental sequence, all of the emission fluorescence intensities decreased. The major peak recorede at 450 nm wavelength was not found to be detectable after 40 minutes of irradiation perios and upon further irradiation time periods, the trend closed to a linear form. The similar trend was also observed for emission scan fluorescence spectra of 100 kDa fraction of humic acid in the absence of zinc.

Synchronous scan fluorescence spectra of 100 kDa fraction of humic acid in the presence of zinc displayed diverse properties as shown in Figure 4.43. Two major peaks could be detected for 100 kDa fraction of humic acid zinc binary system in the wavelength region of 350 nm to 550 nm. The presence of well defined peaks detected at around wavelength of 300 nm could be considered as specific to the studied system although some minor remarks could also be directed to the system composed of 0.45 µm filtered fraction of humic acid and zinc.

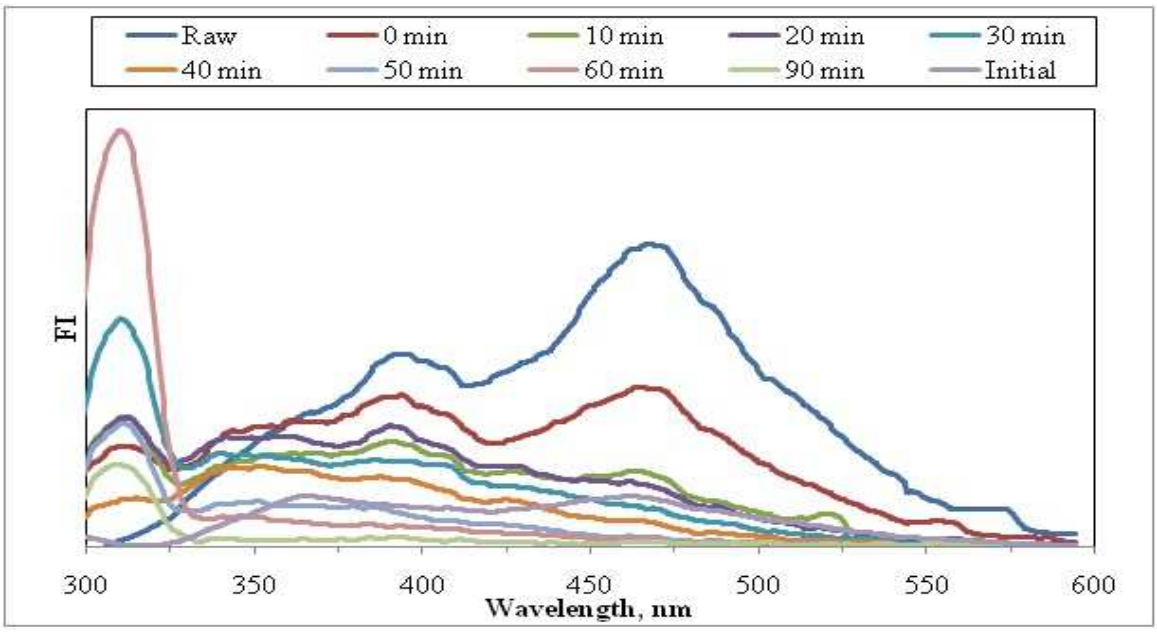

Figure 4.43. Synchronous scan fluorescence spectra of 100 kDa fraction of humic acid during photocatalytic degradation in the presence of zinc (‘’Raw’’ represents 100 kDa fraction of humic acid, ‘’Initial’’ represents 100 kDa fraction of HA and zinc binary system).

From a broader point of view, after 20 minutes of irradiation, the characteristic sharp peak of raw 100kDa fraction of humic acid in the presence of zinc completely disappeared.

4.3.8. Photocatalytic Degradation of 30 kDa Fraction of Humic Acid in the Presence of Zinc

Photocatalytic degradation of 30 kDa fraction of humic acid samples in the presence of zinc were evaluated by UV-vis spectra and fluorescence spectra as well as by the specified UV-vis and fluorescence parameters.

4.3.8.1. UV-vis Spectroscopic Evaluation of 30 kDa Fraction of Humic Acid During Photocatalytic Degradation in the Presence of Zn. As mentioned before, UV-vis spectra of humic acid displayed a monotonously decreasing trend with increasing wavelength. The presence of zinc ions caused a dramatic effect on the UV-vis spectra of humic acid (Figure 4.44). A substantial increase in absorption was observed in the spectral region of 200-235

nm. UV-vis spectra followed the same trend of raw humic acid in the 235-600 nm wavelength regions. Due to the initial very low UV-vis absorbance values of 30 kDa humic acid both in the presence and absence of zinc especially after photocatalytic degradation of humic acid, the UV-vis spectra displayed significantly low absorbance values throughout the whole wavelength region.

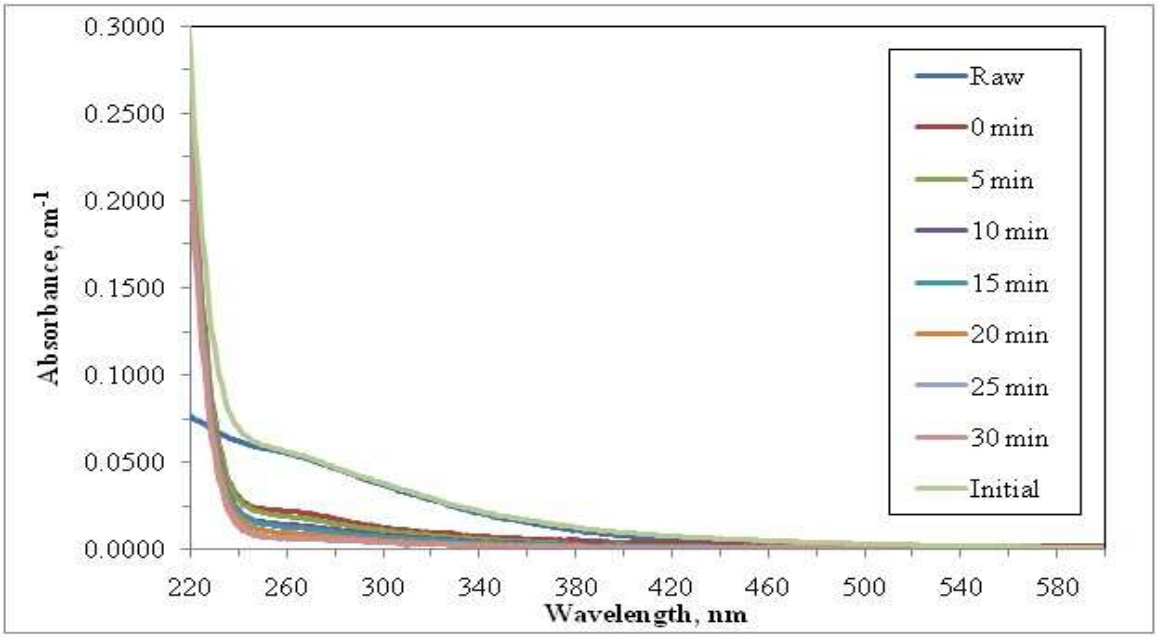

Figure 4.44. UV-vis spectra of 30 kDa fraction of humic acid during photocatalytic degradation in the presence of zinc (‘’Raw’’ represents 30 kDa fraction of humic acid, ‘’Initial’’ represents 30 kDa fraction of HA and zinc binary system).

Photocatalytic degradation of 30 kDa fraction of humic acid was also evaluated in terms of UV-vis parameters as expressed by $Color_{436}$, UV_{365}, UV_{280} and UV_{254} (Figure 4.45). It could be stated that the initial adsorptive removal efficiency of 30 kDa fraction of humic acid and zinc binary system were found to be as 59%, 62% and 60% for UV_{365}, UV_{280} and UV_{254}, respectively. Considering the significant low $Color_{436}$ in 30 kDa fraction of humic acid, the initial adsorptive removal of $Color_{436}$ should not be taken into account. Moreover, significantly higher removal efficiencies were attained for the 30 kDa fraction of humic acid in the presence of zinc in comparison to the 30 kDa fraction of humic acid in the absence of zinc. While 56% of $Color_{436}$ was removed in 10 minutes, 71% removal was

achieved after 30 minutes of irradiation time. UV_{254} was removed from the suspension about 74% and 88% after 10 and 30 minutes of irradiation periods respectively.

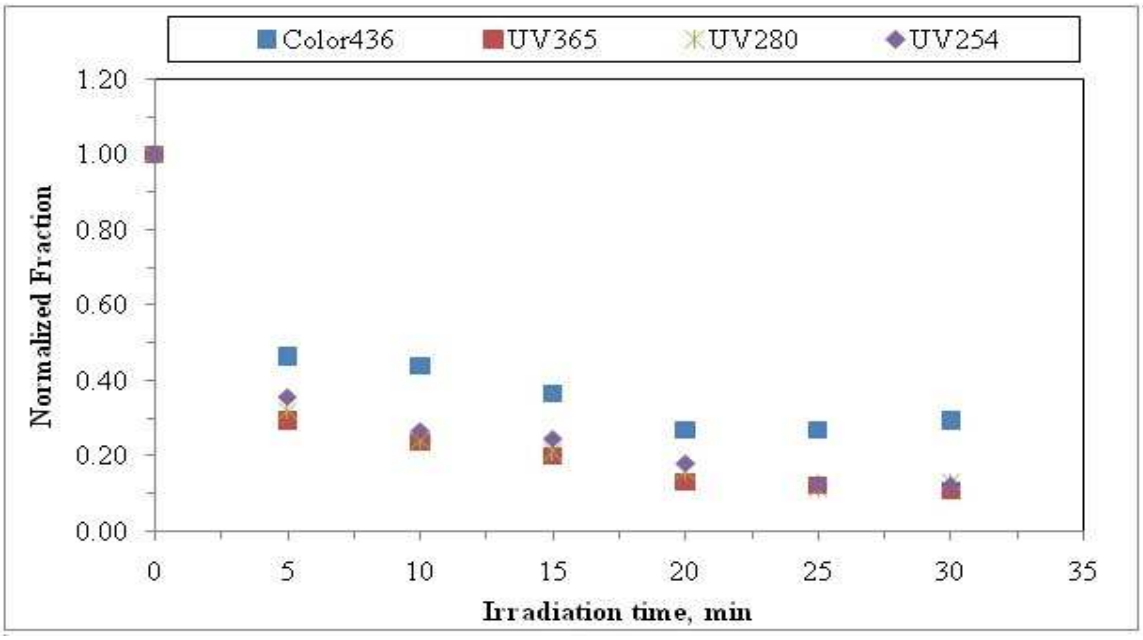

Figure 4.45. Normalized $Color_{436}$, UV_{365}, UV_{280} and UV_{254} values of 30 kDa fraction of humic acid with respect to irradiation time in the presence of zinc.

Almost 89% and 87% degradation was achieved in 30 minutes for UV_{365} and UV_{280}. In long irradiation time periods, such as 60 minutes, no recordable absorbance readings were obtained as could also be verified by the UV-vis absorption spectra.

4.3.8.2. Fluorescence Spectroscopic Evaluation of 30 kDa Fraction of Humic Acid During Photocatalytic Degradation in the Presence of Zn. Emission scan scan fluorescence spectra for oxidized 30 kDa fraction of humic acid in the presence of zinc were shown in Figure 4.46. Raw 30 kDa fraction of humic acid had a peak around 450 nm with relatively high fluorescence intensity with respect to the treated 30 kDa fraction of humic acid samples.

With increasing irradiation time, a gradual decrease in emission fluorescence intensity became evident in the emission scan fluorescence spectra. The spectrum of 10 minutes of reaction period crossed with 15 minutes of irradiation emission scan spectrum.

The similar situation was also observed for the emission fluorescence spectra recorded for 20 and 25 minutes of irradiation periods. Emission scan fluorescence spectra of “initial” displayed significantly lower intensities which were nearly in a linear trend without any significant peak at 450 nm wavelength.

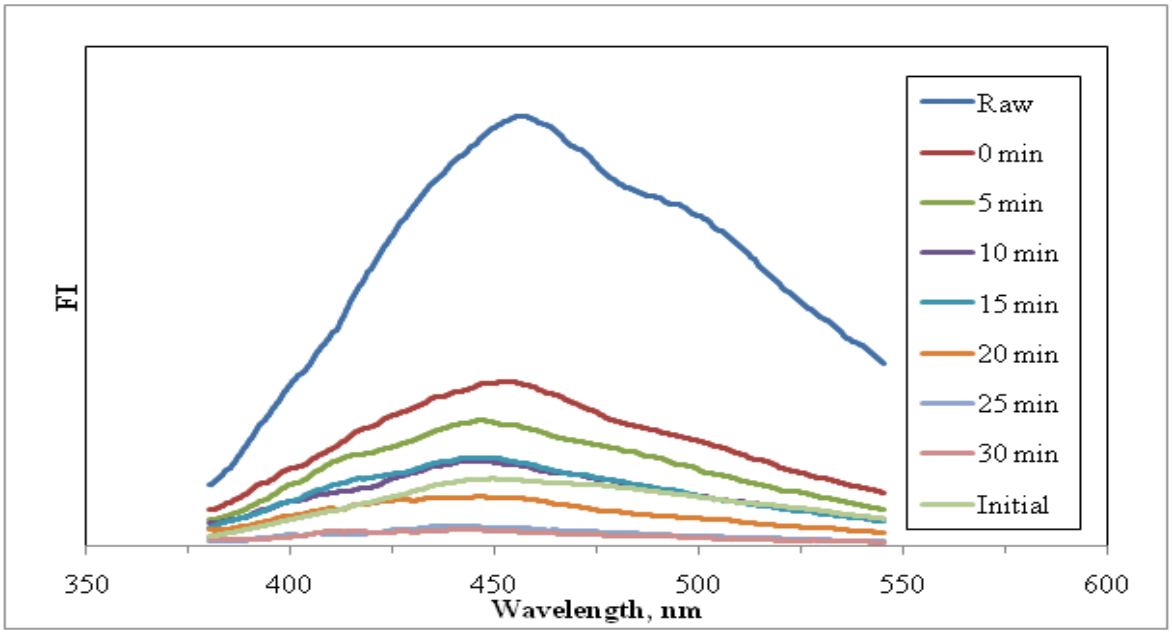

Figure 4.46. Emission scan fluorescence spectra of 30 kDa fraction of humic acid during photocatalytic degradation in the presence of zinc (‘’Raw’’ represents 30 kDa fraction of humic acid, ‘’Initial’’ represents 30 kDa fraction of humic acid and zinc binary system).

Synchronous scan fluorescence spectra of recorded during photocatalytic degradation of 30 kDa fraction of humic acid in the presence of zinc were shown in Figure 4.46. Initial adsorptive removal of 30 kDa fraction of humic acid in the presence of zinc could also be visualized by the synchronous scan fluorescence spectra displaying a quite significant FI decrease at 475 nm wavelength. Following oxidative treatment both the fluorescence spectral features as well as the FI were significantly changed that could also be detected by the spectra recorded even after 10 minutes of irradiation time. Upon further irradiation period of 20 minutes, the synchronous scan fluorescence spectra demostrated a featureless regime.

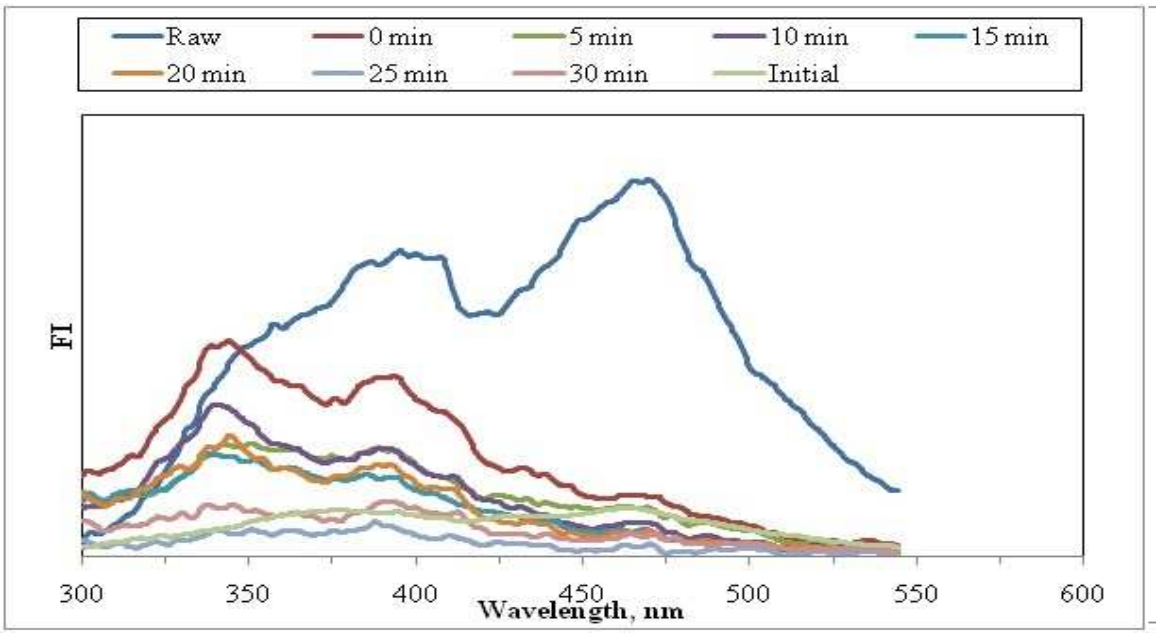

Figure 4.47. Synchronous scan fluorescence spectra of 30 kDa fraction of humic acid during photocatalytic degradation in the presence of zinc (‘’Raw’’ represents 30 kDa fraction of humic acid, ‘’Initial’’ represents 30 kDa fraction of humic acid and zinc binary system).

From a specific point of view, it could also be stated that the peak detected around 300 nm wavelengths for the 100 kDa fraction of humic acid in the presence of zinc could not be detected for this binary system. The reason could be attributed to the specific fluorescence properties of the molecular size fractions of the humic acids both in the absence and presence of zinc.

4.4. Comparative Evaluation of the Photocatalytic Degradation of Humic acid and Its Molecular Size Fractions

For comparison purposes, photocatalytic degradation data of humic acid and its molecular size fractions both in the presence and absence of zinc were evaluated. The removal efficiencies as expressed for the specified UV-vis parameters for raw, 0. 45µm filtered fraction, 100 kDa fraction and 30 kDa fraction of humic acid at 30 min and 60 min of irradiation times were calculated and given at Table 4.2.

Table 4.2. Removal efficiencies of raw humic acid, 0.45 µm filtered fraction, 100 kDa fraction and 30 kDa fraction of humic in the presence and absence of zinc after photocatalytic degradation.

Humic acid and molecular size fractions	Removal efficiency, %							
	$Color_{436}$		UV_{365}		UV_{280}		UV_{254}	
	30 min	60 min	30 min	60 min	30 min	60 min	30 min	60 min
Raw	61	83	57	80	48	71	46	69
0.45 µm ff*	62	81	58	77	50	69	48	67
100 kDa f**	89	99	83	97	76	93	74	93
30 kDa f**	95	-	99	-	91	-	90	-
Binary system; Humic acid and its molecular size fractions in the presence of zinc								
Raw	66	79	63	76	56	68	53	65
0.45 µm ff*	60	76	57	71	51	63	47	60
100 kDa f**	91	98	86	97	76	94	73	93
30 kDa f**	71	-	89	-	87	-	88	-

*filtered fraction, ** fraction

In general, the removal efficiencies of humic acid and its molecular size fractions in the absence of zinc changed in the order as 0.45µm filtered fraction ≤ Raw < 100 kDa < 30 kDa, for the specified UV-vis parameters such as $Color_{436}$ UV_{365}, UV_{280} and UV_{254}. The similar order was also observed for humic acid and its molecular size fractions in the presence of zinc, as 0.45µm filtered fraction < Raw < 100 kDa. It could be stated that 30 min of irradiation period resulted in ≥ 50 % degradation efficiency irrespective of the substrate and condition.

In performing the photocatalytic degradation experiments using humic acid as the substrate, 0.45 µm filters are used for the removal of the photocatalyst (e.g. TiO_2). Through filtration, besides the removal of the suspended photocatalyst particles, humic acid molecules are also expected to pass totally. Moreover, during the preparation step of humic acid solutions, total dissolution of the humic acid sample should be attained. Therefore in principle, raw humic acid and 0.45 µm filtered fraction of humic acid should express equal reactivities towards oxidation.The observed differences could be explained

by the structural and conformational changes that might have been occurred during filtration. Lower molecular size fractions of humic acid displayed higher removel efficiencies for all of the substrates both in the presence and absence of zinc. The reason could be expressed both by considerably lower initial concentrations and experimental conditions. Since photocatalyst dose is one of the major operational parameter in photocatalysis, the higher effective surface area per substrate concentration resulted in higher degradation rate in case of 100 kDa fraction and 30 kDa fraction of humic acid.

In the presence of metal ions under the complexation conditions, a change within the molecular size fractions of humic acids would be expected through the formation of new humic moieities induced by intra- and intermolecular bridging (Uyguner, 1999; Uyguner and Bekbolet, 2007; Uyguner and Bekbolet, 2010). The formed metal-humate complex displays distinctly different UV-vis and fluorescence spectral features which could be assessed by instrumental analyses that are presented so far for humic acid and zinc binary system. The resultant effect would be either enhancement or retardation of photocatalytic degradation performance. Considering the presented data, the presence of zinc ions displayed a retardation effect under the specified experimental conditions.

4.5. Kinetic Evaluation

In relation to the UV-vis and fluorescence spectroscopic characterization of raw and 0.45 µm filtered fraction, 100 kDa fraction and 30 kDa fraction of Aldrich humic acid, photocatalytic degradation data were processed using pseudo first order kinetic model.

4.5.1. Kinetic model

Organic compounds (e.g. humic acid) present in the illuminated titania slurry undergo many chain and consecutive reactions. In an ideal case, all intermediate compounds are fully mineralized to carbon dioxide and water. However, under the specified experimental conditions the resultant solutions contained a measurable amount of organic contents either expressed by UV-vis parameters or DOC. Photocatalytic degradation of humic substances are known to obey pseudo first order kinetic (Bekbolet et al., 1998; Bekbolet et al., 2002).

Pseudo first order kinetic model is expressed by the following equation;

$$R = - dA/dt = k A \quad (4.1)$$

The terms represent the following meanings;

R: Pseudo first order rate in terms of the specified UV-vis parameters (m^{-1} min^{-1})

A: Specified UV-vis parameters (m^{-1})

t: Irradiation time (min) and

k: Pseudo first order reaction rate constant (min^{-1}).

The related half life, $t_{1/2}$ (min) values could also be assessed by the Equation (4.2);

$$t_{1/2} = 0.693/k \quad (4.2)$$

According to the data obtained by photocatalytic degradation experiments, pseudo first order reaction rate constants, half-life values, related correlation coefficients of photocatalytic degradation and rates are calculated (R^2 >0.70) and given in respective tables.

4.5.2. Kinetic Modeling of Photocatalytic Degradation of Raw Humic Acid

The kinetic evaluation of the experimental data for the photocatalytic degradation of raw humic acid revealed the following pseudo first order kinetic model parameters for $Color_{436}$, UV_{365}, UV_{280} and UV_{254} as presented in Table 4. 3. Pseudo first order degradation rate constansts (k, min^{-1}) were found to be $2.39x10^{-2}$, $2.21x10^{-2}$, $1.73x10^{-2}$ and $1.61x10^{-2}$ for the UV-vis parameters specified as $Color_{436}$, UV_{365}, UV_{280} and UV_{254}, respectively. Lower rate constants were attained with respect to photocatalytic degradation of humic acid in the presence of copper ions (Uyguner and Bekbolet, 2010). The removal of color forming moieties was found to be relatively faster than the UV absorbing centers (~ > 30%) as expressed by UV_{280} and UV_{254}.

Table 4.3. Pseudo first order kinetic model parameters for the photocatalytic degradation of raw humic acid.

Parameter	k, min^{-1}	$t_{1/2}$, min	Rate, m^{-1} min^{-1}
$Color_{436}$	$2.39x10^{-2}$	29	0.1957
UV_{365}	$2.21x10^{-2}$	31	0.3660
UV_{280}	$1.73x10^{-2}$	40	0.6548
UV_{254}	$1.61x10^{-2}$	43	0.7084

The corresponding half life ($t_{1/2}$, min) values were found to be in the range of 29-43 min. Photocatalytic degradation rates (R, m^{-1} min^{-1}) were calculated by using the kinetic rate equation (4.1.) and expressed by the decreasing order of $UV_{254} > UV_{280} > UV_{365} > Color_{436}$. Uyguner and Bekbolet (2005a), studied the pseudo first order model reactions and reaction rate constants k (min^{-1}) for humic acid removal were found to be decreasing in the range of $2.98x10^{-2}$ to $2.01x10^{-2}$ for specified UV-vis parameters of $Color_{436}$, UV_{365}, UV_{280} and UV_{254}.

4.5.3. Kinetic Modeling of Photocatalytic Degradation of Raw Humic Acid in the Presence of Zinc

The kinetic evaluation of the experimental data for the photocatalytic degradation of raw humic acid in the presence of 0.1 mg mL^{-1} zinc revealed the following pseudo first order kinetic model parameters for $Color_{436}$, UV_{365}, UV_{280} and UV_{254} as presented in Table 4.4.

Pseudo first order degradation rate constants (k, min^{-1}) were found to be $2.48x10^{-2}$, $2.18x10^{-2}$, $1.70x10^{-2}$ and $1.54x10^{-2}$ for the UV-vis parameters specified as $Color_{436}$, UV_{365}, UV_{280} and UV_{254}, respectively. The corresponding half life ($t_{1/2}$, min) values were in the range of 28-45 min. Photocatalytic degradation rates (R, m^{-1} min^{-1}) were calculated by using the rate equation (4.1) expressed by removals in the decreasing order of $UV_{254} > UV_{280} > UV_{365} > Color_{436}$.

Table 4.4. Pseudo first order kinetic model parameters for the photocatalytic degradation of raw humic acid in the presence of zinc.

Parameter	k, min^{-1}	$t_{1/2}$, min	Rate, m^{-1} min^{-1}
$Color_{436}$	$2.48x10^{-2}$	28	0.2031
UV_{365}	$2.18x10^{-2}$	32	0.3610
UV_{280}	$1.70x10^{-2}$	41	0.6434
UV_{254}	$1.54x10^{-2}$	45	0.6776

The presence of zinc ions altered the pseudo first order kinetic model rate constants by ≤ 5% for all of the specified parameters. The removal rates were also found to be comparatively similar to the raw humic acid photocatalytic degradations profile. The reason could be attributed to the considerably low concentrations of zinc with respect to humic acid concentration. The free binding sites of humic acids could still be available for the pre-adsorption of humic acid onto TiO_2 surface. The color forming moieties as well as the UV absorbing centers were removed by adsorption onto TiO_2 surface by ≤ 40% both in the presence and the absence of zinc ions.

4.5.4. Kinetic Modeling of Photocatalytic Degradation of 0.45 µm Filtered Fraction of Humic Acid

The kinetic evaluation of the experimental data for the photocatalytic degradation of 0.45 µm filtered fraction of revealed the following pseudo first order kinetic model parameters for $Color_{436}$, UV_{365}, UV_{280} and UV_{254} as presented in Table 4.5.

Pseudo first order degradation rate constansts (k, min^{-1}) were found to be $2.73x10^{-2}$, $2.36x10^{-2}$, $1.79x10^{-2}$ and $1.63x10^{-2}$ for the UV-vis parameters specified as $Color_{436}$, UV_{365}, UV_{280} and UV_{254}, respectively. The removal of color forming moieties was found to be relatively faster than the UV absorbing centers (> 35%) as expressed by UV_{280} and UV_{254}. The corresponding half life ($t_{1/2}$, min) values were in the range of 25-43 min. Table 4.5.

Table 4.5. Pseudo first order kinetic model parameters for the photocatalytic degradation of 0.45 µm filtered fraction of humic acid.

Parameter	k, min^{-1}	$t_{1/2}$, min	Rate, m^{-1} min^{-1}
$Color_{436}$	$2.73x10^{-2}$	25	0.2050
UV_{365}	$2.36x10^{-2}$	29	0.3722
UV_{280}	$1.79x10^{-2}$	39	0.6668
UV_{254}	$1.63x10^{-2}$	43	0.7069

Photocatalytic degradation rates (R, m^{-1} min^{-1}) were calculated by using the rate equation (4.1) expressed by the decreasing order of UV_{254} > UV_{280} > UV_{365} > $Color_{436}$. Considering that the 0.45µm filtered fraction of humic acid should express similarities with raw humic acid, the pseudo first order degradation kinetic parameters were also expected to be similar (Tables 4.3 and Table 4.5).

4.5.5. Kinetic Modeling of Photocatalytic Degradation of 0.45 µm Filtered Fraction of Humic Acid in the Presence of Zinc

The kinetic evaluation of the experimental data for the photocatalytic degradation of 0.45 µm filtered fraction of humic acid in the presence of 0.1 mg L^{-1} zinc revealed the following pseudo first order kinetic model parameters for $Color_{436}$, UV_{365}, UV_{280} and UV_{254} as presented in Table 4.6.

Table 4.6. Pseudo first order kinetic model parameters for the photocatalytic degradation of 0.45 µm filtered fraction of humic acid in the presence of zinc.

Parameter	k, min^{-1}	$t_{1/2}$, min	Rate, m^{-1} min^{-1}
$Color_{436}$	$2.58x10^{-2}$	27	0.1938
UV_{365}	$2.56x10^{-2}$	27	0.4037
UV_{280}	$2.33x10^{-2}$	30	0.8679
UV_{254}	$2.34x10^{-2}$	30	1.0149

Pseudo first order degradation rate constansts (k, min^{-1}) were found to be $2.58x10^{-2}$, $2.56x10^{-2}$, $2.33x10^{-2}$ and $2.34x10^{-2}$ for the UV-vis parameters specified as $Color_{436}$, UV_{365}, UV_{280} and UV_{254}, respectively. The corresponding half life ($t_{1/2}$, min) values were in the range of 27-30 min. Photocatalytic degradation rates (R, m^{-1} min^{-1}) were calculated by using the rate equation (4.1) expressed by the decreasing order of UV_{254} > UV_{280} > UV_{365} > $Color_{436}$. Photocatalytic degradation rate constants calculated for the specified UV-vis parameters indicated similar reactivities expressing the role of complexation resulting in conformational alterations. These changes in binary system structure might lead to the formation of new sites open to TiO_2 surface interactions. The effect of the presence of zinc ions on the photocatalytic degradation performance of 0.45 µm filtered fraction of humic acid could be regarded as insignificant for $Color_{436}$ and UV_{365} whereas a slight enhancement in the removal rate could be indicated for UV_{280} and UV_{254}.

4.5.6. Kinetic Modeling of Photocatalytic Degradation of 100 kDa Fraction of Humic Acid

The kinetic evaluation of the experimental data for the photocatalytic degradation of 100 kDa fraction of humic acid revealed the following pseudo first order kinetic model parameters for $Color_{436}$, UV_{365}, UV_{280} and UV_{254} as presented in Table 4.7.

Table 4.7. Pseudo first order kinetic model parameters for the photocatalytic degradation of 100 kDa fraction of humic acid.

Parameter	k, min^{-1}	$t_{1/2}$, min	Rate, m^{-1} min^{-1}
$Color_{436}$	$6.51x10^{-2}$	11	0.1959
UV_{365}	$5.47x10^{-2}$	13	0.3785
UV_{280}	$4.39x10^{-2}$	16	0.7639
UV_{254}	$4.26x10^{-2}$	16	0.8742

Pseudo first order degradation rate constansts (k, min^{-1}) were calculated as $6.51x10^{-2}$, $5.47x10^{-2}$, $4.39x10^{-2}$ and $4.26x10^{-2}$ for the UV-vis parameters specified as $Color_{436}$, UV_{365}, UV_{280} and UV_{254}, respectively. The removal of color forming moieties was found to be relatively faster than the UV absorbing centers (~ > 30%) as expressed by UV_{280} and

UV_{254}. The corresponding half life ($t_{1/2}$, min) values were in the range of 11-16 min. Photocatalytic degradation rates (R, m^{-1} min^{-1}) were calculated by using the rate equation (4.1) expressed by the decreasing order of $UV_{254} > UV_{280} > UV_{365} > Color_{436}$. The pseudo first order kinetic parameters displayed considerably higher removal efficiencies for 100 kDa fraction of humic acid with respect to both 0.45 µm filtered fraction of humic acid and raw humic acid. The enhancement factor could be regarded as two fold for all of the specified UV-vis parameters.

4.5.7. Kinetic Modeling of Photocatalytic Degradation of 100 kDa Fraction of Humic Acid in the Presence of Zinc

The kinetic evaluation of the experimental data for the photocatalytic degradation of 100 kDa fraction of humic acid in the presence of 0.1 mg L^{-1} zinc revealed the following pseudo first order kinetic model parameters for $Color_{436}$, UV_{365}, UV_{280} and UV_{254} as presented in Table 4.8.

Pseudo first order degradation rate constansts (k, min^{-1}) were found to be $4.25x10^{-2}$, $4.57x10^{-2}$, $4.32x10^{-2}$ and $4.33x10^{-2}$ for the UV-vis parameters specified as $Color_{436}$, UV_{365}, UV_{280} and UV_{254}, respectively. The corresponding half life ($t_{1/2}$, min) values were in the range of 15-16 min. Photocatalytic degradation rates (R, m^{-1} min^{-1}) were calculated by using the rate equation (4.1) expressed by the decreasing order of $UV_{254} > UV_{280} > UV_{365} > Color_{436}$.

Table 4.8. Pseudo first order kinetic model parameters for the photocatalytic degradation of 100 kDa fraction of humic acid in the presence of zinc.

Parameter	k, min^{-1}	$t_{1/2}$, min	Rate, m^{-1} min^{-1}
$Color_{436}$	$4.25x10^{-2}$	16	0.1279
UV_{365}	$4.57x10^{-2}$	15	0.3162
UV_{280}	$4.32x10^{-2}$	16	0.7517
UV_{254}	$4.33x10^{-2}$	16	0.8885

The presence of zinc ions altered the photocatalytic degradation rates of 100 kDa fraction of humic acid with respect to the 0.45 µm filtered fraction of humic acid and raw humic acid. However, a retardation effect could be noticed with respect to the conditions specified by the absence of zinc ions.

4.5.8. Kinetic Modeling of Photocatalytic Degradation of 30 kDa Fraction of Humic Acid

The kinetic evaluation of the experimental data for the photocatalytic degradation of 30 kDa fraction of revealed the following pseudo first order kinetic model parameters for $Color_{436}$, UV_{365}, UV_{280} and UV_{254} as presented in Table 4.9.

Pseudo first order degradation rate constansts (k, min^{-1}) were found to be $8.78x10^{-2}$, $12.53x10^{-2}$, $7.93x10^{-2}$ and $8.06x10^{-2}$ for the UV-vis parameters specified as $Color_{436}$, UV_{365}, UV_{280} and UV_{254}, respectively. The corresponding half life ($t_{1/2}$, min) values were in the range of 6-9 min. Photocatalytic degradation rates (R, m^{-1} min^{-1}) were calculated by using the rate equation (4.1) expressed by the decreasing order of $UV_{254} > UV_{280} > UV_{365} > Color_{436}$.

Table 4.9. Pseudo first order kinetic model parameters for the photocatalytic degradation of 30 kDa fraction of humic acid.

Parameter	k, min^{-1}	$t_{1/2}$, min	Rate, m^{-1} min^{-1}
$Color_{436}$	$8.78x10^{-2}$	8	0.0360
UV_{365}	$12.5x10^{-2}$	6	0.1754
UV_{280}	$7.93x10^{-2}$	9	0.3695
UV_{254}	$8.06x10^{-2}$	9	0.4570

Significantly higher photocatalytic degradation rate constants were achieved for 30 kDa fraction of humic acid with respect to the higher molecular weight fractions.

4.5.9. Kinetic Modeling of Photocatalytic Degradation of 30 kDa Fraction of Humic Acid in the Presence of Zinc

The kinetic evaluation of the experimental data for the photocatalytic degradation of 30 kDa fraction of humic acid in the presence of 0.1 mg L^{-1} zinc revealed the following pseudo first order kinetic model parameters for $Color_{436}$, UV_{365}, UV_{280} and UV_{254} as presented in Table 4.10.

Table 4.10. Pseudo first order kinetic model parameters for the photocatalytic degradation of 30 kDa fraction of humic acid in the presence of zinc.

Parameter	k, min^{-1}	$t_{1/2}$, min	Rate, m^{-1} min^{-1}
$Color_{436}$	$3.77x10^{-2}$	18	0.0154
UV_{365}	$6.48x10^{-2}$	11	0.0907
UV_{280}	$6.20x10^{-2}$	11	0.2889
UV_{254}	$6.33x10^{-2}$	11	0.3589

Pseudo first order degradation rate constansts (k, min^{-1}) were found to be $3.77x10^{-2}$, $6.48x10^{-2}$, $6.20x10^{-2}$ and $6.33x10^{-2}$ for the UV-vis parameters specified as $Color_{436}$, UV_{365}, UV_{280} and UV_{254}, respectively. The corresponding half life ($t_{1/2}$, min) values were in the range of 11-18 min. Photocatalytic degradation rates (R, m^{-1} min^{-1}) were calculated by using the rate equation (4.1) expressed by the decreasing order of $UV_{254} > UV_{280} > UV_{365} > Color_{436}$. The presence of zinc ions displayed a slight decrease in degradation rates for 30 kDa fraction of humic acid respect to 0.45 µm filtered fraction of humic acid and raw humic acid. However, a slight retardation effect could be noticed with respect to 100 kDa fraction of humic acid. Moreover, a considerably significant retardation effect could be explained by the possible competitive complexation and oxidation-reduction reactions taking place in the medium that include zinc ions. In the presence of metal ions, because of the possible complex formation between humic acid and metal ions, rearrangement of the electrostatic forces between the place and formation of a micelle like cage structure by metal ion-bridging interactions might be expected (Ghosh and Schnitzer, 1980; Puchalski et al., 1992).

4.6. Adsorption Studies of Humic Acid

Batch adsorption experiments were conducted with raw humic acid and its different molecular size fractions, such as 0.45 μm filtered fraction, 100 kDa fraction and 30 kDa fractions and TiO_2. The results were presented under appropriate subheadings for the humic acid and molecular size fraction in the presence and absence of zinc. Considering the photocatalytically effective photocatalyst doses, the TiO_2 loadings changed in the range of 0.1-1.0 mg $mL^{-1.}$ Zinc concentration was kept constant in all experiments as 0.1 mg L^{-1}.

Adsorption isotherms were modeled by using Freundlich (Equation 2.18) and Langmuir (Equation 2.19) adsorption models by using the specified UV-vis parameters as $Color_{436}$, UV_{365}, UV_{280} and UV_{254}. Previous studies carried by Suphandag (1998 and 2006) and Bas (2001), reported the adsorption capacity of humic acids on semi- conductor powders. The adsorption capacity of humic acid was investigated under different pH conditions onto three different crystal structures of TiO_2 powders that the range changed from 0.1 mg mL^{-1} to 1.0 mg mL^{-1}. It was also reported that the crystal structures of TiO_2 powders affect the adsorption and desorption behavior of humic acid. Higher adsorption efficiencies were observed for Degussa P-25. Adsorption efficiencies of two commercial humic acids (Aldrich and Roth) were evaluated at different pH conditions and it was concluded that Aldrich humic acid has higher adsorption efficiency due to the differences in the structure and chemical composition.

4.6.1. Adsorption of Raw Humic Acid onto TiO_2

The adsorption profiles of humic acid samples attained after batch adsorption experiments were evaluated by UV-vis spectra and fluorescence spectra as well as by the specified UV-vis and fluorescence parameters. The dose change of TiO_2 for the samples were shown in the figures starting from 0.1 to 1.0 mg mL^{-1} that initial represented either the humic acid solution or humic acid and zinc binary system.

4.6.1.1. UV-vis Spectroscopic Evaluation of Raw Humic Acid Adsorption onto TiO_2. As seen in Figure 4.48, UV-vis spectra of humic acid adsorption onto TiO_2 showed a gradually declining trend with respect to the increasing wavelength in the 200-600 nm regions.

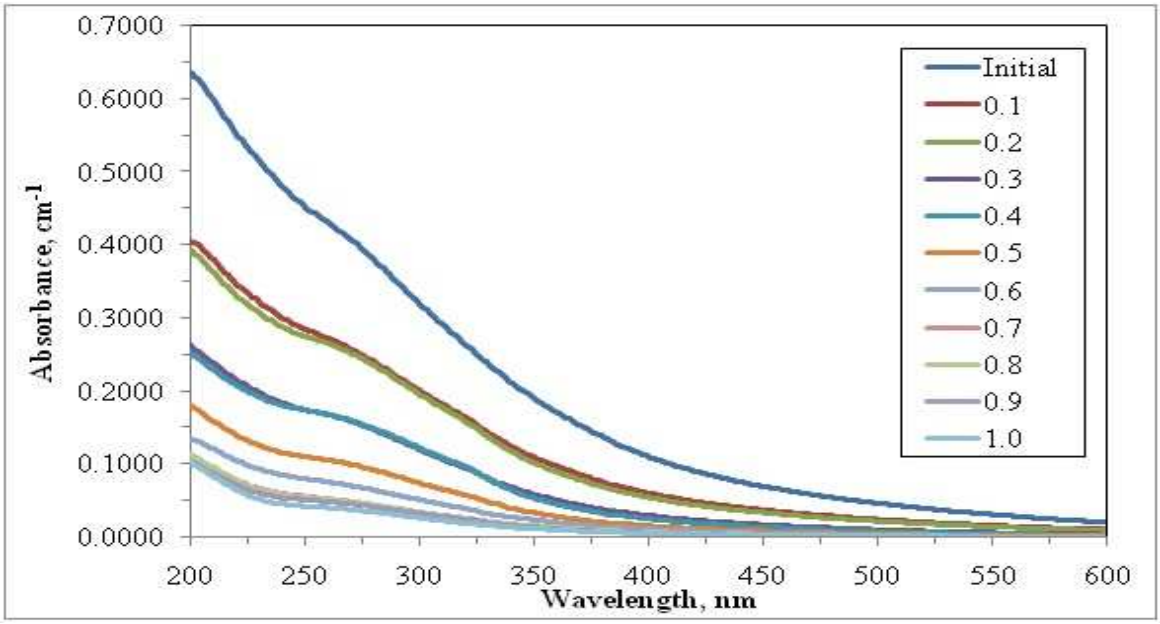

Figure 4.48. UV-vis spectra of raw humic acid adsorption onto TiO_2 (Initial represents raw humic acid).

While initial humic acid shows the highest trend, by the adsorption of raw humic acid onto dose of 0.1 mg mL^{-1} TiO_2, UV-vis spectra displayed a significant decrease. Moreover, the UV-vis spectra showed that adsorption onto 0.1 mg mL^{-1} and 0.2 mg mL^{-1} TiO_2 doses have similar trend. Also, for the case of 0.3 mg mL^{-1} and 0.4 mg mL^{-1} TiO_2 doses, the UV-vis spectra followed the same trend with declining absorbance recordings. After adsorption of raw humic acid onto 0.6 mg mL^{-1} TiO_2 dose, there were no significant changes in UV-vis spectra. Also, it could be easily noticed that, especially for higher TiO_2 loadings, there were no significantly characteristic absorbance recordings after 400 nm wavelength.

A similar adsorption profile was also derived for humic acid with an initial concentration of 50 mg L^{-1} (Ulker, 2008). The lower TiO_2 doses (0.1mg mL^{-1} – 0.2 mg

mL^{-1}) provided considerably lower surface area for the successive adsorption of humic moieties resulting in similar UV-vis spectral pattern. The trend in the UV-vis adsorption profiles obviously reflected in the specified UV-vis parameters.

4.6.1.2. Fluorescence Spectroscopic Evaluation of Raw Humic Acid Adsorption onto TiO_2. Emission scan fluorescence spectra of raw humic acid adsorption onto TiO_2 were displayed in Figure 4.49.

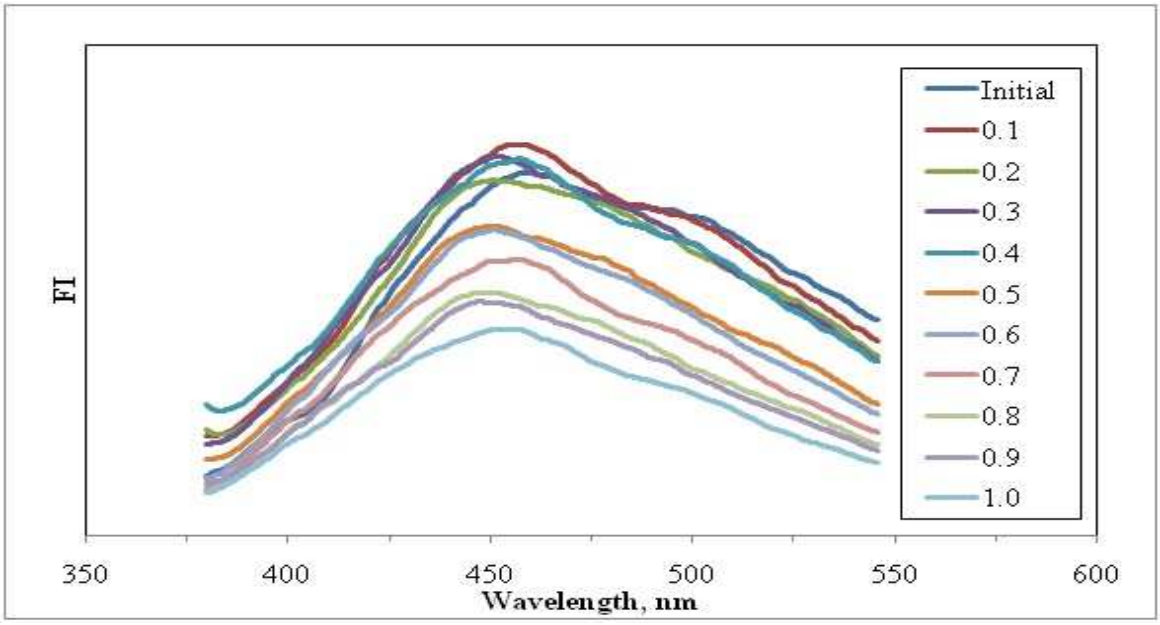

Figure 4.49. Emissions scan fluorescence spectra of raw humic acid adsorption onto TiO_2 (Initial represents raw humic acid).

In accordance with the conditions set forward for raw humic acid, the emission scan fluorescence spectra of the samples were recorded by excitation at 360 nm which resulted in a continuously decreasing trend in fluorescence intensity at λ_{max}=450 nm with respect to increasing TiO_2 dose for raw humic acid. The adsorption of raw humic acid onto minimum dose, 0.1 mg mL^{-1} TiO_2, gave the highest fluorescence intensity. While highest dose, 1.0 mg mL^{-1} TiO_2 had the lowest fluorescence intensity, the spectrum of adsorption onto 0.5 mg mL^{-1} TiO_2 overlapped the recorded emission scan spectrum for the adsorption onto 0.6 mg mL^{-1} TiO_2. The observed differences in UV-vis and that emission scan fluorescence spectra of humic acid indicated the adsorption results in the formation of new fluorophores

although a systematic removal of UV-vis absorbing centers were recorded with respect to increasing TiO_2 doses.

Synchronous fluorescence spectra of raw humic acid adsorption onto TiO_2 were displayed in Figure 4.50. Raw humic acid displayed two peaks at 370 nm and 470 nm wavelengths which were dissappeared after adsorption onto 0.7 mg mL^{-1} TiO_2 dose.

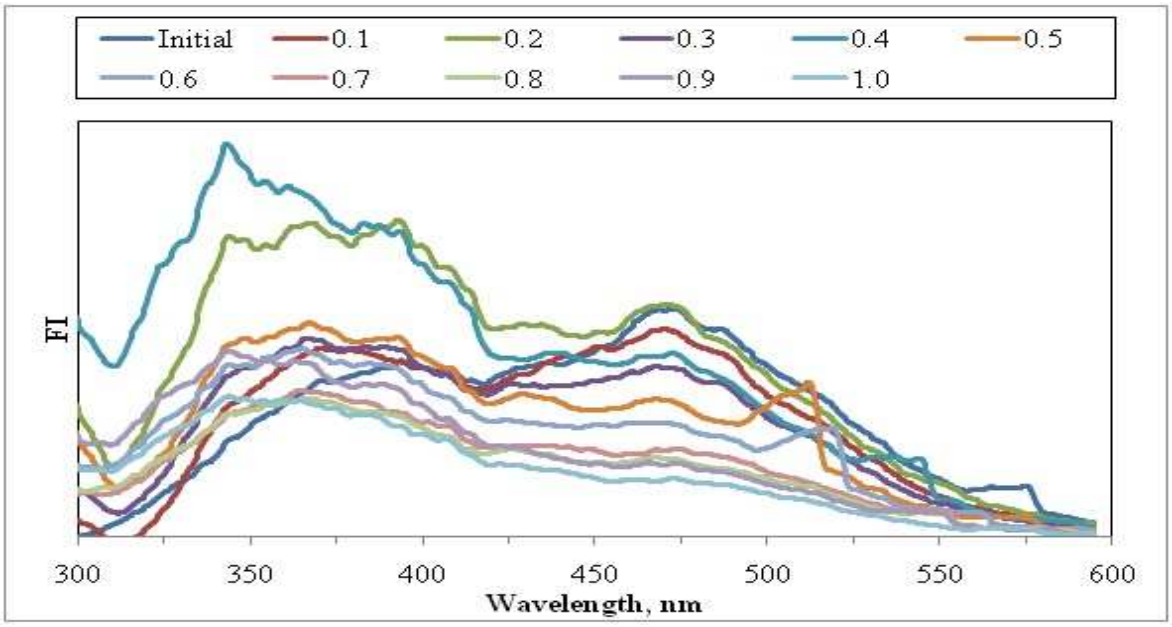

Figure 4.50. Synchronous scan fluorescence spectra of raw humic acid adsorption onto TiO_2 (Initial represents raw humic acid).

The highest fluorescence intensities were observed for adsorption onto 0.4 mg mL^{-1} and 0.2 mg mL^{-1} TiO_2 doses with peaks about 350 nm wavelengths. The lowest FI was recorded for the adsorption of raw humic acid onto 1.0 mg mL^{-1} TiO_2 dose.

4.6.1.3. Adsorption Isotherm Modeling of Raw Humic Acid. The adsorption data were evaluated in terms of Freundlich and Langmuir adsorption models.

Freundlich adsorption model. The Freundlich model assumes that adsorbent forms multiple layer coverage on the surface of adsorbate and the adsorption sites are heterogeneous; that, they have different binding energies (Schnoor, 1996). Freundlich

adsorption model isotherms were displayed in the following Figures 4.51 and 4.52 for $Color_{436}$ and UV_{254}, respectively. The observed trend in the shape of the adsorption isotherm expressed a similar surface attraction for both of the parameters. Freundlich adsorption model isotherms for UV_{365} and UV_{280} were presented in Appendix A.

As seen in Figure 4.51, C_e values varied between 0.37 – 4.24 m^{-1} for $Color_{436}$ depending on the amount of TiO_2 in the range of 0.1-1.0 mg mL^{-1}. The corresponding values of q_A calculated were found to be in the range of 149.60 – 722 $m^{-1}g^{-1}$.

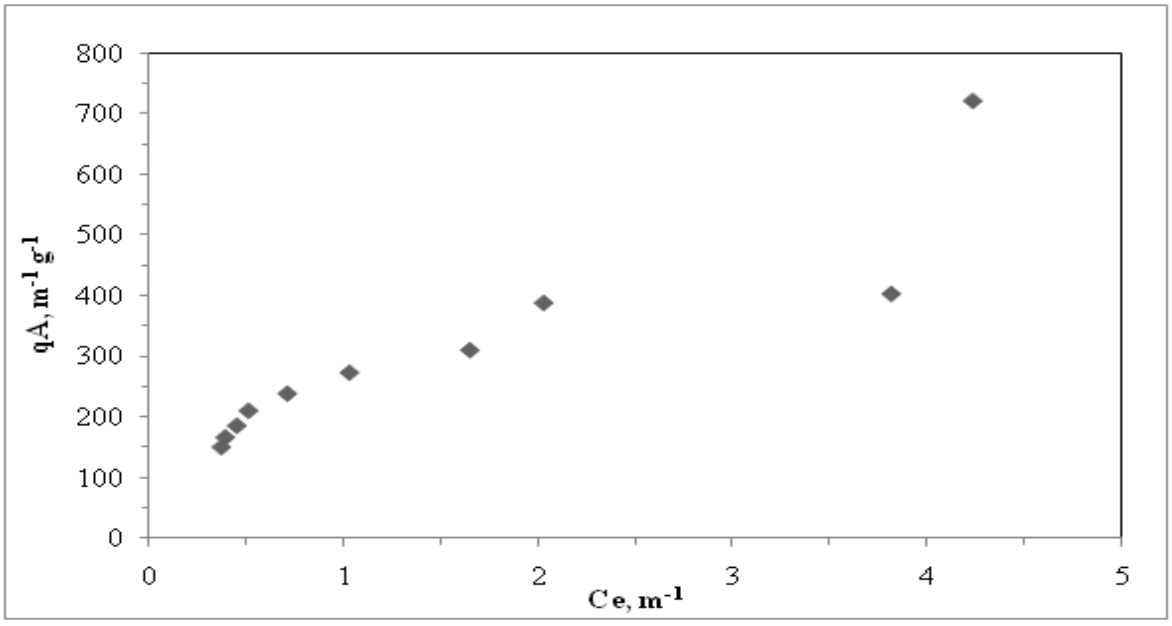

Figure 4.51. Freundlich adsorption isotherm of $Color_{436}$ of raw humic acid onto TiO_2.

As illustrated in Figure 4.52, the equilibrium contents, C_e values varied between 4.21– 27.95 m^{-1} for $UV_{254.}$ The values of q_A calculated to be in the range of 802.60 – 3278 $m^{-1}g^{-1}$ for the corresponding C_e values. It could also be stated that the adsorption isotherms showed similar trend both in terms of $Color_{436}$ and UV_{254} parameters. ΔC_e values for raw humic acid were calculated as 3.87 m^{-1} and 23.74 m^{-1} for $Color_{436}$ and UV_{254} respectively. On the other hand, Δq_A were found to be 572.4 $m^{-1}g^{-1}$ and 2475.4 $m^{-1}g^{-1}$ for $Color_{436}$ and UV_{254} respectively.

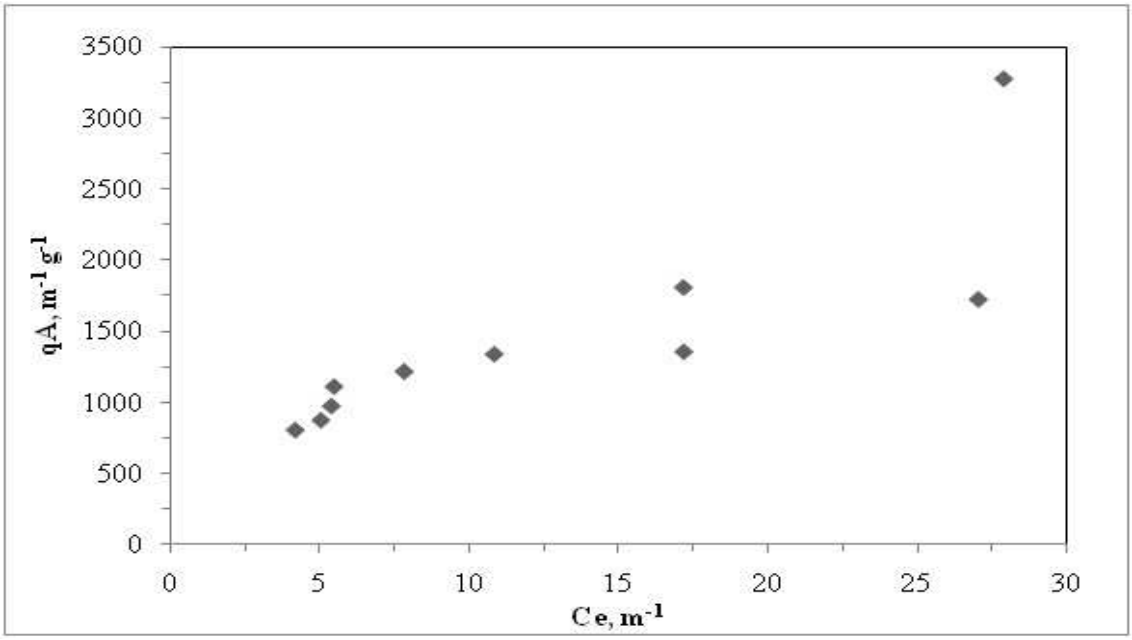

Figure 4.52. Freundlich adsorption isotherm of UV_{254} of raw humic acid onto TiO_2.

Freundlich adsorption model (Equation 2.18) was applied to the data obtained for UV-vis spectroscopic parameters i.e. $Color_{436}$, UV_{365}, UV_{280} and UV_{254} and isotherm model coefficients; adsorption capacity, K_f, and adsorption strength, 1/n, for the adsorption of raw humic acid onto TiO_2 were listed in Table 4.11 ($R^2 \geq 0.70$).

Table 4.11. Freundlich isotherm model parameters for the adsorption of raw humic acid onto TiO_2.

Humic acid	K_f	1/n
$Color_{436}$	267.9	0.498
UV_{365}	332.4	0.517
UV_{280}	399.1	0.489
UV_{254}	398.0	0.518

According to Table 4.11, adsorption capacity constant (K_f) for $Color_{436}$, displayed the lowest value. Adsorption capacity constants for UV absorbing centers (UV_{280}, and UV_{254}) were approximately found to be equal to each other. Adsorption intensity (1/n) values for $Color_{436}$, UV_{365}, UV_{280} and UV_{254} were found to be very close (~ = 0.5) to each other being

lower than 1, expressing that the adsorption bond was strong and the capacity tended to be independent of C_e.

Langmuir adsorption model. Langmuir adsorption isotherms of raw humic acid for UV-vis parameters as $Color_{436}$ and UV_{254} were given in Figure 4.53 and Figure 4.54, respectively. The Langmuir isotherms attained for UV_{365} and UV_{280} parameters were presented in Appendix B.

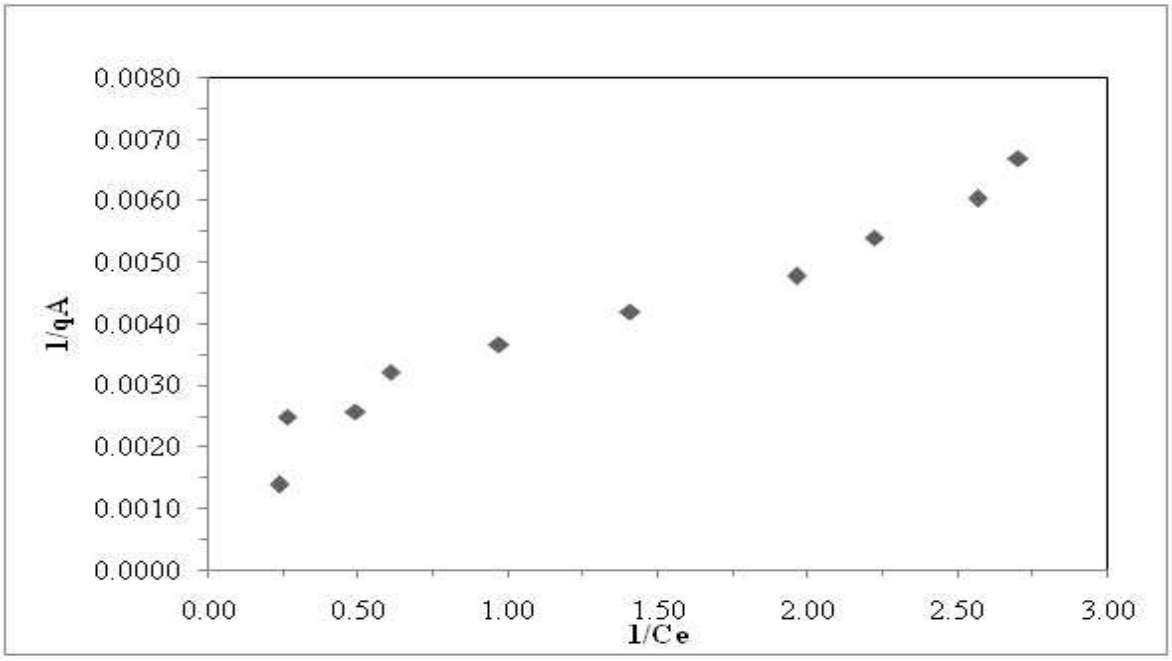

Figure 4.53. Langmuir adsorption isotherm of $Color_{436}$ of raw humic acid onto TiO_2.

Langmuir adsorption isotherms showed similar trends both in terms of $Color_{436}$ and UV_{254} parameters. In general the observed close linearity could also be modeled by Langmuir adsorption isotherm model (Equation 2.19).

Langmuir isotherm model coefficients; binding constant, K, and the maximum quantity adsorbable when all adsorption sites were occupied, q_{max}, for the adsorption of raw humic acid onto TiO_2 were listed in Table 4.12 ($R^2 \geq 0.80$).

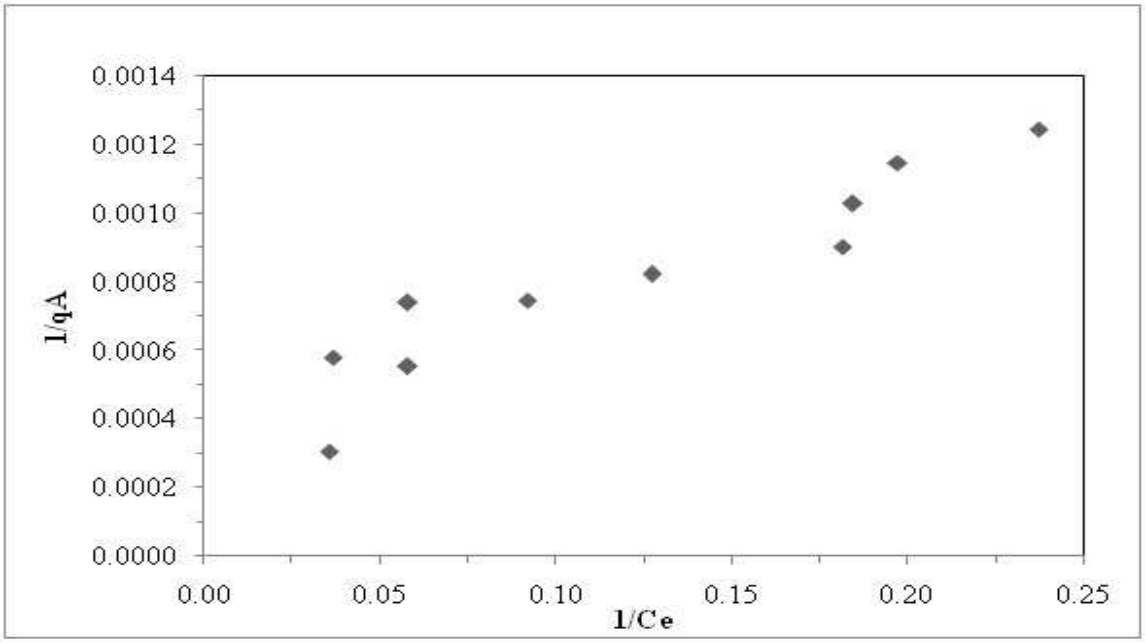

Figure 4.54. Langmuir adsorption isotherm of UV_{254} of raw humic acid onto TiO_2.

Table 4.12. Langmuir isotherm model parameters for the adsorption of raw humic acid onto TiO_2.

Humic acid	q_{max}	K
$Color_{436}$	578	1.006
UV_{365}	1149	0.394
UV_{280}	2174	0.140
UV_{254}	2703	0.103

According to Table 4.12, q_{max} and K values for both the UV_{280} and UV_{254} were very close to each other. There was approximately 79% difference between q_{max} values of $Color_{436}$ and UV_{254}. The difference between K values of $Color_{436}$ and UV_{254} was about 90%. The Langmuir isotherm binding constants, K, of UV-vis parameters were found to be in the order of $Color_{436} > UV_{365} > UV_{280} > UV_{254}$. The maximum quantity adsorbable when all adsorption sites were occupied, q_{max}, could be assessed by the order of $UV_{254} > UV_{280} > UV_{365} > Color_{436}$.

4.6.2. Adsorption of 0.45 µm Filtered Fraction of Humic Acid onto TiO_2

In order to evaluate the effect of different size fractions on adsortion properties of humic acid, experiments were carried out with 0.45 µm filtered fraction of humic acid.

4.6.2.1. UV-vis Spectroscopic Evaluation of 0.45 µm Filtered Fraction of Humic Acid Adsorption onto TiO_2. UV-vis spectra displayed a logarithmic decaying trend for all of the samples obtained after adsorption of 0.45µm filtered fraction of humic acid onto TiO_2 (Figure 4.55). It could be easily seen that the significant decreases were occured with the addition of increased dose of TiO_2.

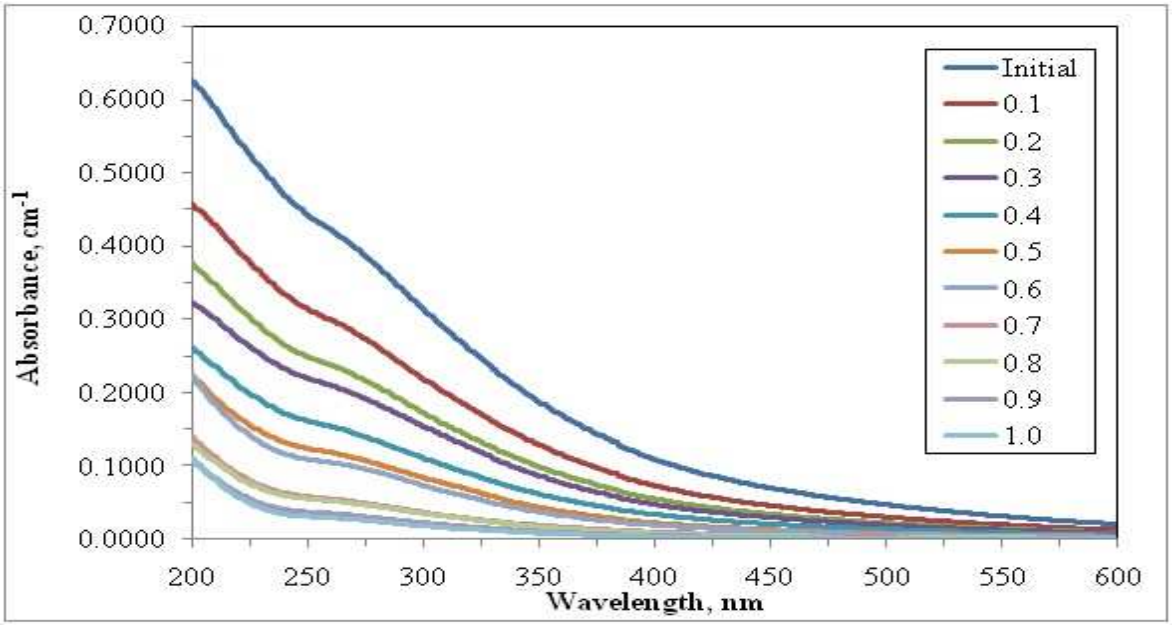

Figure 4.55. UV-vis spectra of 0.45 µm filtered fraction of humic acid adsorption onto TiO_2 (Initial represents 0.45 µm filtered fraction of humic acid).

UV-vis spectra showed that adsorption of 0.45µm filtered fraction of humic acid onto 0.7 mg mL^{-1} and 0.8 mg mL^{-1} TiO_2 displayed similar trend overlapping on each other. Moreover, in the case of 0.9 mg mL^{-1} and 1.0 mg mL^{-1} TiO_2 doses the UV-vis spectra followed the same overlapping trend. The reason coud be attributed to the probable saturation of the surface adsorption sites.

4.6.2.2. Fluorescence Spectroscopic Evaluation of 0.45 µm Filtered Fraction of Humic Acid Adsorption onto TiO_2. Emission scan fluorescence spectra of 0.45µm filtered fraction of humic acid samples were displayed in Figure 4.56. The fluorescence spectra of the samples were recorded by excitation at 360 nm causing a major peak at the wavelength of 450 nm. Although TiO_2 dose dependent general decreasing trend in fluorescence intensity could be visualized, the maximum fluorescence intensity was observed for the adsorption of 0.45µm filtered fraction of humic acid onto 0.1 mg mL^{-1} TiO_2. Especially after adsorption onto 0.6 mg mL^{-1} TiO_2, it became easier to observe the emission FI decrease. As expected, the lowest FI was seen for adsorption of 0.45µm filtered fraction of humic acid onto 1.0 mg mL^{-1} TiO_2.

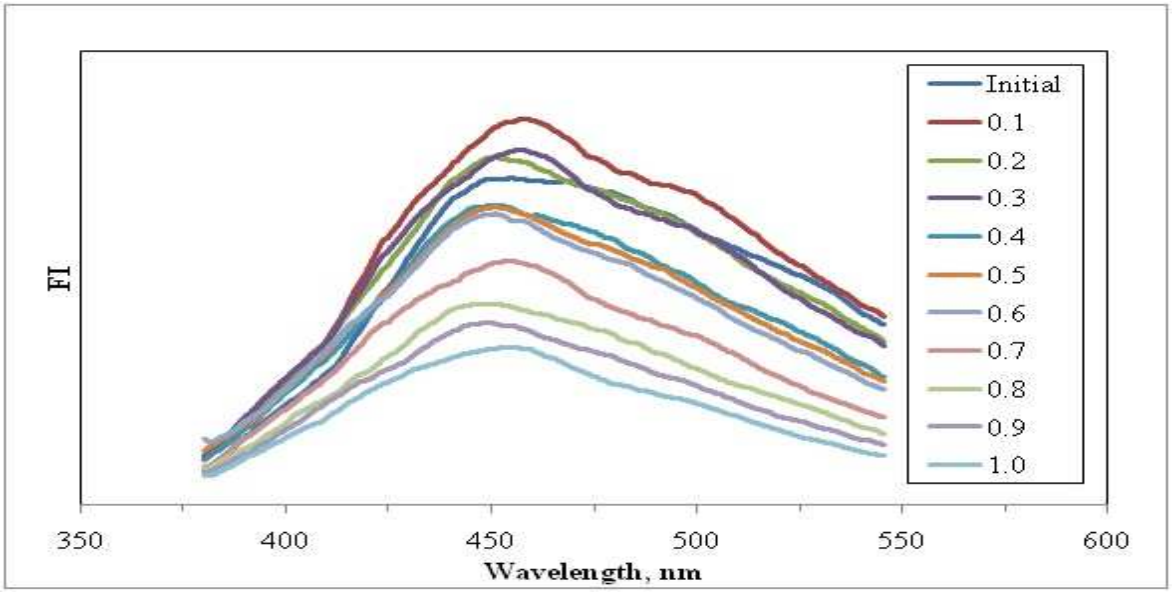

Figure 4.56. Emission scan fluorescence spectra of 0.45µm filtered fraction of humic acid adsorption onto TiO_2 (Initial represents 0.45 µm filtered fraction of humic acid).

Synchronous scan fluorescence spectra recorded for the adsorption of 0.45µm filtered fraction of humic acid were shown in Figure 4.57. Synchronous scan fluorescence spectra for 0.45µm filtered fraction of humic acid displayed a sharp peak around wavelength of 470 nm. There was also a moderate peak around 370 nm wavelengths with a comparatively lower intensity.

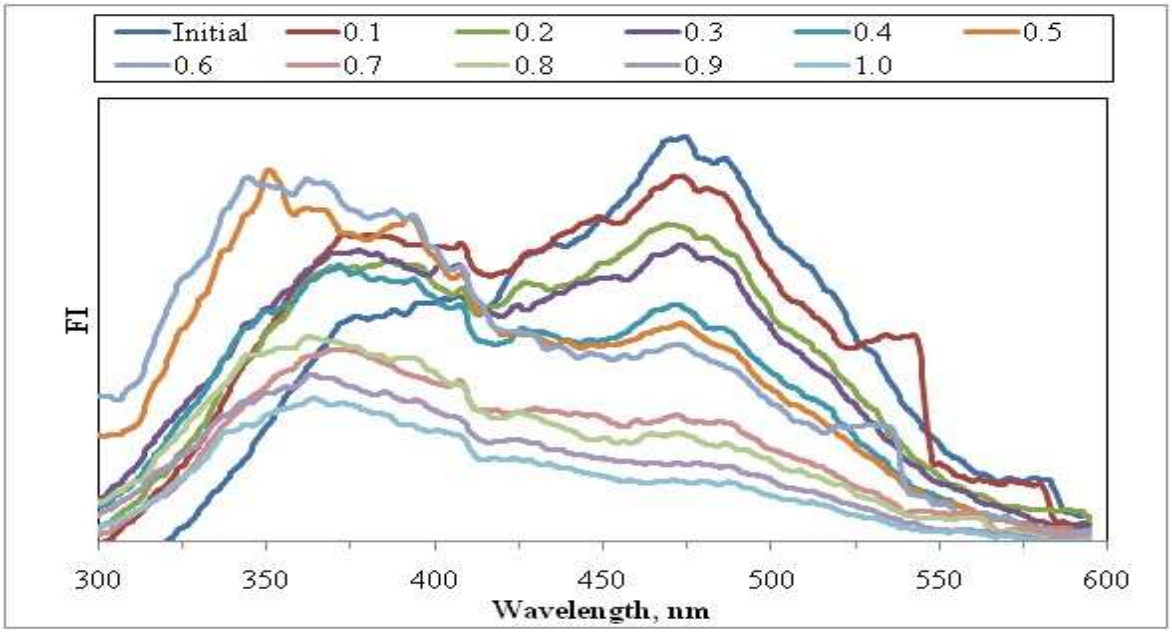

Figure 4.57. Synchronous scan fluorescence spectra of 0.45µm filtered fraction of humic acid adsorption onto TiO_2 (Initial represents 0.45 µm filtered fraction of humic acid).

After adsorption onto higher dosage of TiO_2, the characteristic sharp peak of for 0.45µm filtered fraction of humic acid at 470 nm wavelength completely disappeared. On the other hand, a new peak at 350 wavelengths was noticed. At this wavelength, similar fluorescence intensities were recorded for adsorption of 0.45µm filtered fraction of humic acid onto higher dosages of TiO_2. After adsorption onto higher dosage of TiO_2, such as 1.0 mg mL^{-1} TiO_2, the synchronous scan fluorescence intensity of the major peak recorded at 470 nm wavelength decreased to lower values.

4.6.2.3. Adsorption Isotherm Modeling of 0.45 µm Filtered Fraction of Humic Acid. The adsorption data were evaluated in terms of Freundlich and Langmuir adsorption models.

Freundlich adsorption model. Freundlich adsorption model isotherms were displayed in Figure 4.58 and Figure 4.59 for $Color_{436}$ and UV_{254}, respectively. Freundlich isotherms for UV_{365} and UV_{280} were presented in Appendix A. As illustrated in Figure 4.58, C_e values varied between 0.25 - 5.19 m^{-1} for $Color_{436}$ depending on the amount of TiO_2 present in solution. The values of q_A calculated to be in the range of 151.80 - 530 $m^{-1}g^{-1}$ for the corresponding C_e values. As seen in Figure 4.59, C_e values varied between 3.05 –30.76 m^{-1}

for UV_{254}. The values of q_A calculated to be in the range of 806.40 - 2522 $m^{-1}g^{-1}$ for the corresponding C_e values.

ΔC_e and Δq_A values for 0.45 μm fractionated humic acid were found to be 4.94 m^{-1} and 378.2 $m^{-1}g^{-1}$, respectively at $Color_{436}$. ΔC_e and Δq_A for UV_{254} were calculated as 27.71 m^{-1} and 1715.6 $m^{-1}g^{-1}$, respectively. Adsorption isotherms showed similar trend both in terms of $Color_{436}$ and UV_{254} parameters. This exhibited trend would have agreed well with the C-curve type isotherm that an initial slope remains independent of adsorptive concentration until the maximum possible adsorption was achieved.

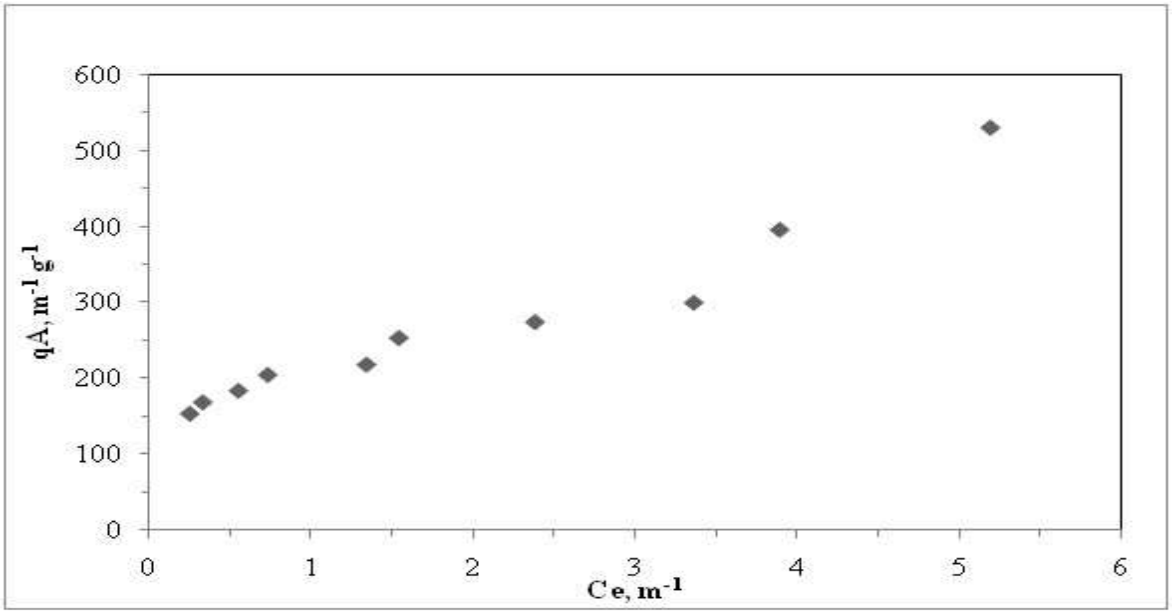

Figure 4.58. Freundlich adsorption isotherm of $Color_{436}$ of 0.45 μm filtered fraction of humic acid onto TiO_2.

In comparison to the adsorption data attained for raw humic acid (Figures 4.51. and 4.52) comparatively similar adsorption isotherms were attained except for the lower doses. The reason could be attributed to the presence of low concentrations of TiO_2 doses leading to lower surface area exposed for adsorption of the humic moieties. On the other hand, the neutral pH conditions served an invariable background for the surface charges attained both on TiO_2 and humic fractions.

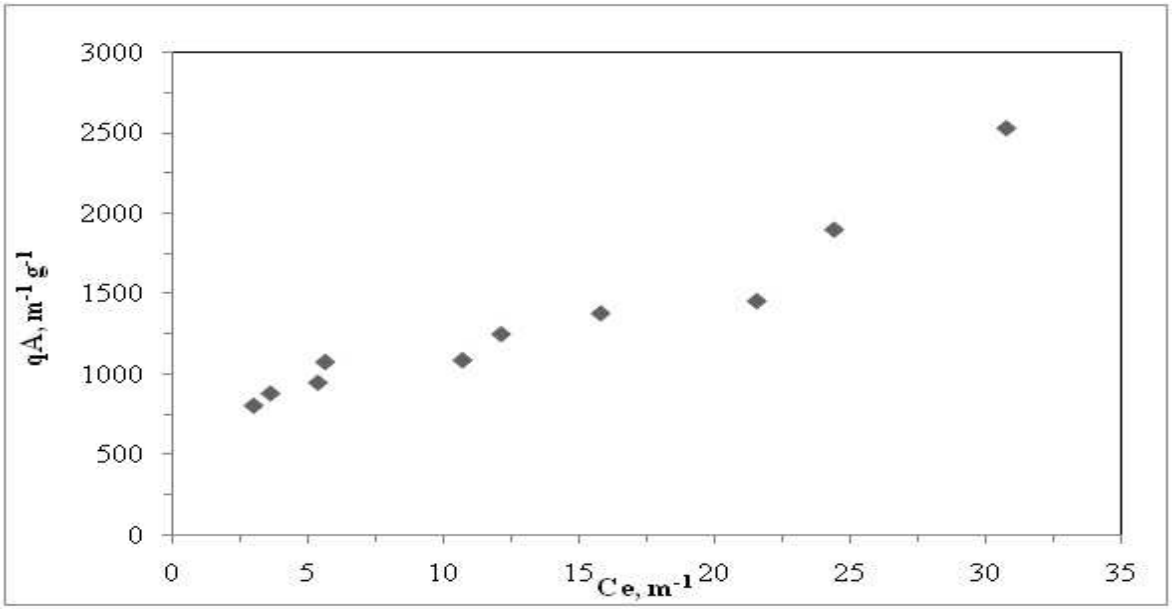

Figure 4.59. Freundlich adsorption isotherm of UV_{254} of 0.45 μm filtered fraction of humic acid onto TiO_2.

Freundlich adsorption model was applied to the data obtained for UV-vis spectroscopic parameters i.e. $Color_{436}$, UV_{365}, UV_{280} and UV_{254}. Isotherm model coefficiens; adsorption capacity, K_f, and adsorption strength, 1/n, for the adsorption of 0.45 μm filtered fraction of humic acid onto TiO_2 were listed in Table 4.13 ($R^2 \geq 0.70$).

Table 4.13. Freundlich isotherm model parameters for the adsorption of 0.45 μm filtered fraction of humic acid onto TiO_2.

Humic acid	K_f	1/n
$Color_{436}$	227.8	0.349
UV_{365}	331.3	0.365
UV_{280}	467.7	0.391
UV_{254}	489.9	0.404

According to Table 4.13, adsorption capacity constant for $Color_{436}$ gave the lowest value when adsorption capacity constants for UV absorbing centers (UV_{280}, and UV_{254}) were approximately equal to each other. Adsorption capacity constant of $Color_{436}$ was

nearly half of adsorption capacity constant of UV_{254}. 1/n values for $Color_{436}$, UV_{365}, UV_{280} and UV_{254} were very closed to each other and found to be lower than 1, it shows that the adsorption bond was strong and the capacity tended to be independent of Ce.

Langmuir adsorption model. Langmuir adsorption isotherms of 0.45µm filtered fraction of humic acid for $Color_{436}$ and UV_{254} were given in the Figure 4.60 and Figure 4.61, respectively. Langmuir adsorption isotherms for UV_{365} and UV_{280} were presented in Appendix B.

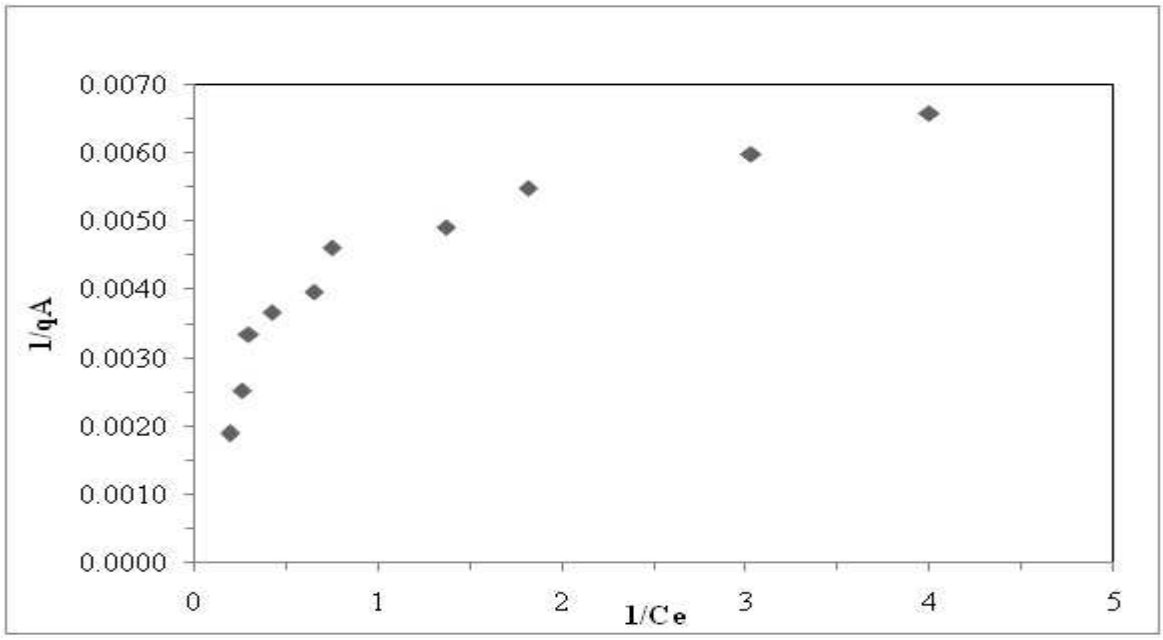

Figure 4.60. Langmuir adsorption isotherm of $Color_{436}$ of 0.45µm filtered fraction of humic acid onto TiO_2.

As seen in Figure 4.60 and Figure 4.61, Langmuir adsorption isotherms showed similar trend both in terms of $Color_{436}$ and UV_{254} parameters. Comparing the Langmuir adsorption isotherm profiles attained for raw humic acid (Figure 4.53 and Figure 4.54), the observed profiles could be expressed as displaying similar properties. The reason could be attributed to the prevailing considerably similar attractions between the TiO_2 surface and the humic moities either raw or 0.45µm filtered fraction of humic acid.

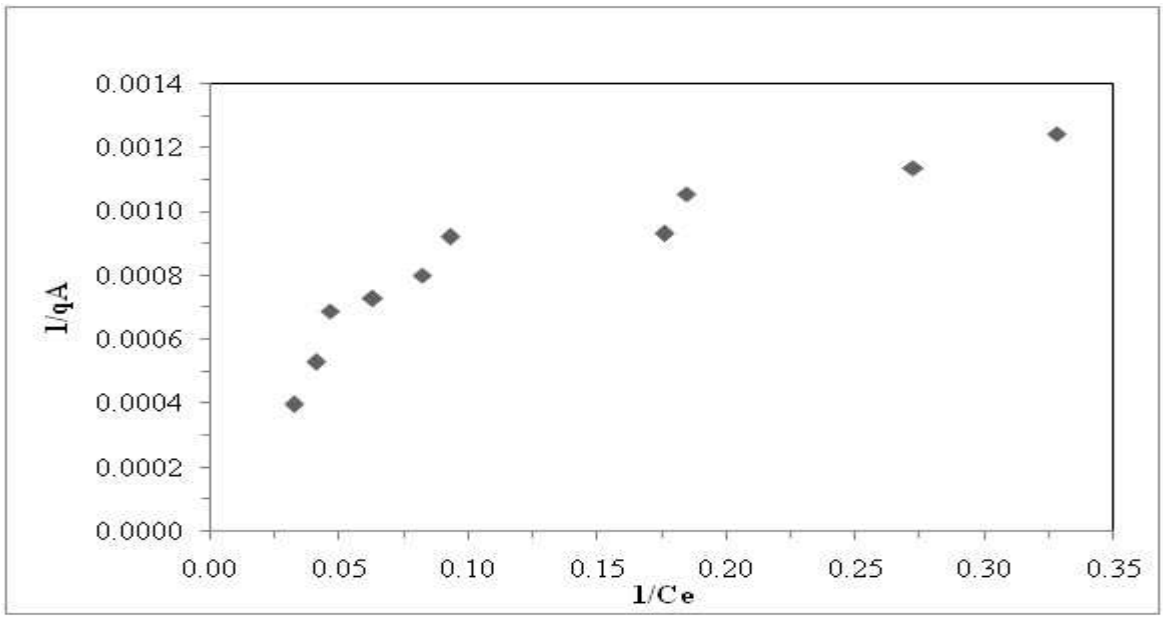

Figure 4.61. Langmuir adsorption isotherm of UV_{254} of 0.45µm filtered fraction of humic acid onto TiO_2.

Langmuir isotherm model coefficients; binding constant, K, and the maximum quantity adsorbable when all adsorption sites were occupied, q_{max}, for the adsorption of 0.45 µm filtered fraction of humic acid onto TiO_2 were listed in Table 4.14 ($R^2 \geq 0.80$)

Table 4.14. Langmuir isotherm model parameters for the adsorption of 0.45 µm filtered fraction of humic acid onto TiO_2.

Humic acid	q_{max}	K
$Color_{436}$	336	2.893
UV_{365}	694	1.036
UV_{280}	1587	0.296
UV_{254}	1887	0.226

According to Table 4.14, q_{max} and K values for both the UV_{280} and UV_{254} were very close to each other. There was approximately 82% difference between q_{max} values of $Color_{436}$ and UV_{254}.The difference between K values of $Color_{436}$ and UV_{254} was about 92%. The Langmuir isotherm binding constants, K, of UV-vis parameters were found to be in

the order of $Color_{436}$>UV_{365} >UV_{280} >UV_{254}. The maximum quantity adsorbable when all adsorption sites were occupied, q_{max}, could be assessed by the order of UV_{254} > UV_{280} > UV_{365} > $Color_{436}$.

4.6.3. Adsorption of 100 kDa Fraction of Humic Acid onto TiO_2

In order to investigate the molecular size effect on adsortion properties of humic acid, experiments were carried out with 100 kDa fraction of humic acid.

4.6.3.1. UV-vis Spectroscopic Evaluation of 100 kDa Fraction of Humic Acid Adsorption onto TiO_2. UV-vis spectra displayed a logarithmic decaying shape for all samples obtained after adsorption of 100 kDa fraction of humic acid (Figure 4.62). After the adsorption onto 0.5 mg mL^{-1} TiO_2, there were no significant absorbance decreases, the higher dosages of TiO_2 showed similar overlapping trend on each other.

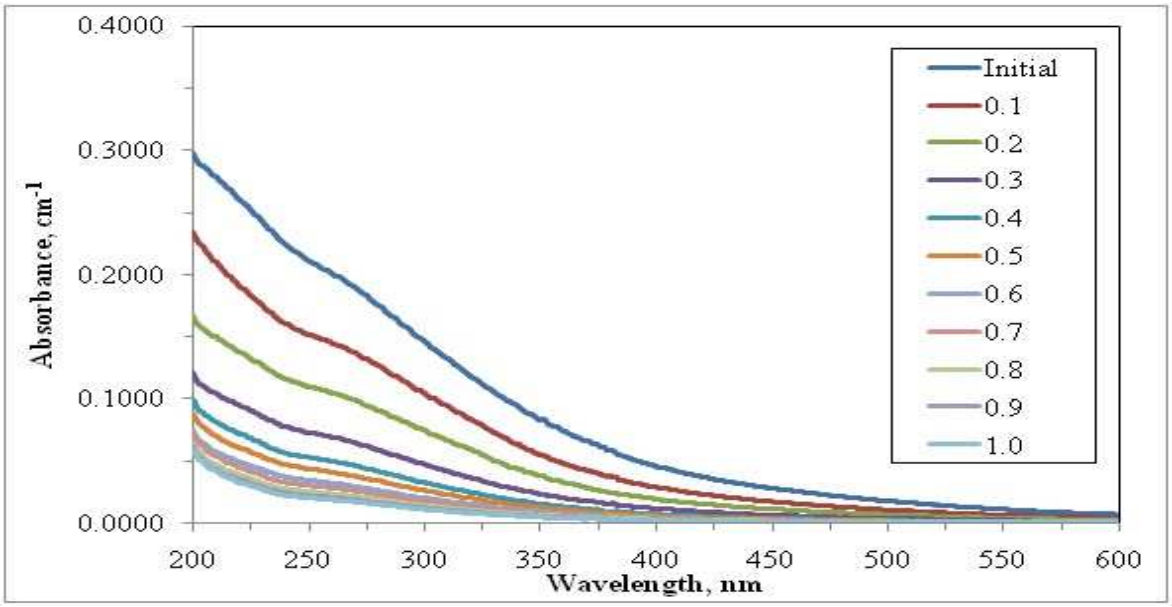

Figure 4.62. UV-vis spectra of 100 kDa fraction of humic acid adsorption onto TiO_2 (Initial represents 100 kDa fraction of humic acid).

When the absorbance values of 100 kDa fraction of humic acid were compared with raw humic acid, it could be easily seen that the values of 100 kDa fraction of humic acid was less than half of the absorbance values of raw humic acid.

4.6.3.2. Fluorescence Spectroscopic Evaluation of 100kDa Fraction of Humic Acid Adsorption onto TiO_2. Emission scan fluorescence spectra of 100 kDa fraction of humic acid adsorption onto TiO_2 were displayed in Figure 4.63.

The fluorescence spectra of the samples were recorded by excitation at 360 nm which resulted in a major peak at the wavelength of 450 nm. Although TiO_2 dose loading dependent general decreasing trend in fluorescence intensity could be visualized, the maximum fluorescence intensity was observed for adsorption of 100 kDa fraction of humic acid onto lower dose as 0.1 mg mL^{-1} TiO_2. Starting from 0.1 mg mL^{-1} TiO_2 to 1.0 mg mL^{-1} TiO_2 dose, all of the fluorescence intensities were decreased. The lowest FI values were reached after adsorption of 100 kDa fraction of humic acid onto 1.0 mg mL^{-1} TiO_2. The reason could be attributed to the TiO_2 dose dependent successive elimination of the fluorophoric groups of the 100 kDa fraction of humic acid acting simultaneously during adsorption onto TiO_2 surface.

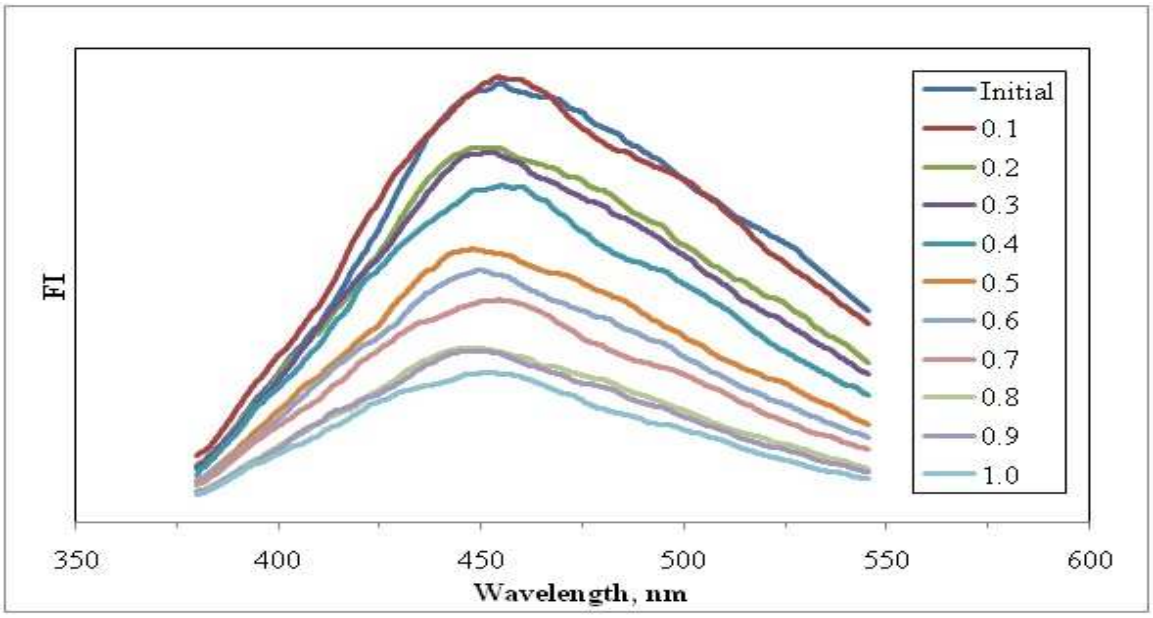

Figure 4.63. Emission scan fluorescence spectra of 100 kDa fraction of humic acid adsorption onto TiO_2 (Initial represents 100 kDa fraction of humic acid).

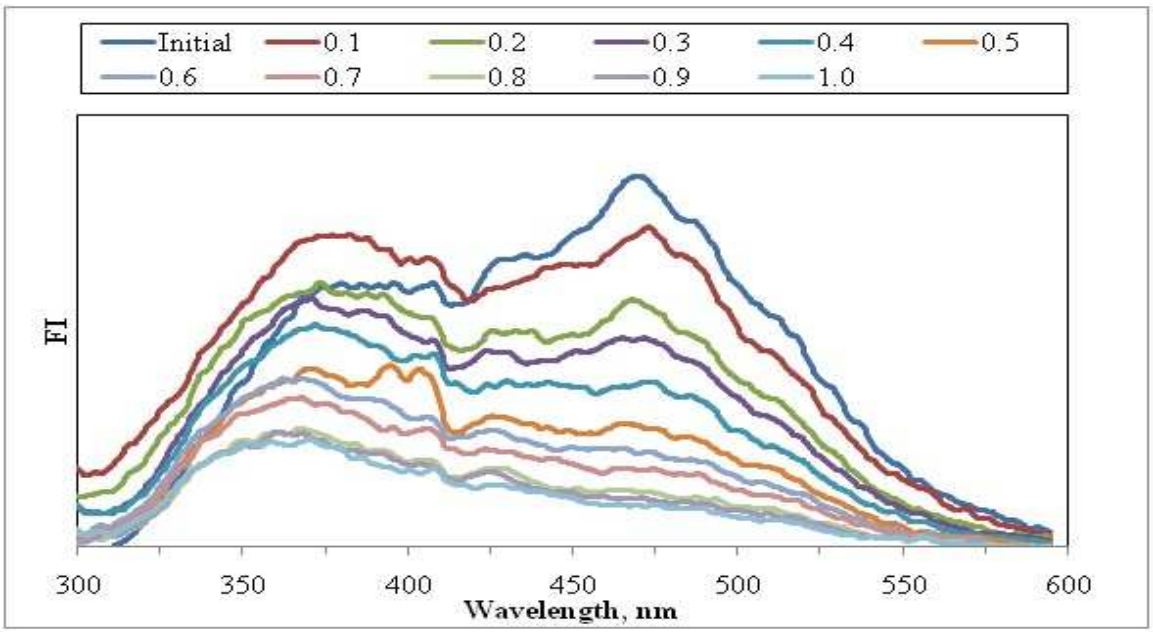

Figure 4.64. Synchronous scan fluorescence spectra of 100 kDa fraction of humic acid adsorption onto TiO_2 (Initial represents 100 kDa fraction of humic acid).

Synchronous scan fluorescence spectra recorded for the adsorption of 100 kDa fraction of humic acid were shown in Figure 4.64. The synchronous scan fluorescence spectra for 100 kDa fraction of humic acid displayed a sharp peak around wavelength of 470 nm. There was also a moderate peak at 370 nm wavelength with a comparatively lower intensity. After adsorption of 100 kDa fraction of humic acid onto higher TiO_2 doses, the characteristic peak of 100 kDa fraction of humic acid at 470 nm wavelength completely disappeared.

4.6.3.3. Adsorption Isotherm Modeling of 100kDa Fraction of Humic Acid. The adsorption data were evaluated in terms of Freundlich and Langmuir adsorption models.

Freundlich adsorption model. The adsorption isotherms for $Color_{436}$ and UV_{254} changes of humic acids were given in the Figure 4.65 and Figure 4.66. Freundlich adsorption isotherms for UV_{365} and UV_{280} were presented in Appendix A. Figure 4.65 indicated that C_e values were changed between 0.17 – 1.98 m^{-1} for $Color_{436}$ depending on the amount of TiO_2 present in solutions. The values of q_A calculated to be in the range of 60.40 - 242 $m^{-1}g^{-1}$ for the corresponding C_e values.

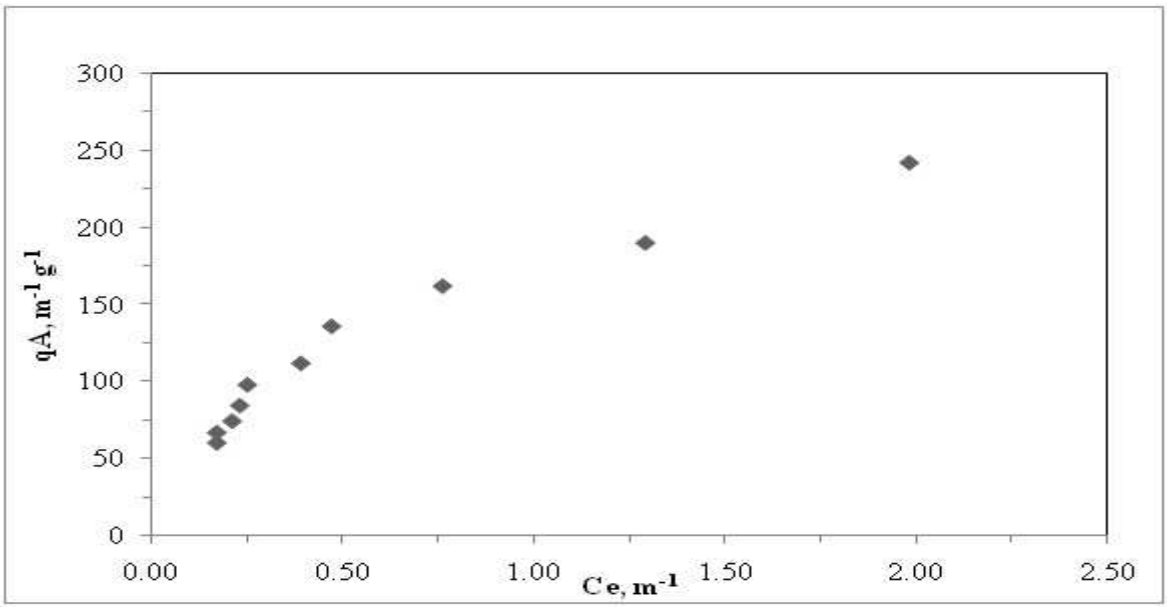

Figure 4.65. Freundlich adsorption isotherm of $Color_{436}$ of 100 kDa fraction of humic acid onto TiO_2.

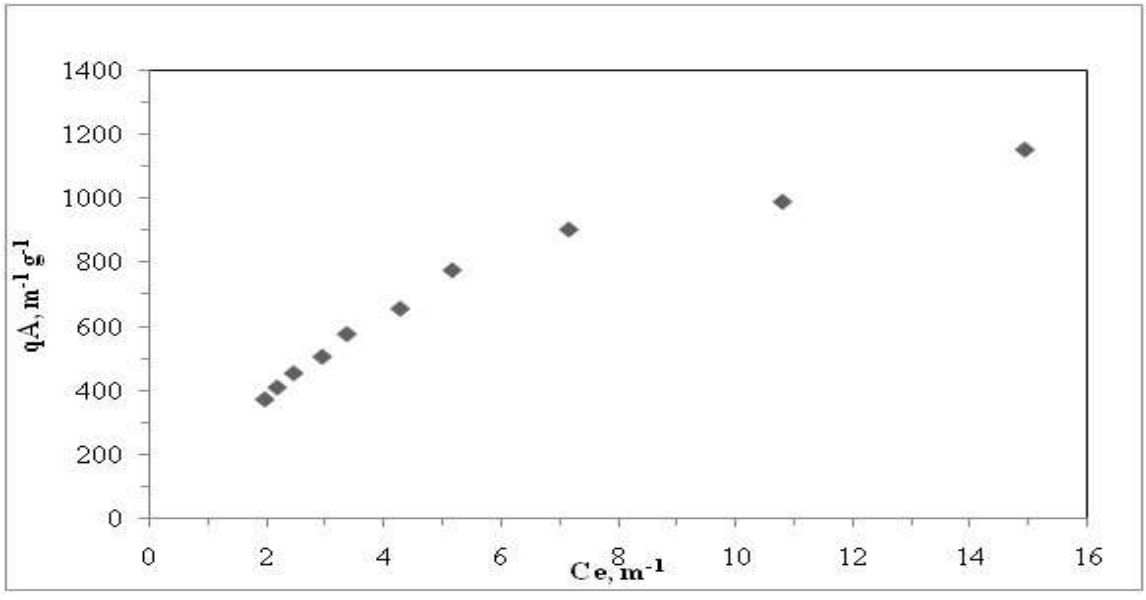

Figure 4.66. Freundlich adsorption isotherm of UV_{254} of 100 kDa fraction of humic acid onto TiO_2.

As seen in Figure 4.66, C_e values varied between 1.96 – 14.94 m^{-1} for $UV_{254.}$ The values of q_A calculated to be in the range of 374.80 - 1152 $m^{-1}g^{-1}$ for the corresponding C_e values. The adsorption isotherms show similar trend both in terms of $Color_{436}$ and UV_{254} parameters. ΔC_e and Δq_A values for 100 kDa fraction of humic acid were 1.81 m^{-1} and 181.6 $m^{-1}g^{-1}$, respectively at $Color_{436}$. ΔC_e and Δq_A for UV_{254} were 12.98 m^{-1} and 777.2 $m^{-1}g^{-1}$, respectively. This exhibited trend was agreed with the L-curve type isotherm which was the resultant effect of high relative affinity of the adsorbent particies for the absorbate at low surface coverage coupled with a decreasing amount of adsorbing surface remaining as the surface excess of the absorbate increases.

Freundlich adsorption model was applied to the data obtained for UV-vis spectroscopic parameters i.e. $Color_{436}$, UV_{365}, UV_{280} and UV_{254}. Isotherm model coefficiens; adsorption capacity, K_f, and adsorption strength, 1/n, for the adsorption of 100 kDa fraction of humic acid onto TiO_2 were listed in Table 4.15. ($R^2 \geq 0.70$)

Table 4.15. Freundlich isotherm model parameters for the adsorption of 100 kDa fraction of humic acid onto TiO_2.

Humic acid	K_f	1/n
$Color_{436}$	178.3	0.527
UV_{365}	232.5	0.514
UV_{280}	285.6	0.517
UV_{254}	281.3	0.552

According to Table 4.16, adsorption capacity constants for both the UV absorbing centers and the color forming chromophoric groups were found to be very close to each other. There was approximately 37% difference between the adsorption capacity of $Color_{436}$ and UV_{254}. 1/n values were found to be lower than one, it indicates that the adsorption bond was strong; the capacity tends to be independent of C_e. The observed case expressed unfavorable adsorption.

Langmuir adsorption model. Langmuir adsorption isotherms of 100 kDa fraction of humic acid for $Color_{436}$ and UV_{254} were given in the Figure 4.67 and Figure 4.68, respectively.

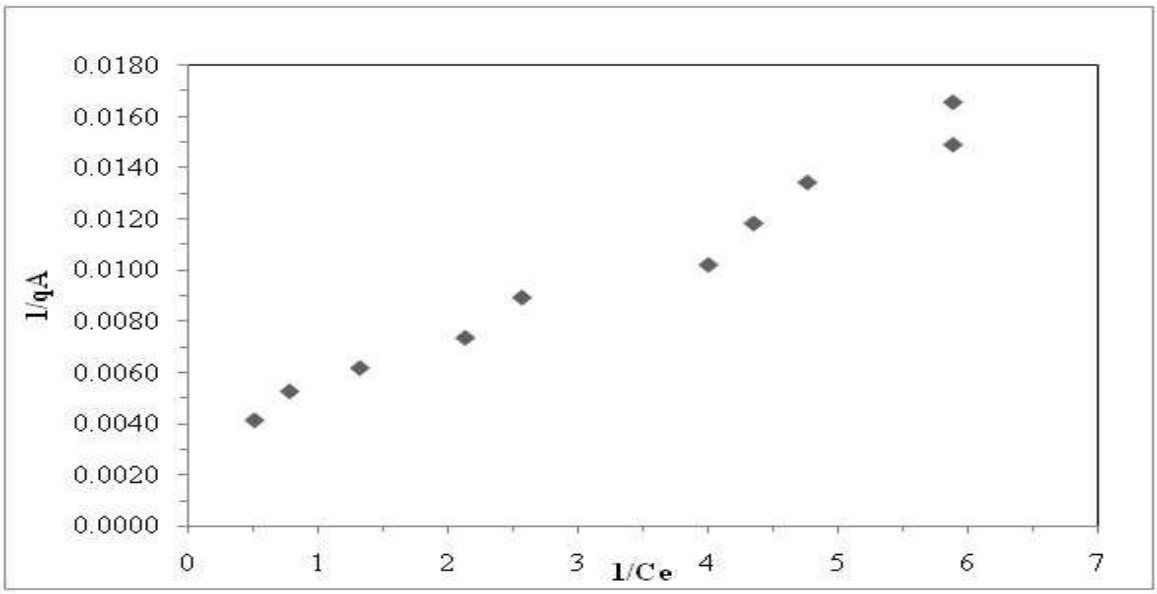

Figure 4.67. Langmuir adsorption isotherm of $Color_{436}$ of 100 kDa fraction of humic acid onto TiO_2.

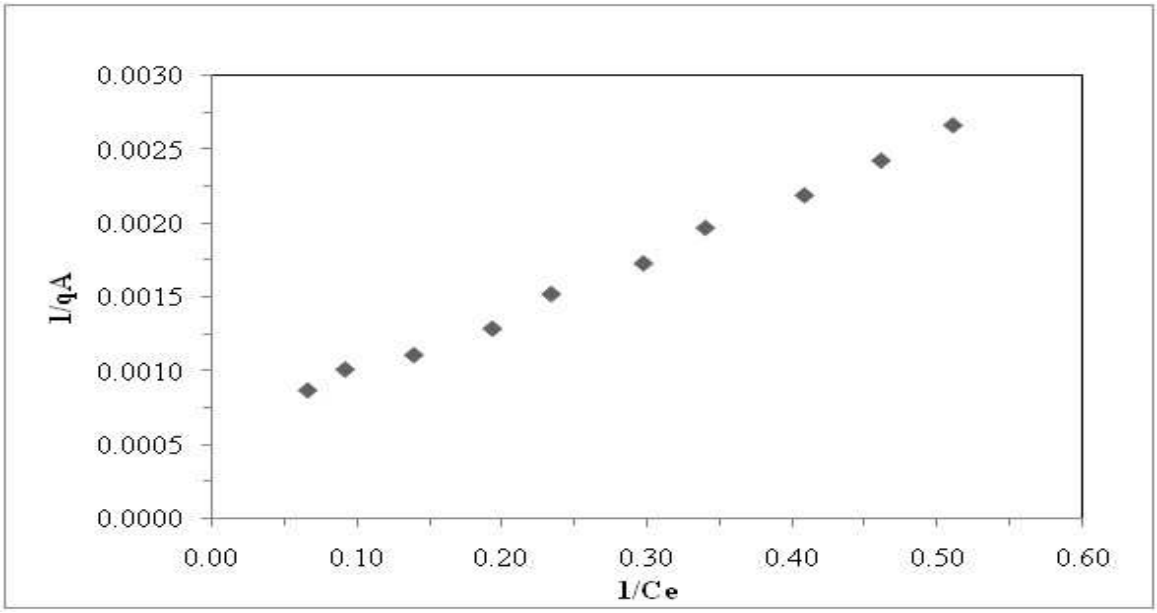

Figure 4.68. Langmuir adsorption isotherm of UV_{254} of 100 kDa fraction of humic acid onto TiO_2.

Langmuir adsorption isotherms for UV_{365} and UV_{280} were presented in Appendix B.

As seen in Figure 4.67 and Figure 4.68, Langmuir adsorption isotherms show similar trend both in terms of $Color_{436}$ and UV_{254} parameters. This exhibited trend would have agreed well with the linear pattern. Langmuir isotherm model coefficients; binding constant, K, and the maximum quantity adsorbable when all adsorption sites were occupied, q_{max}, for the adsorption of 100 kDa fraction of humic acid onto TiO_2 were listed in Table 4.16 ($R^2 \geq 0.80$).

Table 4.16. Langmuir isotherm model parameters for the adsorption of 100 kDa fraction of humic acid onto TiO_2.

Humic acid	q_{max}	K
$Color_{436}$	309	1.571
UV_{365}	529	0.892
UV_{280}	1351	0.214
UV_{254}	1754	0.142

According to Table 4.17, q_{max} and K values for both the UV_{280} and UV_{254} were very close to each other. There was approximately 82% difference between q_{max} values of $Color_{436}$ and UV_{254}.The difference between K values of $Color_{436}$ and UV_{254} was about 91%. The Langmuir isotherm binding constants, K, of UV-vis parameters were found to be in the order of $Color_{436}$>UV_{365} >UV_{280} >UV_{254}. The maximum quantity adsorbable when all adsorption sites were occupied, q_{max}, could be assessed by the order of UV_{254}>UV_{280}>UV_{365}>$Color_{436}$.

4.6.4. Adsorption of 30 kDa Fraction of Humic Acid onto TiO_2

In order to evaluate the molecular size effect on adsortion properties of humic acid, experiments were also carried out with 30 kDa fraction of humic acid.

4.6.4.1. UV-vis Spectroscopic Evaluation of 30kDa Fraction of Humic Acid Adsorption onto TiO_2. UV-vis spectra of the 30 kDa fraction of humic acid displayed a decaying trend for all samples in the 200-600 nm wavelength regions (Figure 4.69).

Considering the initial UV-vis spectral features of the 30 kDa fraction of humic acid, the attained absorbance recordings were significantly lower than the higher molecular weight fractions. Even for adsorption of 30 kDa fraction of humic acid onto comparatively lower TiO_2 loadings (e.g. 0.1 mg mL^{-1}), UV-vis spectra approached to very low absorbance values.

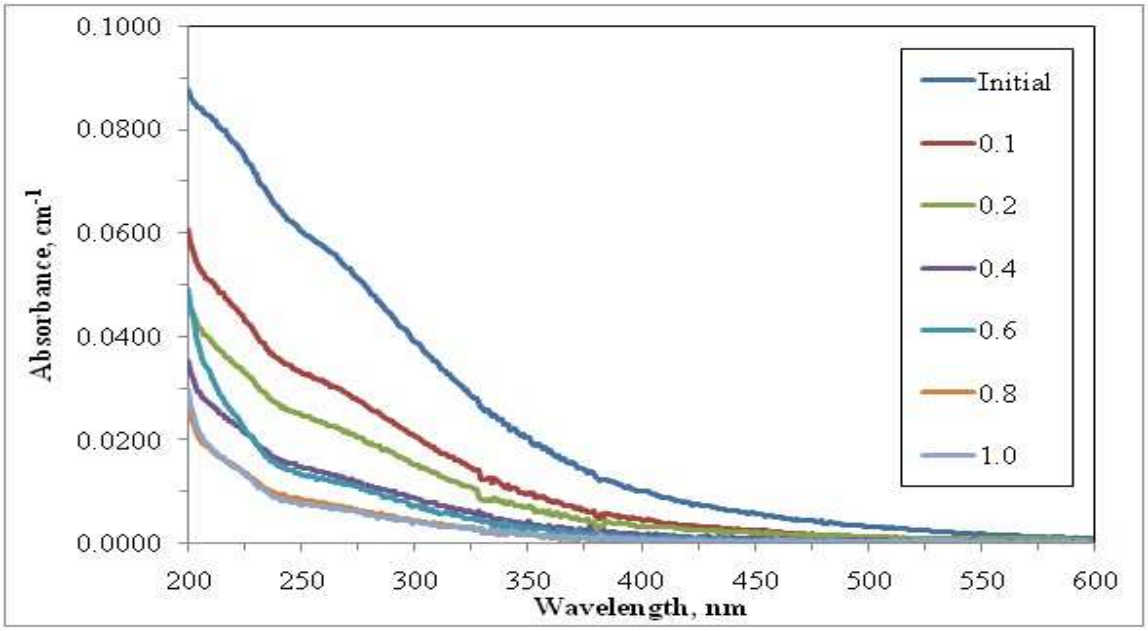

Figure 4.69. UV-vis spectra of 30 kDa fraction of humic acid adsorption onto TiO_2 (Initial represents 30 kDa fraction of humic acid).

4.6.4.2. Fluorescence Spectroscopic Evaluation of 30kDa Fraction of Humic Acid Adsorption onto TiO_2. Emission scan fluorescence spectra for 30 kDa fraction of humic acid were shown in Figure 4.70. "Initial" 30 kDa fraction of humic acid has a peak around 450 nm with relatively high fluorescence intensity. Adsorption of 30 kDa fraction of humic acid onto TiO_2 surface with increasing loadings, a gradual decrease in fluorescence intensity became evident in the emission scan fluorescence spectra. The similar situation was also observed between the cases of 0.8 mg mL^{-1} to 1.0 mg mL^{-1} TiO_2 doses. As presented previously for 100 kDa fraction of humic acid, the observed gradual decrease could also be expressed by the prevailing dose dependent similar surface attractions.

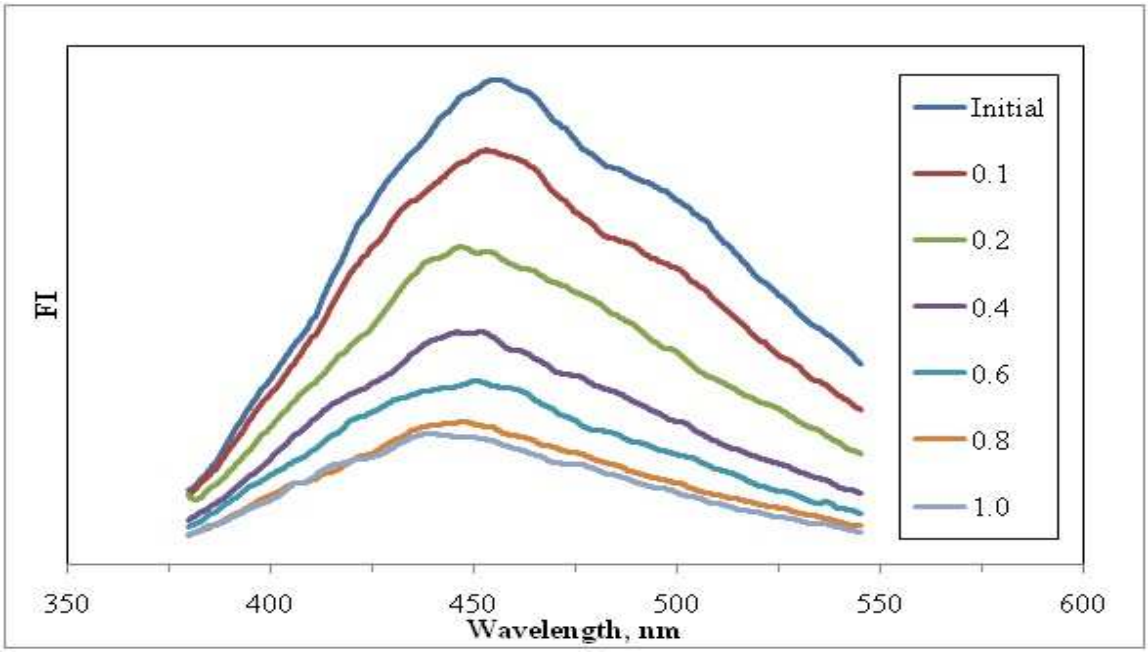

Figure 4.70. Emission scan fluorescence spectra of 30 kDa fraction of humic acid adsorption onto TiO_2 (Initial represents 30 kDa fraction of humic acid).

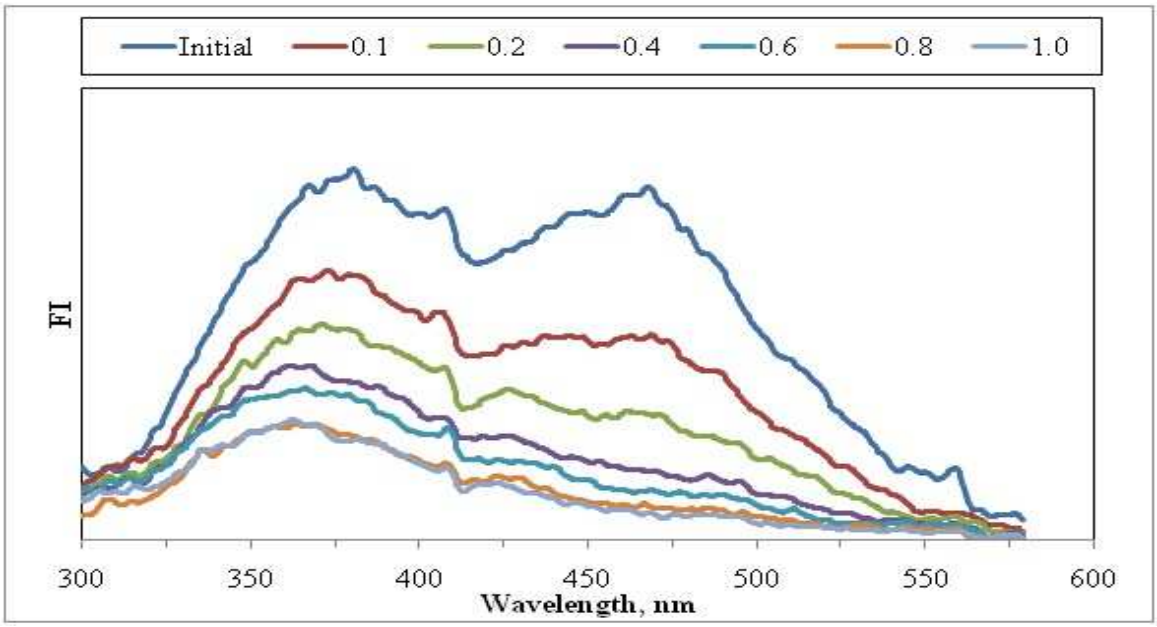

Figure 4.71. Synchronous scan fluorescence spectra of 30 kDa fraction of humic acid adsorption onto TiO_2 (Initial represents 30 kDa fraction of humic acid).

Synchronous scan spectra of 30 kDa fraction of humic acid were shown by Figure 4.71. The synchronous scan fluorescence spectra for 30 kDa fraction of humic acid displayed sharp peaks around wavelength of 470 nm and 380 nm. After adsorption onto higher dosages of TiO_2, the characteristic sharp peaks of 30 kDa fraction of humic acid at 470 nm and 380 nm wavelengths completely disappeared. It was also observed that the trend of 0.8 mg mL-1 and 1.0 mg mL^{-1} TiO_2 doses was crossed to each other.

4.6.4.3. Adsorption Isotherm Modeling of 30kDa Fraction of Humic Acid. The adsorption data were evaluated in terms of Freundlich and Langmuir adsorption models.

Freundlich adsorption model. The adsorption isotherms for $Color_{436}$ and UV_{254} changes of humic acids were given in the Figure 4.72 and Figure 4.73 respectively. The Freundlich adsorption isotherms for UV_{365} and UV_{280} were presented in Appendix A. Figure 4.72 indicated that C_e values varied between 0.05 – 0.29 m^{-1} for $Color_{436}$ depending on the amount of TiO_2 present in solution. The values of q_A calculated to be in the range of 12.20 – 74 $m^{-1}g^{-1}$ for the corresponding C_e values.

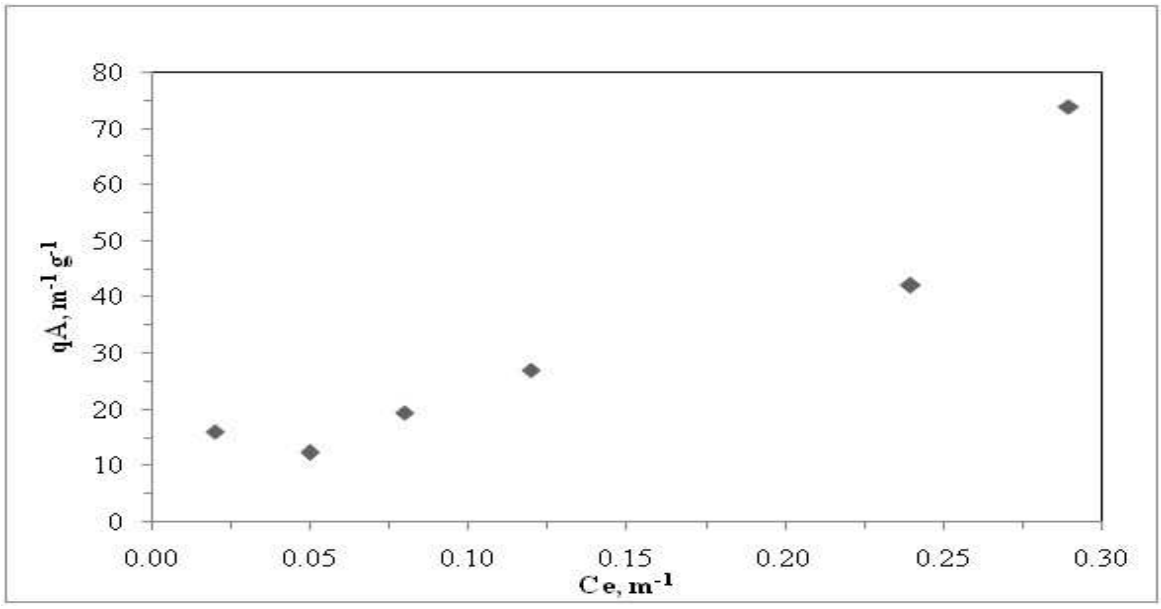

Figure 4.72. Freundlich adsorption isotherm of $Color_{436}$ of 30 kDa fraction of humic acid onto TiO_2.

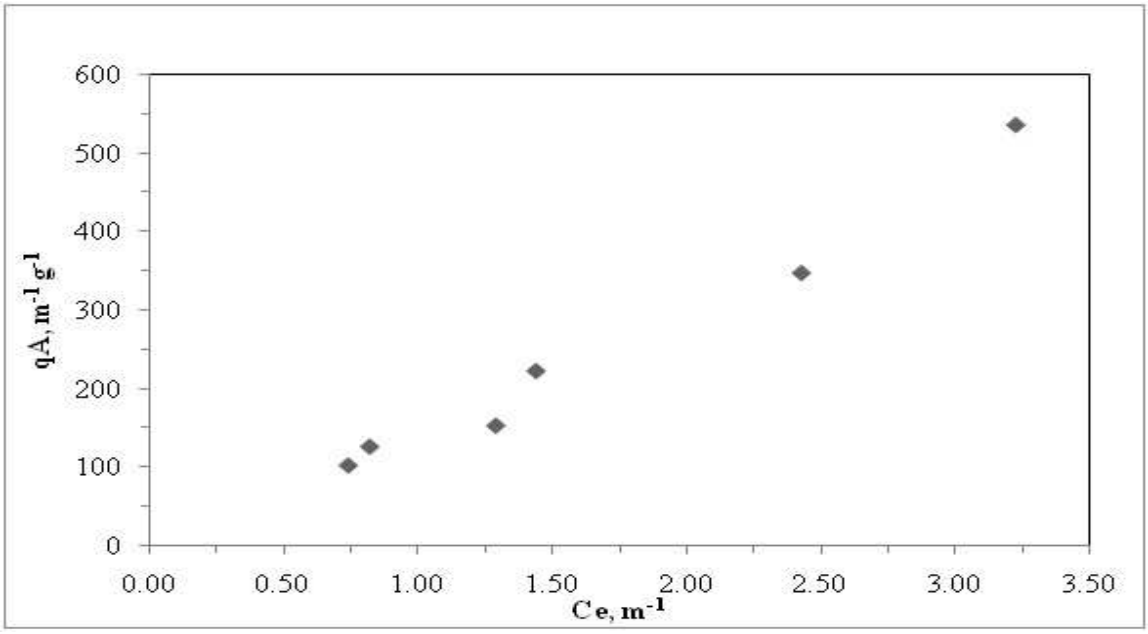

Figure 4.73. Freundlich adsorption isotherm of UV_{254} of 30 kDa fraction of humic acid onto TiO_2.

As observed in Figure 4.73, C_e values varied between 0.74 – 3.23 m^{-1} for $UV_{254.}$ The values of q_A calculated to be in the range of 103.40 - 536 $m^{-1}g^{-1}$ for the corresponding C_e values. ΔC_e and Δq_A values for 30 kDa fractionated humic acid were 0.24 m^{-1} and 61.80 $m^{-1}g^{-}1$, respectively at $Color_{436}$. ΔC_e and Δq_A for UV_{254} were 2.49 m^{-1} and 639.4 $m^{-1}g^{-1}$, respectively. Freundlich adsorption model parameters were presented in Table 4.17.

Table 4.17. Freundlich isotherm model parameters for the adsorption of 30 kDa fraction of humic acid onto TiO_2.

Humic acid	K_f	1/n
$Color_{436}$	103.1	0.579
UV_{365}	191.2	0.879
UV_{280}	158.1	1.016
UV_{254}	142.2	1.065

According to Table 4.17, adsorption capacity constants for both the UV absorbing centers and the color forming chromophoric groups were found to be very close to each

other. There was approximately 27% difference between the adsorption capacity of $Color_{436}$ and UV_{254}. On the other hand, for the adsorption strength, 1/n, value of UV_{254} was calculated as 46% higher than value of $Color_{436}$.

Langmuir adsorption model. Langmuir adsorption isotherm of 30 kDa fraction of humic acid for UV_{254} as the sole parameter was given in the Figure 4.74. Langmuir isotherm model coefficients; binding constant, K, and the maximum quantity adsorbable when all adsorption sites were occupied, q_{max}, for the adsorption of 30 kDa fraction of humic acid onto TiO_2 were listed in Table 4.18 ($R^2 \geq 0.80$).

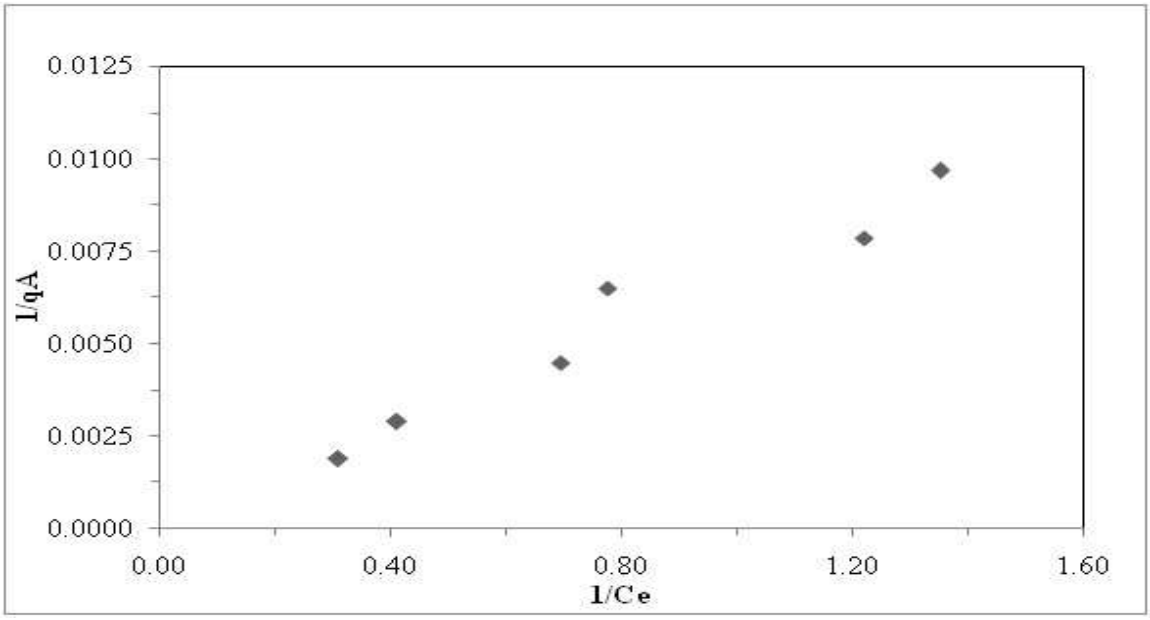

Figure 4.74. Langmuir adsorption isotherm of UV_{254} of 30 kDa fraction of humic acid onto TiO_2.

Table 4.18. Langmuir isotherm model parameters for the adsorption of 30 kDa fraction of humic acid onto TiO_2.

	q_{max}	K
UV_{365}, m^{-1}	196	1.662
UV_{280}, m^{-1}	4545	0.036
UV_{254}, m^{-1}	100 000	0.0014

The Langmuir isotherm binding constants, K, of UV-vis parameters were found to be in the order of UV_{365} >UV_{280} >UV_{254}. The maximum quantity adsorbable when all adsorption sites were occupied, q_{max}, could be assessed by the order of UV_{254} > UV_{280} > UV_{365}. $Color_{436}$ was not a significant parameter for 30 kDa fraction of humic acid because of very low initial absorbance values.

For the comparative evaluation of the adsorption parameters of different molecular fractions of humic acid, K and q_{max} values were given in order. The Langmuir isotherm binding constants, K, of different molecular fractions were found to be in the order of 0.45µm filtered fraction >100 kDa >Raw. The maximum quantity adsorbable when all adsorption sites were occupied, q_{max}, could be assessed by the order of Raw > 0.45µm filtered fraction >100 kDa.

4.6.5. Adsorption of Raw Humic Acid onto TiO_2 in the Presence of Zinc

Adsorption experiments in the presence of zinc were conducted by using raw humic acid and its different molecular size fractions, such as 0.45 µm filtered fraction, 100 kDa, and 30 kDa fractions of humic acid solution. TiO_2 loadings were changed in the range of 0.1-1.0 mg mL^{-1} and zinc concentration was kept constant in all experiments as 0.1 mg L^{-1}.

4.6.5.1. UV-vis Spectroscopic Evaluation of Raw Humic Acid Adsorption onto TiO_2 in the Presence of Zinc. As mentioned before, UV-vis spectra of humic acid adsorption onto TiO_2 in the presence of zinc displayed a monotonously decreasing trend increasing wavelength (Figure 4.75). Up to ~240 nm wavelength, humic acid in the presence of zinc showed the highest absorbance recordings. However, after 240 nm wavelength, it was crossed over the raw humic acid spectra (Figure 4.32). As explained in ‘’Photocatalytic degradation of humic acid in the presence of zinc’’ section; in the presence of zinc, a substantial increase in adsorption was observed in the spectral region of 200-235 nm. The UV-vis spectra followed the same trend of raw humic acid in the 235-600 nm wavelength regions.

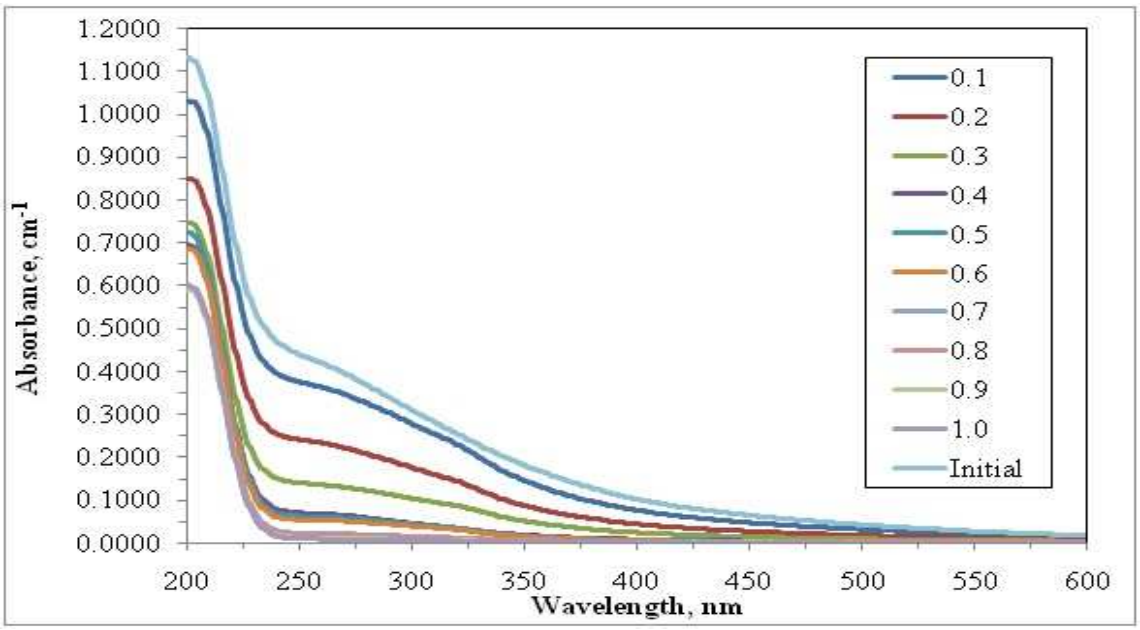

Figure 4.75. UV-vis spectra of raw humic acid adsorption onto TiO_2 in the presence of zinc (Initial represents raw humic acid and zinc binary system).

Comparison of the UV-vis spectra of the raw humic acid onto TiO_2 in the absence of zinc ions distinctly indicated the role of zinc and humic interaction with the TiO_2 surface (Figure 4.48 and Figure 4.75). Increasing doses of the adsorbent displayed significantly different spectral pattern in the 225nm- 500 nm regions. The effect of adsorption onto higher TiO_2 dosages was shown by the UV-vis spectra especially recorded after 0.7 mg mL^{-1} TiO_2 dose. It was observed that there were no characteristic absorbance recordings after this dose. While in the absence of zinc, the values became close to zero after 400 nm wavelength, this conditions were provided at ~250 nm for the experiments in the presence of zinc.

4.6.5.2. Fluorescence Spectroscopic Evaluation of Raw Humic Acid Adsorption onto TiO_2 in the Presence of Zinc. Emission scan fluorescence spectra of raw humic acid duringe adsorption in the presence of zinc samples were displayed in Figure 4.76. It could be stated that the excitation wavelength of 360 nm caused a major peak in the region of 450 nm. It was also recorded for the raw humic acid in the absence of zinc.

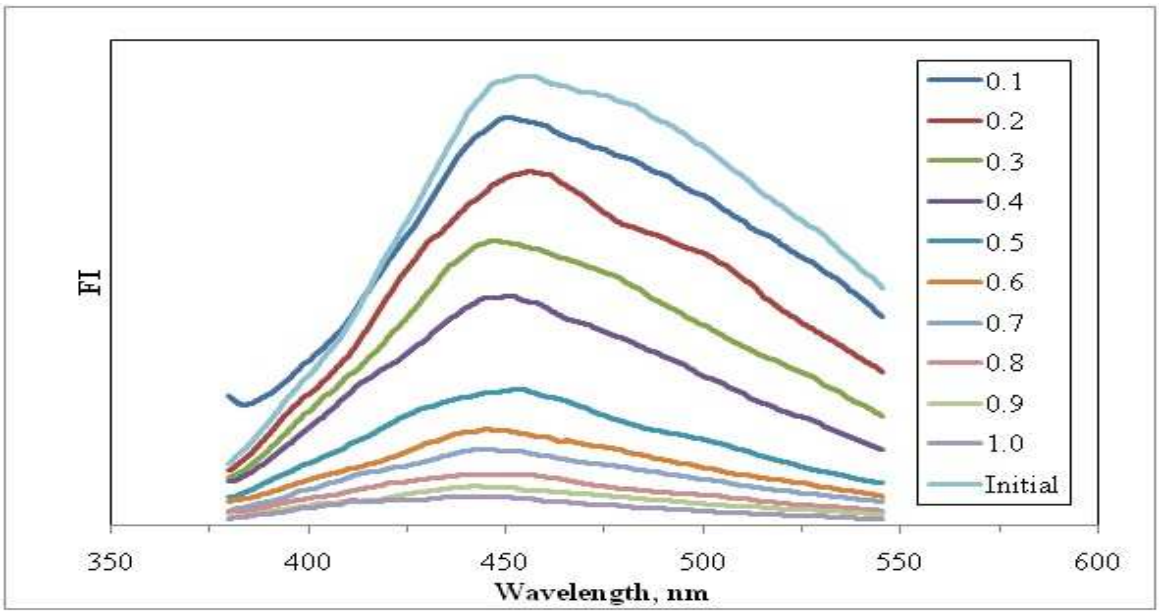

Figure 4.76. Emission scan fluoresence spectra of raw humic acid adsorption onto TiO_2 in the presence of zinc (Initial represents raw humic acid and zinc binary system).

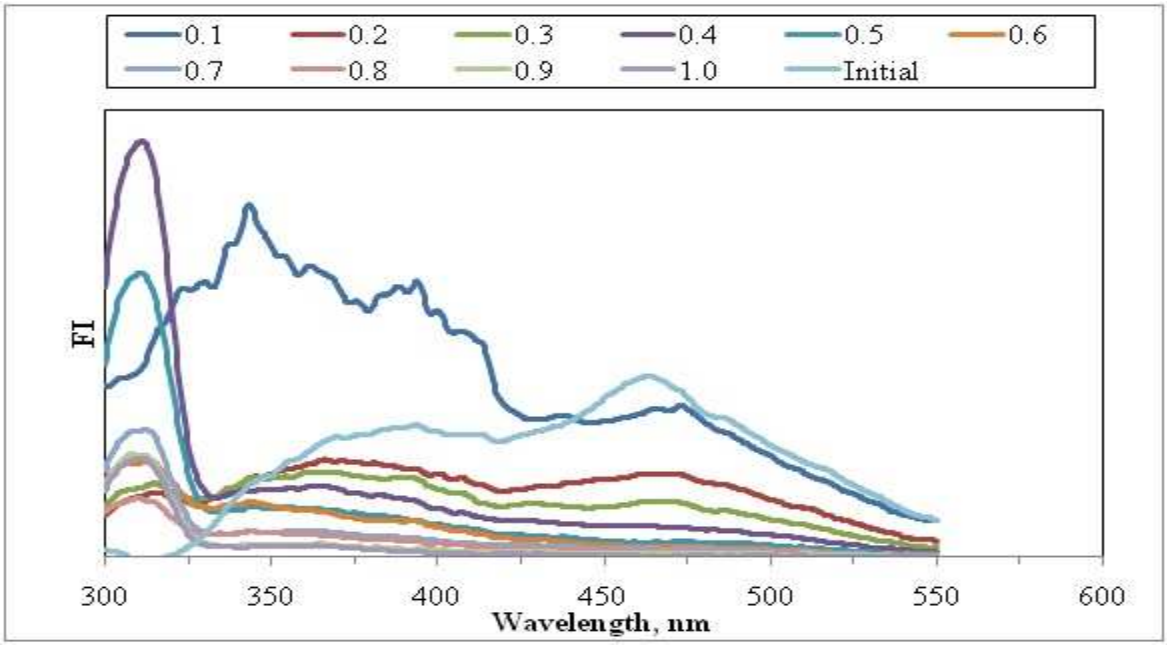

Figure 4.77. Synchronous scan fluorescence spectra of raw humic acid adsorption onto TiO_2 in the presence of zinc (Initial represents raw humic acid and zinc binary system).

As seen in Figure 4.76, a continuously decreasing trend in FI at λ_{max}=450 nm was observed with respect to increasing TiO_2 dose for raw humic acid adsorption onto TiO_2 in the presence of zinc. The raw humic acid and zinc binary system had the highest fluorescence trend. The peak was not found to be detectable upon higher TiO_2 doses such as 0.7 mg mL^{-1}, the trend closed to linear form. The synchronous scan fluorescence spectra recorded for the adsorption of raw humic acid in the presence of zinc were shown in Figure 4.77. As seen in the Figure 4.77, a continuously decreasing trend in FI at λ_{max}=470 nm was observed with respect to increasing TiO_2 dose for raw humic acid. While adsorption dependent fluorescence intensity displayed a decreasing trend with increasing dose of TiO_2 except 0.1 mg mL^{-1} TiO_2 dose, two new peaks were observed approximately at 345 and 395 nm wavelength with adsorption of raw humic acid onto the lowest dose, 0.1 mg mL^{-1} TiO_2. Also, the significant peaks were detected at around wavelength of 300nm.

4.6.5.3. Adsorption Isotherm Modeling of Raw Humic Acid in the Presence of Zinc. The adsorption data were evaluated in terms of Freundlich and Langmuir adsorption models.

Freundlich adsorption model. Freundlich adsorption isotherms for $Color_{436}$ and UV_{254} changes of humic acids were given in the Figure 4.78 and Figure 4.79 respectively. The Freundlich adsorption isotherms for UV_{365} and UV_{280} were presented in Appendix A. Figure 4.78 indicated that C_e values varied between 0.08 – 5.30 m^{-1} for $Color_{436}$ depending on the amount of TiO_2 present in solution. The values of q_A calculated to be in the range of 152.40 – 480 $m^{-1}g^{-1}$ for the corresponding C_e values.

As illustrated in Figure 4.79, C_e values varied between 0.88 – 36.99 m^{-1} for UV_{254}. The values of q_A calculated to be in the range of 869 – 1468 $m^{-1}g^{-1}$ for the corresponding C_e values. The adsorption isotherms showed similar trends both in terms of $Color_{436}$ and UV_{254} parameters. ΔC_e and Δq_A values for raw humic acid were calculated as 5.22 m^{-1} and 327.60 $m^{-1}g^{-1}$ respectively for $Color_{436}$. On the other hand for UV_{254} parameter, ΔC_e and Δq_A were calculated as 36.11 m^{-1} and 599 $m^{-1}g^{-1}$ respectively. The isotherm could be expressed by an L-type isotherm.

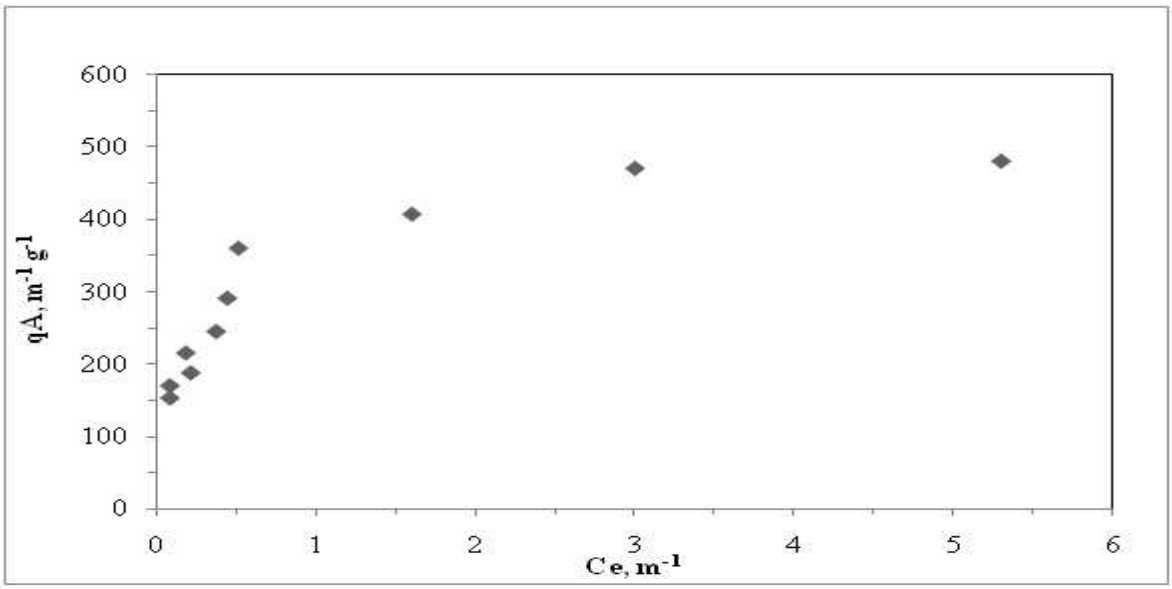

Figure 4.78. Freundlich adsorption isotherm of $Color_{436}$ of raw humic acid onto TiO_2 in the presence of zinc.

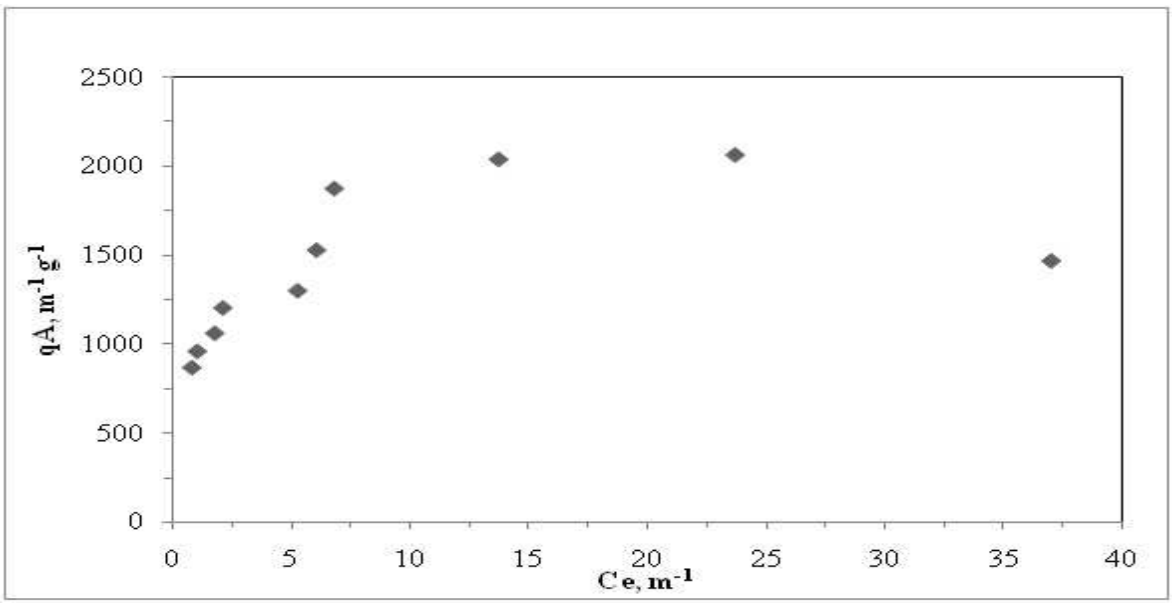

Figure 4.79. Freundlich adsorption isotherm of UV_{254} of raw humic acid onto TiO_2 in the presence of zinc.

Freundlich adsorption model was applied to the data obtained for UV-vis spectroscopic Isotherm model coefficiens; adsorption capacity, K_f, and adsorption strength, 1/n, for the adsorption of raw humic acid onto TiO_2 in the presence of zinc were listed in Table 4.19 ($R^2 \geq 0.70$).

Table 4.19. Freundlich isotherm model parameters for the adsorption of raw humic acid onto TiO_2 in the presence of zinc.

Humic acid	K_f	1/n
$Color_{436}$	340.4	0.284
UV_{365}	540.4	0.259
UV_{280}	891.9	0.181
UV_{254}	989.6	0.204

Adsorption capacity, K_f, for $Color_{436}$ was lower than UV absorbing centers. 1/n values for $Color_{436}$, UV_{365}, UV_{280} and UV_{254} were closed to each other. 1/n values were found to be lower than one; which indicates that the capacity tends to be independent of concentration. They express unfavorable adsorption intensities. Considerably higher K_f values were attained in the presence of zinc for UV_{365}, UV_{280} and UV_{254} contrary to the adsorption intensity factor as expressed by 1/n (Table 4.11).

Langmuir adsorption model. Langmuir adsorption isotherms of raw humic acid in the presence of zinc for $Color_{436}$ and UV_{254} were given in the Figure 4.80 and Figure 4.81, respectively. Langmuir adsorption isotherms for UV_{365} and UV_{280} were presented in Appendix B.

When the Langmuir adsorption isotherms of raw humic acid in the presence of zinc for all UV parameters were compared with Langmuir adsorption isotherms of raw humic acid in the absence of zinc, it was observed that the $1/C_e$ values in the presence of zinc were became 5 times higher than in the absence of zinc (Figures 4.53 and 4.54). On the other hand, $1/q_A$ values were nearly constant with no significant change. The role of complexation of zinc ions with humic moieties did not significantly later the adsorption profiles of raw humic acid onto TiO_2 surface as expressed by Langmuir adsorption model.

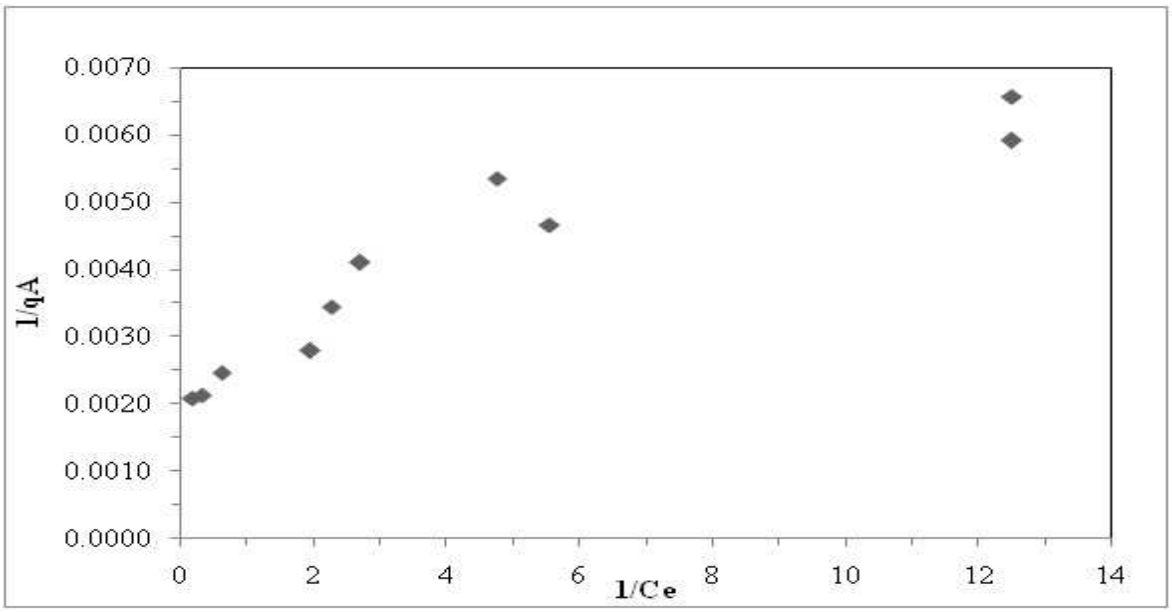

Figure 4.80. Langmuir adsorption isotherm of $Color_{436}$ of raw humic acid onto TiO_2 in the presence of zinc.

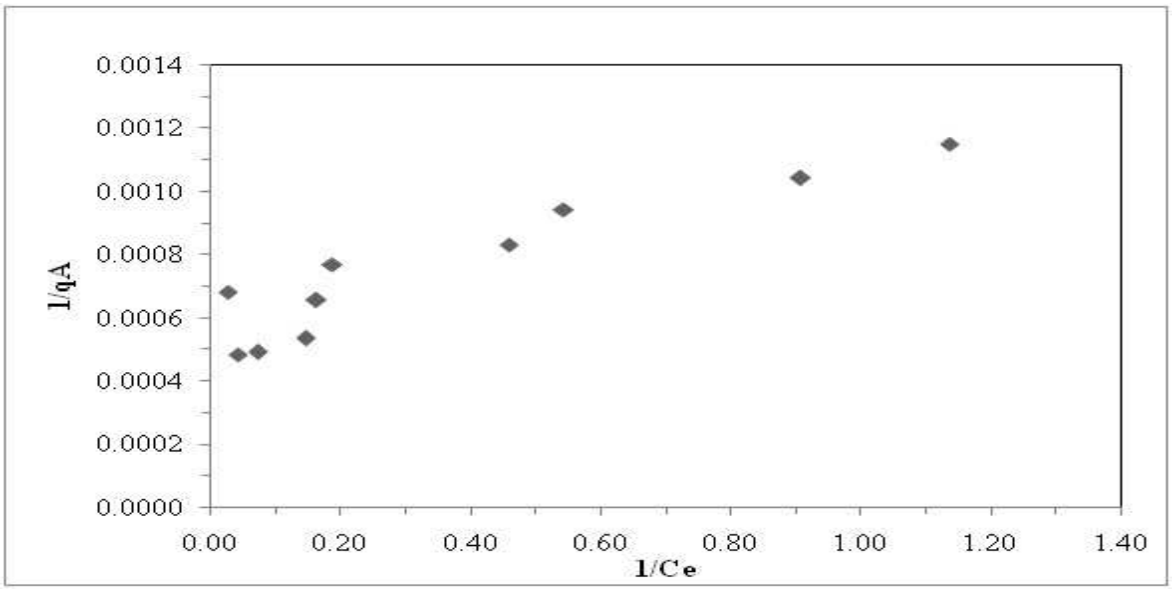

Figure 4.81. Langmuir adsorption isotherm of UV_{254} of raw humic acid onto TiO_2 in the presence of zinc.

Langmuir isotherm model coefficients; binding constant, K, and the maximum quantity adsorbable when all adsorption sites were occupied, q_{max}, for the adsorption of raw humic acid onto TiO_2 in the presence of zinc were listed in Table 4.20 ($R^2 \geq 0.80$).

Table 4.20. Langmuir isotherm model parameters for the adsorption of raw humic acid onto TiO_2 in the presence of zinc.

Humic acid	q_{max}	K
$Color_{436}$	394	7.938
UV_{365}	769	3.940
UV_{280}	1471	1.360
UV_{254}	1818	0.982

According to Table 4.20, q_{max} and K values for both the UV_{280} and UV_{254} were close to each other. There was approximately 78% difference between q_{max} values of $Color_{436}$ and UV_{254}. The difference between K values of $Color_{436}$ and UV_{254} was about 88%. The Langmuir isotherm binding constants, K, of UV-vis parameters were found to be in the order of $Color_{436} > UV_{365} > UV_{280} > UV_{254}$. The maximum quantity adsorbable when all adsorption sites were occupied, q_{max}, could be assessed by the order of $UV_{254} > UV_{280} > UV_{365} > Color_{436}$.

When the values of K and q_{max} were compared to the adsorption of raw humic acid in the absence of zinc, K values became ~8 times higher than adsorption of humic acid binding constants, K, with the addition of zinc. On the other hand, q_{max} values were decreased about 32% with the addition of zinc to adsorption experiments.

4.6.6. Adsorption of 0.45 μm Filtered Fraction of Humic Acid onto TiO_2 in the Presence of Zinc

0.45 μm filtered fraction of humic acid samples were evaluated by UV-vis spectra and fluorescence spectra as well as by the specified UV-vis and fluorescence parameters.

4.6.6.1. UV-vis Spectroscopic Evaluation of 0.45 µm Filtered Fraction of Humic Acid Adsorption onto TiO_2 in the Presence of Zinc. As seen in the Figure 4.82, the UV-vis spectra of 0.45 µm filtered fraction of humic acid showed a gradually declining trend with the respect to increasing wavelength in the 200-600 nm regions. The effect of the presence of zinc can be observed at ≤ 240 nm wavelength with higher absorbance values than raw 0.45 µm filtered fraction of humic acid. As mentioned in photocatalytic degradation section, the presence of zinc ions caused a dramatic effect on the UV-vis spectra of humic acid (Figure 4.36). An essential increase in absorption was observed in the spectral region of 200-235 nm. The UV-vis spectra followed the same trend of raw 0.45 µm filtered fraction of humic acid in the 235-600 nm wavelength region.

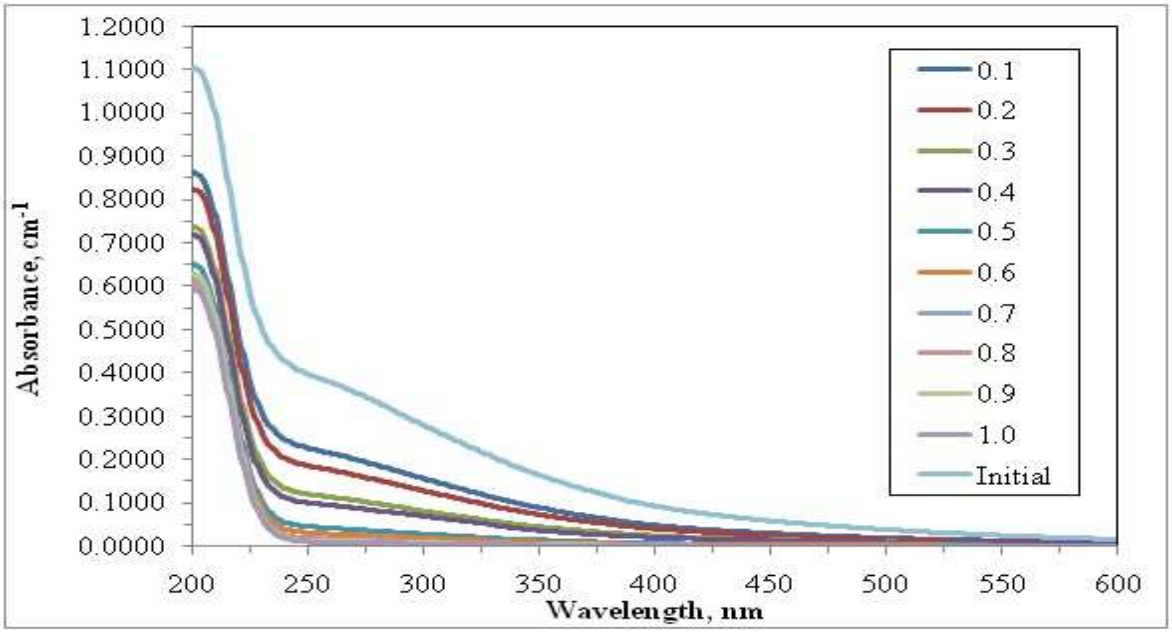

Figure 4.82. UV-vis spectra of 0.45µm filtered fraction of humic acid adsorption onto TiO_2 in the presence of zinc (Initial represents 0.45µm filtered fraction of humic acid and zinc binary system).

While in the absence of zinc, the absorbance values were became close to zero after 400 nm wavelength, these conditions were provided at lower than 250 nm for 0.45 µm filtered fraction of humic acid adsorption onto TiO_2 in the presence of zinc.

4.6.6.2. Fluorescence Spectroscopic Evaluation of 0.45 µm Filtered Fraction of Humic Acid Adsorption onto TiO_2 in the Presence of Zinc. Emission scan fluorescence spectra of 0.45µm filtered fraction of humic acid adsorption onto TiO_2 in the presence of zinc samples were displayed in Figure 4.83. It could be stated that the excitation wavelength of 360 nm caused a major peak in the region of 450 nm as was also recorded for 0.45 µm filtered fraction of humic acid in the absence of zinc. The emission scan spectra of fluorescence intensities displayed a declining trend with respect to increasing TiO_2 dose from 0.1 to 1.0 mg mL^{-1}.

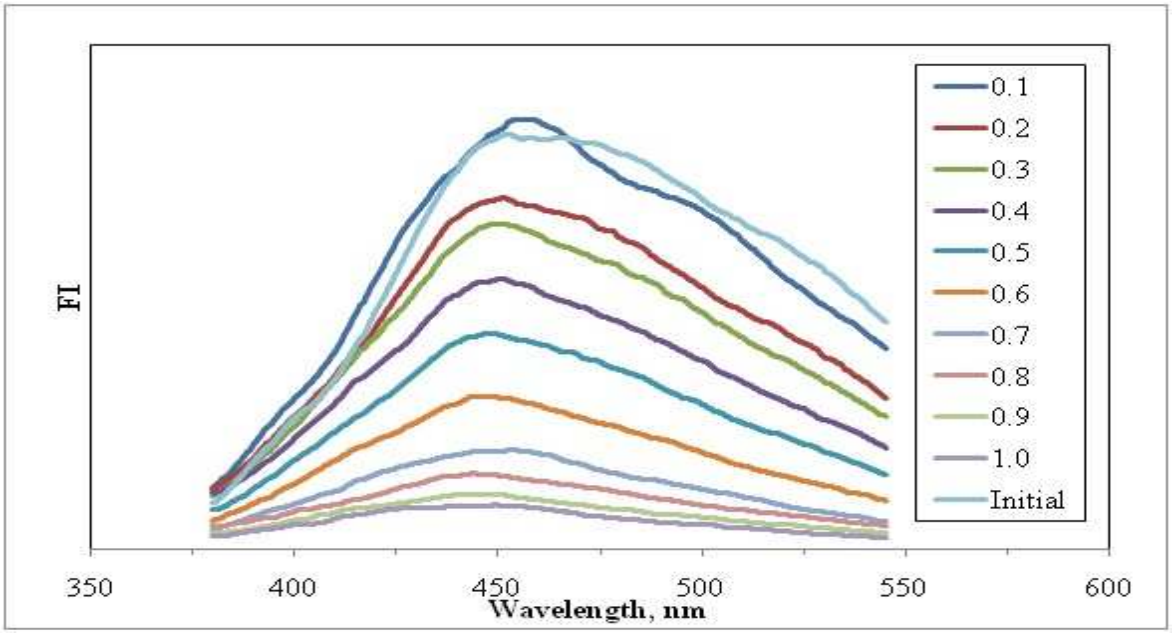

Figure 4.83. Emission scan fluorescence spectra of 0.45 µm filtered fraction of humic acid adsorption onto TiO_2 in the presence of zinc (Initial represents 0.45µm filtered fraction of humic acid and zinc binary system).

While the trend of adsorption onto the lowest adsorbent dose had the highest fluorescence intensity, the spectrum of 0.45µm filtered fraction of humic acid and zinc combination had similar fluorescence intensities with low changes. Upon the adsorption onto 0.8 mg mL^{-1} TiO_2 dose, the peak at 450 nm wavelength was dissappeared and became a linear form.

Synchronous scan spectra of 0.45 µm filtered fraction of humic acid in the presence of zinc as illustrated by Figure 4.84 displayed a declining of fluorescence intensities. As explained in the adsorption studies of humic acid in the absence of zinc; the synchronous scan fluorescence spectra for 0.45 µm filtered fraction of humic acid displayed a sharp peak around wavelength of 470 nm.

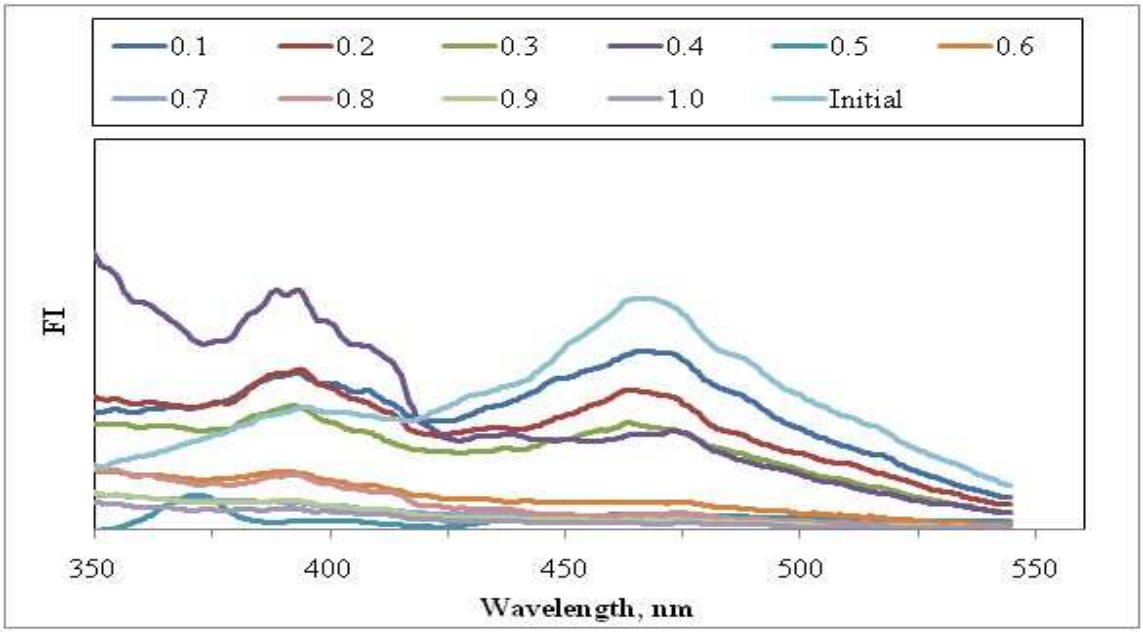

Figure 4.84. Synchronous scan fluorescence spectra of 0.45 µm filtered fraction of humic acid adsorption onto TiO_2 in the presence of zinc (Initial represents 0.45µm filtered fraction of humic acid and zinc binary system).

There was also a moderate peak around 395 nm wavelengths with a comparatively lower intensity. 0.45µm filtered fraction of humic acid and zinc binary system had the highest trend in Figure 4.84. Adsorption of 0.45 µm filtered fraction of humic acid onto increased TiO_2 doses, the adsorption equilibrium was reached while the major peak at 470 nm was disappeared. On the other hand, adsorption onto the highest TiO_2 doses gave major peak at 400 nm wavelengh with high fluorescence intensities. The presence of different peaks at different wavelengths could be attributed to the presence of zinc.

4.6.6.3. Adsorption Isotherm Modeling of 0.45 μm Filtered Fraction of Humic Acid in the Presence of Zinc. The adsorption data were evaluated in terms of Freundlich and Langmuir adsorption models.

Freundlich adsorption model. Freundlich adsorption isotherms for $Color_{436}$ and UV_{254} changes of humic acids were given in the Figure 4.85 and Figure 4.86 respectively. The Freundlich adsorption isotherms for UV_{365} and UV_{280} were presented in Appendix A.

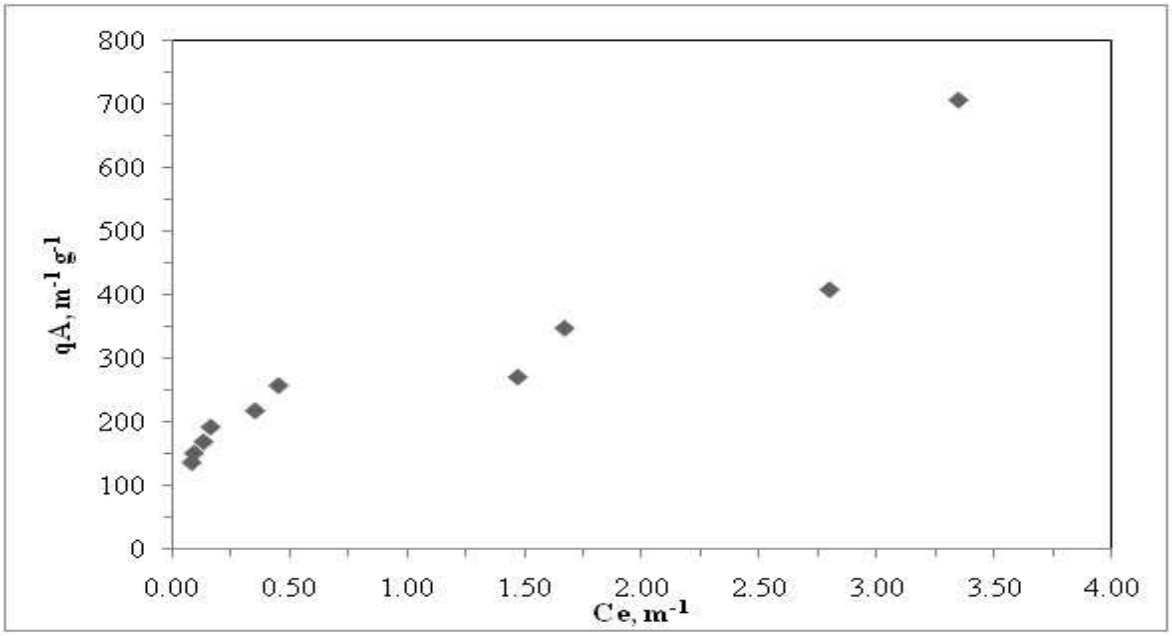

Figure 4.85. Freundlich adsorption isotherm of $Color_{436}$ of 0.45 μm filtered fraction of humic acid onto TiO_2 in the presence of zinc.

C_e values varied between 0.08 – 3.35 m^{-1} for $Color_{436}$ depending on the amount of TiO_2 present in solution as shown in Figure 4.85. The values of q_A calculated to be in the range of 136 – 706 $m^{-1}g^{-1}$ for the corresponding C_e values. As seen in Figure 4.86, C_e values varied between 0.85 – 22.09 m^{-1} for $UV_{254.}$ The values of q_A calculated to be in the range of 783.6 -3588 $m^{-1}g^{-1}$ for the corresponding C_e values. The adsorption isotherms show similar trend both in terms of $Color_{436}$ and UV_{254} parameters. ΔC_e and Δq_A values for 0.45 μm filtered humic acid were 3.27 m^{-1} and 570 $m^{-1}g^{-1}$, respectively at $Color_{436}$. ΔC_e and Δq_A for UV_{254} were 21.24 m^{-1} and 2804.4 $m^{-1}g^{-1}$, respectively. The isotherm exhibited S- curve type isotherm.

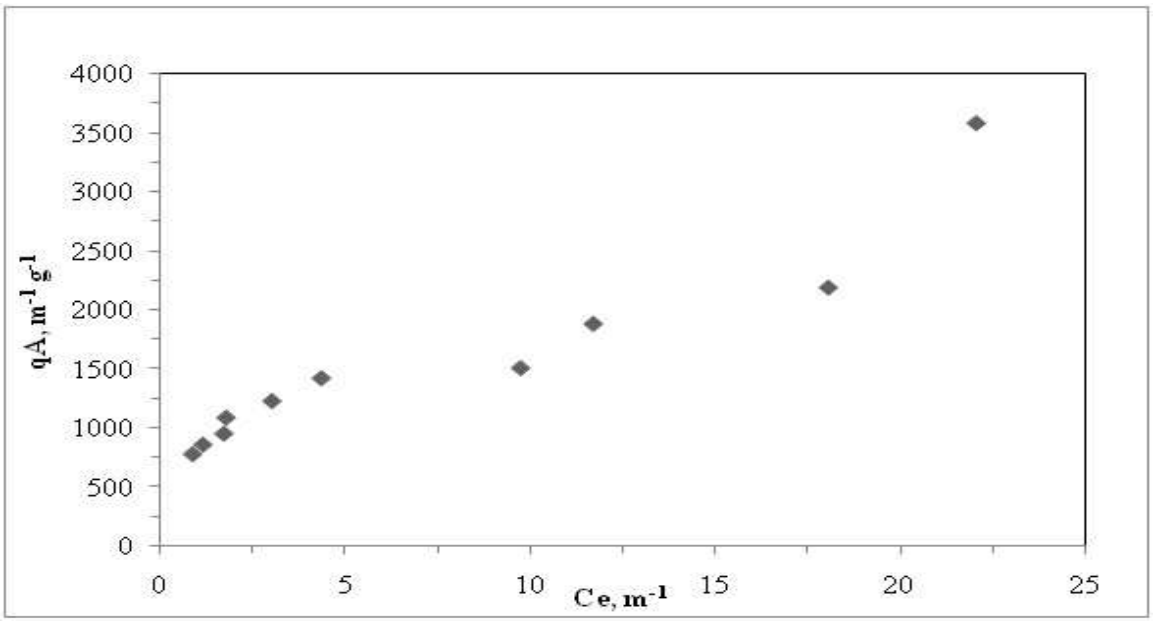

Figure 4.86. Freundlich adsorption isotherm of UV_{254} of 0.45 μm filtered fraction of humic acid onto TiO_2 in the presence of zinc.

Freundlich adsorption model was applied to the data obtained for UV-vis spectroscopic parameters i.e. $Color_{436}$, UV_{365}, UV_{280} and UV_{254}. Isotherm model coefficiens; adsorption capacity, K_f, and adsorption strength, 1/n, for the adsorption of 0.45μm filtered fraction of humic acid onto TiO_2 in the presence of zinc were listed in Table 4.21 ($R^2 \geq 0.70$).

Table 4.21. Freundlich isotherm model parameters for the adsorption of 0.45 μm filtered fraction of humic acid onto TiO_2 in the presence of zinc.

Humic acid	K_f	1/n
$Color_{436}$	321.9	0.329
UV_{365}	516.1	0.322
UV_{280}	765.7	0.370
UV_{254}	813.0	0.376

According to Table 4.21, adsorption capacities of 0.45 μm filtered fraction of humic acid in the presence of zinc were found to be higher than the adsorption capacities of 0.45 μm fractionated humic acid for each parameter. The adsorption capacity constant for $Color_{436}$ gave the lowest value when adsorption capacity constants for UV absorbing centers (UV_{280}, and UV_{254}) were approximately equal to each other. There was a 60% difference between the K_f values of $Color_{436}$ and UV_{254}. 1/n values for $Color_{436}$, UV_{365}, UV_{280} and UV_{254} were very closed to each other and found to be lower than 1, it shows that the adsorption bond was strong and the capacity tended to be independent of Ce.

Langmuir adsorption model. Langmuir adsorption isotherms of 0.45μm filtered fraction of humic acid in the presence of zinc for $Color_{436}$ and UV_{254} were given in the Figure 4.87 and Figure 4.88, respectively. Langmuir adsorption isotherms of UV_{365} and UV_{280} were presented in Appendix B. As seen in Figure 4.87 and Figure 4.88, Langmuir adsorption isotherms showed similar trend both in terms of $Color_{436}$ and UV_{254} parameters. The Langmuir adsorption isotherms of 0.45μm filtered fraction of humic acid in the presence of zinc for all UV parameters were compared with Langmuir adsorption isotherms of 0.45μm filtered fraction of humic acid in the absence of zinc.

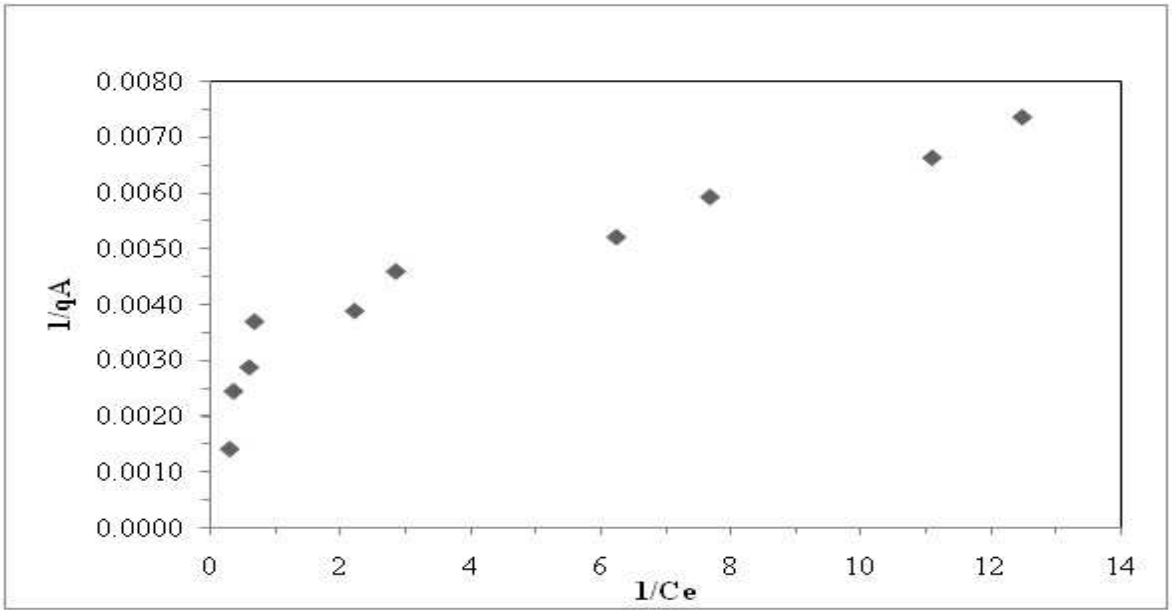

Figure 4.87. Langmuir adsorption isotherm of $Color_{436}$ of 0.45μm filtered fraction of humic acid onto TiO_2 in the presence of zinc.

It was observed that the $1/C_e$ values in the presence of zinc were became four times higher than the experiments in the absence of zinc. On the other hand, $1/q_A$ values were nearly constant with no significant change.

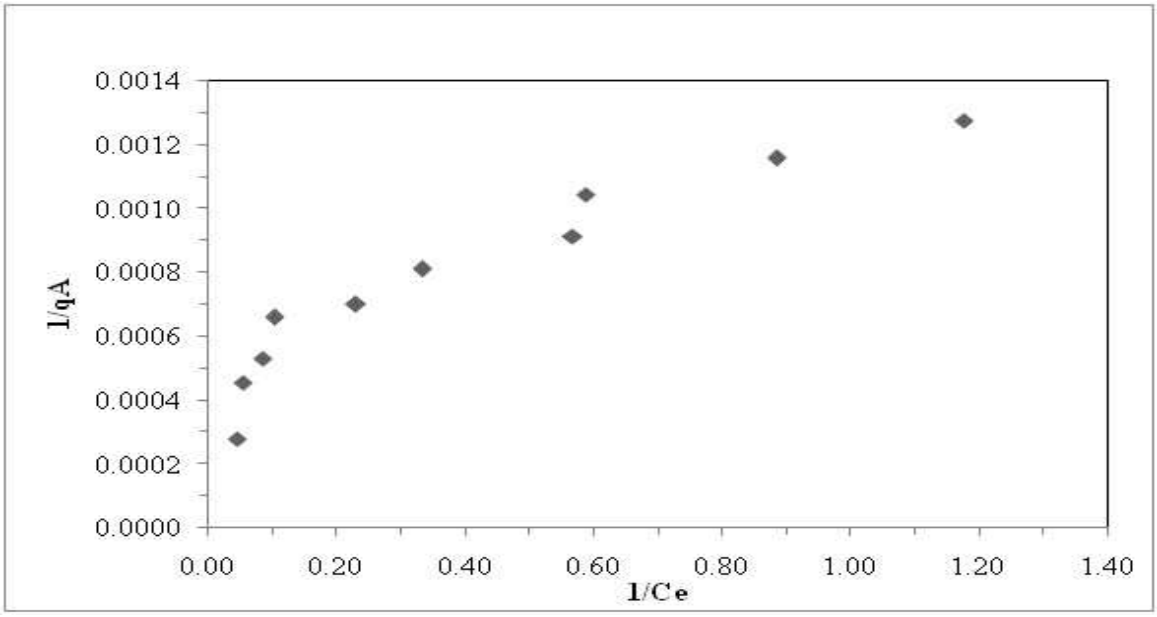

Figure 4.88. Langmuir adsorption isotherm of UV_{254} of 0.45µm filtered fraction of humic acid onto TiO_2 in the presence of zinc.

Langmuir isotherm model coefficients; binding constant, K, and the maximum quantity adsorbable when all adsorption sites were occupied, q_{max}, for the adsorption of 0.45 µm filtered fraction of humic acid onto TiO_2 in the presence of zinc were listed in Table 4.22 ($R^2 \geq 0.80$).

Table 4.22. Langmuir isotherm model parameters for the adsorption of 0.45 µm filtered fraction of humic acid onto TiO_2 in the presence of zinc.

Humic acid	q_{max}	K
$Color_{436}$	373	6.874
UV_{365}	709	4.274
UV_{280}	1818	0.797
UV_{254}	2128	0.610

According to Table 4.22, q_{max} and K values for both the UV_{280} and UV_{254} were very close to each other. There was approximately 82% difference between q_{max} values of $Color_{436}$ and UV_{254}. The difference between K values of $Color_{436}$ and UV_{254} was about 91%. The Langmuir isotherm binding constants, K, of UV-vis parameters were found to be in the order of $Color_{436}$>UV_{365} >UV_{280} >UV_{254}.The maximum quantity adsorbable when all adsorption sites were occupied, q_{max}, could be assessed by the order of UV_{254} > UV_{280} > UV_{365} > $Color_{436}$. When the values of K and q_{max} were compared to the adsorption of 0.45 µm filtered fraction of humic acid in the absence of zinc, K values became about three times higher than adsorption of humic acid binding constants, K, with the addition of zinc. On the other hand, q_{max} was decreased about 10% with the addition of zinc to adsorption experiments.

4.6.7. Adsorption of 100 kDa Fraction of Humic Acid onto TiO_2 in the Presence of Zinc

The humic acid samples attained by adsorption were evaluated by UV-vis spectra and fluorescence spectra as well as by the specified UV-vis and fluorescence parameters.

4.6.7.1. UV-vis Spectroscopic Evaluation of 100 kDa Fraction of Humic Acid Adsorption onto TiO_2 in the Presence of Zinc. UV-vis spectra displayed a logarithmic decaying shape for all samples obtained after adsorption of 100 kDa fraction of humic acid in the presence of zinc. However, the humic acid in the presence of zinc have higher absorbance recordings up to 240 nm, it can be reached the same trend with initial humic acid at ~ 350 nm wavelength. UV-vis spectra displayed significantly low absorbance values throughout the whole wavelength region especially after 250 nm wavelength. After adsorption of 100 kDa fraction of humic acid onto 0.3 mg mL^{-1} TiO_2 and more than this dose, the trends crossed to each other with low differences.

In comparison to the UV-vis spectra recorded for 100 kDa fraction of humic in the absence of humic acid (Figure 4.62) significantly different trend in the lower wavelength range (< 250 nm) was observed due to the complexation behavior of zinc ions and humic moieities.

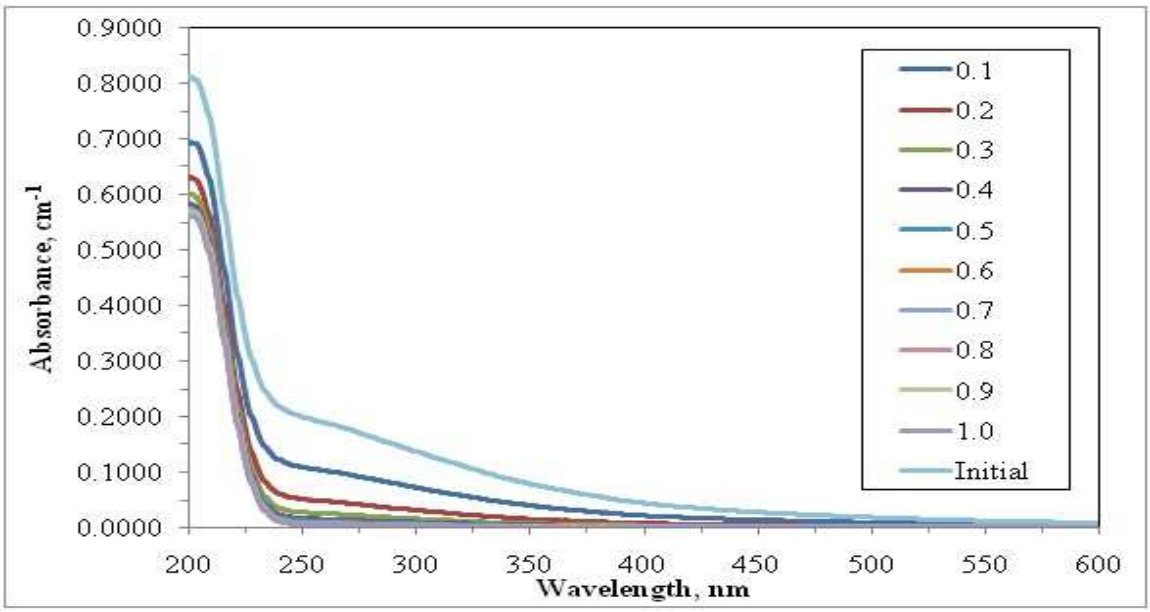

Figure 4.89. UV-vis spectra of 100 kDa fraction of humic acid adsorption onto TiO_2 in the presence of zinc (Initial represents 100 kDa fraction of HA and zinc binary system).

As explained in photocatalytic degradation of humic acid in the presence of zinc, the presence of zinc ions caused a dramatic effect on the UV-vis spectra of 100 kDa fraction humic acid (Figure 4.40). A significant increase in absorption was observed in the spectral region of 200-235 nm. The UV-vis spectra followed the same trend of 100 kDa fraction of humic acid in the 235-600 nm wavelength regions. Moreover, the UV-vis spectra displayed a $\Delta Abs \leq 0.003$ in the wavelength region of 230-350 nm followed by a complete overlapping trend in the wavelength region of 350-600 nm.

4.6.7.2. Fluorescence Spectroscopic Evaluation of 100 kDa Fraction of Humic Acid Adsorption onto TiO_2 in the Presence of Zinc. Significant changes in the shape of emission scan fluorescence spectra of 100 kDa fraction of humic acid adsorption onto TiO_2 in the presence of zinc were seen in Figure 4.90. The maximum fluorescence intensity peak was recorded at 450 nm wavelength in accordance with the previously investigated other humic acid and humic acid zinc binary systems. Starting from adsorption onto 0.1 to 1.0 mg mL^{-1} TiO_2 doses, all of the fluorescence intensities were decreased.

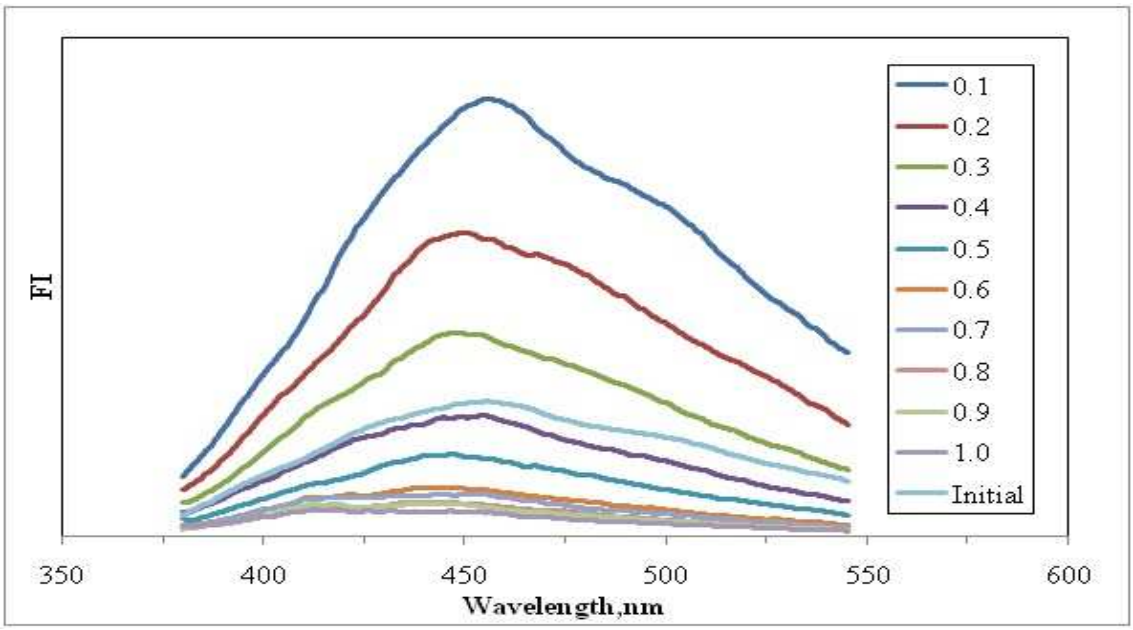

Figure 4.90. Emission scan fluorescence spectra of 100 kDa fraction of humic acid adsorption onto TiO_2 in the presence of zinc (Initial represents 100 kDa fraction of HA and zinc binary system).

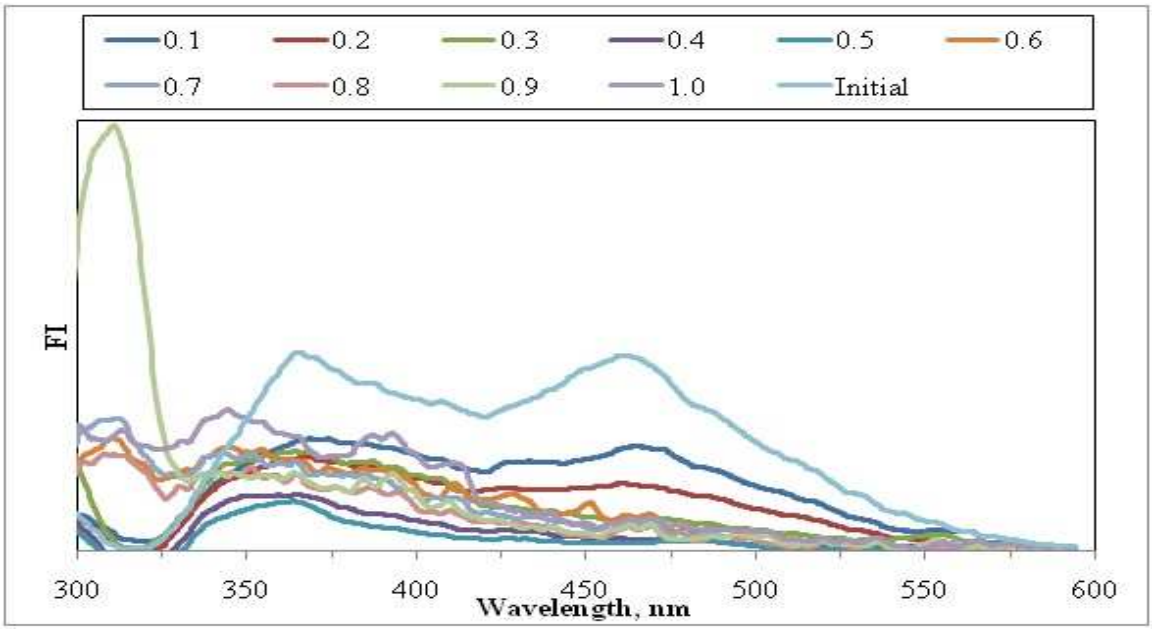

Figure 4.91. Synchronous scan fluorescence spectra of 100 kDa fraction of humic acid adsorption onto TiO_2 in the presence of zinc (Initial represents 100 kDa fraction of HA and zinc binary system).

The emission fluorescence intensity peak was not found to be detectable upon adsorption of 100 kDa fraction of humic acid onto 0.5 mg mL^{-1} TiO_2 dose, and the trend closed to a linear form. The "initial" binary system exhibited a similar trend between the adsorption doses of 0.3 mg mL^{-1} and 0.4 mg mL^{-1} TiO_2. The synchronous fluorescence spectra of 100 kDa fraction of humic acid adsorption onto TiO_2 in the presence of zinc were given in Figure 4.91. Although the recorded synchronous fluorescence spectra were not found to be discriminative, the adsorptive removal of fluorophoric groups could still be detectable with a decreasing trend for zinc and humic acid binary system.

4.6.7.3. Adsorption Isotherm Modeling of 100 kDa Fraction of Humic Acid in the Presence of Zinc. The adsorption data were evaluated in terms of Freundlich and Langmuir adsorption models.

Freundlich adsorption model. Freundlich adsorption isotherms for $Color_{436}$ and UV_{254} changes of humic acids were given in the Figures 4.92 and 4.93. Freundlich adsorption isotherms for UV_{365} and UV_{280} were presented in Appendix A.

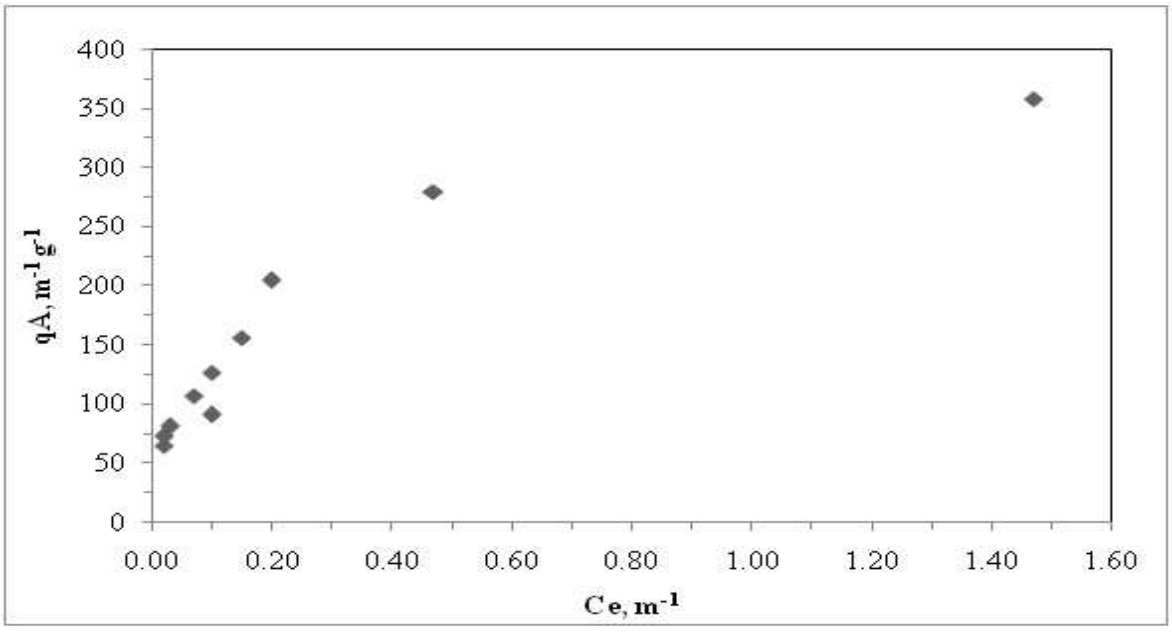

Figure 4.92. Freundlich adsorption isotherm of $Color_{436}$ of 100 kDa fraction of humic acid onto TiO_2 in the presence of zinc.

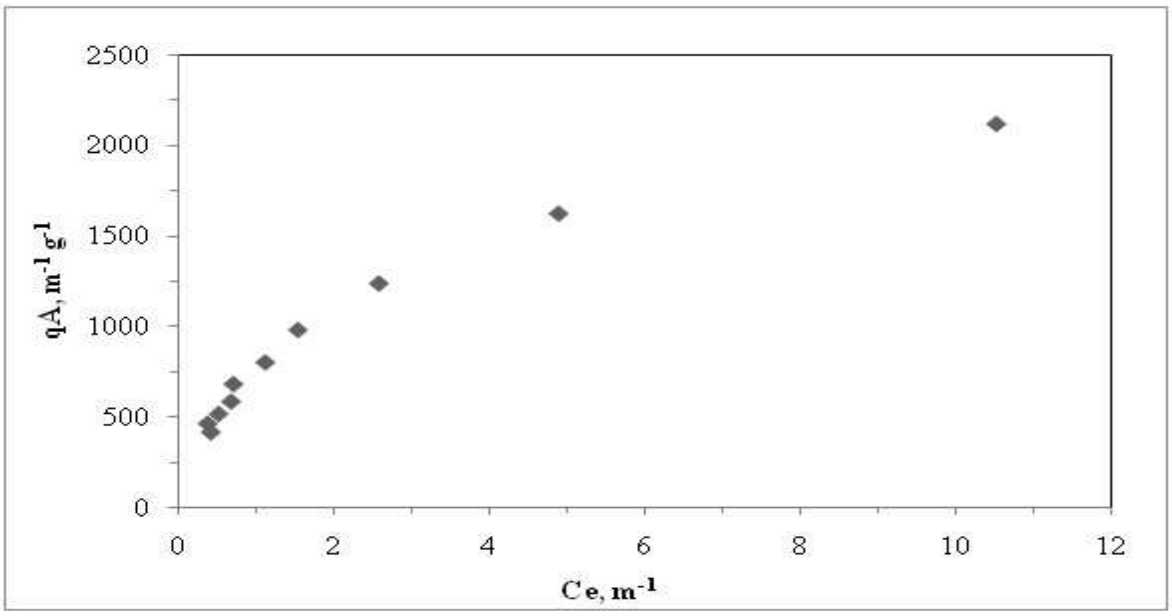

Figure 4.93. Freundlich adsorption isotherm of UV_{254} of 100 kDa fraction of humic acid onto TiO_2 in the presence of zinc.

Figure 4.92 indicated that C_e values varied between 0.02 – 1.47 m^{-1} for $Color_{436}$ depending on the amount of TiO_2 present in solution. The values of q_A calculated to be in the range of 64.80 - 358 $m^{-1}g^{-1}$ for the corresponding C_e values. As seen in Figure 4.93, C_e values varied between 0.44 – 10.54 m^{-1} for $UV_{254.}$ The values of q_A calculated to be in the range of 413.40 - 2114 $m^{-1}g^{-1}$ for the corresponding C_e values. The adsorption isotherms show similar trend both in terms of $Color_{436}$ and UV_{254} parameters. ΔC_e and Δq_A values for 100 kDa fraction of humic acid were 1.45 m^{-1} and 293.2 $m^{-1}g^{-1}$, respectively at $Color_{436}$. ΔC_e and Δq_A for UV_{254} were 10.1 m^{-1} and 1700.6 $m^{-1}g^{-1}$, respectively. This exhibited trend was agreed with L- curve type isotherm which was typically concave to the concentration axis and generally characterized by an initial slope that does not increase with adsorbate in the solution.

Freundlich adsorption model was applied to the data obtained for UV-vis spectroscopic parameters i.e. $Color_{436}$, UV_{365}, UV_{280} and UV_{254}. Isotherm model coefficiens; adsorption capacity, K_f, and adsorption strength, 1/n, for the adsorption of 100 kDa fraction of humic acid onto TiO_2 in the presence of zinc were listed in Table 4.23 ($R^2 \geq$ 0.70).

Table 4.23. Freundlich isotherm model parameters for the adsorption of 100 kDa fraction of humic acid onto TiO_2 in the presence of zinc.

Humic acid	K_f	1/n
$Color_{436}$	329.8	0.412
UV_{365}	509.2	0.394
UV_{280}	710.9	0.482
UV_{254}	720.2	0.499

Adsorption intensity for $Color_{436}$ was lower than UV absorbing centers. On the other hand, adsorption intensities for each UV-vis parameter were found to be lower than one, it indicated that the adsorption bond was strong, the capacity tended to be independent of Ce. According to Table 4.23, adsorption capacities of 100 kDa fraction of humic acid onto TiO_2 in the presence of zinc were found to be higher than in the absence of zinc.

Langmuir adsorption model. Langmuir adsorption isotherms of 100 kDa fraction of humic acid in the presence of zinc for $Color_{436}$ and UV_{254} were given in the Figure 4.94 and Figure 4.95, respectively. Langmuir adsorption isotherms of UV_{365} and UV_{280} were presented in Appendix B.

When the Langmuir adsorption isotherms of 100 kDa fraction of humic acid in the presence of zinc for all UV parameters were compared with Langmuir adsorption isotherms of 100 kDa fraction of humic acid in the absence of zinc, it was observed that the $1/C_e$ values in the presence of zinc were 5-10 times higher than in the absence of zinc (Figure 4.67 and Figure 4.68). On the other hand, $1/q_A$ values were nearly the same with no significant change. The isotherms attained under both conditions could be successfully modeled by Langmuir model and the model parameters could be compared.

Langmuir isotherm model coefficients; binding constant, K, and the maximum quantity adsorbable when all adsorption sites were occupied, q_{max}, for the adsorption of 100 kDa fraction of humic acid onto TiO_2 in the presence of zinc were listed in Table 4.24 ($R^2 \geq 0.80$).

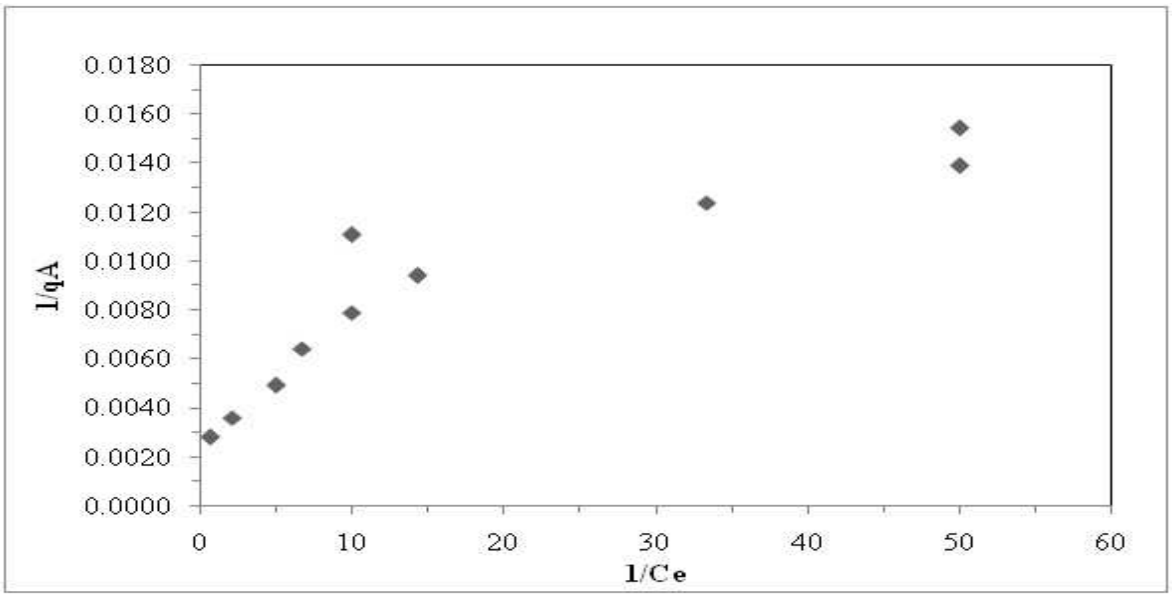

Figure 4.94. Langmuir adsorption isotherm of $Color_{436}$ of 100 kDa fraction of humic acid onto TiO_2 in the presence of zinc.

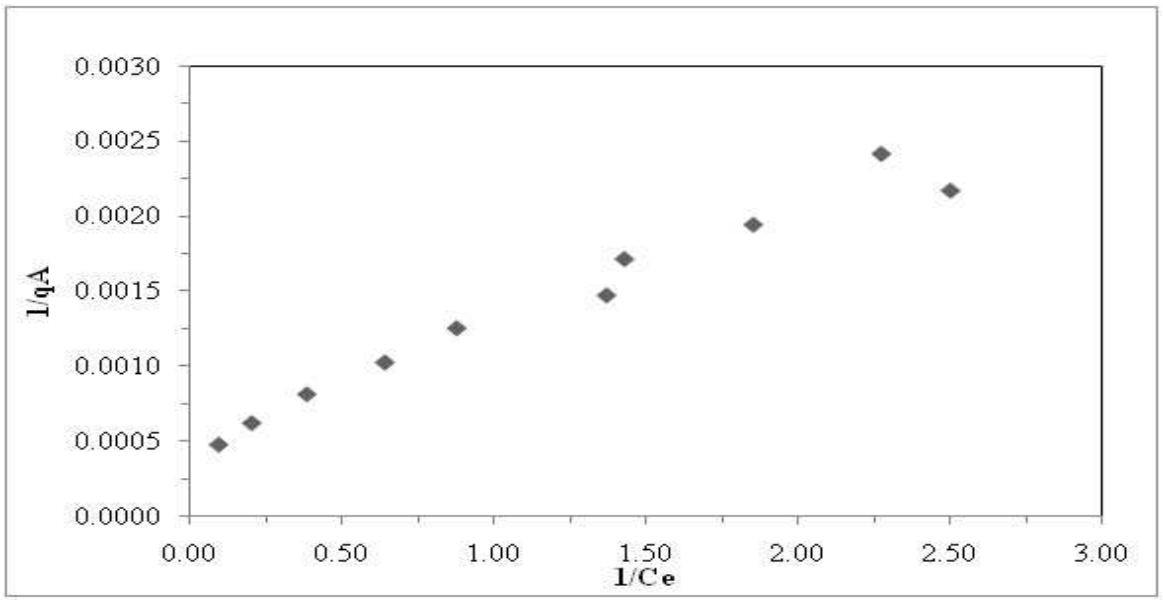

Figure 4.95. Langmuir adsorption isotherm of UV_{254} of 100 kDa fraction of humic acid onto TiO_2 in the presence of zinc.

According to Table 4.24, q_{max} and K values for both the UV_{280} and UV_{254} were close to each other. There was approximately 90% difference between q_{max} values of $Color_{436}$ and UV_{254}.The difference between K values of $Color_{436}$ and UV_{254} was about 97%.

Table 4.24. Langmuir isotherm model parameters for the adsorption of 100 kDa fraction of humic acid onto TiO_2 in the presence of zinc.

Humic acid	q_{max}	K
$Color_{436}$	200	23.81
UV_{365}	398	14.78
UV_{280}	1515	1.100
UV_{254}	2000	0.649

The Langmuir isotherm binding constants, K, of UV-vis parameters were found to be in the order of $Color_{436}$>UV_{365} >UV_{280} >UV_{254}. The maximum quantity adsorbable when all adsorption sites were occupied, q_{max}, could be assessed by the order of UV_{254} > UV_{280} > UV_{365} > $Color_{436}$.

4.6.8. Adsorption of 30 kDa Fraction of Humic Acid onto TiO_2 in the Presence of Zinc

30 kDa fraction of humic acid samples were evaluated by UV-vis spectra and fluorescence spectra as well as by the specified UV-vis and fluorescence parameters.

4.6.8.1. UV-vis Spectroscopic Evaluation of 30kDa Fraction of Humic Acid Adsorption onto TiO_2 in the Presence of Zinc. Considering the initial UV-vis spectral features of the 30 kDa fraction of humic acid, the attained absorbance recordings were significantly lower than the considerably higher molecular weight fractions. The raw absorbance values of 30 kDa fraction of humic acid were about 95% and 87% less than raw humic acid for $Color_{436}$ and $UV_{254,}$ respectively. As could be seen at other fractions, 30 kDa fraction of humic acid in the presence of zinc gave a similar trend with increasing wavelength.

The presence of zinc ions caused a dramatic effect on the UV-vis spectra of humic acid (Figure 4.44). A significant increase in absorption was observed in the spectral region of 200-235 nm. The UV-vis spectra followed the same trend of 30 kDa fraction humic acid in the 235-600 nm wavelength regions.

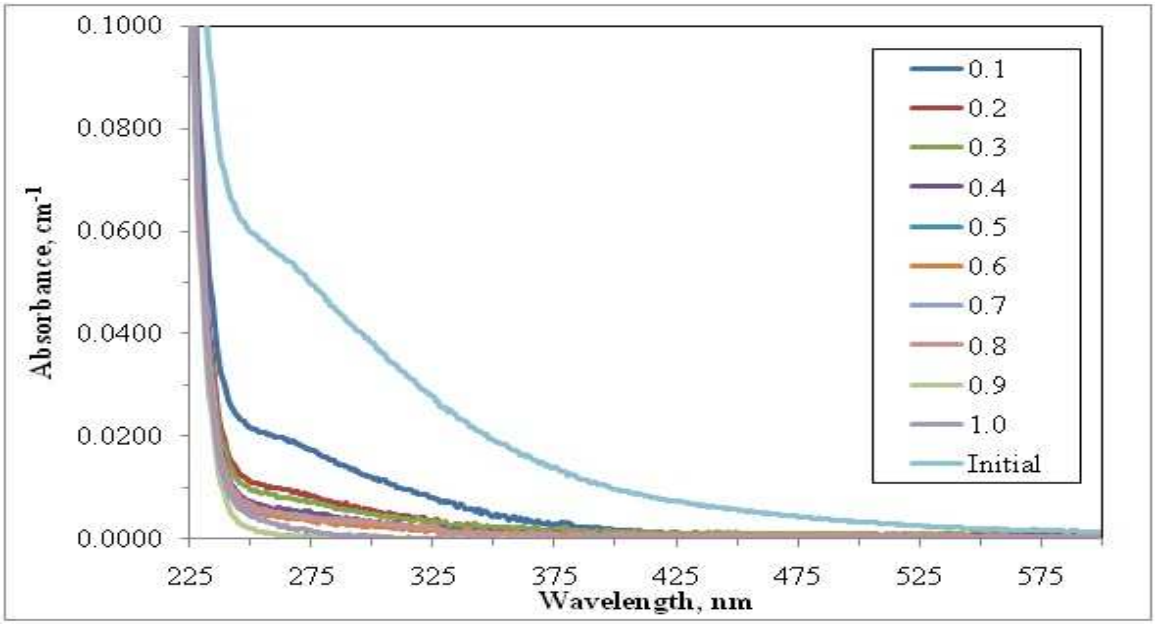

Figure 4.96. UV-vis spectra of 30 kDa fraction of humic acid adsorption onto TiO_2 in the presence of zinc (Initial represents 30 kDa fraction of HA and zinc binary system).

Especially, after adsorption of 30 kDa fraction of humic acid onto 0.3 mg mL^{-1} TiO_2 dose, no significant absorbance changes were observed. Even for lower TiO_2 loadings (0.1 mg mL^{-1}), UV-vis spectra was reached to very low absorbance values.

4.6.8.2. Fluorescence Spectroscopic Evaluation of 30kDa Fraction of Humic Acid Adsorption onto TiO_2 in the Presence of Zinc. Emission scan fluorescence spectra for 30 kDa fraction of humic acid Adsorption onto TiO_2 in the presence of zinc were shown in Figure 4.97. Raw 30 kDa fraction of humic acid had a peak around 450 nm with relatively high fluorescence intensity with respect to the other 30 kDa fraction of humic acid samples.

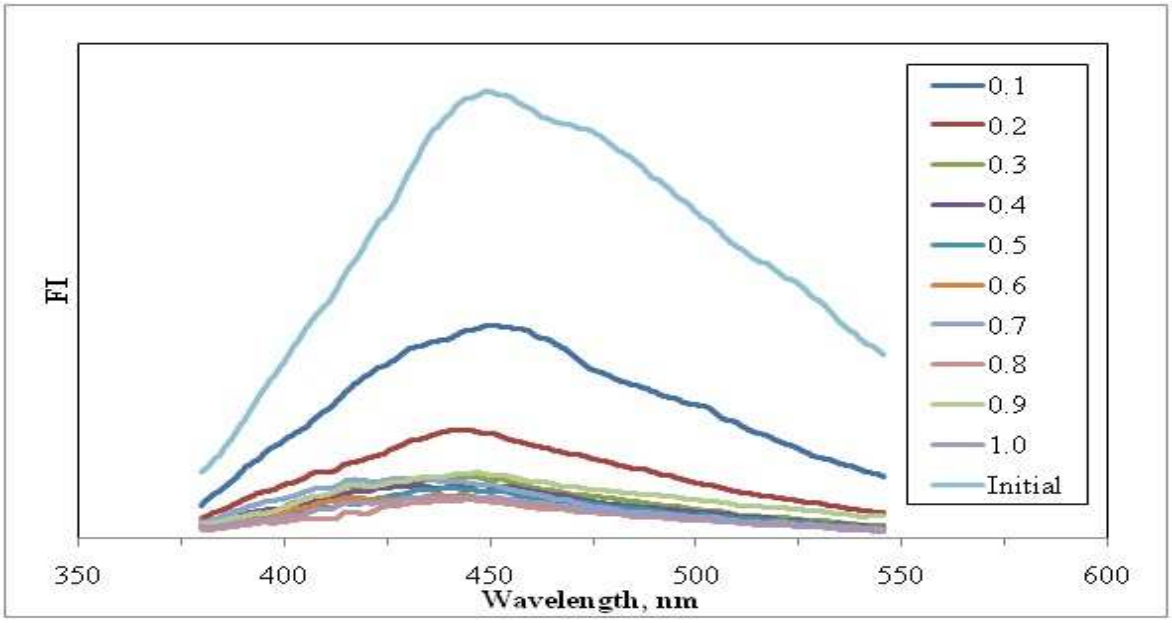

Figure 4.97. Emission scan fluorescence spectra of 30kDa fraction of humic acid adsorption onto TiO_2 in the presence of zinc (Initial represents 30 kDa fraction of HA and zinc binary system).

Zinc and humic acid binary system had lower fluorescence intensities than raw 30 kDa fraction of humic acid. With increasing TiO_2 dose, a gradual decrease in fluorescence intensity became evident in the emission fluorescence spectra. Initial adsorptive removal of 30 kDa fraction of humic acid in the presence of zinc could be visualized by the synchronous scan fluorescence spectra displaying a significant FI decrease. The spectrum upon the adsorption of 30 kDa fraction of humic acid onto 0.2 mg mL^{-1} TiO_2 dose crossed with higher doses of TiO_2 emission spectrum. The peak at 450 nm wavelength was dissappeared with adsorption of 30 kDa fraction of humic acid onto higher doses of TiO_2. The binary system of zinc and raw 30 kDa fraction of humic acid gave the highest trend for emission scan spectra.

Synchronous scan spectra of 30 kDa fraction of humic acid in the presence of zinc were shown in Figure 4.98. As seen in Figure 4.98, a continuously decreasing trend in FI at λ_{max}=380 nm and λ_{max}=470 nm was observed with respect to increasing TiO_2 dose for 30 kda fraction of humic acid as well as the higher molecular weight fractions of humic

acid. Zinc and raw 30 kDa fraction of humic acid binary system had the highest fluorescence intensities.

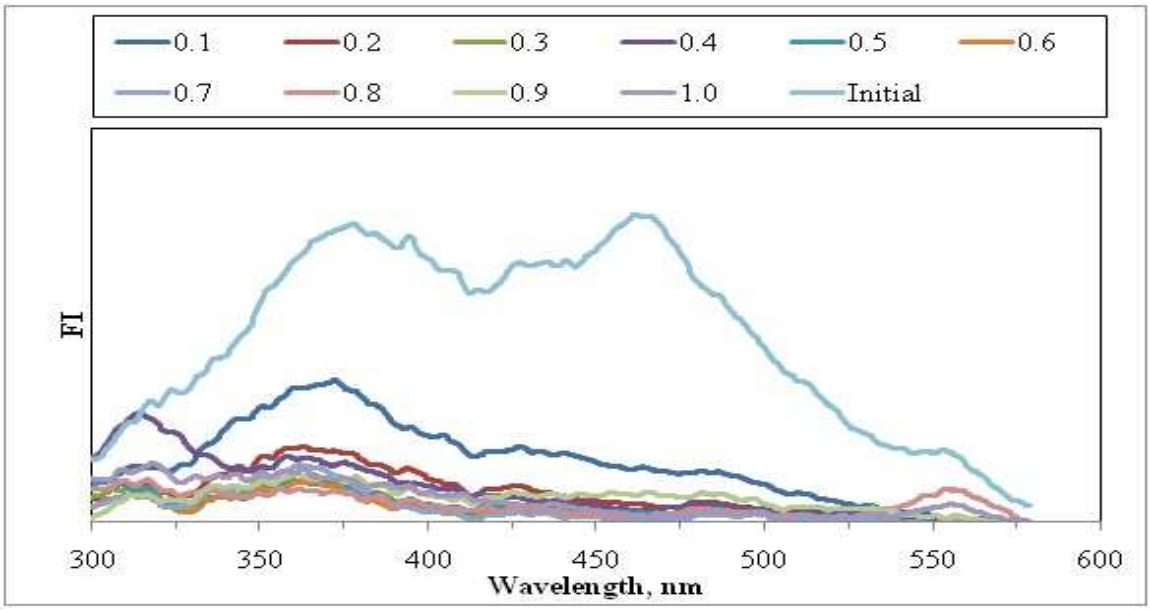

Figure 4.98. Synchronous scan fluorescence spectra of 30 kDa fraction of humic acid adsorption onto TiO_2 in the presence of zinc (Initial represents 30 kDa fraction of HA and zinc binary system).

The spectrum attained upon the adsorption of 30 kDa fraction of humic acid onto 0.2 mg mL^{-1} TiO_2 dose crossed over with the emission spectrum recorded for higher doses of TiO_2. The peaks at 380 and 470 nm wavelengths were dissappeared with the adsorption of 30 kDa fraction of humic acid onto higher doses of TiO_2.

4.6.8.3. Adsorption Isotherm Modeling of 30 kDa Fraction of Humic Acid in the Presence of Zinc. The adsorption data were evaluated in terms of Freundlich and Langmuir adsorption models.

Freundlich adsorption model. Freundlich adsorption isotherms for $Color_{436}$ and UV_{254} changes of humic acids were given in the Figure 4.99 and Figure 4.100 respectively. The Freundlich adsorption isotherms for UV_{365} and UV_{280} were presented in Appendix A.

Because of low absorbance recordings of 30 kDa fraction of humic acid, it becomes difficult to observe the changes with increased TiO_2 loadings. Especially for $Color_{436}$, the absorbance values of initial humic acid were very low (0.0041 cm^{-1}). After adsorption onto increased dose of TiO_2, these values were close to zero value. It could be said that $Color_{436}$ was not a significant parameter for 30 kDa fraction of humic acid. As illustrated in Figure 4.99, C_e values varied between 0.01 – 0.08 m^{-1} for $Color_{436}$ depending on the amount of TiO_2 present in solution. The values of q_A were found to be in the range of 8.00 – 66.00 $m^{-1}g^{-1}$ for the corresponding C_e values.

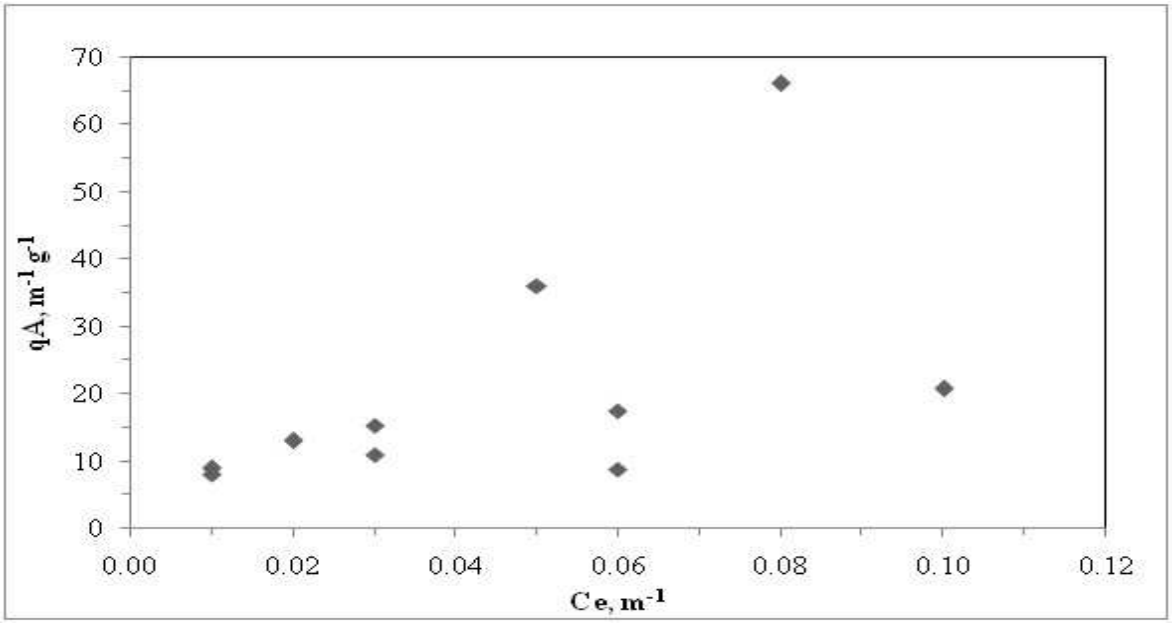

Figure 4.99. Freundlich adsorption isotherm of $Color_{436}$ of 30 kDa fraction of humic acid onto TiO_2 in the presence of zinc.

As seen in Figure 4.100, C_e values varied between 0.35 -2.07 m^{-1} for $UV_{254.}$ The values of q_A calculated to be in the range of 106.40 – 720 $m^{-1}g^{-1}$ for the corresponding C_e values. The calculated ΔC_e and Δq_A values for 30 kDa fraction of humic acid were found to be 0.07 m^{-1} and 58.00 $m^{-1}g^{-1}$ respectively for $Color_{436}$. On the other hand, the calculated ΔC_e and Δq_A for UV_{254} parameter were 1.72 m^{-1} and 613.6 $m^{-1}g^{-1}$ respectively. Comparatively higher ΔC_e were calculaed for the adsorption of 30 kDa fraction of humic acid onto in the absence of zinc.

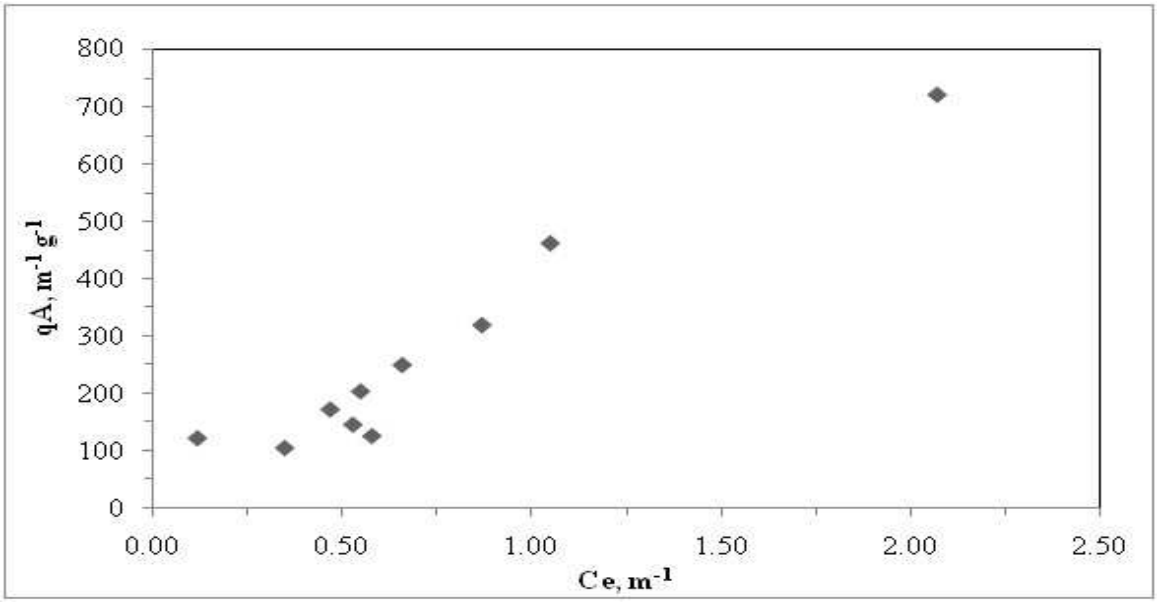

Figure 4.100. Freundlich adsorption isotherm of UV_{254} of 30 kDa fraction of humic acid onto TiO_2 in the presence of zinc.

Langmuir adsorption model. Langmuir adsorption isotherm modeling could not be verified for $Color_{436}$ and UV_{254} of 30 kDa fraction of humic acid.

4.7. Comparative Evaluation For Adsorption of Humic Acids Onto TiO_2

Because of the surface oriented nature of the photocatalytic degradation systems, adsorption the the target compounds had a prominent influence on the degradation mechanism. To investigate the effect of a certain TiO_2 dosage on photocatalytic degradation of humic acid using and adsorption of humic acid onto TiO_2 under similar conditions, the TiO_2 dose was chosen as 0.1 mg mL^{-1}. In this respect, the dark adsorption data obtained for t=0 min and adsorption data attained under equilibrium conditions for raw, 0.45 µm filtered fraction, 100 kDa fraction and 30 kDa fraction of humic acid were compared in the absence and the presence of zinc.

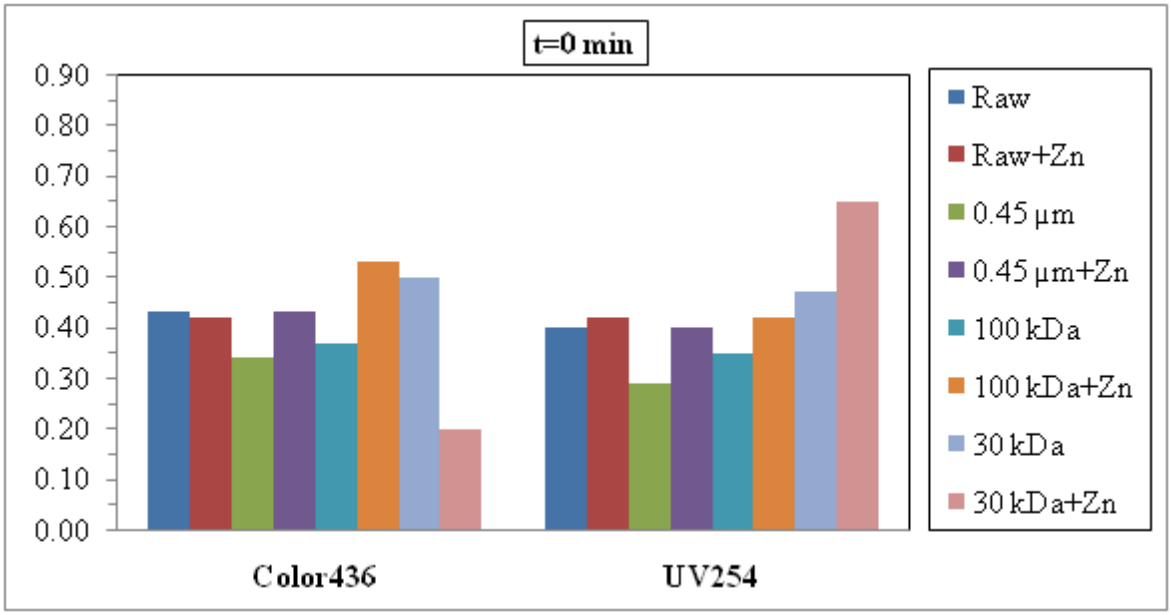

Figure 4.101. Comparison of instantaneous $Color_{436}$ and UV_{254} removals upon introduction of 0.1 mg mL^{-1} TiO_2 in the presence and absence of zinc.

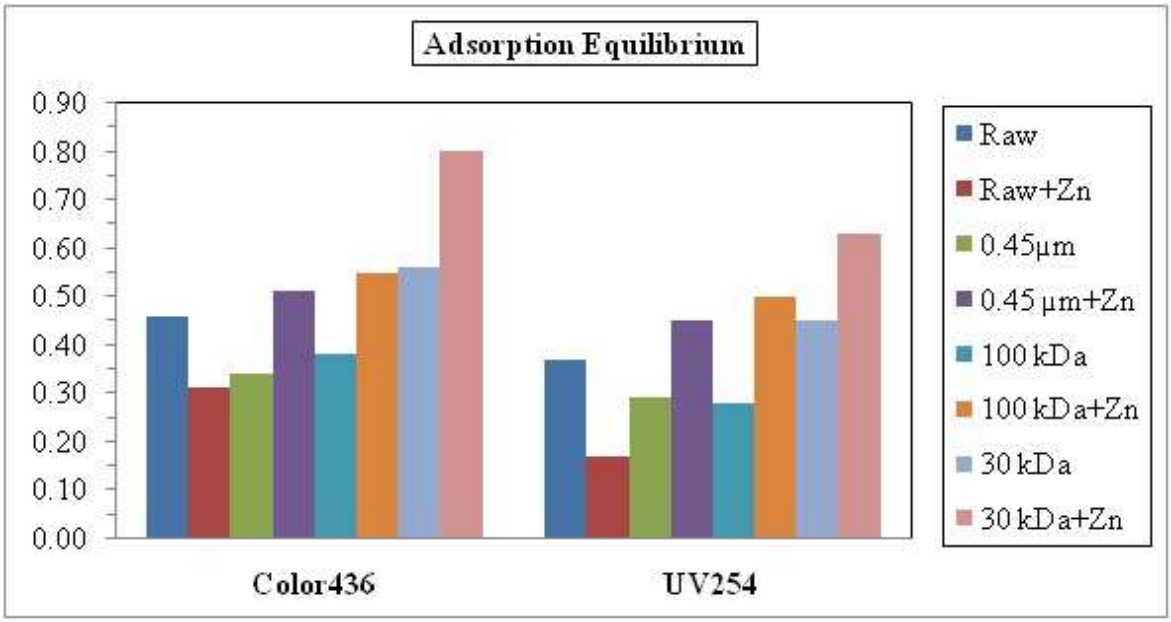

Figure 4.102. Comparison of adsorptive removals of $Color_{436}$ and UV_{254} under equilibrium conditions for the dosage of 0.1 mg mL^{-1} TiO_2 in the presence and absence of zinc.

As observed from Figure 4.101 and Figure 4.102, the dark adsorption data obtained for t=0 min and adsorption data attained under equilibrium conditions for raw humic acid were nearly same for $Color_{436}$. On the other hand, the removal that obtained prior to photocatalytic degradation of raw humic acid gave higher percentages than equilibrium conditions in the presence of zinc. The similar conditions were observed for UV_{254}. In the absence of zinc, instantaneous UV_{254} removals upon introduction of 0.1 mg mL^{-1} TiO_2 and adsorptive removals of UV_{254} under equilibrium conditions for the same dose of TiO_2 had nearly same values. However, in the presence of zinc, data obtained for t=0 min had higher removal percentages than data attained under equilibrium conditions for raw humic acid.

The dark adsorption data obtained for t=0 min and adsorption data attained under equilibrium conditions for 0.45µm filtered fraction of humic acid were exactly same for $Color_{436}$. The removal that obtained prior to photocatalytic conditions gave nearly same percentages with equilibrium conditions in the presence of zinc. In the absence of zinc, instantaneous UV_{254} removals upon introduction of TiO_2 and adsorptive removals of UV_{254} under equilibrium conditions for the same dose of TiO_2 had exactly same values. However, in the presence of zinc, data obtained for t=0 min had close removal percentages with data attained under equilibrium conditions for 0.45µm filtered fraction of humic acid with negligible changes.

Similar conditions were observed for 100 kDa fraction of humic acid. In the absence of zinc, instantaneous $Color_{436}$ removal upon introduction of 0.1 mg mL^{-1} TiO_2 and adsorptive removals of $Color_{436}$ under equilibrium conditions for the same dose of TiO_2 had exactly same values. In the presence of zinc, data obtained for t=0 min had nearly same removal percentages with data attained under equilibrium conditions for 100 kDa fraction of humic acid for $Color_{436}$. In the absence of zinc, instantaneous UV_{254} removals upon introduction of TiO_2 and adsorptive removals of UV_{254} under equilibrium conditions for the same dose of TiO_2 had close values with changes $\leq$ 7%. On the other hand, the removal that obtained prior to photocatalytic conditions gave similar percentages with equilibrium conditions in the presence of zinc.

As seen in Figure 4.101 and Figure 4.102, the dark adsorption data obtained for t=0 min and adsorption data attained under equilibrium conditions for 30 kDa fraction of

humic acid were nearly same for $Color_{436}$. On the other hand, the removal that obtained prior to photocatalytic degradation of 30 kDa fraction of humic acid gave very lower percentages than equilibrium conditions in the presence of zinc. It could be explained by $Color_{436}$ being not a significant parameter for 30 kDa fraction of humic acid. In the absence of zinc, instantaneous UV_{254} removals upon introduction of 0.1 mg mL^{-1} TiO_2 and adsorptive removals of UV_{254} under equilibrium conditions for the same dose of TiO_2 had nearly similar values. Moreover, in the presence of zinc, data obtained for t=0 min had close percentages with data attained under equilibrium conditions for 30 kDa fraction of humic acid.

The adsorptive removal by adsorption under equilibrium conditions were changed for $Color_{436}$ as 0.45µm filtered fraction < 100 kDa < Raw < 30 kDa. The order of removal was observed for experiments in the presence of zinc, such as Raw < 0.45µm filtered fraction < 100 kDa < 30 kDa. The adsorptive removal by adsorption under equilibrium conditions were changed for UV_{254} as 100 kDa < 0.45µm filtered fraction < Raw < 30 kDa. The order of removal percentages was observed for experiments in the presence of zinc, such as Raw < 0.45µm filtered fraction < 100 kDa < 30 kDa.

For raw humic acid, the equilibrium adsorptive removal decreased in the presence of zinc. There was 32-54% difference between the results that were attained in the absence and the presence of zinc. For 0.45µm filtered fraction of humic acid, the equilibrium adsorptive removal increased in the presence of zinc revealing ~ 34% difference due to the absence and the presence of zinc. For 100 kDa fraction of humic acid, the removal also increased in the presence of zinc (31-44% difference). Almost 30% difference was attained for 30 kDa fraction of humic acid in the absence and the presence of zinc.

5. CONCLUSION

In this study, photocatalytic degradation and adsorption experiments were carried out to investigate the complex interactions between the surface properties of titanium dioxide and the molecular size dependent fractions of the humic acid. The effects of zinc ions on the nonselective photocatalytic degradation of humic acid in aqueous medium were investigated. The adsorption properties were also evaluated by using Freundlich and Langmuir adsorption isotherms. The role of the metal ion complexation as expressed by the "binary system effect" on the photocatalytic degradation efficiency of humic acids with respect to molecular size fractions was deduced.

The photocatalytic degradation experiments were conducted with different molecular size fractions such as raw, 0.45 µm filtered fraction, 100 kDa fraction and 30 kDa fraction of Aldrich humic acid solution in the presence and the absence of zinc ion. Addition to the UV-vis and fluorescence spectroscopic characterization of raw and 0.45 µm filtered fraction, 100 kDa fraction and 30 kDa fraction of Aldrich humic acid, photocatalytic degradation data were processed using pseudo first order kinetic model. Photocatalytic degradation rates (R, m^{-1} min^{-1}) were attained in a decreasing order of $UV_{254} > UV_{280} > UV_{365} > Color_{436}$ for raw, 0.45 µm filtered fraction, 100 kDa fraction and 30 kDa fraction of humic acid.

For raw humic acid, the removal of color forming moieties was found to be faster (~ > 30%) than the UV absorbing centers as expressed by UV_{280} and UV_{254}. The presence of zinc ions altered the pseudo first order kinetic model rate constants of raw humic acid by ≤ 5% for all of the specified parameters. In the presence of zinc, the removal rates were found to be similar to the raw humic acid photocatalytic degradations profile. The reason could be attributed to low concentrations of zinc with respect to humic acid concentration. Also, the free binding sites of humic acids could still be available for the pre-adsorption of humic acid onto TiO_2 surface.

For 0.45 µm filtered fraction of humic acid, the removal of color forming moieties was observed faster (> 35%) than the UV absorbing centers. The pseudo first order

degradation kinetic parameters of 0.45µm filtered fraction of humic acid had similarities with raw humic acid. The effect of the presence of zinc ions on the photocatalytic degradations of 0.45 µm filtered fraction of humic acid could be regarded as insignificant for $Color_{436}$ and UV_{365} whereas a slight enhancement in the removal rate could be observed for UV_{280} and $UV_{254.}$

For 100 kDa fraction of humic acid, the removal of color forming moieties was found to be relatively faster (~ > 30%) than the UV absorbing centers. The pseudo first order kinetic parameters displayed considerably higher removal efficiencies for 100 kDa fraction of humic acid with respect to both 0.45 µm filtered fraction of humic acid and raw humic acid. The enhancement factor could be regarded as two fold for all of the specified UV-vis parameters. The presence of zinc ions changed the photocatalytic degradation rates of 100 kDa fraction of humic acid with respect to the 0.45 µm filtered fraction of humic acid and raw humic acid. However, a retardation effect could be noticed with respect to the conditions specified by the absence of zinc ions.

For 30 kDa fraction of humic acid, significantly higher photocatalytic degradation rate constants were achieved for 30 kDa fraction of humic acid with respect to the higher molecular weight fractions. The presence of zinc ions displayed a slight decrease in degradation rates for 30 kDa fraction of humic acid respect to 0.45 µm filtered fraction of humic acid and raw humic acid. However, a slight retardation effect could be noticed with respect to 100 kDa fraction of humic acid. Moreover, a considerably significant retardation effect could be explained by the possible competitive complexates and oxidation-reduction reactions taking place in the medium that include zinc ions.

While raw and 0.45 µm filtered fraction of humic acid had similar properties, pseudo first order reaction rate constants, k (min^{-1}) were increased with decreasing molecular fractions of humic acid in the presence and the absence of zinc. On the other hand, a decrease in degradation rates was observed for decreasing molecular size fractions in the presence and also in the absence of zinc. When removal percentages at t=0 were studied, a slight enhancement was observed for the experiments in the presence of zinc. On the other hand, while the removal efficiencies were studied for longer irradiation time periods, it could be easily seen that in the presence of zinc the removal efficiencies at t=60 min

irradiation time were decreased for raw, 0.45 µm filtered fraction, 100 kDa fraction and 30 kDa fraction of humic acid. The retardation effect observed on the photocatalytic degradation of humic acid could be explained by the adsorption of zinc ions on humic acid or the surface of TiO_2 resulting in blockage of active sites of the photocatalyst.

The adsorption experiments were conducted with different molecular size fractions such as raw, 0.45 µm filtered fraction, 100 kDa fraction and 30 kDa fraction of Aldrich humic acid solution in the presence and the absence of zinc ion. Addition to the UV-vis and fluorescence spectroscopic characterization of raw and 0.45 µm filtered fraction, 100 kDa fraction and 30 kDa fraction of Aldrich humic acid, the adsorption data were fitted Freundlich and Langmuir adsorption models.

Freundlich adsorption model parameters showed some changes as;

In the absence of zinc, K_f values changed as raw > 0.45 µm filtered fraction > 100 kDa > 30 kDa for $Color_{436}$. K_f values changed as 0.45 µm filtered fraction > raw > 100 kDa > 30 kDa for UV_{254}. In the presence of zinc, K_f values changed as raw > 100 kDa > 0.45 µm filtered fraction for $Color_{436}$. K_f values changed for UV_{254} as raw > 0.45 µm filtered fraction > 100 kDa. No distinct isotherm could be assessed for 30 kDa fraction. The overall evaluation of 1/n could be expressed by the range of 0.181-1.065. Adsorption intensity (1/n) values which were lower than 1, expressing the adsorption bond was strong and the capacity tended to be independent of C_e.

In the presence of zinc, a general enhancement for K_f values was observed for raw, 0.45 µm filtered fraction, 100 kDa and 30 kDa fraction of humic acid. On the contrary, adsorption intensity (1/n) values were decreased in the presence of zinc.

Langmuir adsorption model parameters showed some changes as;

In the absence of zinc, the maximum quantity adsorbable when all adsorption sites were occupied, q_{max} values changed as raw > 0.45 µm filtered fraction > 100 kDa for $Color_{436}$. q_{max} values changed as raw > 0.45 µm filtered fraction > 100 kDa for UV_{254}. For binding constant, K, the order observed as 0.45 µm filtered fraction > 100 kDa > raw for

$Color_{436}$. K values changed as 0.45 μm filtered fraction > 100 kDa > raw for UV_{254}. In the presence of zinc, q_{max} values changed as raw > 0.45 μm filtered fraction > 100 kDa for $Color_{436}$. q_{max} values changed for UV_{254} as 0.45 μm filtered fraction > 100 kDa > raw. For binding constant, K, the order was observed as 100 kDa > raw > 0.45 μm filtered fraction for $Color_{436}$. K values changed as raw > 100 kDa > 0.45 μm filtered fraction for UV_{254} Adsorption of 30 kDa fraction of humic acid did not fit Langmuir adsorption model and no distinct isotherm could be assessed for 30 kDa fraction.

In the presence of zinc, a general decrease was observed for q_{max} values of raw humic acid. On the other hand, an enhancement was seen for q_{max} values of 0.45 μm filtered fraction of humic acid. The effect of the presence of zinc ions on the q_{max} values of of 100 kDa fraction of humic acid could be observed as a decrease for $Color_{436}$ and UV_{365} whereas a slight enhancement in q_{max} values was observed for UV_{280} and $UV_{254.}$

The effect of the presence of zinc ions on K values of raw, 0.45 μm filtered fraction, 100 kDa fraction and 30 kDa fraction of humic acid could be observed as an enhancement for all specified UV-vis parameters.

As a result of the study, it could be said that, the complexity of the structure of humic acid molecule and the presence of zinc ions in the system can change the photocatalytic oxidation through complex formation, oxidation and adsorption processes. The reason of insignificant changes could be attributed to low concentrations of zinc with respect to humic acid concentration. In groundwater situations where more than one metal was present, the effect of other metals must be considered in predicting metal speciation (Cao et al., 1995).

REFERENCES

Aiken, G. R., McKnight, D. M., Wershaw, R. L., MacCarthy, P. (Eds.), 1985. Humic Substances in Soil, Sediment and Water, John Wiley and Sons, Inc., U.S.A.

Alberts, J. J., Takacs, M., Egeberg, P. K., 2002. Total luminescence spectral characteristics of natural organic matter (NOM) size fractions as defined by ultrafiltration and high performance size exclusion chromatography (HPSEC). Organic Geochemistry, 33, 817-828.

Apostoli, P., Cornelis, R., Duffus, J., Hoet, P., Lison, D., Templeton, D., 2006. Elemental Speciation in Human Health Risk Assessment, World Health Organization, Geneva.

Baker, A., 2001. Fluorescence excitation–emission matrix characterization of some sewage-impacted rivers. Environmental Science and Technology, 35, 948–953.

Bas, T., 2001. Humic Acid and Oxide Surface Interactions: Adsorption, Desorption and Surface Charge Effects, M. S. Thesis, Bogazici University.

Bekbolet, M., Balcioglu, I., 1996. Photocatalytic degradation kinetics of humic acid in aqueous TiO_2 dispersions: The influence of hydrogen peroxide and bicarbonate ion. Water Science and Technology, 34, 73–80.

Bekbolet, M., Cecen, F., Ozkosemen, G., 1996. Photocatalytic oxidation and subsequent adsorption characteristic of humic acids. Water Science and Technology, 34, 65-72.

Bekbolet, M., Ozkosemen, G., 1996. A preliminary investigation on the photocatalytic degradation of a model humic acid. Water Science and Technology, 33, 189-194.

Bekbolet, M., Boyacioglu, Z., Ozkaraova, B., 1998. The influence of solution matrix on the photocatalytic removal of color from natural waters. Water Science and Technology, 38, 155–162.

Bekbolet, M., Suphandag, A. S., Uyguner, C. S., 2002. An investigation of the photocatalytic efficiencies of TiO_2 powders on the decolorisation of humic acids. Journal of Photochemistry and Photobiology A: Chemistry, 148, 121-128.

Bennett, L. E., Darikas, M., 1993. The evaluation of color in natural waters. Water Research, 27, 1209-1218.

Benoit, F. M., Helleur, R., Malaiyandi, M., Ramaswamy S., Williams, D.T., 1993. Soil fulvic acid degradation by ozone in aqueous medium. Ozone Science and Engineering, 15, 19-38.

Brady, N. C., 1990. The Nature and Properties of Soils, 10th edition, Macmillan Publishing Company, New York, 286–291.

Camper, A. K., 2004. Involvement of humic substances in regrowth. International Journal of Food Microbiology, 92, 355–364.

Cao, Y., Conklin, M., Betterton, E., 1995. Competitive complexation of trace metals with dissolved humic acid. Environmental Health Perspectives, 103, 29-32.

Carp, O., Huisman, C. L., Reller, A., 2004. Photoinduced reactivity of titanium dioxide. Solid State Chemistry, 32, 33–177.

Carvalho, E. R., Martin-Neto, L., Miloria, D. M. B. P., Rocha, J. C., Julio, C. R., Rosa, A.H., 2004. Interactions of chlorine with tropical aquatic fulvic acids and formation of intermediates observed by fluorescence spectroscopy. Journal of Brazilian Chemical Society, 15, 421-426.

Christl, I., Kretzschmar, R., 2001. Relating ion binding by fulvic and humic acids to chemical composition and molecular size. I. Proton binding. Environmental Science and Technology, 35, 2505–2511.

Edzwald, J. K., Becker, W. C., Wattier, K. L., 1985. Surrogate parameters for monitoring organic matter and THM precursors. Journal of American Water Works Association, 77, 122-132.

Essington, M. E., 2004. Soil and Water Chemistry: An Integrative Approach, CRC Press LLC, Boca Raton, FL.

Fearing, D. A., Banks, J., Guyetand, S., Eroles, C. M., Jefferson, B., Wilson, D., Hillis, P., Campbell, A. T., Parsons, S. A., 2004. Combination of ferric and MIEX for the treatment of a humic rich water. Water Research, 38, 2551-2558.

Ghosh, K., Schnitzer, M., 1980. Macromolecular structures of humic substance. Soil Science, 129, 266–276.

Giles, C. H., MacEwan, T. H., Nakhwa, S. N., Smith, D., 1960. Studies in adsorption. A system classification of solution adsorption isotherms and its use in diagnosis of adsorption and in measurement of specific surface areas of solids. Journal of Chemical Society, 3973-3993.

Goel, S., Hozalski, R. M., Bouwer, E. J., 1995. Biodegradation of NOM: Effect of NOM source and ozone dose. Journal of the American Water Works Association, 87, 90–105.

Goslan, E. H., Fearing, D. A., Banks, J., Wilson, D., Hillis, P., Campbell, A. T., Parsons, S. A., 2002. Seasonal variations in the disinfection by-product precursor profile of a reservoir water. Journal of Water Supply: Research and Technology–AQUA, 51, 475–482.

Guy R. D., Chakrabarti C. L.. 1976. Studies of metal-organic interactions in model systems pertaining to natural waters. Canadian Journal of Chemistry, 54, 2600-2611.

Hatchard, C. G., Parker, C. A., 1956. A new sensitive chemical actinometer. II. Potassium ferrioxalate as a standard chemical actinometer, Proceedings of the Royal Society of London. Series A, Mathematical and Physical Sciences, 235, 518–536.

Heijerick D. G., De Schamphelaere K. A. C., Janssen C. R., 2002. Biotic ligand model development predicting Zn toxicity to the alga *Pseudokirchneriella subcapitata*: Possibilities and limitations. Comparative Biochemistry and Physiology, Part C, 133, 207-218.

Helz G. R., Huggett R. J., Hill J. M., 1975. Behavior of Mn, Fe, Cu, Zn, Cd, and Pb discharged from a wastewater treatment plant into an estuarine environment. Water Research, 9, 631-636.

Hoigné, J., 1998. Chemistry of Aqueous Ozone and Transformation of Pollutants by Ozone and Advanced Oxidation Processes. In Hrubec, J., (Ed), The Handbook of Environmental Chemistry, Part C, Quality and Treatment of Drinking Water II, Springer, Heidelberg, 5, 83-143.

Hu, C. Z., Liu, H. J, Qu, J. H., Wang, D. S., Ru, J., 2006. Coagulation behavior of aluminum salts in eutrophic water: Significance of Al_{13} species and pH control. Environmental Science and Technology, 40, 325-331.

İstanbul Büyükşehir Belediyesi, İstanbul Su ve Kanalizasyon İdaresi Home Page, http://www.iski.gov.tr/web/statik.aspx?KID=1000811, (accessed August 2010).

Kainulainen, T., Tuhkanen, T., Vartiainen, T., Heinonen-Tanski H, Kalliokoski, P., 1994. The effect of different oxidation and filtration processes on the molecular size distribution of humic material. Water Science and Technology, 30, 169-174.

Karabacakoğlu, E., 1998. Photocatalytic Oxidation Efficiency of Titanium Dioxide in Hard Waters, M.S. Thesis, Boğaziçi University.

Kavcar, P., Sofuoğlu, A., Sofuoğlu, S. C., 2009. A health risk assessment for exposure to trace metals via drinking water ingestion pathway. International Journal of Hygiene and Environmental Health, 212, 216-227.

Khan, E., Babcock, R. W., Viriyavejakul, S., Suffet, I. H., Stenstorm, M. K., 1998. Biodegradable dissolved organic carbon for indication wastewater reclamation plant performance and treated wastewater quality. Water Environmental Research, 70, 1033–1040.

Kinniburgh, D. G., Van Riemsdijk, W. H., Koopal, L. K., Borkovec, M., Benedetti, M. F. Avena, M. J., 1999. Ion binding to natural organic matter: competition, heterogeneity, stoichiometry and thermodynamic consistency. Colloids and Surfaces A: Physicochemical and Engineering Aspects, 151, 147–166.

Kipton, H., Powell, J., Town, R. M., 1992. Solubility and fractionation of humic acid; Effect of pH and ionic medium. Analytica Chimica Acta, 267, 47–54.

Kitis, M., Kaplan, S. S., 2007. Advanced oxidation of natural organic matter using hydrogen peroxide and iron-coated pumice particles. Chemosphere, 68, 1846–1853.

Korshin, G. V., Kumke, M. U., Li C. W., Frimmel, F. H., 1999. Influence of chlorination on chromophores and fluorophores in humic substances. Environmental Science and Technology, 33, 1207–1212.

Kulovaara, M., Metsämuuronen, S., Nystrom, M., 1999. Effects of aquatic humic substances on a hydrophobic ultrafiltration membrane. Chemosphere 38, 3485–3496.

Letterman, R. D., 1999. Water Quality and Treatment. A Handbook of Community Water Supplies, 5th Edition, McGraw-Hill, USA.

Litter, M. I., 1999. Heterogeneous photocatalysis, transition metal ions in photocatalytic systems. Catalysis B: Environmental, 23, 89–114.

Lloyd, T.B., Showak, W., 1984. Zinc and Zinc Alloys. In Grayson M., (Ed.) Kirk-Othmer Encyclopedia of Chemical Technology, 3rd Edition, John Wiley and Sons, New York, 24, 835-836.

Lombnæs, P., Chang A. C., Singh, B. R., 2008. Organic ligand, competing cation, and pH effects on dissolution of zinc in soils. Pedosphere, 18, 92-101.

Manahan, S. E., 2001. Fundamentals of Environmental Chemistry, CRC Press, LLC, Boca Raton, FL.

Melin, E. S., Ødegaard, H., 1999. Biofiltration of ozonated humic water in expanded clay aggregate filters. Water Science and Technology, 40, 165–172.

Mills, A., Le Hunte, S., 1997. An overview of semiconductor photocatalysis. Journal of Photochemistry and Photobiology A: Chemistry, 108, 1–35.

Murray, C. A., Parsons, S. A., 2004. Removal of NOM from drinking water: Fenton's and photo-Fenton's processes. Chemosphere, 54, 1017–1023.

Paquin P. R., Gorsuch J. W., Apte S., 2002. The biotic ligand model: A historical overview. Comparative Biochemistry and Physicology, 133, 3-35.

Peng, X., Luan, Z., Zhang, H., 2006. Montmorillonite-Cu(II)/Fe(III) oxides magnetic material as adsorbent for removal of humic acid and its thermal regeneration. Chemosphere, 63, 300–306.

Petala, M. D., Zouboulis, A. I., 2006. Vibratory shear enhanced processing membrane filtration applied for the removal of natural organic matter from surface waters. Journal of Membrane Science, 269, 1–14.

Peuravuori, J., Koivikko, R., Pihlaja, K., 2002. Characterization, differentiation and classification of aquatic humic matter separated with different sorbents: Synchronous scanning fluorescence spectroscopy. Water Research, 36, 4552-4562.

Pichat, P., 1997. Heterogeneous Photocatalysis. In Ertl, G., Knozinger, H., Weitkamp, J. (Eds.), Handbook of Heterogeneous Catalysis, Wiley-VCH, Weinheim, 4, 2111-2122.

Piccolo, A., 2002. The supramolecular structure of humic substances: A novel understanding of humus chemistry and implications in soil science. Advances in Agronomy, 75, 57 -133.

Puchalski, M. M., Morra, M. J., Wandruszka, R. V., 1992. Fluorescence quenching of synthetic organic compounds by humic materials. Environmental Science and Technology, 26, 1787–1792.

Rook, J. J., 1974. Formation of haloforms during chlorination of natural waters. Water Treatment and Examination. 23, 234–243.

Richardson, S. D., 1998. Drinking Water Disinfection By-Products. In Meyers, R. A. (Ed.), Encyclopedia of Environmental Analysis and Remediation, John Wiley and Sons, New York. 3, 1398–1421.

Santore R. C., Mathew R., Paquin P. R., Toro, D., 2002. Application of the biotic ligand model to predicting zinc toxicity to rainbow trout, fathead minnow, and *Daphnia magna*. Comparative Biochemistry and Physiology, 133, 271-285.

San Vicente de la Riva, B., Costa-Fernadez, J. M., Pereiro, R., Sanz-Medel, A., 2002. Spectrafluorimetric method for the rapid screening of toxic heavy metals in water samples. Analytica Chimica Acta, 451, 203–210.

Schnoor, J. L., 1996. Environmental Modeling: Fate and Transport of Pollutants in Water, Air and Soil. John Wiley and Sons, Inc, New York, USA.

Selcuk, H., Sene, J. J., Anderson, M. A., 2003. Photoelectrocatalytic humic acid degradation kinetics and effect of pH, applied potential and inorganic ions. Journal of Chemical Technology and Biotechnology, 78, 979–984.

Selcuk, H., Bekbolet, M., 2008. Photocatalytic and photoelectrocatalytic humic acid removal and selectivity of TiO_2 coated photoanode. Chemosphere, 73, 854-858.

Selim H. M., Iskandar I. K., 1999. Fate and Transport of Heavy Metals in the Vadose Zone, Lewis Publishers, USA.

Senesi, N., 1990. Molecular and quantitative aspects of the chemistry of fulvic acid and its interactions with metal ions and organic chemicals, Part II: The fluorescence spectroscopy approach. Analytica Chimica Acta, 232, 77–106.

Senesi, N., Loffredo, E., 1999. The Chemistry of Soil Organic Matter. In Sparks, D.L. (Ed.), Soil Physical Chemistry, 2nd Edition. CRC Press, Boca Raton, 239–370.

Siddiqui, M.S., Amy, G.L., Murphy, B.D., 1997. Ozone enhanced removal of natural organic matter from drinking water sources, Water Research, 31, 3098-3106.

Singer, P. C., 1999. Humic substances as precursors for potentially harmful disinfection by-products. Water Science and Technology, 40, 25–30.

Sobecka, S. B., Tomaszewska, M., Morawski, A. W., 2006. Removal of humic acids by the ozonation–biofiltration process. Desalination, 198, 265–273.

Sposito, G., 1989. The Chemistry of Soils, Oxford University Press, New York.

Standard Methods for the Examination of Water and Wastewater, 1999. APHA, AWWA, WPCF, 20th Edition, American Water Works Association, Washington D.C., USA.

Stevenson, F. J., 1982. Humus Chemistry: Genesis, Composition, Reactions, Wiley and Sons, New York.

Stevenson, F. J., 1994. Humus Chemistry: Genesis, Composition, Reactions, 2nd Edition, John Wiley and Sons, New York.

Suffet, I. H., MacCarthy, P., 1989. Aquatic Humic Substances: Influence on Fate and Treatment of Pollutants, Advances in Chemistry Series 219, American Chemical Society, Washington DC.

Suphandag, S. A., 1998. Adsorption Capacity of Natural Organic Matter on Semiconductor Powders, M. S. Thesis, Bogazici University.

Suphandag, S. A., 2006. Evaluation of Natural Organic Matter-Metal Oxide Adsorption Isotherms Under Influential Structural Concepts, Ph.D. Thesis, Bogazici University.

Thurman, E. M., Malcolm, R.L., 1981. Preparative isolation of aquatic humic substances. Environmental Science and Technology. 15, 463–466.

Tipping, E., 1998. Humic ion-binding model VI: An improved description of the interactions of protons and metal ions with humic substances. Aquatic Geochemistry, 4, 3–48.

Toor, R., Mohseni, M., 2007. UV-H_2O_2 based AOP and its integration with biological activated carbon treatment for DBP reduction in drinking water. Chemosphere, 66, 2087-2095.

Uyguner, C. S., 1999. Trace-level Metals and Natural Organic Matter Interactions: Oxidative/Adsorptive Removal Pathways, M. S. Thesis, Bogazici University.

Uyguner, C. S., Bekbolet, M., 2004. Evaluation of humic acid, chromium (VI) and TiO_2 ternary system in relation to adsorptive interactions. Applied Catalysis B: Environmental, 49, 267-275.

Uyguner, C. S., 2005. Elucidation of the Photocatalytic Removal Pathways of Humic Substances: Progress Towards Mechanistic Explanations, Ph.D. Thesis, Bogazici University.

Uyguner, C. S., Bekbolet, M., 2005a. Evaluation of humic acid photocatalytic degradation by UV–vis and fluorescence spectroscopy. Catalysis Today, 101, 267–274.

Uyguner, C. S., Bekbolet, M., 2005b. A comparative study on the photocatalytic degradation of humic substances of various origins. Desalination, 176, 167-176.

Uyguner, C. S., Bekbolet, M., 2007. Contribution of metal species to the heterogeneous photocatalytic degradation of natural organic matter. International Journal of Photoenergy.

Uyguner, C. S., Suphandag, S. A., Kerc, A., Bekbolet, M., 2007. Evaluation of adsorption and coagulation characteristics of humic acids preceded by alternative advanced oxidation techniques. Desalination, 210, 183-193.

Uyguner C. S., Bekbolet, M., 2010. TiO_2-assisted photocatalytic degradation of humic acids: effect of copper ions. Water Science and Technology, 2581-2590.

Ulker, Y., 2008. Effect of Fractionation on the Sorption Properties of NOM onto Modified TiO_2 Surface, M. S. Thesis, Bogazici University.

vanLoon, G. W., Duffy, S. J., 2000. Environmental Chemistry, Oxford University Press, Inc., New York.

Volk, C. J., LeChevallier, M. W., 2002. Effects of conventional treatment on AOC and BDOC levels. Journal of the American Water Works Association, 94, 112–123.

Wandruszka, R., 2000. Humic acids: Their detergent qualities and potential uses in pollution remediation. Geochemical Transactions, 1, 10-15.

Weber, J. W., 1972. Physicochemical Processes for Water Quality Control. John Wiley and Sons, Inc., U.S.A, 199-259.

Yoon, S. H., Lee, C. H., Kim, K. J., Fane, A. G., 1998. Effects of calcium ion on the fouling of nanofilter by humic acid in drinking water production. Water Research, 32, 2180–2186.

APPENDIX A

Freundlich Adsorption Isotherms of Humic Acids

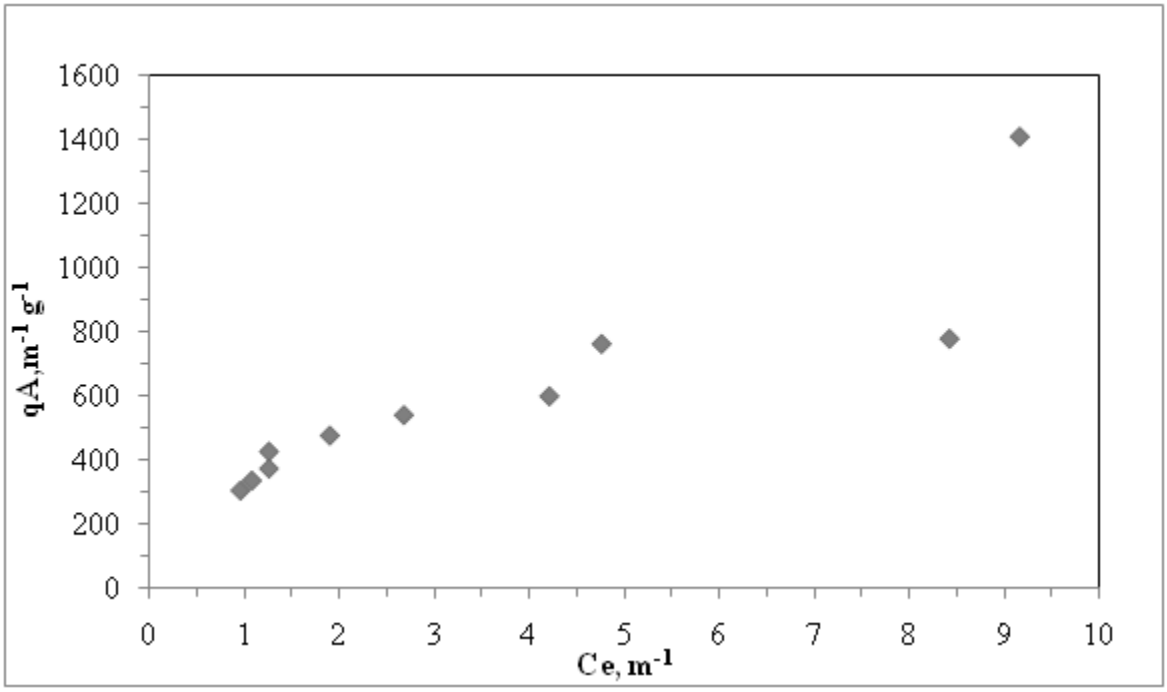

Figure A.1. Freundlich adsorption isotherm of UV_{365} of raw humic acid onto TiO_2.

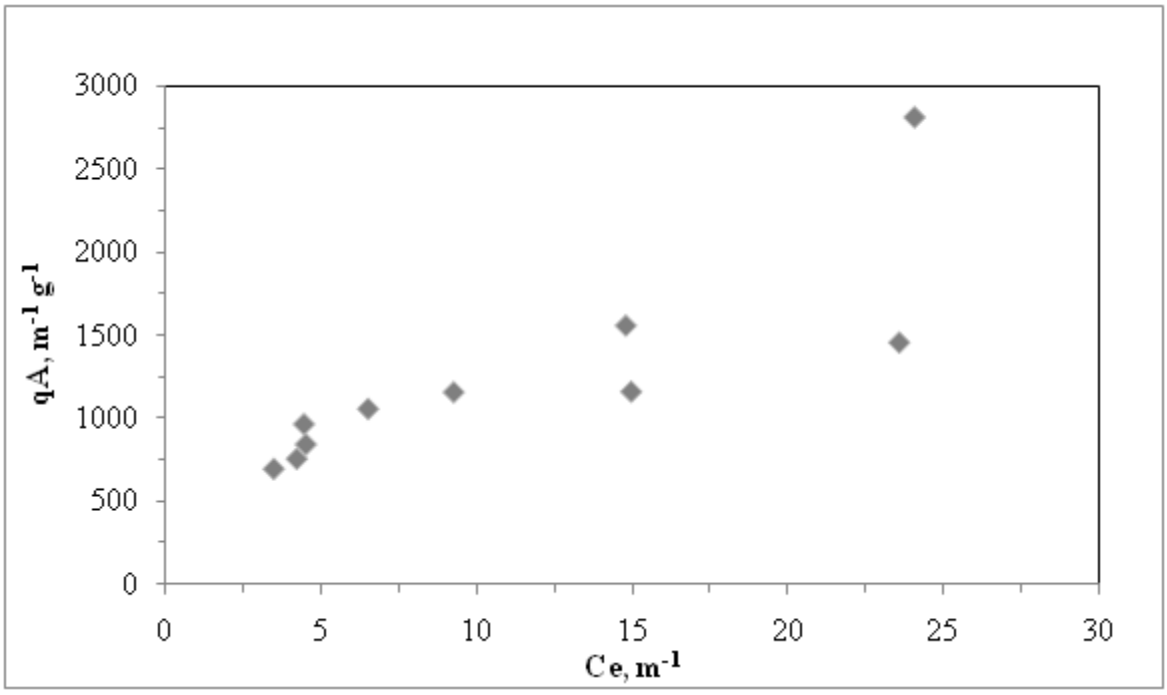

Figure A.2. Freundlich adsorption isotherm of UV_{280} of raw humic acid onto TiO_2.

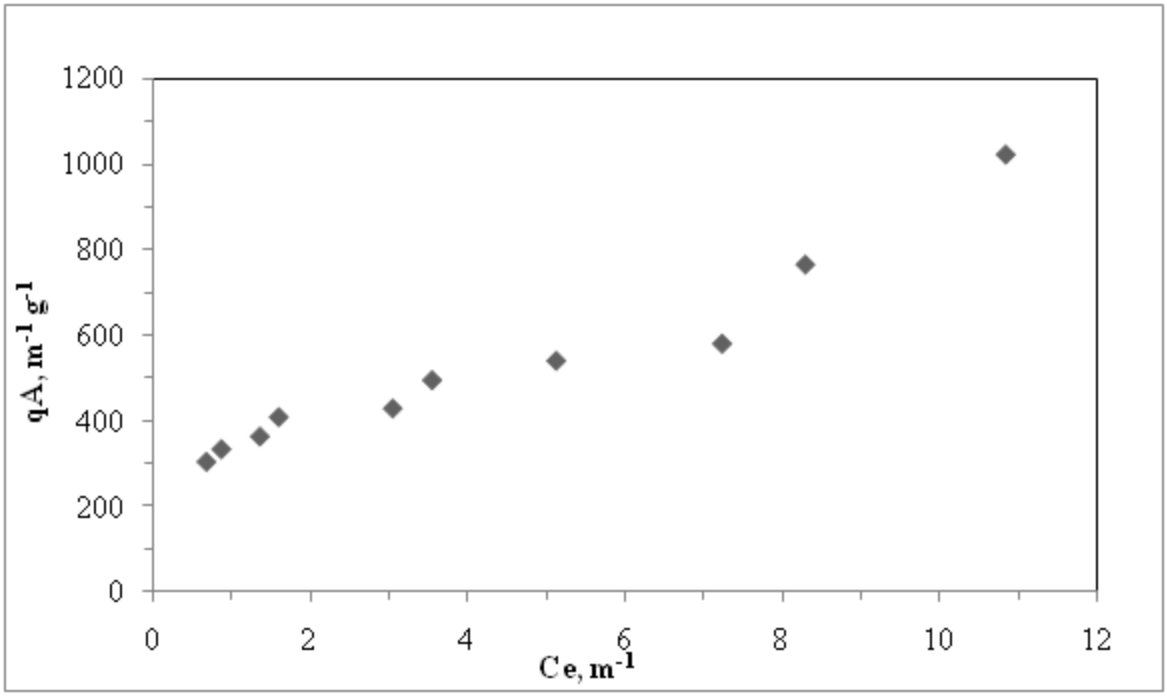

Figure A.3. Freundlich adsorption isotherm of UV_{365} of 0.45µm filtered fraction of humic acid onto TiO_2.

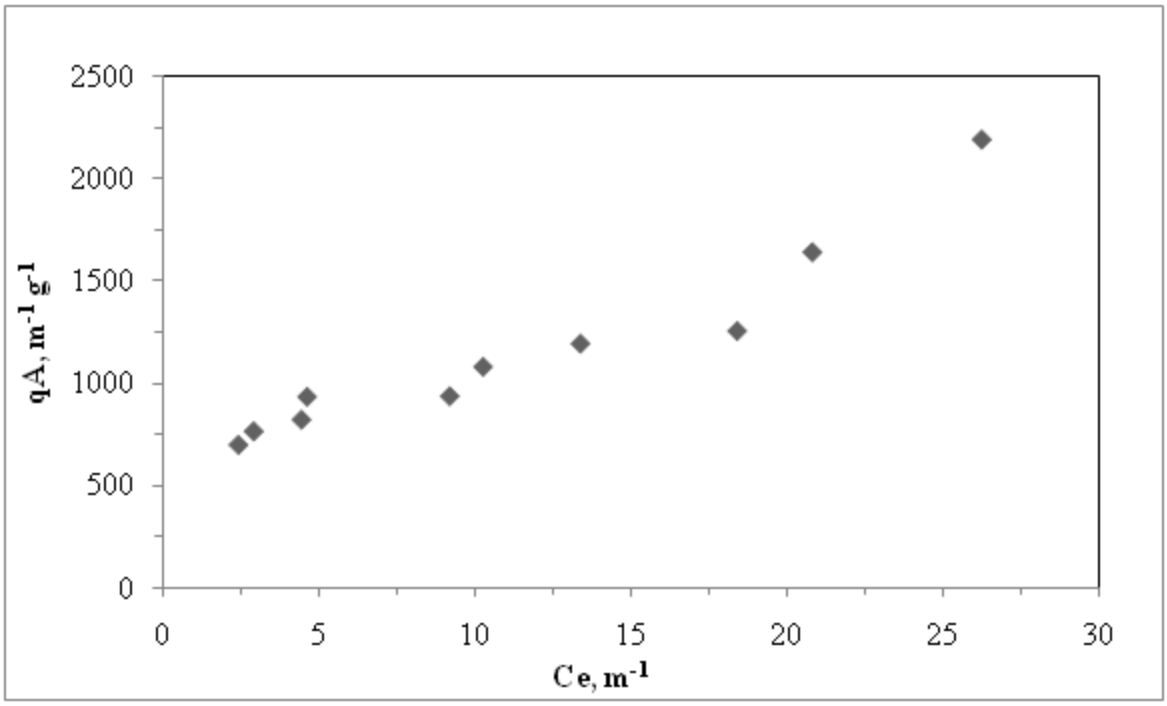

Figure A.4. Freundlich adsorption isotherm of UV_{280} of 0.45µm filtered fraction of humic acid onto TiO_2.

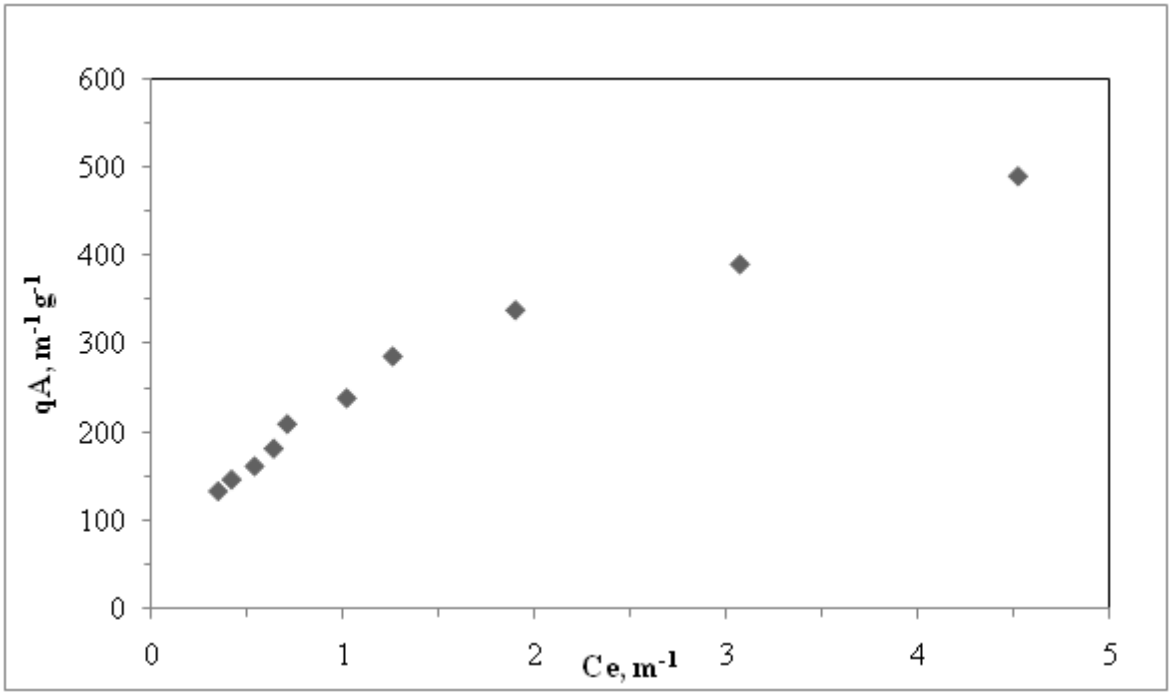

Figure A.5. Freundlich adsorption isotherm of UV_{365} of 100 kDa fraction of humic acid onto TiO_2.

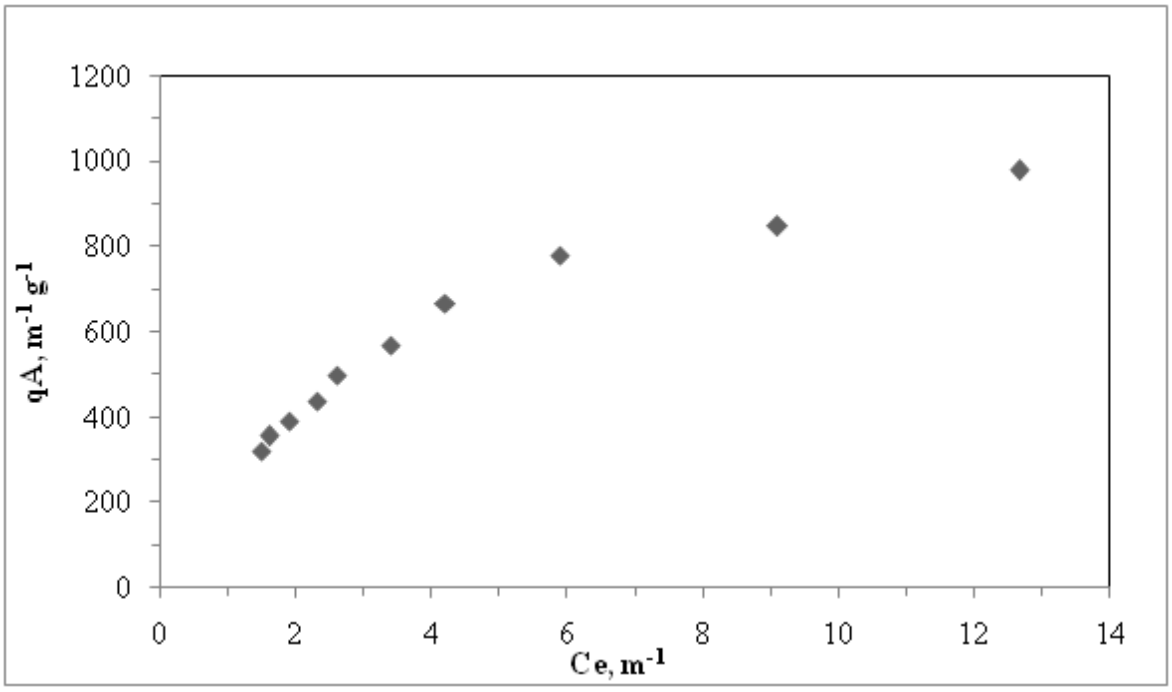

Figure A.6. Freundlich adsorption isotherm of UV_{280} of 100 kDa fraction of humic acid onto TiO_2.

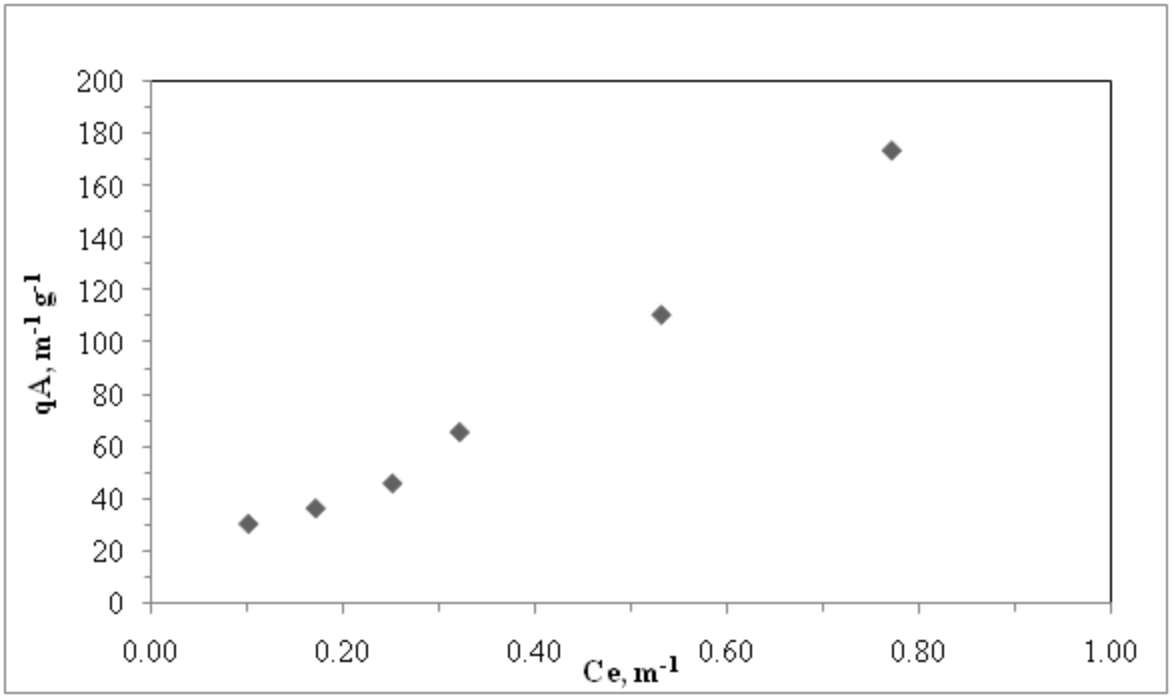

Figure A.7. Freundlich adsorption isotherm of UV_{365} of 30 kDa fraction of humic acid onto TiO_2.

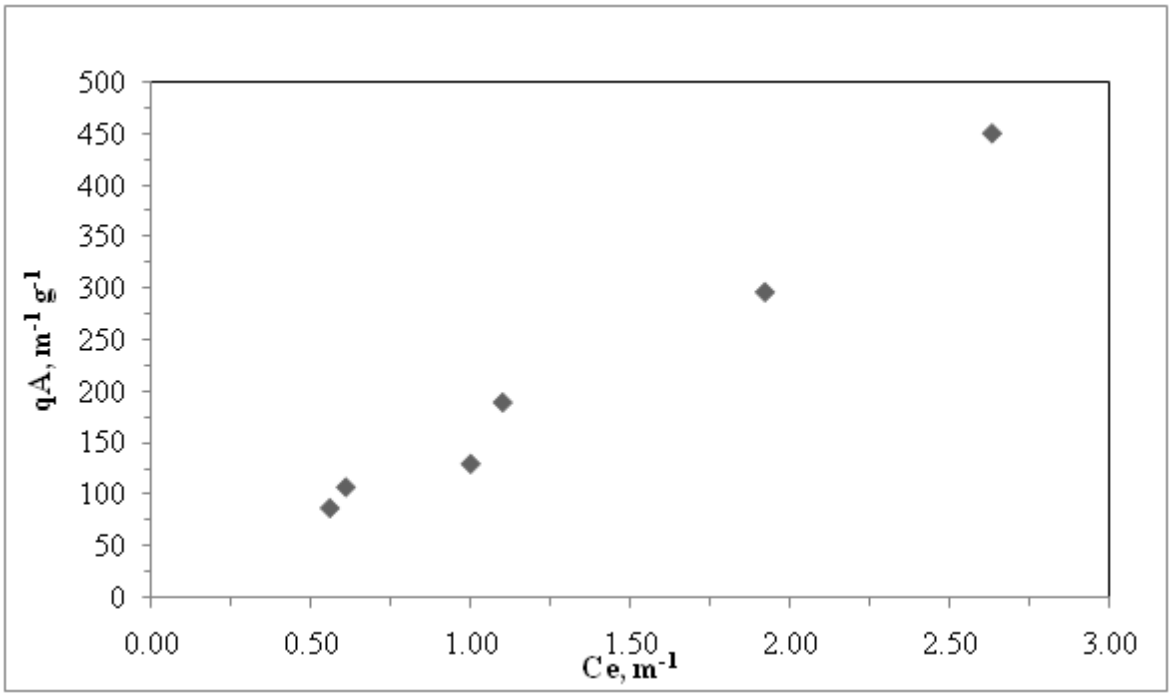

Figure A.8. Freundlich adsorption isotherm of UV_{280} of 30 kDa fraction of humic acid onto TiO_2.

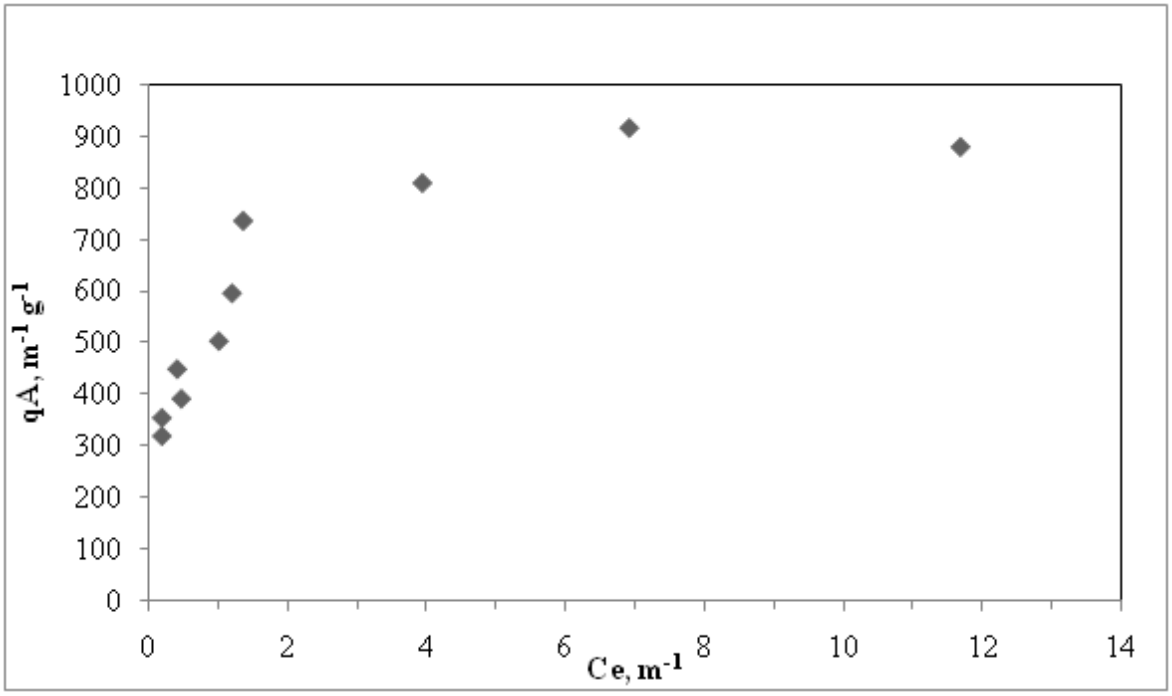

Figure A.9. Freundlich adsorption isotherm of UV_{365} of raw humic acid onto TiO_2 in the presence of zinc.

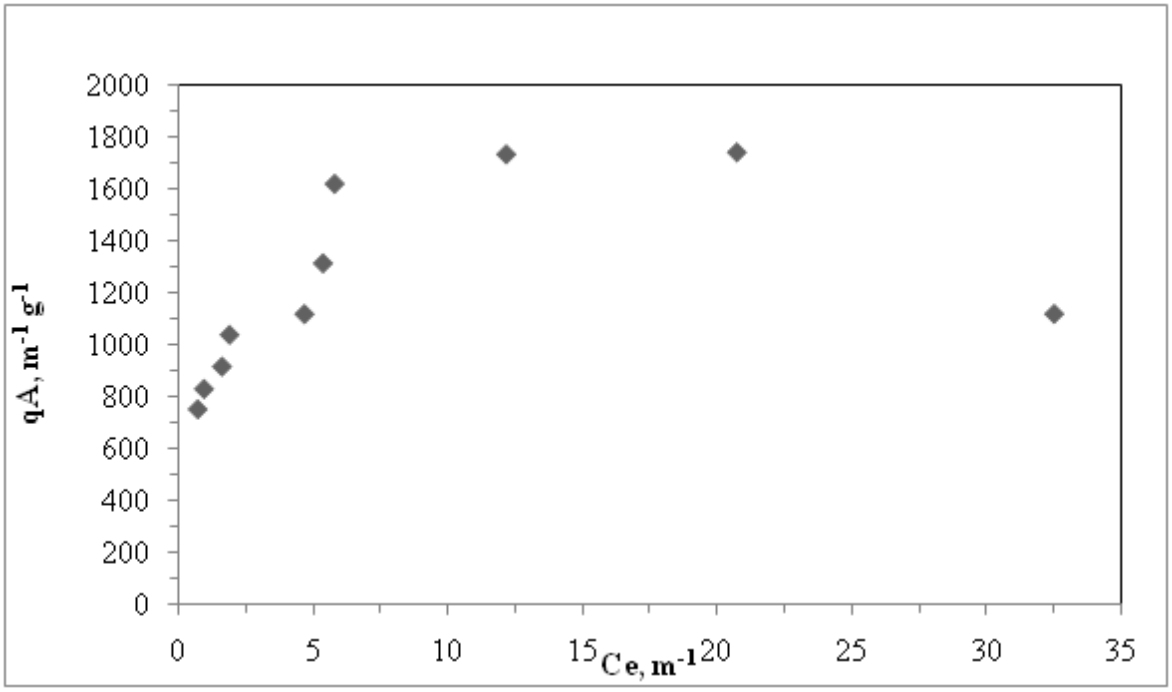

Figure A.10. Freundlich adsorption isotherm of UV_{280} of raw humic acid onto TiO_2 in the presence of zinc.

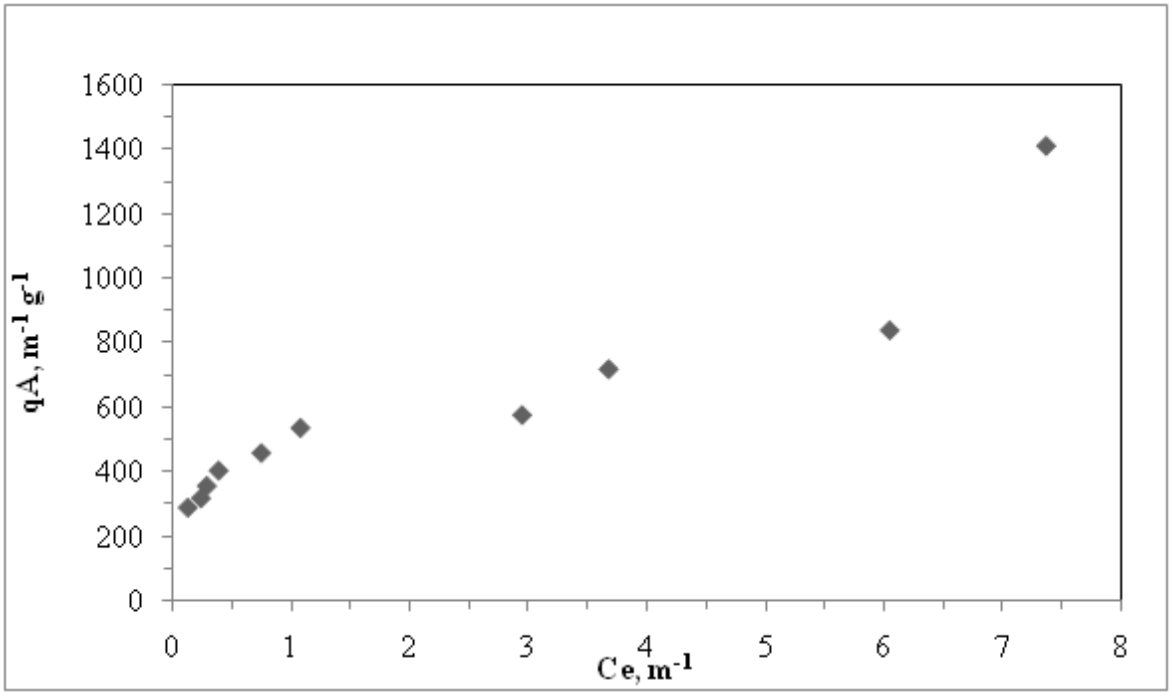

Figure A.11. Freundlich adsorption isotherm of UV_{365} of 0.45µm filtered fraction of humic acid onto TiO_2 in the presence of zinc.

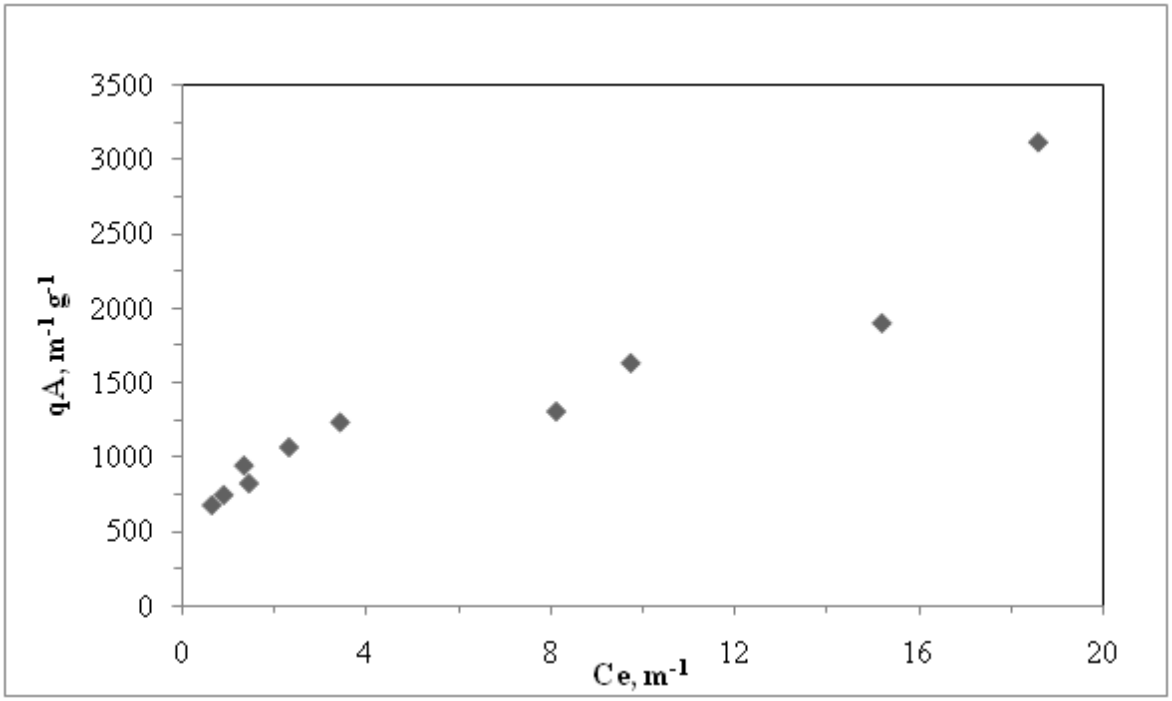

Figure A.12. Freundlich adsorption isotherm of UV_{280} of 0.45µm filtered fraction of humic acid onto TiO_2 in the presence of zinc.

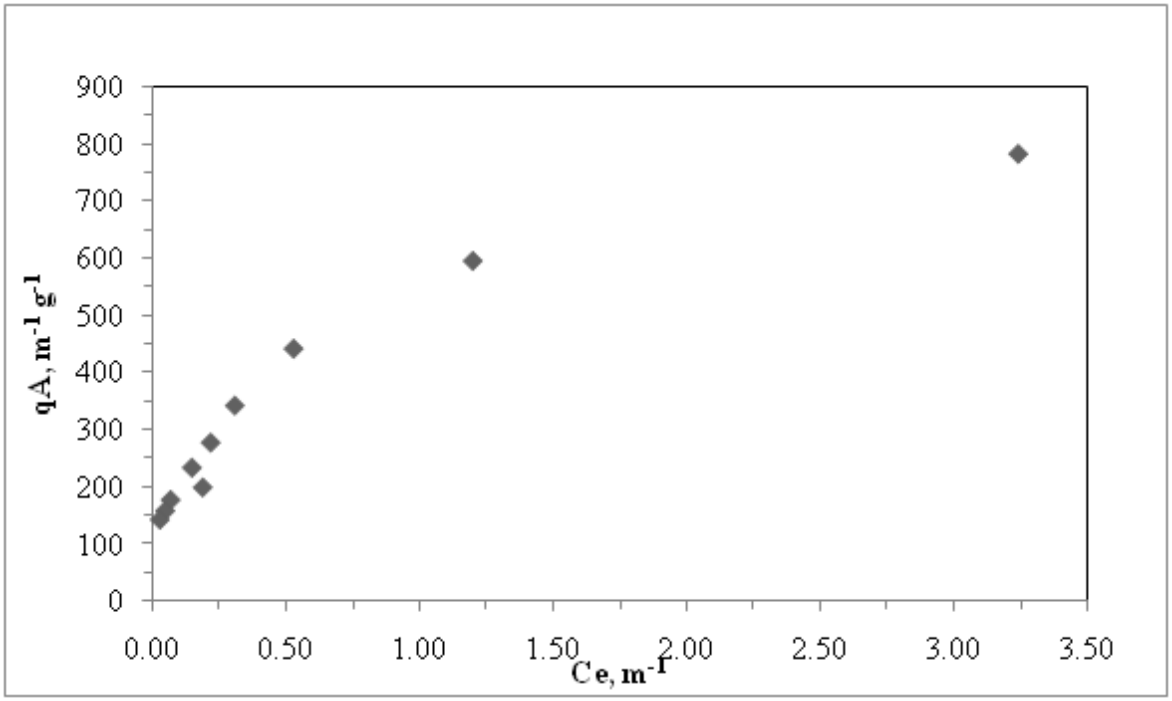

Figure A.13. Freundlich adsorption isotherm of UV_{365} of 100 kDa fraction of humic acid onto TiO_2 in the presence of zinc.

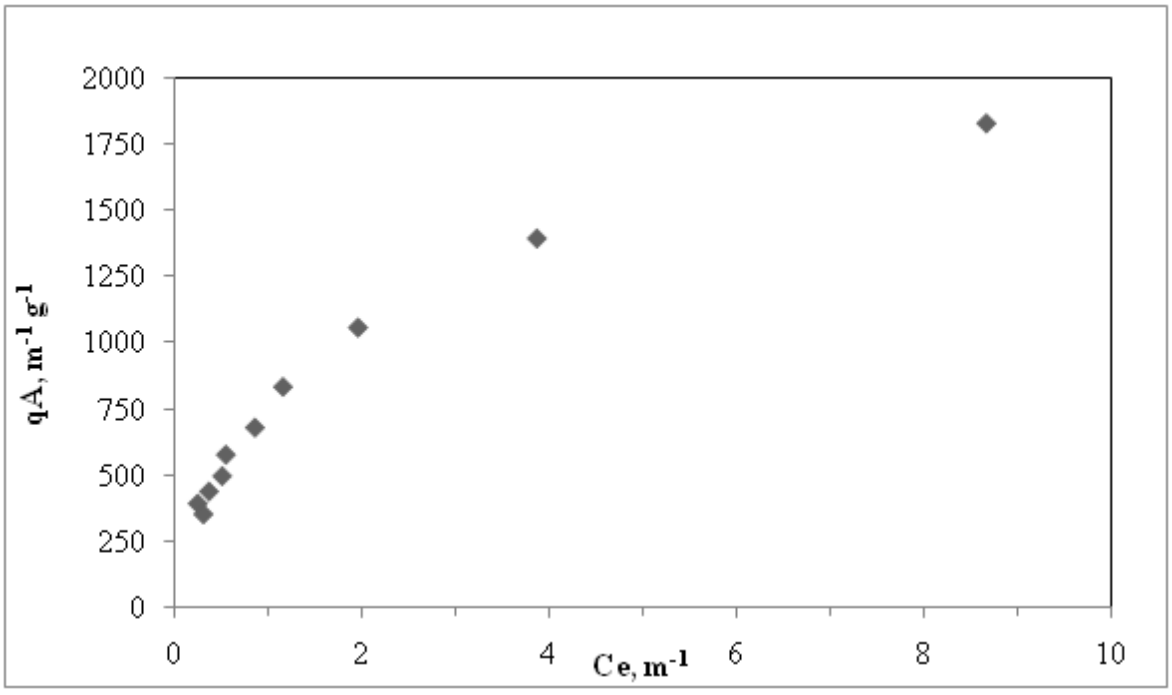

Figure A.14. Freundlich adsorption isotherm of UV_{280} of 100 kDa fraction of humic acid onto TiO_2 in the presence of zinc.

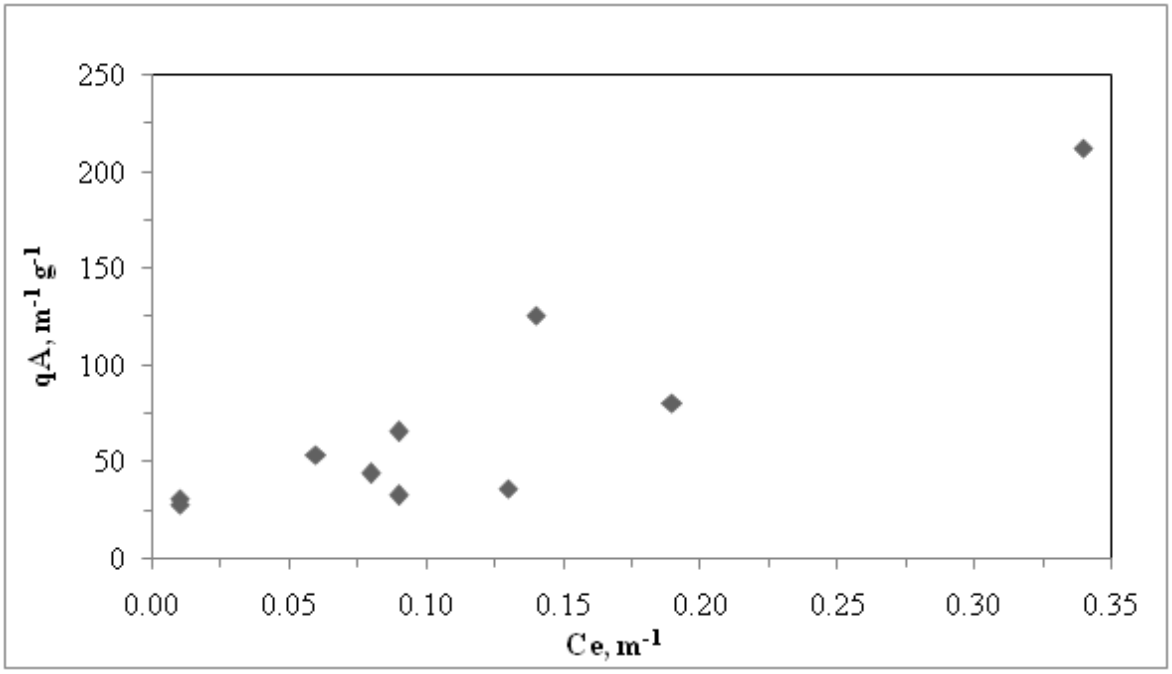

Figure A.15. Freundlich adsorption isotherm of UV_{365} of 30 kDa fraction of humic acid onto TiO_2 in the presence of zinc.

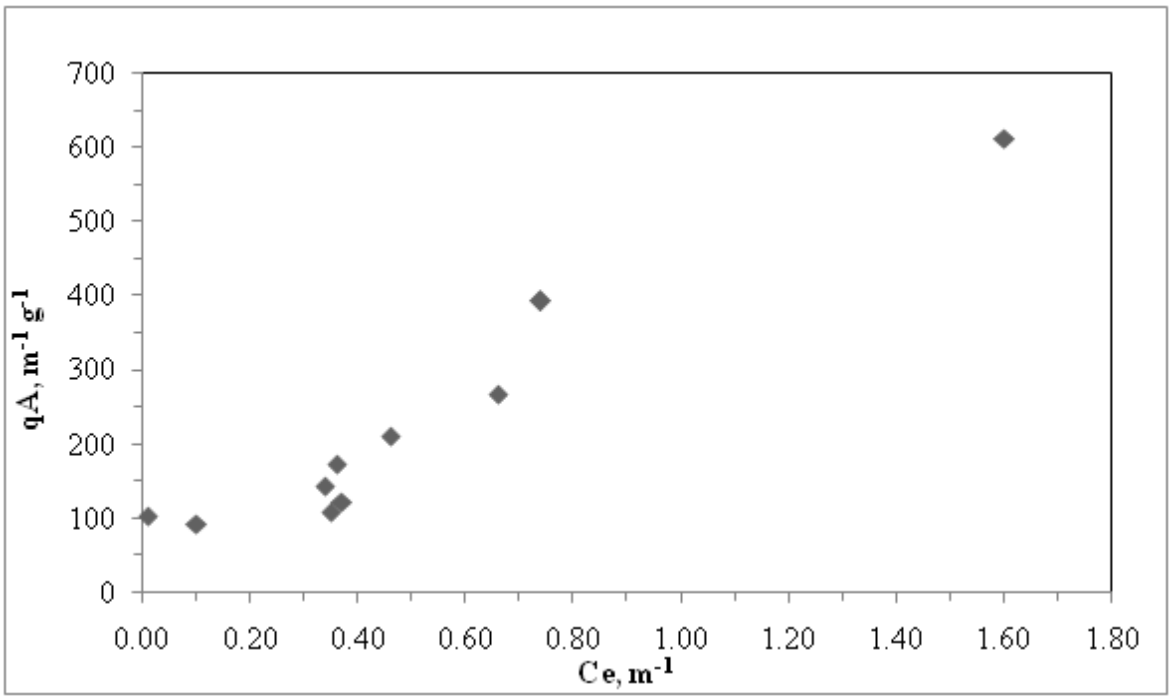

Figure A.16. Freundlich adsorption isotherm of UV_{280} of 30 kDa fraction of humic acid onto TiO_2 in the presence of zinc.

APPENDIX B

Langmuir Adsorption Isotherms of Humic Acids

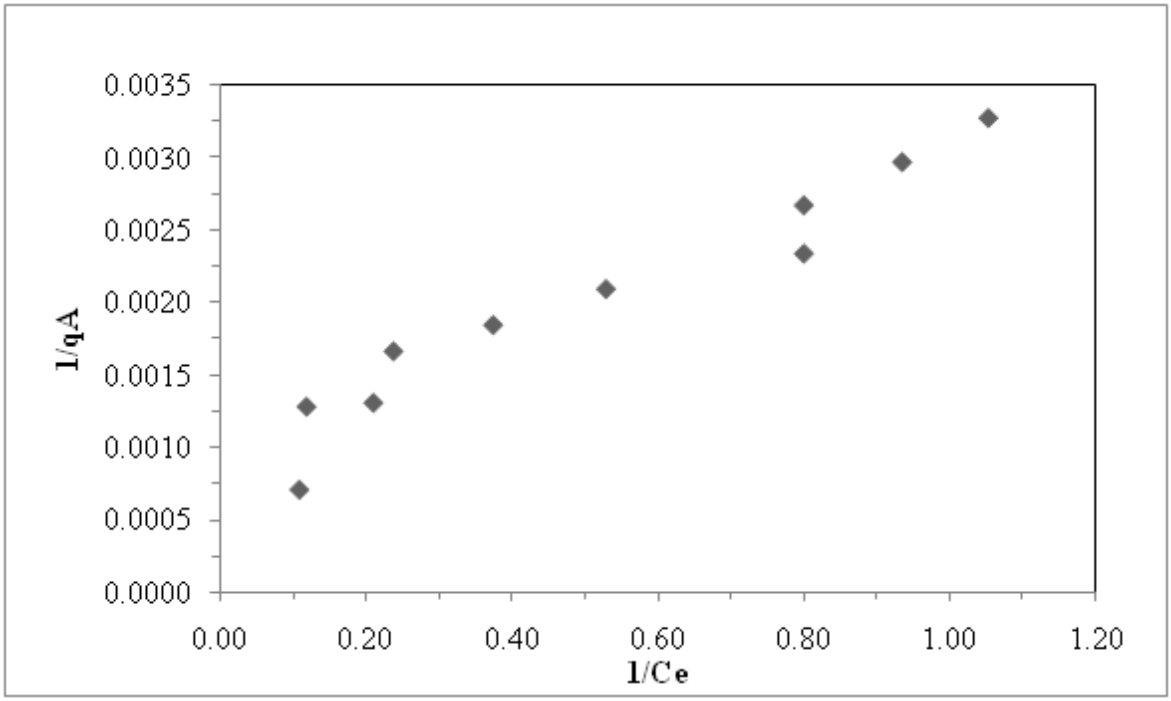

Figure B.1. Langmuir adsorption isotherm of UV_{365} of raw humic acid onto TiO_2.

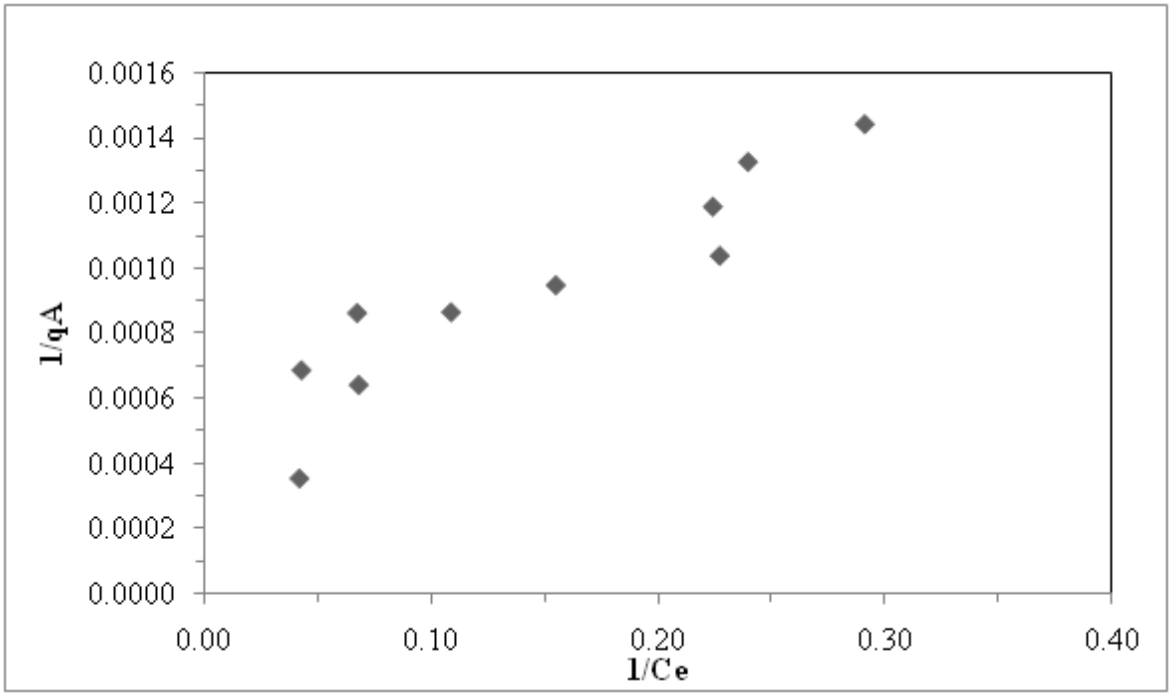

Figure B.2. Langmuir adsorption isotherm of UV_{280} of raw humic acid onto TiO_2.

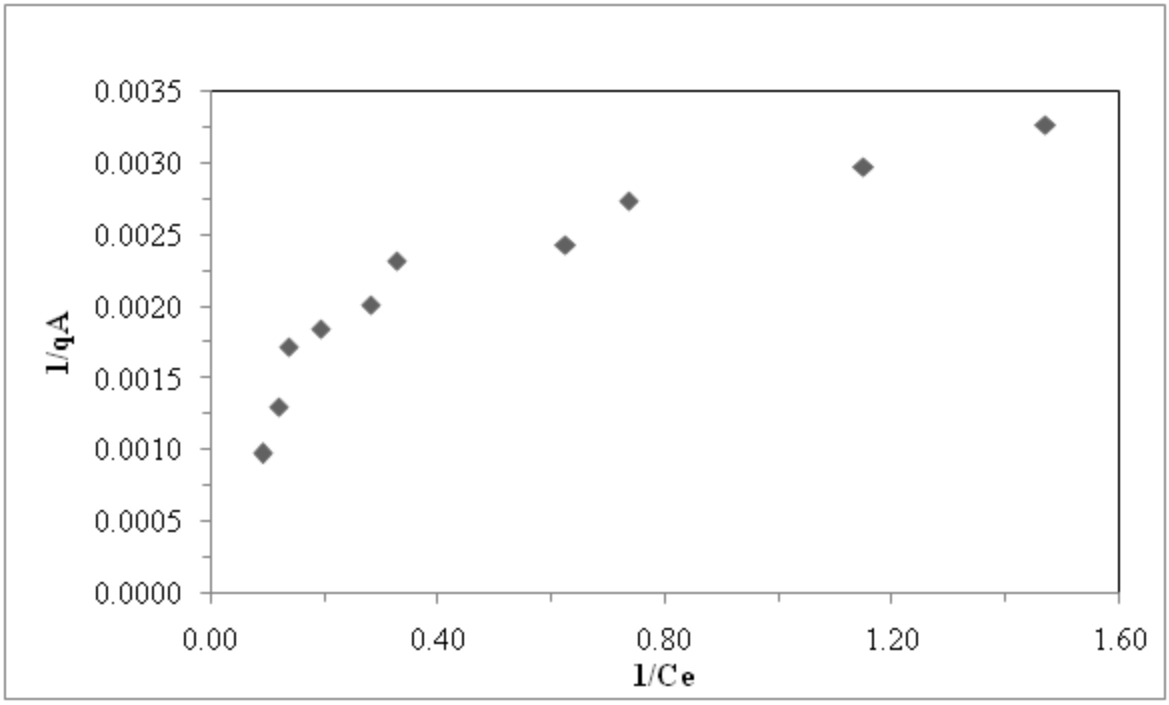

Figure B.3. Langmuir adsorption isotherm of UV_{365} of 0.45µm filtered fraction of humic acid onto TiO_2.

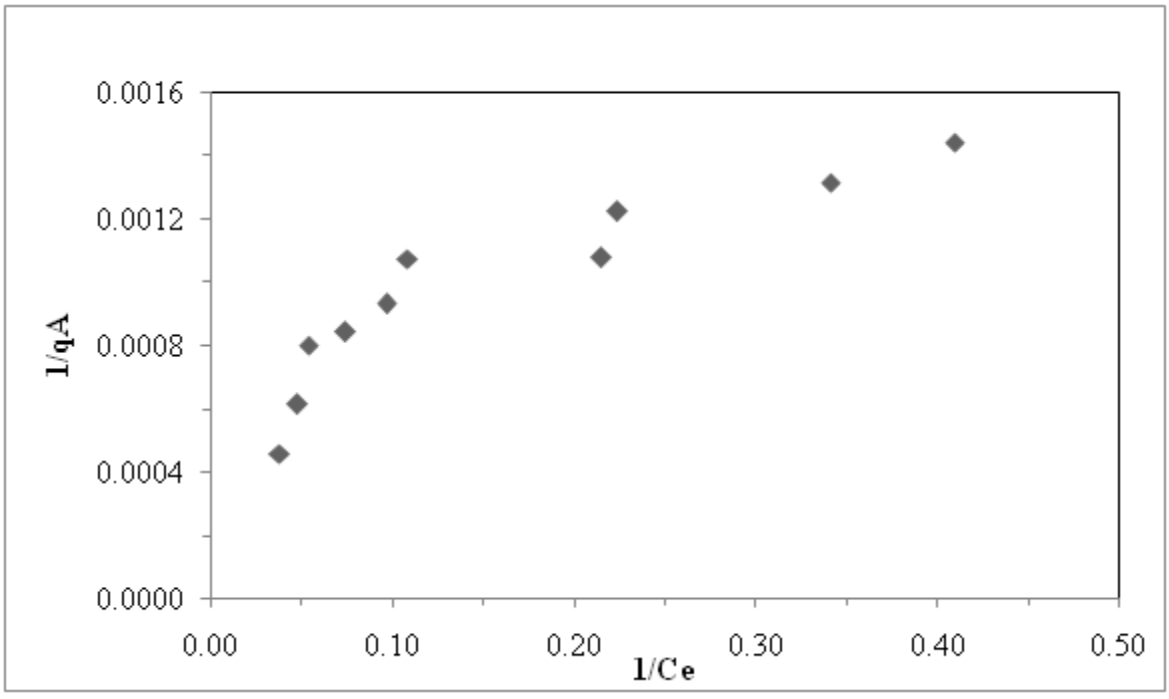

Figure B.4. Langmuir adsorption isotherm of UV_{280} of 0.45µm filtered fraction of humic acid onto TiO_2.

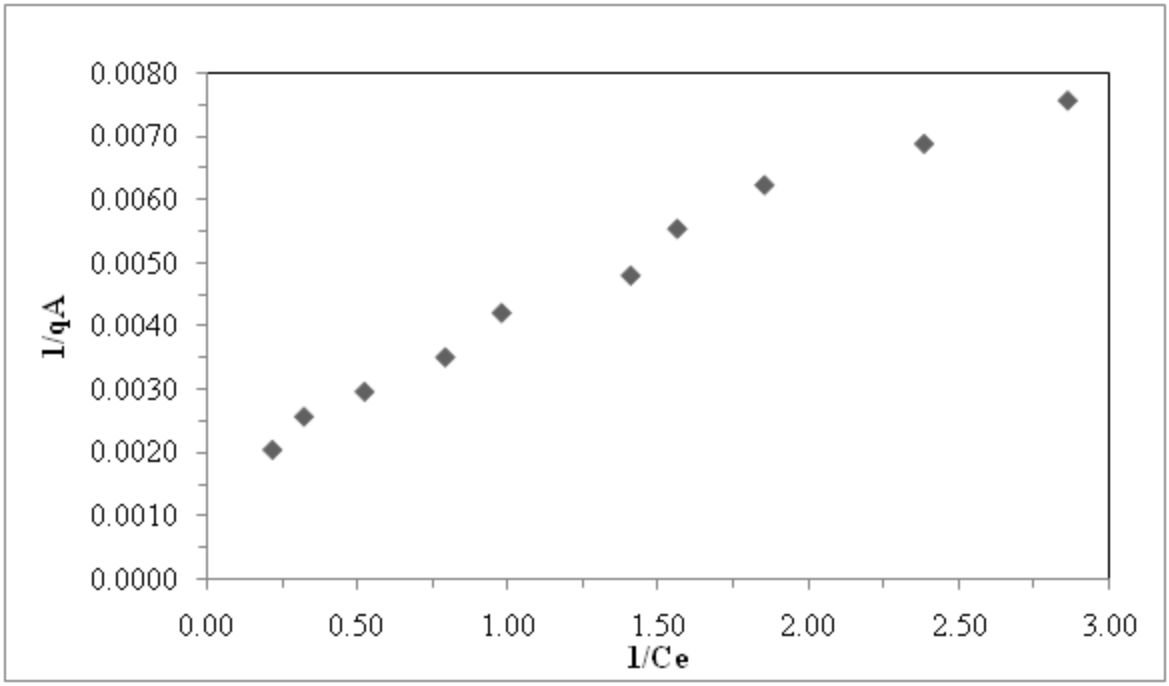

Figure B.5. Langmuir adsorption isotherm of UV_{365} of 100 kDa fraction of humic acid onto TiO_2.

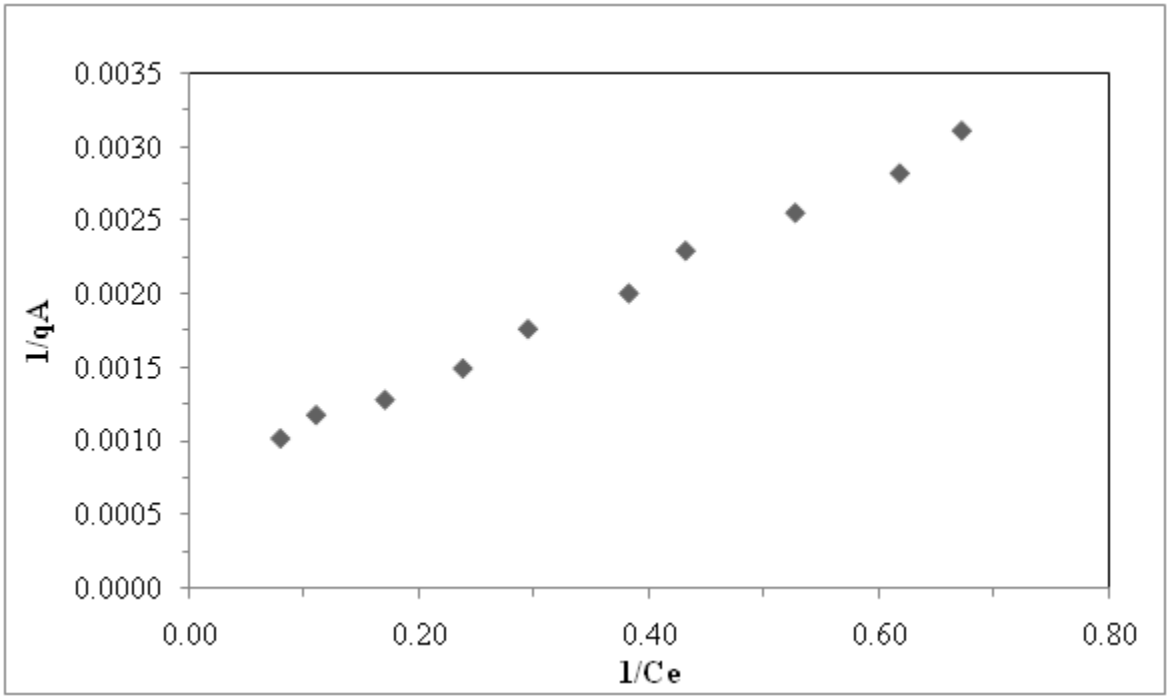

Figure B.6. Langmuir adsorption isotherm of UV_{280} of 100 kDa fraction of humic acid onto TiO_2.

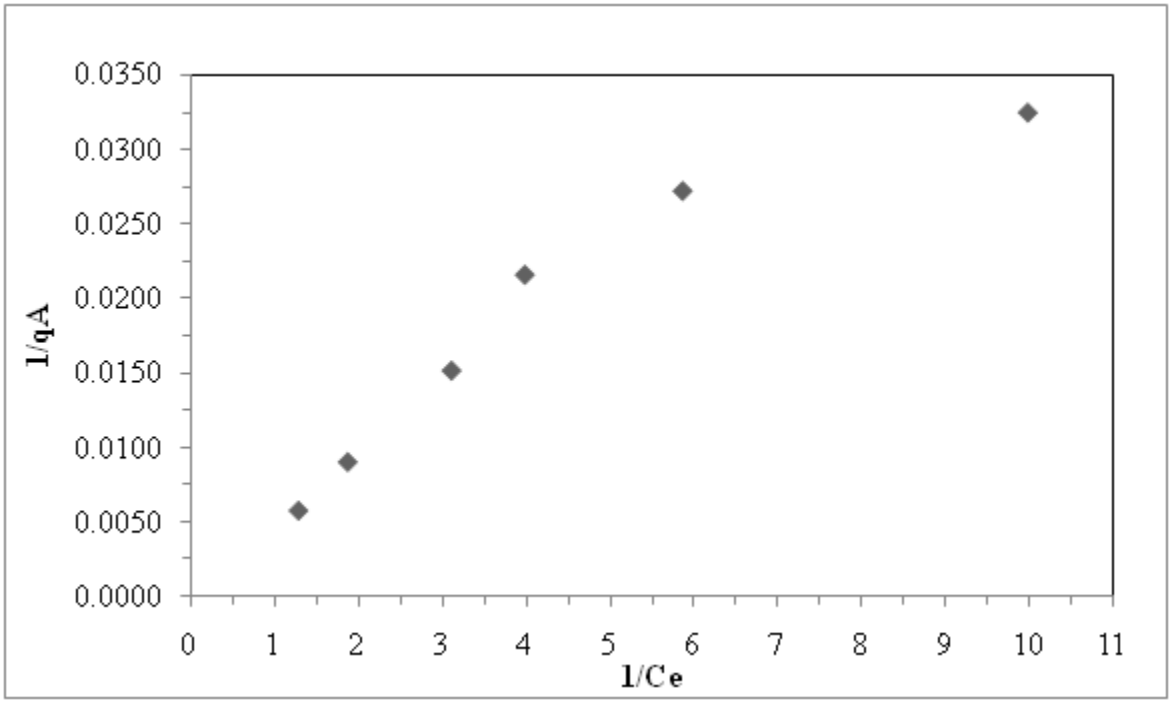

Figure B.7. Langmuir adsorption isotherm of UV_{365} of 30 kDa fraction of humic acid onto TiO_2.

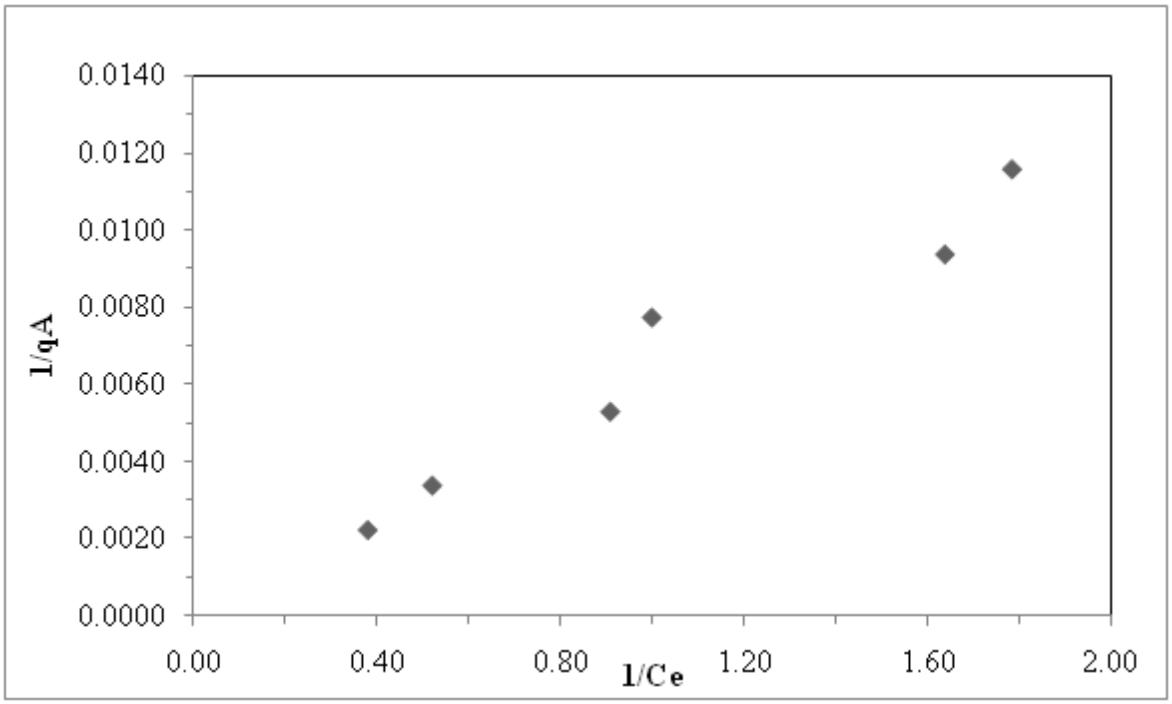

Figure B.8. Langmuir adsorption isotherm of UV_{280} of 30 kDa fraction of humic acid onto TiO_2.

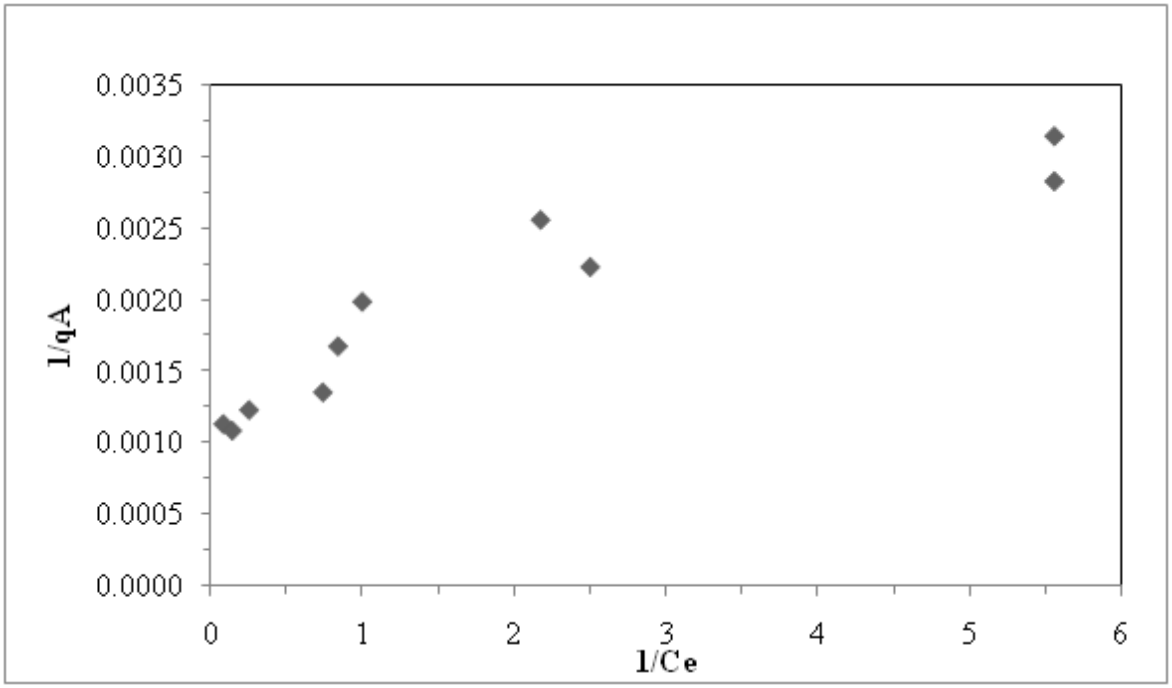

Figure B.9. Langmuir adsorption isotherm of UV_{365} of raw humic acid onto TiO_2 in the presence of zinc.

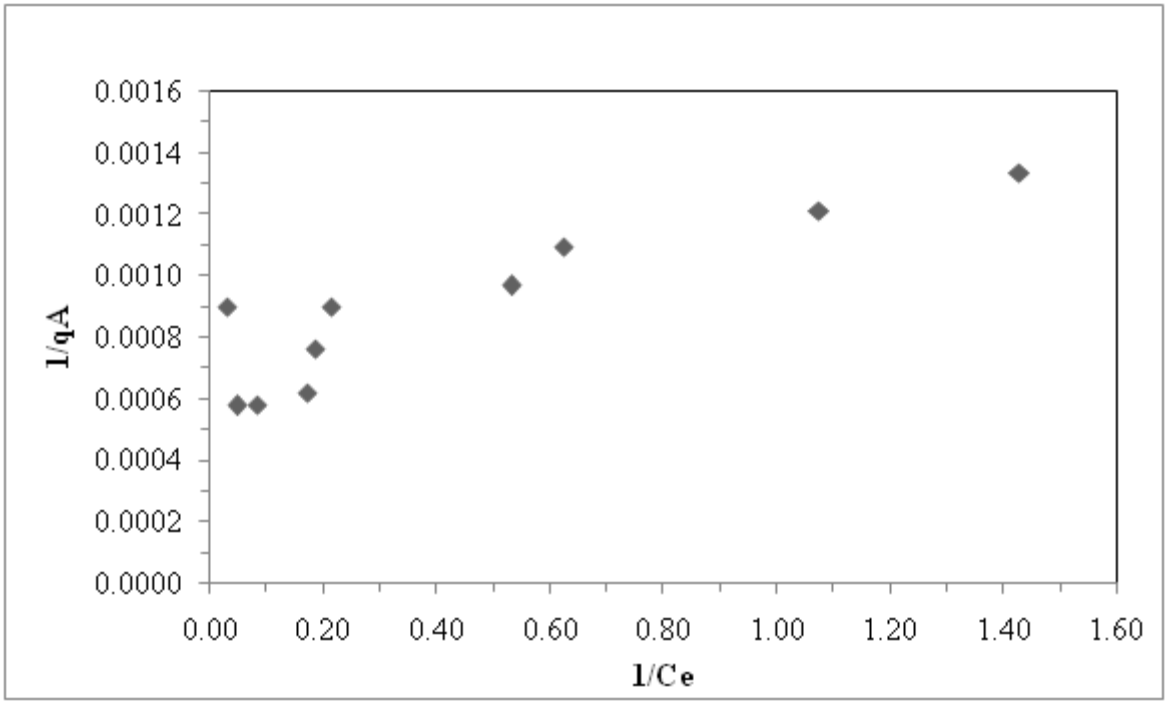

Figure B.10. Langmuir adsorption isotherm of UV_{280} of raw humic acid onto TiO_2 in the presence of zinc.

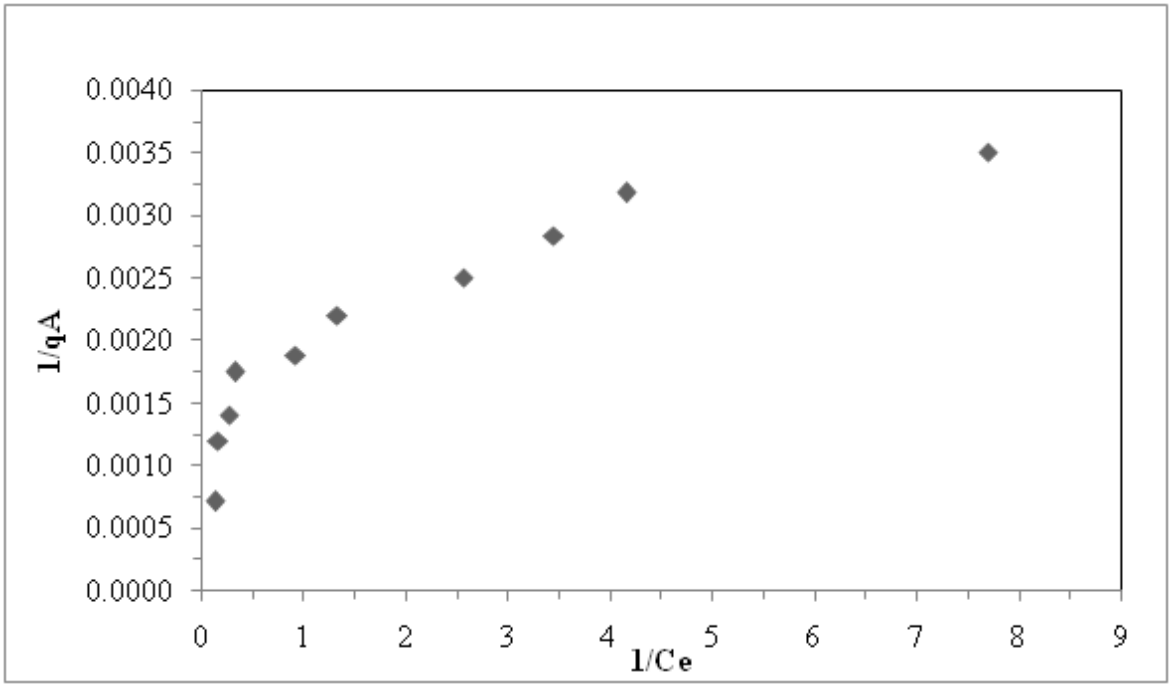

Figure B.11. Langmuir adsorption isotherm of UV_{365} of 0.45µm filtered fraction of humic acid onto TiO_2 in the presence of zinc.

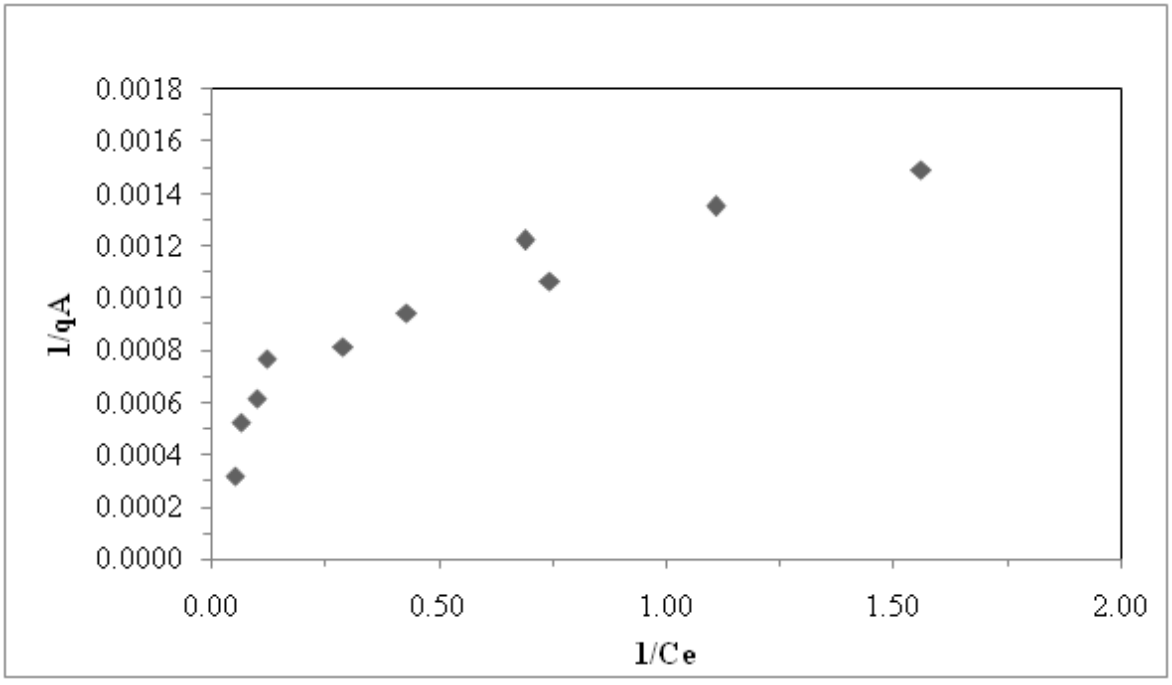

Figure B.12. Langmuir adsorption isotherm of UV_{280} of 0.45µm filtered fraction of humic acid onto TiO_2 in the presence of zinc.

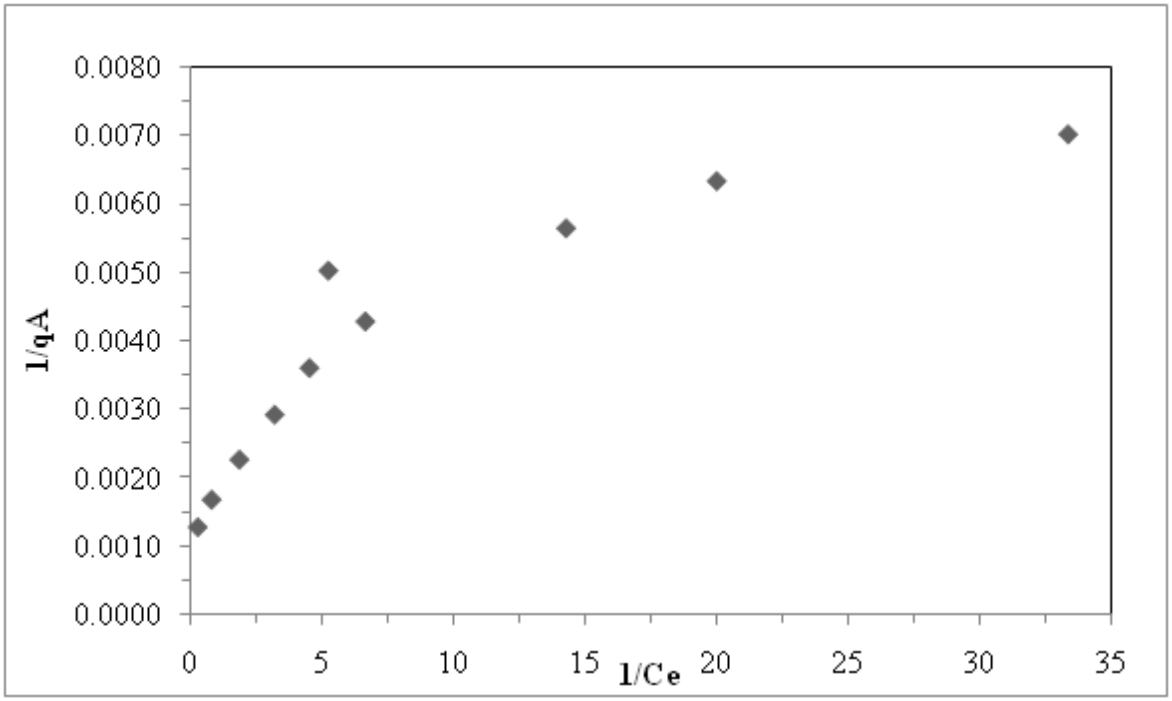

FigureB.13. Langmuir adsorption isotherm of UV_{365} of 100 kDa fraction of humic acid onto TiO_2 in the presence of zinc.

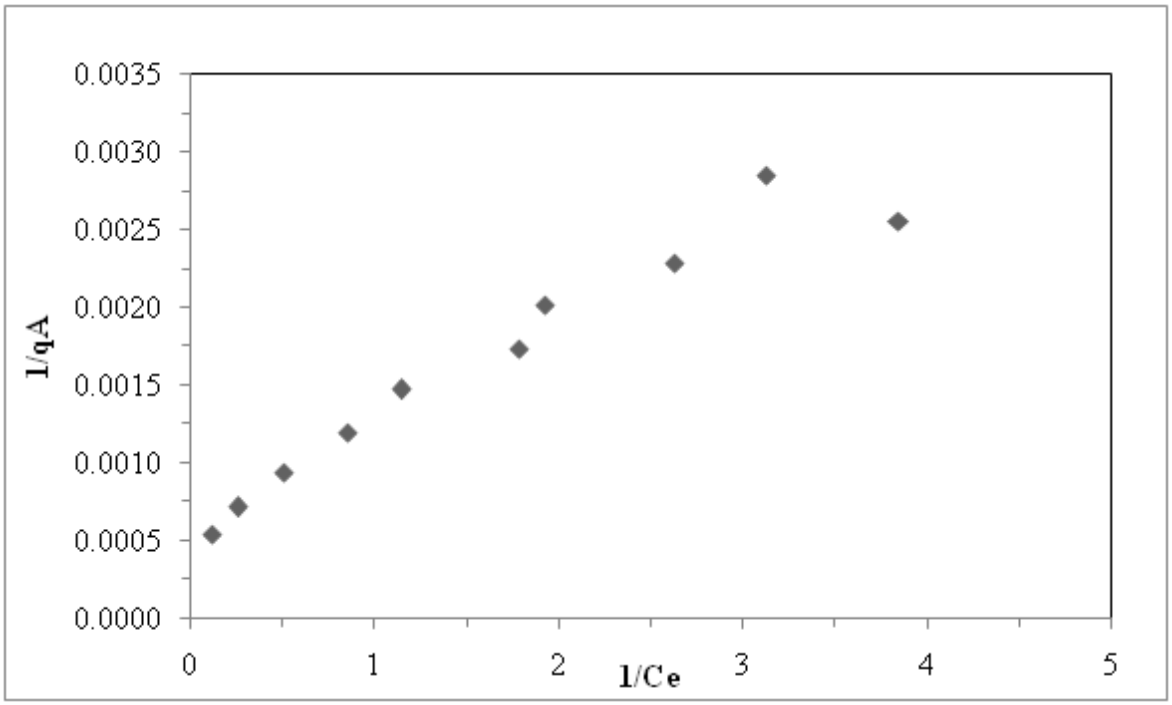

Figure B.14. Langmuir adsorption isotherm of UV_{280} of 100 kDa fraction of humic acid onto TiO_2 in the presence of zinc.

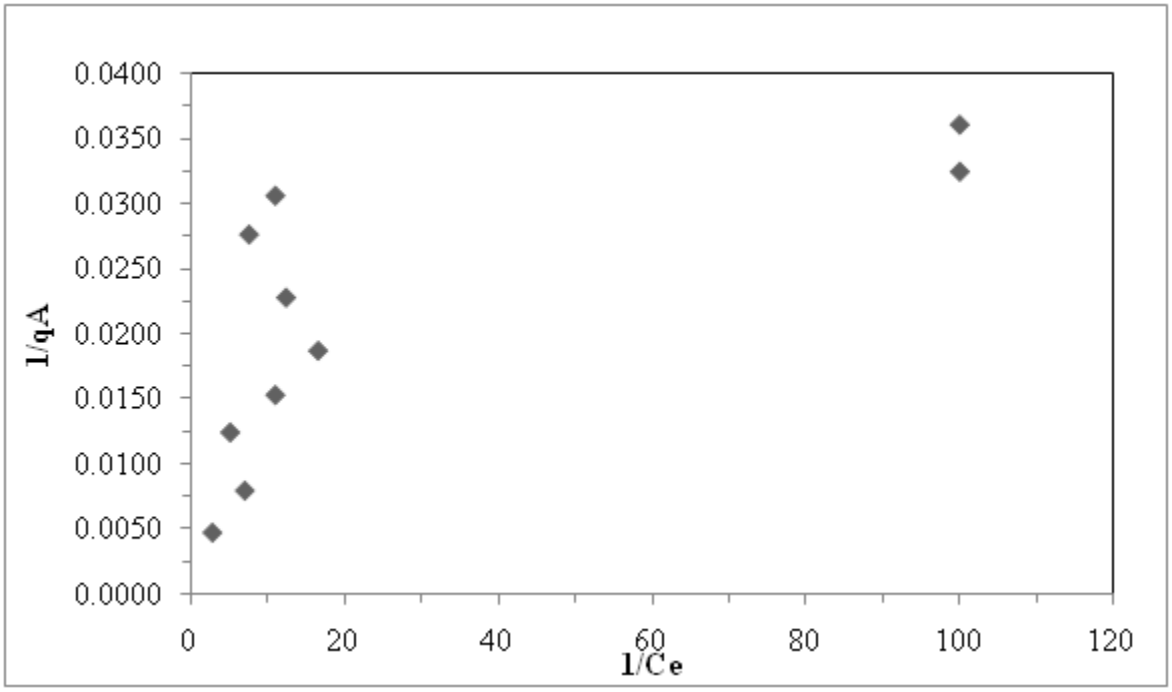

Figure B.15. Langmuir adsorption isotherm of UV_{365} of 30 kDa fraction of humic acid onto TiO_2 in the presence of zinc.

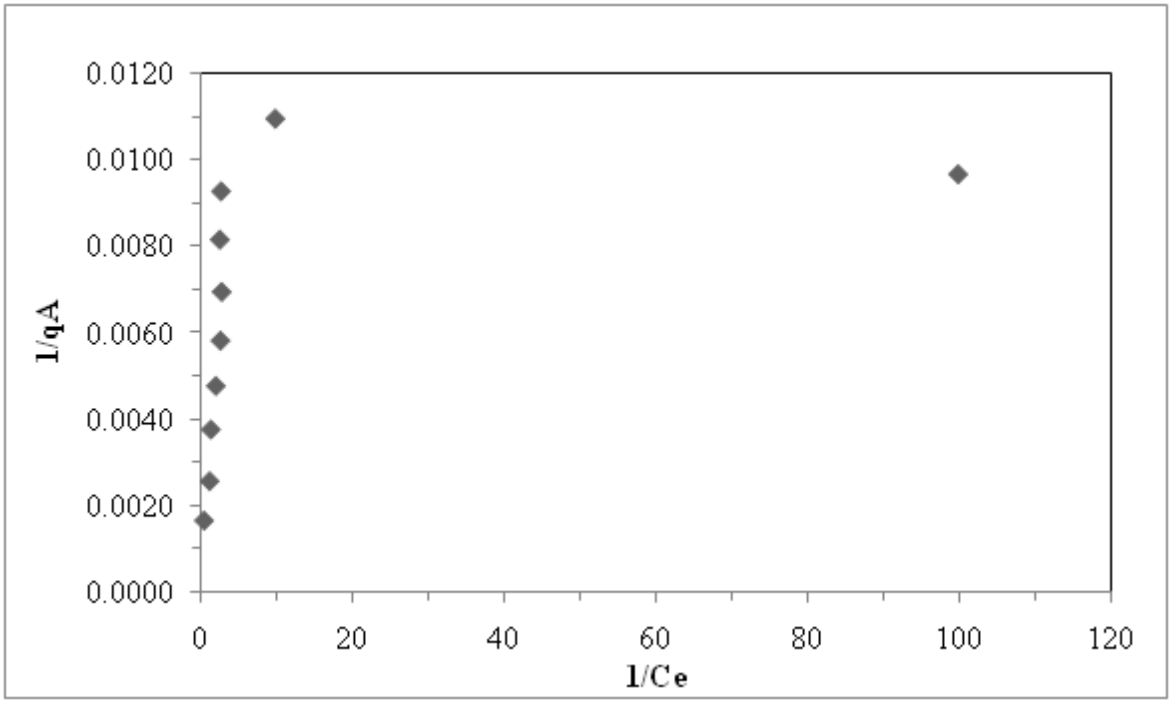

Figure B.16. Langmuir adsorption isotherm of UV_{280} of 30 kDa fraction of humic acid onto TiO_2 in the presence of zinc.